

***DEVELOPMENT OF NEW ANTI COUNTERFEIT  
PRINTING TECHNIQUES FOR PACKAGING***

*Thesis submitted by*

by

**Indrama Das**

Reg No.: D-7/E/914/16

*Doctor of Philosophy (Engineering)*

Printing Engineering Department,  
Faculty Council of Engineering & Technology  
Jadavpur University  
Kolkata, India

**2023**

**Index No. 46/16/E**

*Title of Thesis*

**DEVELOPMENT OF NEW ANTI COUNTERFEIT  
PRINTING TECHNIQUES FOR PACKAGING**

*Under the Guidance of*

Dr. Swati Bandyopadhyay  
Associate Professor,  
Printing Engineering Department,  
Jadavpur University, Kolkata – 700032, India

&

Prof. Alain Trémeau  
Professor, Faculty of Sciences and Technologies  
Hubert Curien Laboratory, UMR CNRS  
Université de Lyon, Université Jean Monnet,  
Saint Etienne, France

## *List of Publication*

### **Journal Publications (3):**

1. Indrama Das, Swati Bandyopadhyay and Alain Trémeau, “Characterization of prints based on microscale image analysis of dot patterns”, Appl Sci, 11 (14), pp. 6634, 2021.
2. Indrama Das, Swati Bandyopadhyay and Alain Trémeau, “Identification of A Fake Medicine Packaging Print From its Dot Sizes and Shape”, International Journal of Engineering Research & Technology (IJERT), IJERTV12IS030199, <http://www.ijert.org> ISSN: 2278-0181, 12 (03), 2023.
3. Indrama Das, Swati Bandyopadhyay and Alain Trémeau, “Identification of Fake Printed Medicine Packaging from a SVM Approach and Dots Shape Features”. International Journal of Computer Applications 185(8), pp. 5-12, 2023.

### **List of Patents (1):**

1. Dr. Swati Bandyopadhyay, Indrama Das., “Method for Introducing Variable Image Watermark on Different Packaged Products and System Thereof”, Patent no.: 410574, Application No.: 202031034457, Intellectual Property India, SL No :033121892, Date of Filing: 11/08/2020, Date of Grant: 31/10/2022.

### **List of Presentations in National / International Conferences/ Workshops/Symposiums (1):**

1. Indrama Das, Swati Bandyopadhyay and Alain Trémeau, “Authenticity of a print for medicine packaging from its dot sizes and shape”, International Conference on Innovations in Engineering and Technology (ICIET-2022), held on JNTU, Hyderabad, pp. 133, 15- 17 September, 2022.



# Proforma – 1

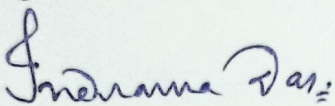
## “Statement of Originality”

I Indrama Das registered on 17<sup>th</sup> November, 2016 do hereby declare that this thesis entitled “Development of New Anti-Counterfeit Printing Techniques for Packaging” contains literature survey and original research work done by the undersigned candidate as part of Doctoral studies.

All information in this thesis have been obtained and presented in accordance with existing academic rules and ethical conduct. I declare that, as required by these rules and conduct, I have fully cited and referred all materials and results that are not original to this work.

I also declare that I have checked this thesis as per the “Policy on Anti Plagiarism, Jadavpur University, 2019”, and the level of similarity as checked by iThenticate software is 7 %.

Signature of Candidate:



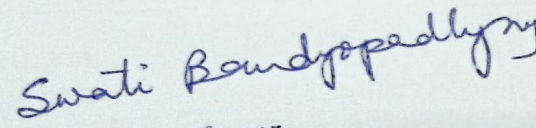
(INDRAMA DAS)

Date: 04.07.2023

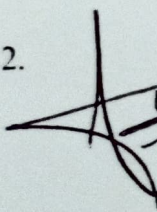
Certified by Supervisor(s):

(Signature with date, seal)

1.

  
Associate Professor  
Printing Engineering Department  
Jadavpur University  
Kolkata

2.

  
~~LABORATOIRE HUBERT CURIEN~~  
UMR CNRS 5516 Université Jean Monnet  
18 rue Pr. Benoît Luras - Bât. F  
FR-2000 SAINT-ETIENNE  
(33) 04 77 91 57 80 / Fax (33) 04 77 91 57 81



## Proforma-2

### CERTIFICATE FROM THE SUPERVISOR

This is to certify that the thesis entitled “**Development Of New Anti-Counterfeit Printing Techniques For Packaging**” submitted by **Indrama Das**, who got her name registered on 17<sup>th</sup> November, 2016, for the award of Ph.D. (Engineering) Degree of Jadavpur University is absolutely based upon her own work under the supervision of **Dr. Swati Bandyopadhyay** and **Prof. Alain Trémeau** and that neither her thesis nor any part of the thesis has been submitted for any degree or any other academic award anywhere before.

*Signature of the Supervisor and Date  
With Official Seal*

*Swati Bandyopadhyay*  
Associate Professor  
Printing Engineering Department  
Jadavpur University  
Kolkata

**Dr. Swati Bandyopadhyay**  
Associate Professor,  
Printing Engineering Department,  
Jadavpur University  
Kolkata – 700 032, India

*Signature of the Supervisor and Date  
with Official Seal*

*Alain Trémeau*  
**LABORATOIRE HUBERT CURIEN**  
UMR CNRS 5516 Université Jean Monnet  
18 rue Pr. Benoît Luras - Bât. F  
F-42000 SAINT-ETIENNE  
(33) 04 77 91 57 80 / Fax (33) 04 77 91 57 81

**Prof. Alain Trémeau**  
Professor, Faculty of Sciences and  
Technologies  
Hubert Curien Laboratory  
UMR CNRS  
Université de Lyon, Université Jean  
Monnet,  
Saint Etienne, France



# ACKNOWLEDGEMENT

We are delighted to present the Ph.D. thesis titled " **Development of New Anti-Counterfeit Printing Techniques for Packaging.**" Completing this thesis has been a truly rewarding and memorable experience, made possible by the guidance and support of esteemed individuals. First and foremost, I express my deepest gratitude to my supervisors, **Dr. Swati Bandyopadhyay** and **Prof. Alain Trémeau**, for their invaluable advice, unwavering support, and patience throughout my doctoral studies. Their extensive knowledge and vast experience have been a constant source of encouragement during my academic research.

I would like to express my sincere gratitude to **Prof. Sivaji Bandyopadhyay**, who has consistently served as a great source of inspiration to me since my time in the master's program.

I extend my sincere thanks to the Indo French Centre for the Promotion of Advanced Research (IFCPAR/CEFIPRA) for their support.

I am grateful to Sergusa Solution Pvt. Ltd. and Etone India Pvt. Ltd. for their assistance.

I am profoundly grateful to my friend, Dr. Mahasweta Mandal, who has supported and helped me. Her valuable suggestions played a significant role in the successful completion of this work. I am also grateful to my friend, Dr. Paulomi Kundu, for her support and assistance for this work.

I would like to express my warm and heartfelt gratitude to my family members for all their greatest moral support, love and patience during this fulfilling experience. I am very grateful to my Parents, my sister and in-laws, for their unwavering, unconditional and affectionate support, which has kept me motivated and confident. My achievements and success are a result of their belief in me.

I want to express special thanks to my husband, who became part of my life during my research work and stood by me through both the joyful and challenging moments.

Most importantly, I express my gratitude to Lord Shiva, whose benevolent blessings and unwavering support have been indispensable in my successful completion of this journey.

*Sudhama Das*



# DEDICATION

I would like to dedicate my thesis to my Parents for their endless love, support, and encouragement throughout my pursuit for education. I hope this achievement will fulfill their dream they envisioned for me.

*Indranil Das*

## TABLE OF CONTENT

➤ <b>ABSTRACT</b> .....	xxii
➤ <b>CHAPTER 1: Introduction</b> .....	1
1.1 Identification of Problem.....	1
1.2 Problem Statement.....	2
1.3 Purpose & Goal.....	3
1.4 Research Objectives.....	3
1.5 Statement of Hypothesis.....	4
1.6 Limitation.....	4
1.7 Overview of Thesis.....	4
➤ <b>CHAPTER 2: Literature Survey</b> .....	6
2.1 Literature review on watermarking process for protecting copyright.....	6
2.2 Literature on microscopic printed Dot shape and parameter.....	10
2.3 Literature review on Automatic dot object detection.....	12
2.4 Literature review on Anticounterfeit packaging.....	13
2.5 Literature review on Gravure printing.....	14
2.6 Literature review on Classification of source by Support Vector Machine....	14
➤ <b>CHAPTER 3: Medicine Package Printing</b> .....	16
3.1 Medicine Packaging.....	16
3.2 Substrate Used for Medicine Packaging.....	18
3.3 Blister Substrate used for Medicine packaging Printing.....	19
➤ <b>CHAPTER 4: Anticounterfeiting techniques used for package printing</b> .....	25
4.1 Anticounterfeiting techniques used for package printing.....	25
4.2. Watermarking process as security feature in anti-counterfeiting.....	27
4.3 Watermarking security and its vulnerability.....	28
4.4 Watermarking by Histogram.....	30
4.5 Anti-counterfeiting measures microscopic dot analysis.....	31
➤ <b>CHAPTER 5: Gravure printing</b> .....	33
5.1 Gravure Cylinder Making.....	34
5.2 The Gravure Printing Unit.....	39
5.3 Gravure Print Parameters.....	41
5.3.1 Gravure Inks.....	45
5.3.1.1 Foil Ink.....	49
➤ <b>CHAPTER 6: Classification through Support Vector Machine</b> .....	52
6.1 Support Vector Machine.....	52
6.1.1 Multiclass classification in SVM.....	53
6.1.2 Type of SVM kernels.....	54

6.1.3	Validation Techniques for Multi-class classification SVM Model.....	56
6.1.4	Confusion Matrix.....	57
6.1.5	SVM step by step process.....	58
6.2	Multiclass classification (M-SVM) model development to classify the Print sample on blister foil.....	59
6.2.1	Generate a classification model to differentiate print and reprint samples using SVM Multi-class classification model.....	59
6.2.2	Cross – validation for training and testing the model.....	59
6.2.3	Evaluation of proposed model.....	61
6.2.4	Implementation.....	61
➤	<b>CHAPTER 7: Experimental Procedure.....</b>	<b>63</b>
	❖ Source Artwork.....	63
	❖ Engraving the Cylinder Pre-press parameters for the artwork.....	64
	❖ Gravure cylinder engraving process.....	65
	❖ Gravure machine unit in the printing press.....	66
	❖ Print substrate and ink.....	67
	❖ Capture/Scan and Engrave Reprint Cylinder for Simulate the counterfeiting process.....	68
	❖ Collection of samples data.....	68
7.1	Method for Introducing Variable Image Watermark on Different Packaged Products and System Thereof.....	70
7.1.1	Source Artwork for watermarking process.....	70
7.1.2	Preparing watermarked image using the MATLAB.....	70
7.1.3	Proposed Watermarking Scheme.....	71
	❖ Proposed Watermark Design.....	72
	❖ Watermark Embedding Scheme.....	73
7.1.4	Steps of the Embedding Watermark into the Host Image.....	74
7.1.5	Quality measures (MSE, PSNR, SSIM) for host images (HI), host images watermarked (HIW), original watermarked print samples (PS-WI) and reprint (simulated counterfeit) samples (RPRS-WI) on A4 paper media.....	75
7.1.6	Quality Measures (by co-relation co-efficient) for host images watermarked (HIW), original watermarked print samples (PS-WI) and reprint (simulated counterfeit) samples (RPRS-WI) on Paper and Foil Media.....	77
7.2	Characterization of Prints Based on Microscale Image Analysis of Dot Patterns.....	78
7.2.1	Source Artwork.....	78
7.2.2	Cylinder Engraving for the artwork.....	79
7.2.3	Microscope instrument and function.....	79
7.2.4	Measurement, Modelling and Analysis at the Microscale of Printed Dots for three colors (CMY) using MATLAB.....	80
7.3	Identification of A Fake Medicine Packaging Print From its Dot Sizes and Shape.....	88
7.3.1	Measurement at the Microscale of Print and Reprint Dots for colors	

(CMY) MATLAB function.....	90
7.4 Identification of fake printed medicine packaging from a SVM approach and dots shape features.....	92
7.4.1 Classification process.....	94
7.4.1.1 Support Vector Machine multi-class for classification.....	94
➤ <b>CHAPTER 8: Result and discussion</b> .....	97
8.1 Experimental results and discussions for Variable Image Watermark Process.....	97
8.2 Experimental Results obtain from Prints Based on Microscale Image Analysis of Dot Patterns.....	119
8.3 Experimental Results obtain from print and reprint Dot Sizes and Shape.....	130
8.4 Experimental Results obtain from a Support Vector Machine approach and dots shape features.....	144
➤ <b>CHAPTER 9: Conclusion &amp; Future Scope</b> .....	168
➤ <b>CHAPTER 10: Reference</b> .....	170
➤ <b>List of Figures</b> .....	xii
➤ <b>List of Tables</b> .....	xix
➤ <b>Abbreviations</b> .....	xxi

## List of Figures:

Fig 3.1: Blister Pack medicines.....	20
Fig 3.2: The basic configuration of blister packaging.....	20
Fig 3.3: The basic components of blister packaging.....	22
Fig 3.4: A common method for assembling blister packaging.....	24
Fig 5.1: Gravure Printing Process.....	33
Fig 5.2: (a) Copper Plating (b) Polishing Copper Plated Cylinder.....	35
Fig.5.3: Flow chart showing the EME cylinders making processes.....	36
Fig.5.4: Different Stylus angels.....	37
Fig.5.5: Engraving Head.....	37
Fig.5.6. Images show (a) EME engraving process, (b) EME engraved cell on Cu plated cylinder.....	37
Fig.5.7: Electromechanical Engraving of Cylinder.....	38
Fig.5.8: Electromechanical engraving Machine.....	38
Fig.5.9: Gravure cylinder.....	40
Fig.5.10: Gravure printing unit.....	40
Fig.5.11: Microstructure of Gravure Cell.....	41
Fig.5.12: Cell and Cell wall.....	42
Fig.5.13: (a)Pyramidal Electronic Engraved Cells (b) Cell angle of compression.....	43
Fig.5.14: Varying Cell Depth for Highlight, Middle-tone and Shadow.....	43
Fig.5.15: Thin cell walls for shadows (L) and thick cell walls for highlights (R).....	44
Fig.6.1: Schematic Diagram Image of SVM.....	52
Fig.6.2: (a)Binary Classification (b) Multi- class Classification.....	53
Fig.6.3: Block diagram of Multiclass classification SVM Input-Output.....	58
Fig.6.4: Six-fold cross validation for Dataset – Print (P1, P2, P3) and Reprint (R1, R2, R3).....	61
Fig.6.5: Block diagram of Multi-class SVM model in this study.....	61
Fig.7.1: Source Images ((a)Lena, (b) Baboon, (c) Avion, (d) Peppers).....	62
Fig.7.2: Reference image IT8.7/3 Color Chart.....	63
Fig.7.3: Combined artwork for variable image watermark and microscopic dot shape analysis engraved on cylinder.....	63
Fig.7.4: Gravure cylinder engraving parameters set in the pre-press using Art-Pro software.....	64
Fig.7.5: HELL machine for cylinder engraving (electromechanical).....	64
Fig.7.6: Gravure Printing press.....	64
Fig.7.7: (a) Substrate blister foil (b) Printing on blister foil using engraved cylinder.....	66
Fig.7.8: Flow Chart Original Print Process and Simulated Counterfeiting Process.....	67
Fig.7.9: Experimental procedure (step by step process) for data collection.....	68
Fig.7.10: Preparing watermarked image (HIW).....	69
Fig.7.11: Data collection for variable image watermarking analysis.....	70
Fig.7.12: Flow diagram of embedding watermark process.....	72



Fig.7.13: Step by step process of watermarking.....	73
Fig.7.14: Statistical Analysis Flow Chart of comparison for MSE, PSNR, SSIM.....	75
Fig.7.15: Flow Chart of Comparative statistical analysis for the correlation coefficient..	77
Fig.7.16:(a) Selected samples from the IT8.7/3 Color Chart: sample C10—Cyan with 20% ink coverage; sample D10—Magenta with 20% ink coverage, sample E10—Yellow with 20% ink coverage, (b)cropped image of a Rotogravure printed cyan sample magnified $\times 4$ .....	77
Fig.7.17: Lawrence & mayo Microscope.....	78
Fig.7.18: Framework of the proposed image processing pipeline.....	79
Fig.7.19: (a) Example of halftone misregistration for a CMY image with 20% of ink coverage for each channel. (b) The contrast between the cyan dots and the background is sufficient to distinguish them even if the magenta dots are visible in the cyan image. (c) The contrast between the magenta dots and the background is enough to distinguish them even if the cyan dots are visible in the magenta image. (d) Separating magenta dots from yellow dots is not possible in the yellow image. (e) In order to correctly identify yellow dots, magenta dots that have been segmented in the magenta image are excluded from the yellow image.....	80
Fig.7.20:(a) Typical halftoning scheme for yellow ( $0^\circ$ ), cyan ( $15^\circ$ ), black ( $45^\circ$ ) and magenta ( $75^\circ$ ) ([1]). (b) An example of a rosette pattern that can occur with a different color halftoning method is shown, with CMYK at $0^\circ$ and a slight shift $\mu\text{m}$ along the X and Y axis.....	81
Fig.7.21:(a) Cyan dots; (b) binary image (with physical dot gain); (c) binary image after removal of dots connected to the borders and noise around dots. The physical dot gain causes printed dots to deform, affecting their shape and size. This deformation produces light cyan elliptical regions due to physical dot gain, while printed dots are represented by dark cyan circular regions.....	82
Fig.7.22: Fig 7.22: Displays a depiction of the step-by-step results obtained. In this example, cyan dots are extracted, measured and analysed. (a)CMY image, (b)Step1: extraction of C channel, (c)Step2: binarization,(d) Step 3.5: isosurface of distance transform, (e) Steps 3.1 to 3.4:removal of noise and irrelevant areas.(f) Step 4:labelling of regions of interest, (g) Step 5: removal of outliers, (h) Step 7: extraction of dots with concavity (ID1/ID2/ID3)or an irregular shape (ID4) defined by a solidity upper than 0.75, (i) extraction of dots with a convex shape (ID5) with a circular equivalent shape, or an elliptic equivalent shape, or another pattern shape.....	83
Fig 7.23: Illustration of the results obtained step by step. In this example magenta dots are extracted, measured and analysed. The red windows correspond to the image areas shown in Fig 7.18. (a) CMY image, (b) Step 1: extraction of Magenta channel, (c) Step 2: binarization, (d) Steps 3.1 to 3.4: removal of noise and irrelevant areas, (e)Step4: labelling of regions of interest, (f)Step5: removal of outliers, (g) Step 7: extraction of dots with a concavity (ID1/ID2/ID3) or an irregular shape (ID4) defined by a solidity upper than 0.75, (h) extraction of dots with a convex shape (ID5) with a circular equivalent shape, or an elliptic equivalent shape, or another pattern shape.....	83

Fig 7.24: (a) CMY image, (b) Step 1:extraction of the Yellow channel, (c) Step 1:Y image after removal of Magenta shadow, (d) Step 2: binarization, (e) Steps 3.1 to 3.4: removal of noise and irrelevant areas,(f) Step 4:labelling of regions of interest,(g) Step 5:removal of outliers,(h)Step 7: extraction of dots with concavity (ID1/ID2/ID3) or an irregular shape (ID4) defined by a solidity upper than 0.75, (i): extraction of dots with a convex shape (ID5) with a circular equivalent shape, or an elliptic equivalent shape, or another pattern shape.....84

Fig.7.25: Categories of dot patterns (convex hulls of dots are highlighted in green, major/minor axis are highlighted in blue, convex hulls of holes are highlighted in red)...85

Fig.7.26: Examples of descriptor values for various patterns. The elliptic bounding box corresponds to the red ellipse. The in scription corresponds to the green ellipse.....87

Fig 7.27: Example of results for two print samples printed with a cell angle of 60°. (a) % of dots belonging to category ID1(0%), ID2(92%), ID3(2%), ID4(less than 1%), ID5(0%), ID6 (5%, most of them are at right of the figure). In total, 92% of dots have a circular shape— see statistical values report in (shown in chapter 8, Table 8.10). (b) % of dots belonging to category ID1 (less than 1%), ID2 (0%), ID3 (less than 1%), ID4 (40%), ID5 (49%, all have a circular shape), ID6 (6%, most of them are the top of the figure). The circular shape is present in 94% of all dots.....87

Fig 7.28: Illustrate example of results for a cyan print with a cell angle of 60° % of dots belonging to category ID1 (34%), ID2 (0%), ID3 (0%), ID4 (0%), ID5 (55%), ID6 (11%, most of them are at the border of the figure). In total, 62% of dots have an elliptic shape, while 25%of dots have an elongated shape (less than1% has a circular shape).....88

Fig.7.29: Print sample dot parameters compared with reprint dot parameters.....91

Fig.7.30: Binary images with several dot patterns corresponding to 20% of Cyan and Magenta tints (for Print samples - P1, P2, P3, for Reprint samples - R1, R2, R3).....92

Fig.7.31: Binary images with several dot patterns corresponding of 40% of Cyan and Magenta tints (for Print samples - P1, P2, P3; for Reprint samples - R1, R2, R3).....93

Fig.8.1: (a)PSNR values for HIW, Print (PS-WI) and Reprint (RPRS-WI) for Canon E400.....102

Fig.8.1: (b)SSIM values for HIW, Print (PS-WI) and Reprint (RPRS-WI) for Canon E400.....103

Fig.8.2: (a)PSNR values for HIW, Print (PS-WI) and Reprint (RPRS-WI) images for Canon E610.....104

Fig.8.2: (b)SSIM values for HIW, Print (PS-WI) and Reprint (RPRS-WI) images for Canon E610.....104

Fig.8.3: PSNR values for PS-WI and RPRS-WI of images-(a) Lena (b) Baboon (c) Avion (d) Peppers and SSIM values for PS-WI and RPRS-WI of images-(e) Lena (f) Baboon (g) Avion (h) Peppers using Canon E400.....105-106

Fig.8.4: PSNR values for PS-WI and RPRS-WI of images-(a) Lena (b) Baboon (c) Avion (d) Peppers and SSIM values for PS-WI and RPRS-WI of images-(e) Lena (f) Baboon (g) Avion (h) Peppers using Canon E610.....106-107

Fig.8.5 (a)Histogram of HIW with WZ (b) Histogram of HIW with WX (c)Histogram of PS-WI with WZ (d)Histogram of PS-WI with WX.....	112
Fig.8.6:Co-relation co-efficient of Lena HIW with PS-WI and RPRS-WI on A4 paper.....	113
Fig.8.7:Co-relation co-efficient of Baboon HIW with PS-WI and RPRS-WI on A4 paper.....	113
Fig.8.8:Co-relation co-efficient of Avion HIW with PS-WI and RPRS-WI on A4 paper.....	114
Fig.8.9:Co-relation co-efficient of Peppers HIW with PS-WI and RPRS-WI on A4 paper.....	114
Fig.8.10:Co-relation co-efficient of Avion HIW with PS-WI and RPRS-WI on Foil media.....	115
Fig.8.11:Co-relation co-efficient of Peppers HIW with PS-WI and RPRS-WI on Foil media.....	115
Fig.8.12:Co-relation co-efficient of Avion HIW with PS-WI and RPRS-WI on Foil media.....	116
Fig.8.13:Co-relation co-efficient of Peppers HIW with PS-WI and RPRS-WI and RPRS-WI on Foil media.....	116
Fig.8.14: (a) Magenta dots with 95% of doughnuts oriented in the print direction; (b) Magenta dots with 85% of doughnuts oriented in the print direction. Orientation of the doughnuts vs. print direction.....	123
Fig.8.15. Robustness of the dot patterns detection method relative to the printing device.....	124
Fig.8.16: Robustness of the dot pattern detection method relative to the printing device (a1) CMYK Image (printed with printer P2 and ink DIC) (cyan dots have a cell angle of 30° and magenta dots have a cell angle of 60°), (a2) Another CMYK Image (cyan dots have a cell angle of 30° and magenta dots have a cell angle of 60°), (a3) Another CMYK Image (cyan dots have a cell angle of 30° and magenta dots have a cell angle of 60°), (b1–e3) results step by step for C color channel, (f1–h3) results step by step for M color channel, (i1–k3) results step by step for Y color channels.....	125-127
Fig.8.17: Examples of dot deformation.....	128
Fig.8.18: Analysed image of Print ((a)Cyan 20% patch of Printer 1(P1), (b)Cyan 20% patch of Printer 2(P2), (c)Cyan 20% patch of Printer 3(P3)), (d)Binary image of Cyan20% patch of Printer 1(P1) , (e)Binary image of Cyan20% patch of Printer 2(P2), (f)Binary image of Cyan20% patch of Printer 3(P3)) and Reprint ((a-1)Cyan 20% patch of Re-printer 1(R1), (b-1)Cyan 20% patch of Re-printer 2(R2), (c-1)Cyan 20% patch of Re-printer 3(R3)), (d-1)Binary image of Cyan20% patch of Re-printer 1(R1), (e-1)Binary image of Cyan20% patch of Re-printer 2(R2), (f-1)Binary image of Cyan20% patch of Re-printer 3(R3)).....	130
Fig.8.19: Analysed image of Print ((a)Magenta 20% patch of Printer 1(P1), (b)Magenta 20% patch of Printer 2(P2), (c)Magenta 20% patch of Printer 3(P3)), Binary images of Print ((d)Binary image of Magenta 20% patch of Printer 1(P1), (e)Binary image of Magenta 20% patch of Printer 2 (P2), (f)Binary image of Magenta 20% patch of Printer 3(P3)) and Re-print ((a-1) Magenta 20% patch of Printer 1(R1), (b-1) Magenta 20% patch of Printer 2	

(R2), (c-1) Magenta 20% patch of Printer 3(R3)), Binary images of Re-print ((d-1) Binary image of Magenta 20% patch of Re-printer 1(R1) , (e-1) Binary image of Magenta 20% patch of Re-printer 2(R2) , (f-1) Binary image of Magenta 20% patch of Re-printer 3(R3)).....130

Fig.8.20: Analysed image of Print ((a) Yellow 20% patch of Printer 1(P1), (b) Yellow 20% patch of Printer 2(P2), (c) Yellow 20% patch of Printer 3(P3)), Binary images of Print ((d) Binary image of Yellow 20% patch of Printer 1(P1), (e) Binary image of Yellow 20% patch of Printer 2 (P2), (f) Binary image of Yellow 20% patch of Printer 3(P3)) and Re-print ((a-1) Yellow 20% patch of Printer 1(R1), (b-1) Yellow 20% patch of Printer 2 (R2), (c-1) Yellow 20% patch of Printer 3(R3)), Binary images of Re-print ((d-1) Binary image of Yellow 20% patch of Re-printer 1(R1) , (e-1) Binary image of Yellow 20% patch of Re-printer 2(R2) , (f-1) Binary image of Yellow 20% patch of Re-printer 3(R3)).....131

Fig.8.21: Analysed image of Print ((a) Black 20% patch of Printer 1(P1), (b) Black 20% patch of Printer 2(P2), (c) Black 20% patch of Printer 3(P3)), Binary images of Print ((d) Binary image of Black 20% patch of Printer 1(P1), (e) Binary image of Black 20% patch of Printer 2 (P2), (f) Binary image of Black 20% patch of Printer 3(P3)) and Re-print ((a-1) Black 20% patch of Printer 1(R1), (b-1) Black 20% patch of Printer 2 (R2), (c-1) Black 20% patch of Printer 3(R3)) Binary images of Re-print ((d-1) Binary image of Black 20% patch of Re-printer 1(R1) , (e-1) Binary image of Black 20% patch of Re-printer 2(R2) , (f-1) Binary image of Black 20% patch of Re-printer 3(R3)).....131

Fig.8.22: Cyan 20% patch Average Dot Area.....132

Fig.8.23: Cyan 40% patch Average Dot Area.....132

Fig.8.24: Cyan 50% patch Average Dot Area.....132

Fig.8.25: Magenta 20% patch Average Dot Area.....132

Fig.8.26: Magenta 40% patch Average Dot Area.....132

Fig.8.27: Magenta 50% patch Average Dot Area.....132

Fig.8.28: Yellow 20% patch Average Dot Area.....133

Fig.8.29: Yellow 40% patch Average Dot Area.....133

Fig.8.30: Yellow 50% patch Average Dot Area.....134

Fig.8.31: Black 20% patch Average Dot Area.....133

Fig.8.32: Black 40% patch Average Dot Area.....133

Fig.8.33: Black 50% patch Average Dot Area.....134

Fig.8.34(a, b, c): Major axis of cyan print and reprint.....134-135

Fig.8.35(a, b, c): Minor axis of cyan print and reprint.....134-135

Fig.8.36(a, b, c): Eccentricity of cyan print and reprint.....136

Fig.8.37(a, b, c): Major axis of magenta print and reprint.....136-137

Fig.8.38(a, b, c): Minor axis of magenta print and reprint.....136-137

Fig.8.39(a, b, c): Eccentricity of magenta print and reprint.....137-138

Fig.8.40(a, b, c): Major axis of yellow print and reprint.....138-139

Fig.8.41(a, b, c): Minor axis of yellow print and reprint.....138-139

Fig.8.42(a, b, c): Eccentricity of yellow print and reprint.....139-140

Fig.8.43(a, b, c): Major axis of black print and reprint.....140-141

Fig.8.44(a, b, c): Minor axis of black print and reprint.....140-141

Fig.8.45(a, b, c): Eccentricity of black print and reprint.....141-142

Fig.8.46: Scatter plots for 20% of Cyan for Print sample (P1, P2, P3) and Reprint sample (R1, R2, R3) (a) Original data Area vs. Perimeter before classification (b) Predicted data Area vs. Perimeter after SVM Classification.....144

Fig.8.47: Scatter plots for 20% of Magenta for Print sample (P1, P2, P3) and Reprint sample (R1, R2, R3) (a) Original data Perimeter vs Area before classification (b) Predicted data Perimeter vs Area after classification.....144

Fig.8.48: Scatter plots for 20% of Yellow for Print sample (P1, P2, P3) and Reprint sample (R1, R2, R3) (a) Original data Perimeter vs Area before classification (b) Predicted data Perimeter vs Area after classification.....145

Fig.8.49: Scatter plots for 20% of Black for Print sample (P1, P2, P3) and Reprint sample (R1, R2, R3) (a) Original data Perimeter vs. Area before classification (b) Predicted data Perimeter vs. Area after classification.....145

Fig.8.50: Scatter plots for 40% of Cyan for Print sample (P1, P2, P3) and Reprint sample (R1, R2, R3) (a) Original data Perimeter vs. Area before classification (b) Predicted data Perimeter vs. Area after classification.....146

Fig.8.51: Scatter plots for 40% of Magenta for Print sample (P1, P2, P3) and Reprint sample (R1, R2, R3) (a) Original data Perimeter vs. Area before classification (b) Predicted data Perimeter vs. Area after classification.....146

Fig.8.52: Scatter plots for 40% of Yellow for Print sample (P1, P2, P3) and Reprint sample (R1, R2, R3) (a) Original data Perimeter vs. Area before classification (b) Predicted data Perimeter vs. Area after classification.....147

Fig.8.53: Scatter plots for 40% of Black for Print sample (P1, P2, P3) and Reprint sample (R1, R2, R3) (a) Original data Perimeter vs. Area before classification (b) Predicted data Perimeter vs. Area after classification.....147

Fig.8.54: Scatter plots for 50% of Cyan for Print sample (P1, P2, P3) and Reprint sample (R1, R2, R3) (a) Original data Perimeter vs. Area before classification (b) Predicted data Perimeter vs. Area after classification.....148

Fig.8.55: Scatter plots for 50% of Magenta for Print sample (P1, P2, P3) and Reprint sample (R1, R2, R3) (a) Original data Perimeter vs. Area before classification (b) Predicted data Perimeter vs. Area after classification.....148

Fig.8.56: Scatter plots for 50% of Yellow for Print sample (P1, P2, P3) and Reprint sample (R1, R2, R3) (a) Original data Perimeter vs. Area before classification (b) Predicted data Perimeter vs. Area after classification.....149

Fig.8.57: Scatter plots for 50% of Black for Print sample (P1, P2, P3) and Reprint sample (R1, R2, R3) (a) Original data Perimeter vs. Area before classification (b) Predicted data Perimeter vs. Area after classification.....149

Fig.8.58: Scatter plots for 20% of Cyan for Print sample (P1, P2, P3) and Reprint sample (R1, R2, R3) (a) Original data Eccentricity vs. Area before, (b) Predicted data Eccentricity vs. Area after classification.....150

Fig.8.59: Scatter plots for 20% of Magenta for Print sample (P1, P2, P3) and Reprint sample (R1, R2, R3) (a) Original data Eccentricity vs. Area before, (b) Predicted data Eccentricity vs. Area after classification.....150

Fig.8.60: Scatter plots for 20% of Yellow for Print sample (P1, P2, P3) and Reprint sample (R1, R2, R3) (a) Original data Eccentricity vs. Area before, (b) Predicted data Eccentricity vs. Area after classification.....151

Fig.8.61: Scatter plots for 20% of Black for Print sample (P1, P2, P3) and Reprint sample (R1, R2, R3) (a) Original data Eccentricity vs. Area before classification (b) Predicted data Eccentricity vs. Area after classification.....151

Fig.8.62: Scatter plots for 40% of Cyan for Print sample (P1, P2, P3) and Reprint sample (R1, R2, R3) (a) Original data Eccentricity vs. Area before classification (b) Predicted data Eccentricity vs. Area after classification.....152

Fig.8.63: Scatter plots for 40% of Magenta for Print sample (P1, P2, P3) and Reprint sample (R1, R2, R3) (a) Original data Eccentricity vs. Area before classification (b) Predicted data Eccentricity vs. Area after classification.....152

Fig.8.64: Scatter plots for 40% of Yellow for Print sample (P1, P2, P3) and Reprint sample (R1, R2, R3) (a) Original data Eccentricity vs. Area before classification (b) Predicted data Eccentricity vs. Area after classification.....153

Fig.8.65: Scatter plots for 40% of Black for Print sample (P1, P2, P3) and Reprint sample (R1, R2, R3) (a) Original data Eccentricity vs. Area before classification (b) Predicted data Eccentricity vs. Area after classification.....153

Fig.8.66: Scatter plots for 50% of Cyan for Print sample (P1, P2, P3) and Reprint sample (R1, R2, R3) (a) Original data Eccentricity vs. Area before classification (b) Predicted data Eccentricity vs. Area after classification.....154

Fig.8.67: Scatter plots for 50% of Magenta for Print sample (P1, P2, P3) and Reprint sample (R1, R2, R3) (a) Original data Eccentricity vs. Area before classification (b) Predicted data Eccentricity vs. Area after classification.....154

Fig.8.68: Scatter plots for 50% of Yellow for Print sample (P1, P2, P3) and Reprint sample (R1, R2, R3) (a) Original data Eccentricity vs. Area before classification (b) Predicted data Eccentricity vs. Area after classification.....155

Fig.8.69: Scatter plots for 50% of Black for Print sample (P1, P2, P3) and Reprint sample (R1, R2, R3) (a) Original data Eccentricity vs. Area before classification (b) Predicted data Eccentricity vs. Area after classification.....155

## List of Table:

Table 6.1: Confusion matrix.....	56
Table 7.1: Set parameters for engraving on Gravure cylinder.....	64
Table 7.2: Set parameters for Gravure printing.....	65
Table 7.3: Set parameters for foil ink.....	66
Table 7.4: Set range for the expiry date and batch number.....	71
Table 7.5: Representation Expiry date and Batch number in binary.....	71
Table 8.1: Histogram of Host Image (HI) and Host Image with Watermark softcopy (HIW).....	97
Table 8.2: Comparison results between different methods using the PSNR (without any attacks).....	98
Table 8.3: Comparison result between different methods using the SSIM (without any attacks).....	99
Table 8.4(a). Experimental analysis the Print samples (HIW vs PS-WI) and Re-print samples (simulated counterfeited sample) (HIW vs RPRS-WI) in Canon E400 printer cum scanner.....	100
Table 8.4(b). Experimental analysis the Print samples (HIW vs PS-WI) and Re-print samples (simulated counterfeited sample) (HIW vs RPRS-WI) in Canon E610 printer cum scanner.....	101
Table 8.5: Histogram of Host Image with Watermark softcopy (HIW), Print sample image (PS-WI) and Reprint sample image (RPRS-WI) on A4 media (Scan using Canon E400(Scanner S1)).....	108
Table 8.6: Histogram of Host Image with Watermark softcopy (HIW), Printed and Scanned Watermarked Image (PS-WI) and RePrinted and ReScanned Watermarked Image (RPRS-WI) on foil from Printer P1 and scanner S1.....	109
Table 8.7: Histogram of different Host Images with Watermark softcopy (HIW), Print sample image (PS-WI) and Reprint sample image (RPRS-WI) on foil from Printer P1 and scanner S1 for verification.....	110
Table 8.8: Dot shape parameters values of Magenta dots.....	119
Table 8.9: Dot shape parameters values of Cyan dots. The most significant values are in bold.....	121
Table 8.10: Dot shape parameters values of Yellow dots. The most significant values are in bold.....	122
Table 8.11- (a) Confusion Matrix of SVM Classification results for 20% cyan print and reprint.....	156
Table 8.11- (b)Confusion Matrix of SVM Classification results for 20% magenta print and reprint.....	157
Table 8.11- (c) Confusion Matrix of SVM Classification results for 20% yellow print and reprint.....	157
Table 8.11- (d) Confusion Matrix of SVM Classification results for 20% black print and reprint.....	158
Table 8.12- (a) Confusion Matrix of SVM Classification results for 40% cyan print and reprint.....	158

Table 8.12- (b) Confusion Matrix of SVM Classification results for 40% magenta print and reprint.....	159
Table 8.12- (c) Confusion Matrix of SVM Classification results for 40% yellow print and reprint.....	159
Table 8.12 (d) Confusion Matrix of SVM Classification results for 40% black print and reprint.....	160
Table 8.13- (a) Confusion Matrix of SVM Classification results for 50% Cyan print and reprint.....	160
Table 8.13 (b) Confusion Matrix of SVM Classification results for 50% Magenta print and reprint.....	161
Table 8.13- (c) Confusion Matrix of SVM Classification results for 50% Yellow print and reprint.....	161
Table 8.13- (d) Confusion Matrix of SVM Classification results for 50% Black print and reprint.....	162
Table 8.14(a) – the overall accuracy $A_{cc}$ and harmonic mean $F_h$ for each print and reprint using SVM for classification for 20% of Cyan.....	162
Table 8.14(b) – the overall accuracy $A_{cc}$ and harmonic mean $F_h$ for each print and reprint using SVM for classification for 20% of Magenta.....	162
Table 8.14(c) – the overall accuracy $A_{cc}$ and harmonic mean $F_h$ for each print and reprint using SVM for classification for 20% of Yellow.....	163
Table 8.14(d) – the overall accuracy $A_{cc}$ and harmonic mean $F_h$ for each print and reprint using SVM for classification for 20% of Black.....	163
Table 8.15(a) – the overall accuracy $A_{cc}$ and harmonic mean $F_h$ of each print and reprint using SVM for classification for 40% of Cyan.....	163
Table 8.15(b) – the overall accuracy $A_{cc}$ and harmonic mean $F_h$ of each print and reprint using SVM for classification for 40% of Magenta.....	163
Table 8.15(c) – the overall accuracy $A_{cc}$ and harmonic mean $F_h$ for each print and reprint using SVM for classification for 40% of Yellow.....	164
Table 8.15(d) – the overall accuracy $A_{cc}$ and harmonic mean $F_h$ for each print and reprint using SVM for classification for 40% of Black.....	164
Table 8.16(a) – the overall accuracy $A_{cc}$ and harmonic mean $F_h$ for each print and reprint using SVM for classification for 50% of Cyan.....	164
Table 8.16(b) – the overall accuracy $A_{cc}$ and harmonic mean $F_h$ for each print and reprint using SVM for classification for 50% of Magenta.....	164
Table 8.16(c) – the overall accuracy $A_{cc}$ and harmonic mean $F_h$ for each print and reprint using SVM for classification for 50% of Yellow.....	165
Table 8.16(d) – the overall accuracy $A_{cc}$ and harmonic mean $F_h$ for each print and reprint using SVM for classification for 50% of Black.....	165



**Abbreviations:**

HI- Host Image.

HIW- Host Image Watermarked.

PS-WI - Printed and Scanned Watermarked Image.

RPRS-WI - RePrinted and ReScanned Watermarked Image.

ED - Expiry Date.

BN - Batch Number.

SVM – Support Vector Machine

# ABSTRACT

The originality of products is of serious concern nowadays and packaging has a major role in it. Package printing becomes critical as fake medicines, expired/counterfeited food products can be easily packed and sold if printed with proper color combination. Secure packaging is one of the essential techniques to avoid counterfeiting. Often the out-of-date medicines or packaged food products or cosmetics are sold by changing the expiry date of the product which can cause severe health hazard. In recent years, printing technology has helped to fight against counterfeiting, a plea threatening citizen safety and impacting the financial health of food and pharmaceutical packaging industries. The authentication of the packaging is considered as an important step in the investigation of suspected counterfeits of packaged products. Due to the advancement of printing technologies, the emergence of counterfeits with a better appearance may be observed. In the recent years, due to the easy access of the high-quality printing technologies, the importance of package printing security has been increased to prevent the counterfeiting of packages. Hence it is important to identify whether a printed package is printed by original food or medicine manufacturers or their authorized printers or it is printed by counterfeiters. Scanning or photographing the package and reprinting is one approach for forging an authentic package sample. To simulate it, the original sample is being scanned/photographed and then reprinted using a variety of digital cameras, mobile cameras, scanners, and other devices.

This study will help to identify the authenticity of a printed package. Undoubtedly it will have a great impact on the packaging industry to check the authenticity and validity of the packaged product. This study has proposed four potential methods to distinguish an original print document from a reprint document (which may be simulated as counterfeited). Firstly, this research has suggested a method by creating a variable image watermark in order to protect batch number and expiry date of different packaged products. The idea of image watermarking is to hide some important information in the form of data bits inside the host image which will ascertain the authenticity of the product and which cannot be easily copied or printed. In this proposed work, a non-blind watermarking technique has been developed so that it cannot be easily copied or printed. The idea of this watermarking is to imperceptibly embed a small amount of secret information in an image, which is called a watermark, so that when any test print is studied properly, it can be identified whether it is printed in original printer by the manufacturer or it is counterfeited. More particularly this non-blind dynamic watermark is designed on the basis of product batch number and expiry date and is embedded into an image and stored in a 16-bit buffer wherein each of the said 16-bits are embedded into specific intensity values in the host image. The application of the watermark is in food and medicine industry as well as in many other industries.

In the experimental process, the reference target chart IT 8.7/3 has been printed using three different gravure printers (P1, P2, P3). Gravure printing process is widely acceptable for flexible package printing, specially on films and foil. In this study, blister foil is used as the substrate as it is mostly used in pharmaceutical industries and food packaging for its light weight, chemical inertness and impermeability to air and water. The images of print samples

are then captured using camera. The images are printed again in the same three printers and then the samples are named as reprint samples (R1, R2, R3). The second study has demonstrated another method to identify an original print document from a reprint document (which may be simulated as counterfeited product) using microscopic dot parameter analysis of color patches from standard color chart IT8.7/3. The samples printed in the gravure process are analysed using the Lays & Mayo microscope with 4x zoom and ScopeImage 9.0 microscope software. The analysis at microscopic scale of original print documents shows some specific dot shapes which depend on the printing parameters as well as the printing device used. We can, therefore, draw the assumption that the dot shapes can be used as a fingerprint to differentiate a print from a reprint. In the third study, the reference target chart IT 8.7/3 has been printed using three different gravure printers (P1, P2, P3). The images of print samples are then captured using camera. The images are printed again in the same three printers and then the samples are named as reprint samples (R1, R2, R3). The parameters like dot area, major axis, minor axis and eccentricity of cyan, magenta, yellow and black tints for print and reprint samples are measured using MATLAB R2018a. Canny edge detection algorithm has been applied on the microscopic images. Then the boundaries of the objects are being calculated by detecting the contours of the detected edge dots in the samples. From the results, it has been observed that the dot shape parameters may be used to distinguish the print sample from reprint sample. Fourthly, a multi-classification-based method Support Vector Machine (SVM) have been utilized using shape descriptor index features for print and reprint source identification.

The experimental results show that the proposed methods can successfully differentiate original print from its scanned/photographed (simulated counterfeits) reprints which can be effectively used to prevent counterfeiting in medicine, food processing or other industries and have the scope of commercialisation in order to prevent the great challenge of counterfeiting of medicines and other products. The suggested method successfully classified the print and reprint sample at different dot percentages with a high rate of accuracy.

# Chapter 1

## INTRODUCTION

### 1. INTRODUCTION

The problem of authentication of products are of grave concerns today as fake products can be easily marketed by effective package printing. The problem becomes more critical specially in case of packaging of foods, medicine, confectionaries and other healthcare products as it may create serious health hazards. Often the expiry dates are changed and reprinted to sell exhaust products and is a major concern in a world of global exchanges. In recent years, printing technology has helped to fight against counterfeiting, a plea threatening citizen safety and impacting the financial health of pharmaceutical packaging or food and beverages packaging industries. The package printing can help in defining the packaged product identity, providing useful information, and expressing customer needs. The growth of fake package prints is growing to a great extent due to the development of printing technology. The original print may be counterfeited utilizing high-quality printers. Hence the security of package printing took a special attention in recent years, as a result of the accessibility of high-quality printing technology to avoid counterfeiting of packaging which is a great social problem. The counterfeiting of medicine or food packaging is one of the major problems for our society. Therefore, the process of authentication is very much needed to protect original products from counterfeiters. Counterfeiting medicine and healthcare products are the heinous crime and hence packaging of this sector needs special attention. The easiest way to counterfeit medicine packages is to Scan or take image of the package and reprint it.

#### 1.1 IDENTIFICATION OF PROBLEM

Packaging plays a significant role in the authentication or validation of the product. The market of counterfeited medicine is growing rapidly. It creates serious health hazards and even treatment failure or death. Moreover, it becomes a great challenge for original pharmaceutical companies. They are facing huge revenue loss for it and the most important thing is that the reputations of their brand names are at stake. Printing and packaging play a very important role for any packaging products because the customer buys the product based on its appearance and information provided on the package. Packaging plays an essential role as marketing tool to differentiate a product and to convey a certain message or brand image to highlight the package products aspects for consumers. The pharmaceutical or food packaging should carry the information on the correct usage of dosage forms, their contents, about the packed product such as date of manufacturing, expiry date, lot number etc. If the package print content has only text, it is easier to copy it by carefully selecting font color and size. When an image is introduced, there is no other option but to take its image. Multi-color image makes the system more critical. The easiest way to make a fake or duplicate package is to scan or take photograph of the real one and reproduce it again. Medicines industry have been the centre of attraction for the counterfeiters due to the high prices of medicine, lack of authentication of medicine package prints and lack of prosecutions and penalties. In Pharmaceutical packaging context, the packaging should carry certain features to prevent the medicine from counterfeiting. Therefore,

the security feature is required to identify the package printing counterfeiting. Undoubtedly it will have a great impact on the packaging industry to check the authenticity and validity of the packaged product. Therefore, this study has focused on the authenticity of medicine packaging. Beside this, the cost of high technology security features involves high cost which may cause price escalation of medicine. Hence low-cost print authentication solutions are needed.

## **1.2 PROBLEM STATEMENT**

Recently, the counterfeiting of pharmaceutical, food and beverage packaging is a worldwide issue. Counterfeiting of consumer goods is a critical problem which causes various negative impacts for consumers, enterprises and the whole economic ecosystem. Secure packaging is one of the main solutions to help enterprises protect their brand against this concern. Anti-counterfeit labels and packaging is one of the essential techniques to avoid counterfeiting. Often the expiry dates of the packaged products are changed to sell the outdated products which cause severe kinds of health hazard. The printed packs or its ancillary printed components act as a tool to identify the product.

The gravure printing process is used to print on the blister foil which is widely accepted as substrate in pharmaceutical or food packaging industry due to its inertness, impermeability and light weight properties. Gravure printing is considered as major printing technology for the flexible packaging industry. Scanning or photographing the package and reprinting it is one approach for forging an authentic package sample. The original sample may be scanned using a variety of digital cameras, mobile cameras, scanners, and other devices and then reprinted. Several hardware and software solutions may make it simple to manage or manipulate a single-color hue. Managing of multi-color printing would be quite challenging task. In most cases, some built-in security features could be used to identify whether printed samples are counterfeited or not. The present work is mainly focused to provide security feature based on variable image watermarking for authenticating expiry date and batch number of medicine package. Most of the work has been done on the blind watermarking algorithms, which is embedded the binary watermark in the blue part of an RGB image in the spatial domain. Therefore, this present study is making effort for creating a variable image watermark in order to protect batch number and expiry date of different packaged products. The idea of image watermarking is to hide some important information in the form of data bits inside the host image which will ascertain the authenticity of the product and which cannot be easily copied or printed.

Much of the previous research has focused on the security issues of the offset or digital prints. Little study has been conducted about the security issues of gravure printing process. Moreover, most of the studies have been performed on papers. Few works have been conducted on the blister foil. The blister foil is widely accepted as package substrate in the pharmaceutical industry due to its inertness, light weight and chemical resistance properties. Based on the color information and microscale analysis, it is possible to identify the fake pharmaceuticals packaging products. This present study has developed an approach to identify the authentic prints using identifying parameters like Dot area, Perimeter, Circularity, Eccentricity, Solidity, Major and Minor axis of the microscopic printed dots in package prints. So, the watermarking and micro-scale dot structure have been explored as important feature to differentiate between original and scanned reprinted samples using gravure printing process.

### **1.3 PURPOSE AND GOAL**

The issue of authenticating counterfeited pharmaceutical items with blister foil packaging has been studied in this work. This study will help to identify the authenticity of a printed package. Undoubtedly it will have a great impact not only on the packaging industry but also on the society in general. This study has proposed four potential methods to distinguish an original print document from a reprint document (which may be simulated as counterfeited). The samples from the print and reprint have been labelled as authentic and counterfeit, respectively. The original print samples are scanned and then the scanned images are reproduced by the counterfeiters. These reproduced samples are very much identical to the authentic samples which are not distinguishable easily by the product manufacturers and consumers. This study has applied variable image watermarking method for identifying the authentic samples in a manner that is robust to printing and scanning. This study also focused on microscopic dot analysis print and reprint sample on the blister foil to distinguish the authentic samples from simulated counterfeited samples. In this study, Four Host Images (HI) sizes of 1 inch x 1 inch with 600dpi resolutions (Lena, Baboon, Avion, Peppers) have been taken for the watermarking and after embedding the information into these images, all watermarked images (HIW) have been engraved on cylinder using electro-mechanical engraving process. The artwork IT8.7/3 color target chart has been engraved as a reference image on the gravure cylinder for microscopic dot analysis. The combined final artwork for variable image watermark and microscopic dot shape analysis has been prepared by Electro-Mechanical engraving process. Three separate gravure printers have been used to collect the print samples. The combined artwork has been printed with cyan, magenta, yellow and black foil inks on the blister foil. Then, in order to imitate the process used by counterfeiters, the print samples are photographed with various cameras and scanners. The scanned images are then printed once again using the same three gravure printers. The goal of this study is to propose non-blind dynamic watermark method in order to protect batch number and expiry date of different packaged products. The application of the watermark is in food and medicine industry as well as in many other industries. This study provides a promising method to distinguish an original print document from a reprinted document based on a pattern recognition process (copy or fake). It proved that a print can be distinguished from a reprint using microscopic analysis of the geometrical shape of printed dots, just like a fingerprint. Moreover, the aim of this study is to measure and identify the print parameters like-dot area, major and minor axis, eccentricity and to check how these parameters can be used to differentiate printed dots from scanned reprinted dots from the samples. If these parameters are carefully monitored, it may help to identify whether the print is original or it is copied and reprinted. In order to identify the source of prints and reprints, a multi-classification-based method called Support Vector Machine (SVM) has been applied.

### **1.4 RESEARCH OBJECTIVES**

The following research objectives have been carried out so as to accomplish the above-mentioned goal:

- To develop a generic watermark method to create a variable image watermark in order to protect batch number and expiry date of different packaged products for printed blister or aluminium foils.
- To analyze the microscopic dot shape structure parameters of color patches printed on aluminium foils using gravure printing process.
- To classify the print and reprint dot shape features to determine the characteristics of dot shape size changes by support vector classification model.
- To identify fake pharmaceuticals packaging products printed using a CMYK (Cyan, Magenta, Yellow, Black) gravure printing machine from color information and microscale analysis.

### **1.5 STATEMENT OF HYPOTHESIS**

Gravure printing is considered as major printing process in medicine packaging or food packaging industry. The blister foil is commonly preferred as packaging substrate to pack the medicines in pharmaceutical packaging. So, this study has focused on the gravure printing process on a blister foil substrate. Different gravure printing machines have been used to print the foil samples with cyan (C), magenta (M), yellow (Y), and black (K) inks. In this proposed work, a non-blind watermarking technique has been developed so that it cannot be easily copied or printed. The idea of this watermarking is to imperceptibly embed a small amount of secret information in an image, which is called a watermark, in the packaging system so that when any test print is observed, it can be identified whether it is printed in original printer by the manufacturer or it is counterfeited. The statistical analysis has shown significant difference between the print and reprint samples. Moreover, the microscopic dot structure analysis has been performed depending on the print parameters like-dot area, major and minor axis, eccentricity. This analysis will help to check how these parameters can be used to differentiate printed dots from scanned reprinted dots from the samples. The print and reprint samples are distinguished using the microscale dot shape descriptor index parameter and statistically.

### **1.6 LIMITATION**

The variable image watermark, color information, and microscopic analysis of printed and scanned reprinted samples from gravure printing machines are the main focus of this study. It will be beneficial for the product manufacturers to determine if a print sample is genuine or counterfeited. In the future, it may be investigated how end users can verify it in pharmacies or by sending photographs to the manufacturers.

### **1.7 THESIS OVERVIEW**

The gravure printing on blister foil substrate, that is widely used for medicine packaging, is the major subject of the present study. The present study draws the assumption that print and reprint copy (by scan-and-print process) of blister foil samples can be differentiated by two ways. A new non-blind dynamic watermark is proposed, where the watermark is designed on the basis of batch number and expiry date and is embedded into an image, by observing the histograms, it

can be easily identified whether it is printed by original manufacturer or not. The differentiation of print and scanned reprint product samples can be done at microscale level using dots shape descriptor index parameters. These parameters have been used to classify print and reprint dot percentage with respect to particular color tint.

An introduction and problem statement are described in Chapter 1. A summary of the prior research for the current study is provided in the literature survey in Chapter 2 of the related work. Chapter 3 discusses the materials used for medicine packaging and their utilities. Chapter 4 explores the techniques employed in package printing to combat counterfeiting. Chapter 5 presents a comprehensive description of the gravure printing process specifically used for pharmaceutical package printing. It includes a discussion on various methods of manufacturing gravure cylinders and their impact on printing output across different gravure printing machines. Chapter 6 introduces the classification methodology using Support Vector Machine. Chapter 7 details the experimental procedure undertaken in this study. Chapter 8 presents the results obtained and provides a thorough discussion of the findings. Finally, in Chapter 9, the study concludes by summarizing key insights and outlining future prospects for research.



# Chapter 2

## LITERATURE SURVEY

### 2.1 Literature review on watermarking process for protecting copyright

Q. Su and B. Chen [1] have introduced a new blind watermarking algorithm that addresses the issue of copyright protection. This algorithm involves the embedding of a binary watermark into the blue component of an RGB image within the spatial domain. This algorithm concentrates mainly on the common attacks, such as JPEG compression, cropping, and adding noise.

K. Thongkor and T. Amornraksa [2] have addressed the problem of extraction process of a watermark from the printed and scanned watermarked document where the watermark image, has been created using black (0) and white (1). Then the watermark bits were first permuted by using Gaussian distribution-based permutation to disperse bits 0s and 1s. Then the numbers of bit 0 and 1 have been balanced by XORing the result with a pseudo-random bit stream generated from a key-based stream cipher. The experimental results have been showed some improvements in term of average NC, calculation has been compared to the previous works.

T. Mantoro et. al [3] have proposed an authentication scheme which embeds watermark object with QR code to validate the printed document, but this scheme requires the watermark image transparency set to 50% and prepares validation link in advance. It is also reported that this scheme set the size of QR to be not less than  $2 \times 2 \text{ cm}^2$  to be able to read the watermarked QR code efficiently.

S. Ibrahim et. al [4, 5] have developed a watermarking scheme capable of removing printing and scanning distortions to authenticate the printed document. In this proposed scheme, the scalar value of watermark named regulation factors has been embedded into each partition of original image. If the regulation factor is bigger, the more visibility of the watermark has been shown in the watermarked image. This adaptive technique provides better security by assigning different regulation factors to different partitions. During the embedding process, a matrix of regulation factor has been generated so that it can be utilized for the extraction process. In the extraction process, the geometric distortion has been first removed, and the watermark is then extracted applying normalization technique. Their scheme helps to avoid attackers from guessing the value of regulation factors but it still has some problems when the rotation distortion has been occurred.

A. Pramila et. al [6, 7] have further presented an autocorrelation and directed periodic pattern-based watermarking method which is robust to the print-cam process. Just Noticeable Difference (JND) method has been applied after printing to evaluate the quality of image. Bilinear interpolation has been used to define the rotation angles of gray coded bit sequence. This method has not been robust against attacks where the watermarked image has been printed, scanned, printed again and then captured.

D. Klein et. al [8] have proposed a watermark method by image hashing and face verification for such an image hash that is resistant to a print-scan transformation. A digital seal has been used to cryptographically signed 2D barcode printed on a document to verify the documents authenticity and integrity.

G. Khadija et. al [9] have developed an image watermarking technique for the print-scan process, combining frame-based perspective rectification with Wiener filter to reduce blurring and tweaks to lessen color degradations. The Fourier watermarking technique yielded superior results than the state-of-the-art of current watermarking techniques, with a total error rate of 1%. Three complimentary adjustments were examined to withstand attacks.

S. H. Amiri and M. Jamzad [10] has proposed method that have addressed the issue of print and scan attack by introducing a model the scanner and printer process. For modelling the print and scan operations it has been presumed that rotation, scaling and clipping, and it has been counted as geometric transforms that happen at the end of operation. Thus, this model has been focused on other operations that has manipulate the input image during the print and scan operations. The neural network has been used in each system to estimate non-linear operations on the input image.

Coltuc D. et. al. [11] explained a new result on regional image watermarking by exact histogram specification. Here, Image has been split in regions and for each region a watermark has been specified. Watermarks have been selected such as image original histogram has preserved. The main improvement of proposed region-based method consists in the marking of the entire image (all the regions) with complementary watermarks. Robustness or fragility of the proposed scheme has been depended on the specified histograms. This scheme has been used sparse histograms, which one achieves not only image authentication, but also, in case of any attack or malicious editing, the detection of the area where image has been altered. The use of histograms as watermarks has the great advantage of a very fast and low complexity detection. It is easy to observe that exact histogram specification has an increasing transform and mage information content has been preserved.

D. Coltuc et. Al [12] have proposed a method that explored the use of exact histogram description for robust watermarking. The basic idea of this proposed robust watermarking technique is to reduce the presence of certain groups of gray levels taking care to preserve the visual appearance of the image. The gray level distribution has been changed in the attacked images.

S. H. Amiri and M. Jamzad [13] has created a robust watermarking technique to mimic the noise addition and nonlinear effects of print and scan attacks. This technique encompasses both noise addition and geometric alterations performed by the operator during the scanning process. The high resilience was achieved by extracting low-influencing coefficients, specifying embedding settings, and removing geometric attacks.

P. Athichitsakul et. al [14,15] have discussed a method based on printing a document fingerprint using an image hashing algorithm. Image-based hashing has been used to extract specific features from multimedia content and produce a hash value. This approach is resistant to attacks from rotation, shearing, brightness, noise, and other print-scan scenario elements. The Discrete

Wavelet Transform (DWT) was employed to extract features from radon coefficients, and the Fast Fourier Transform (FFT) was used to generate a hashing string derived from a cryptographic hashing function. A tiny change in the original input creates a big difference in the hash value.

These articles [16, 17] have presented a pilot-based DCT-based watermarking method to incorporate and detect a low-resolution watermark. To accommodate both random nonlinear local geometry distortions and nonlinear pixel value distortions, the watermark has been inserted and detected within the down sampled low-resolution image. The effect of the print-and-scan method on the watermark has discussed. PSNR values and the Bit Error Ratio (BER) have been computed from the rescanned watermarked pictures of extracted watermark to determine the embedding strength. The experimental findings showed that the suggested technique is resilient and computationally efficient.

A. Pramila [18] has proposed a digital image watermarking technique to improve the resilience of print-cams. The method involves breaking the picture into nine blocks, each of which can store four bits. The watermark is encoded inside the brightness domain and quantized into degrees, and can be extracted with good accuracy at up to 60 degrees of rotation.

W. L. Lin and W. H. Tsai [19] have developed a solution for copyright protection by embedding semi-visible watermarks in picture mosaics to represent bit pairs. This approach is resistant to print-and-scan attacks, allowing the embedded data for copyright evidence to be recovered even after the mosaic has been attacked.

K. Solanki et. al [20] have presented work that uses Differential Index Modulation to conceal information in the phase spectrum of pictures. This technique has been shown to have essential applications in document security and image copyright protection. The print-scan model is composed of three components- effects caused by cropping, colored high-frequency noise, and non-linear effects. The quality of the printed picture is dependent on the printer and toner's condition.

K. W. Mahmoud et. al [21] have developed a watermarking method for use in print security. This strategy is independent of the process of halftoning and based on the statistical characteristics of the task. It is used to establish the authenticity of printed works and differentiate them from forgeries generated using the print/scan process. This project focuses on consumer PS devices such as color inkjet printers and flatbed scanners. The process involved watermarking the image by utilizing low amplitude coded data generated from the high frequency elements of a fractal noise in the out-of-band frequency space, specifically in the region where the half band width exceeds 128. Batch tracking has been made possible by this method.

M. Narong et. al [22] have proposed a pixel-based digital watermarking approach to extract the embedded watermark from printed and scanned watermarked photographs. The watermark has been implanted in a host color picture by changing the image pixel in the blue color channel. The sequence of watermark bits was permuted using XOR and a pseudo-random bit-stream. The image was then printed on a white-colored A4 sheet and a black frame was placed around

the watermarked region. The Normalized Correlation (NC) was computed to determine the precision of the recovered watermark.

Q. Su et. al [23] have proposed a blind watermarking technology for copyright protection of color images in the spatial domain. This unique spatial watermarking approach embeds a color watermark image within a color carrier image and extracts the embedded watermark using the characteristics of the 2D-DFT DC coefficient. The experimental findings suggest that the technique meets the requirements for imperceptibility and outperforms existing methods in terms of resilience and real-time capabilities.

W. Zhang et. al [24] have presented work for digital watermarking technology for printing and the discovery of printing anti-counterfeiting technology that is difficult to replicate, simple to identify, inexpensive, and pollution-free. The research programme incorporated three steps: generation and embedding of watermarks, printing and scanning, and the extraction and detection of watermarks. Research on the effects of printing and scanning attacks on watermarks has demonstrated that the link between invisibility and resistance to printing-scanning attacks may be balanced. However, little study has been conducted on the watermark process's consequences.

Z. Xiao et. al [25] have developed a novel solution against print-scan assaults that combines zero watermarking with Arnold scrambling. The resulting watermark image indices are within an acceptable range, and the impact of the attacks on the embedding procedure was not visible to the human eye. The watermarked image has minimal distortion, making the method robust.

M. K. Kundu and A. Maiti [26] have presented an image-based document with copyright protection against the print-scan process. This study utilizes discrete cosine transformation to provide an undetectable watermarking system. Both the original and extracted watermarks have been analysed for authenticity. Both watermarking and halftoning algorithms have been implemented to determine the degree of degradation and durability in a certain watermarking technique.

Z. Wang et. al [27] have presented a novel approach to evaluating the perceptual quality of images. This evaluation aimed to measure the visibility of errors between a distorted image and a reference image by considering various properties of the human visual system. However, the authors suggest an alternative framework based on the degradation of structural information, assuming that human visual perception is well-suited for extracting structural details from a scene. The authors have created a Structural Similarity Index and demonstrated its potential through the use of intuitive examples. Their work aims to develop quantitative metrics that have the capability to automatically predict the perceived quality of images.

M. B Aliwa et. al [28] have developed a digital image watermarking technique to safeguard digital images against unauthorized alterations and detect hidden information to prevent both malicious and non-malicious attacks. One of the challenges in digital watermarking is achieving a balance among three essential requirements: imperceptibility, capacity, and robustness. These requirements often conflict with each other, leading to a trade-off between fidelity and robustness. To address this issue, the researchers have introduced a novel method for embedding watermarks that simultaneously fulfills the imperceptibility, capacity, and

robustness criteria. They have called this method Adaptively Pixel Adjustment Process based on Medial Pyramid of Embedding Error applied in the falling-off boundary in corners board of the cover image set-of-the Most Significant-Bit-6 blind in spatial domain.

J. Picard et. al [29] have introduced a highly secure identification (ID) document that is resistant to fraud. This document utilizes a fusion of three distinct data hiding technologies: digital watermarking, 2-D bar codes, and Copy Detection Pattern, alongside additional biometric safeguards. Through their research, the team demonstrated that this combination of data hiding technologies effectively safeguards the document against forgery, eliminating the need for supplementary security features. To prevent unauthorized usage of a genuine document, the ID document also covertly stores biometric information, which can be utilized for identification purposes by the detector.

## **2.2 Literature on microscopic printed Dot shape and parameter**

M. Namedanian et. al [30] have studied the characterization of halftone prints on microscopic scale. One of the most important phenomena that impacts print result is dot gain. Porous paper causes optical dot gain, which results in printed dots appearing larger than their actual physical size due to the lateral spread of light. They have developed three approaches based on the Murray-Davies model to obtain the total dot gain. Moreover, this study has suggested another novel approach based on the histogram of microscale images to separate physical from optical dot gain. In, this work the dependency of dot gain and wavelength in color print have been investigated. This study has also discussed, using different wavelengths to separate colors. Based on Namedanian's findings, utilizing distinct angles for each channel has reduced the impact of misregistration. However, this approach has also introduced a visible pattern known as a rosette pattern at a microscale level. The study has reported that the amount of optical dot gain is differed from different types of half toning as the optical dot gain depends on the dot shape perimeter.

A lot of praiseworthy studies have been conducted by Q. Nguyen et. al [31-33] to authenticate printer technologies from microscopic analysis of paper print. Each printed and scanned set of dots (a dot being a binary element) have been affected from a stochastic non-invertible noise which creates the difficulties during the reproduction of the original graphical code. The focus of this study was to create a binary response model by utilizing a micrometric scan of document printing. The parameters of the model are determined by the dots' location and shape. A maximum likelihood estimation algorithm has been suggested to estimate the location, the darkness, the scale and shape parameter of the dot. Furthermore, this study has proposed a probabilistic model that consists of vector parameters describing a spatial interaction binary model with inhomogeneous Markov chain. Additionally, the report highlights the determination of the location and the description of the diverse random structures of the microscopic printed pattern as influenced by those parameters. Nguyen Q. and colleagues [34] conducted a statistical analysis on microscopic printing in order to identify the legitimate printer source. To achieve this, they utilized micro-tags composed of patterns of microscopic printed dots on the paper. The study employed multi-class Support Vector Machine (SVM) and Random Forest (RF) algorithms on five shape descriptor indexes of the micro-printing patterns.

N. Otsu [35] has proposed a method based on an unsupervised histogram thresholding for picture segmentation. A discriminant analysis has been performed to select a threshold automatically from a gray level histogram. This unsupervised histogram thresholding approach is used to minimize intra-class intensity variance; and also the performance of this method is among the best to differentiate ink coverage from paper regions. Postprocessing approaches have been reported to measure, characterize and model the print at the microscale [36]. An optical dot gain characterization tool has been developed. The drawback of this probabilistic model is not suitable for doughnut dots or non-spherical patterns.

E. Olson [37] has discussed analytical instruments that are commonly used to determine the particle size and distribution of fine particles. Image analysis is considered as a useful method for measuring particle shape factors and providing important information that could impact the product behaviour or correlate with a response of interest.

A. Hamblyn [38] has reported a high degree of correlation between the exposed areas within flexo-printed dots and the positioning of topographical indentations on the surfaces of paper and paperboard. The dot geometry, the surface area and geometry of the halftone dot have been intensively studied. Therefore, the size, volume and uniformity of the printed dots have been generated under varying printing conditions. The effect of dot uniformity on the selected halftone models has been discussed. This study has focused on the surface patterning of the printing plate depending on the aspect of pattern and different process parameters affecting optical density and print uniformity. Their study is one of the first to investigate dot patterns with concave geometry and local deformation. Specifically, they have found that doughnuts, which have ring-shaped halftone dots lacking ink in their centre, are caused by the displacement of ink away from the top of the printing feature during substrate contact. This effect is related to the pressure-sensitive nature of the rotogravure printing process. According to Hamblyn, doughnuts have been more visible at high impression pressure, but the origin of this printing defect is still uncertain and the impact of dot top geometry on the defect is still not reported.

The problem of doughnuts on the boundary of dots has been reported in [39,40]. This study has been performed with two different cylinders engraved using chemical etching and two different rotogravure presses. This study has discussed that the signature of engraved cylinder has impacted more on printed patterns in comparison with the signature of gravure printing press. H. Mathes [41] has identified cylinder or plate swelling as the reason of doughnuts formation. Additionally, the aggressive inks and solvents can also lead to swelling and distortion. Moreover, the usage of ink with excessive draw and low viscosity can also contribute to the occurrence of doughnuts. Several studies have discussed that several printing parameters can have a significant impact on the print quality, for example, on printed dot size or on doughnut effect. Sosa R. [42] has suggested that the ink viscosity and the subsequent ink spreading on the substrate are affected by the temperature of the surroundings and/or the operating equipment. The viscosity of inks changes about 3 to 4% per degree Fahrenheit change. Sosa demonstrated that as the ink temperature rises, the dots undergo deformation, leading to an increase in the doughnut effect and an expansion of the dot perimeter.

M.E.A. Kader has reported [43] that the ink filling the gravure cylinder cells takes a concave shape due to the increase of ink temperature, leaving an air bubble trapped between the ink and

the substrate. The study also mentioned that the brightness or lightness of the dots can be analysed based on the solvent content in the ink, with a higher quantity of solvent minimizing the presence of solid ink components. The limitation of this reported dot structure analysis is a visual analysis; no quantitative evaluation of doughnuts has been performed

Joshi et. al. [44] has developed a method to identify the source printer of a printed document via its camera acquired image. This study has worked on the dataset comprised of 2250 images of text document. this study has introduced a single CNN approach, using a two-channel combination of native letter image and its noise residual to identify source printer. This study has described the potential of local deformations of printed patterns at a macroscopic level, such as the finding in the letter "e", can be used to identify a unique print signature.

Oliver et. al. [45] has shown the potential for using the roundness and perimeter of printed dots at a microscopic scale to differentiate between different printer models. Variety of image features and print quality metrics are used to identify significant signature features to discriminate the printing process.

S. Sun et. al [46] have summarized the frequently applied optimization methods from the perspective of machine learning, and studies. This study has also discussed the fundamental principles and advancements of optimization techniques in various fields and approaches to improve the performance.

X. Ying. [47] has identified noise learning as a significant factor contributing to overfitting. To prevent overfitting and enhance classification accuracy, pruning can be used to eliminate less significant or irrelevant data.

### **2.3 Literature review on Automatic dot object detection**

J. Ni et. al [ 48] have developed an integrated method to realize the separation and counting task by images. this technique can be utilized with an image having random colors of circular objects and non-circular objects. Circular Hough transform has been applied to recognise and to count circularly overlapping items, and intelligent edge detection has been used to identify objects' edges. In this method all the objects are successfully detected, segmented, counted and sorted. In various sectors, systems based on infrared sensors are employed for the estimate of items. Using the suggested method, items have been color-coded and quantified, and recorded images of blood smears have been implemented in a system for the cell segmentation and counting of human blood cells.

R. Hussin et. al [49] have suggested an approach based on the detection of mangos on mango trees using color processing techniques as the primary filter. The circular Hough transform (CHT) has been used to determine the objects' edges. The backlight condition has the greatest impact on the image, as the RGB color reflected varies according to the intensity of the light. The grayscale image contains a great deal of noise due to the inability of the grayscale filtering to exclude the low-intensity pixels that have been designated as noise. The CHT may not precisely detect the circular item since it has occasionally linked with other objects and returned an erroneous result.

S. Bindu et. al [50] have proposed a method to recognise things such as mangoes, sunflowers, and buttons put on a surface using techniques such as color processing and the Circular Hough transform (C.H.T). They have focused to detect the various objects from complex backgrounds. This study has used MATLAB as a tool to attain its objective, and Matlab function has been used to get the radius of targeted objects. the objects and remove the background from the image, as well as detect the object. The greatest detection success rate 96.2% has been achieved to detect object from complex backgrounds. Further work in progress involves the identification of many items in a cluster that overlap.

N. Abbas et. al [51] have suggested a method that uses contemporary technology and methodologies to semi-automate the red blood cell quantification procedure in digital images of microscopic thin blood smears. It involves interactive basic cuts and morphological operations for breaking clusters of red blood cells, while counting is performed using a labelling matrix. Experiments have been conducted using a collection of publicly accessible digital images. The proposed method has achieved a sensitivity of 0.997%, an accuracy of 0.998%, a true negative rate of 0.00265%, and an error rate of 0.00137%. The correlation value  $R^2 = 0.997\%$  demonstrates that it also has a significant connection with hand counting.

F. Dembele, et. al [52] have introduced a novel system for detecting objects in input images. This study has employed two techniques, separability filter and the CHT to identify objects in image. Experiments have been conducted to evaluate the performance of the system using 25 images. The maximum success rate has been achieved 96% on the circle template and the lowest success rate was 80%.

## **2.4 Literature review on Anticounterfeit packaging**

OECD has conducted a cutting-edge quantitative analysis of worldwide trends concerning counterfeit and pirated goods. This analysis utilized the most extensive dataset available to date, offering a comprehensive examination of the subject matter. The report provides detailed insights and information to complement the analysis [53]. The report has mentioned about serialization-based product authentication, with a unique identifier (e.g., 2D barcode) which help to track and identify each medical package along the supply chain. However, the process is expensive and may be exposed to getting compromised by counterfeiters. The authentication process for physical products, including documents, goods, and drugs, typically relies on utilizing the stochastic structure of either the materials that make up the product or the printed packaging associated with it. This approach helps verify the authenticity of the product.

The verification process for physical products such as documents, goods, and medicine typically involve the examination of the stochastic structure of either the constituent materials or the printed packaging connected to the product [54]. This method is commonly employed to ensure the authenticity of the product. The study has suggested optical detection of random features in combination with digital signatures based on public key codes to recognize counterfeit objects without using expensive production techniques. This method is applied for protecting banknotes and identity verification of credit- or chipcard holders. In recent times, there has been a substantial increase in the counterfeiting and forgery of documents and product packages. This has been due to advancements in technology, particularly the availability of high-



quality printing and scanning devices. Therefore, the importance of various security elements has been proposed to prevent the images from counterfeiter [55, 56].

I. Tkachenko et al. [ 57] have used a small number of training images and a classical classifier, depending on the Principal Component Analysis or the Non-negative Least Squares, to authenticate medicine packaging. This study has generated text samples using two different gravure printers and two similarly chemically engraved cylinders. Then they have compared the distances between the weighted vector applying PCA.

## **2.5 Literature review on Gravure printing**

A. V. Joshi and S. Bandyopadhyay [58, 59] have introduced a model aimed at predicting print defects or void areas on film substrates in the context of the gravure printing process. Void areas refer to the portions of the substrate where the surroundings remain unprinted due to gel formation in the PVC film during gravure printing. The researchers have performed ANOVA to investigate the impact of various gravure process parameters, including speed, viscosity, hardness, and line screen frequency, on the formation of void areas. By utilizing their proposed Regression model, they successfully predicted the void area and achieved a 65% reduction in void area using their methods for the gravure printing process.

P. Kundu et al. [60] has proposed a method to identify an original print on blister foils with different gravure printing machines using the color gamut volume. The color gamut of the printed sample (original) and a scanned reprinted sample (fake) have been analysed to distinguish between them. Few studies have focused on the authentication of printed blister foil samples using color values and ANN (Artificial Neural Network) model [61] and also to differentiate between the original and duplicate samples of blister foil print sample printed with gravure printing technique using spectral signatures, color differences [62].

M. Mandal and S. Bandyopadhyay [63-67] have studied image stability of package prints to estimate the fading behaviour of prints with time. They have developed different models to assess the lightfastness of prints. This model holds potential for verifying printed expiry dates on packages

L. Xinguang et al [68] have proposed a strategy to explain the gravure printing characteristic curve, which depicts the mechanism of dot transmission. Ink cell shapes, ink viscosity, paper kinds, and reducer components have been varied in the printing press to determine the influence of various factors on printing qualities. The structure of electro-graved ink cells for gravure printing has been determined by the engraving needle, frequency of the electro-graving, and the speed of the cylinder's rotation. The X-Rite Spectro-densitometer has been used to test the densities of each color batch on compression ink cell sheets. Three zones have been designated: the zone of beginning tone, the zone of tone leap, and the zone of density saturation.

## **2.6 Literature review on Classification of source by Support Vector Machine**

Several studies have reported higher classification accuracy using k-nearest neighbors (KNN). These studies have focused for classifying the source printer of the printed document using texture analysis [69-73]. They have utilized a wiener filter to estimate the specific invisible noise associated with each printer, and then analyse the noise texture using a gray level co-occurrence

matrix (GLCM). By extracting features from the GLCM and utilising the features in support vector machine classifier to identify the source printers.

S. Joshi [74] has introduced a system to classify source printers using scanned images of printed documents, using local texture patterns-based features and a single classifier. The system extracts letters using connected component analysis and morphological filtering, preventing forged documents and leaks.

R. Schraml et. al. [75] have discussed a potential intrinsic texture features of the packaging material to authenticate the packaging product. In this study, has discussed the feasibility of a classification-based drug authentication system using image analysis of the cardboard packaging and the texture of the top and bottom blister surfaces was examined. The underlying assumption is that the packaging material of a specific drug exhibits consistent yet distinct textural characteristics that can be used for authentication purposes. To validate the package item's genuineness, the proposed work has described a binary classification problem, where there is a set of negative classes that includes unknown and previously unseen counterfeits. In order to demonstrate the viability of this approach, the research has conducted experimental evaluations which have been used to assess two fundamental requirements in texture classification.

S. Voloshynovskiy. et al. [76] have developed a forensic database FAMOS using microstructure images for authentication purpose.

It has been observed from the above literature that though a lot of watermark techniques have been proposed, none of them have dealt how the expiry date or batch number of an authenticated products can be verified. Little work has been done to differentiate an original package product from its counterfeited one by dot shape features or by using classification techniques. Hence, in this work, a watermark is proposed to authenticate expiry date and batch number of the product. Moreover, dot shape features have been effectively utilized to differentiate between an original print with its scanned reprints. Studies on gravure print parameters are almost negligible. Here gravure printing features have been taken as it is the most popular technique for food and medicine packaging industries. Multiclass classification has not been dealt earlier for gravure print identification. Hence this technique is used to differentiate original prints from its scanned reprints which may be considered as the simulated counterfeited print.

# Chapter 3

## MEDICINE PACKAGING PRINTING

### 3. MEDICINE PACKAGING PRINTING

#### 3.1 Medicine Packaging

Packaging is considered as a key for sale, safety and success. Like other packaged products, Medicine packaging is an art and science of preserving and protecting pharmaceutical product from external damage by enclosing them and biological degradation. A technique for keeping medicines contained from the moment of manufacturing in a unit until usage is called medicine packaging. Medicine packaging need to be designed in such a manner that it will provide protection, identification, product quality, patient comfort, display and needs of security, convenience of handling and delivery. Medicine packaging manufacturers are not only focusing the relatively simple issues such as developing good designs, environment safety and communicating with customers but also, they are more concerned to fight with counterfeiting. Issue of counterfeiting is key concern for both developed and developing countries packaging industry. In the pharmaceutical industry, the type of pharmaceutical packaging selected depends upon its function and type of the material used [77-81]. All packaging materials must be evaluated through testing of selected materials, sterilization, storage and stability studies.

#### ❖ Functions of Pharmaceutical Packaging:

The following functions are provided by the pharmaceutical packaging:

- **Containment:** The primary essential purpose of packaging for pharmaceutical items is to keep the contents contained. The requirements of the product and the production and distribution system must be taken into account when designing high-quality packaging. A good packaging does not allow any leaking, any diffusion and permeation of the product and also any alteration the ingredients of the formulation in its final dosage form. The design of high-quality packaging requires being strong enough to hold the contents when subjected to normal handling.
- **Protection:** A good packaging play an important role in protecting the product from all adverse external conditions that can affect the properties of the product or its quality, which may include temperature, light, moisture, oxygen, biological contamination and mechanical damage. Blister packing is a method that may be used to give this kind of protection.
- **Migration:** The ingredients of ink or substrate should not migrate to the product and interact with it. To prevent migration, aluminium foil or film foil combinations work well.
- **Security:** In Pharmaceutical packaging context, the packaging should carry certain features to prevent the medicine from counterfeiting.

- **Presentation and Information:** The pharmaceutical packaging should carry the information on the correct usage of dosage forms, their contents, about the packed product such as date of manufacturing, expiry date, lot number etc.
- **Identification:** The printed packs or its ancillary printed components act as a tool to identify the product.
- **Convenience:** There are different types of packaging which helps to increase customers' access to products and improve distribution, in easy handling and selling.
- **Tool for Advertising and Marketing of Product:** Packaging plays an essential role as marketing tool to differentiate a product and to convey a certain message or brand image to highlight the pharmaceutical aspects for consumers.

In the pharmaceutical industry, various types of materials such as aluminium strips, blister packs, glass bottles, paper/board, plastic films, rubber, and ampoules, are used as packaging material and carefully selected to pack medicines and provide them secure storage until their use. Important information regarding the manufacturing date, expiring date, and correct usage of dosage forms, ingredients of medicines and their side effects are required to disseminate through the medicine packaging. Clear labeling with correct information needs to be disseminated by packages of pharmaceutical products and this information has been printed using different printing processes on packages. Gravure printing process has extensive usage in the medicine packaging industry. This study has mainly focused on the gravure printing process for blister foil medicine packaging.

#### ❖ **Categories of Pharmaceutical Packaging Materials:**

The pharmaceutical packaging is categorically differentiated into three types of packaging such as primary, secondary, and tertiary.

- **Primary packaging:** Primary packaging system is the first packaging envelope which is in directly physical contact with the medicine. So, the choice of primary packaging material need to be done carefully so that there is no interaction with the medicine during its entire shelf life and it will provide proper containment of pharmaceuticals. There are different types of medicine packaging such as bottles, vials, blister packs, strip packaging, ampoules, and sachet packaging used as primary packaging. The nonreactive substances like aluminium are widely acceptable in the medicine packaging industry. Some polymeric materials such as Polyethylene (PE), Polyvinyl Chloride (PVC), Nylon (Polyamide), Polycarbonate, and Polyethylene terephthalate (PET) are used as medicine packaging.
- **Secondary Packaging:** The secondary packaging components are not in direct touch with the medicines or equipment. This is consecutive covering or package which keeps pharmaceuticals packages in it for their grouping. Cartons and boxes etc. are used for secondary packaging for pharmaceutical products.
- **Tertiary Packaging:** This type of packaging is mainly used to prevent the primary and secondary packaging from the external environment and physical damage. It is required to provide bulk handling and shipping of pharmaceuticals from one place to another. E.g. Containers, barrels, etc. [79,80,82].

### 3.2 Substrates used for Medicine Packaging

The materials are selected for pharmaceutical packaging based on its mechanical properties, biological properties, chemical properties and economical aspects. The material used for medicine packaging must be non-toxic. The following materials are considered in the medicine packaging [79,80,82,84]:

- **Paper and Paper board:**

Papers are normally considered as eco-friendly packaging material as it is bio degradable and recycled easily. Papers are light weight as compared to other packaging material. Permeability to gases and moisture and poor tear resistance are the main the drawback of using papers in packaging. The thickness of the paperboards is higher comparing to paper. The paper board is composed of multiple layers of paper. Paperboards are mainly used for secondary packaging for pharmaceutical products. The limitation of paper and paperboards may be due to its burst factor, strength, possible migration from coating, possibility of tear etc.

- **Glass:**

Glass is hard material and is extensively used in pharmaceutical industries. The glasses are chemically inert, impermeable, strong and rigid. Four types of glasses are used in the pharmaceutical industry such as Type I-Borosilicate glass, Type 2-Treated soda-lime glass, Type III- Regular soda lime glass and Type IV- General Purpose soda lime glass. The choice of different types of glass depends on the characteristics and the intended use of the medicinal products concerned. Ampoules, bottles, vials, syringes and cartridges are made by glass [80,83]. The limitation of glass is due to its fragile character and non-flexibility.

- **Plastic:**

Plastic packages are extremely resistant to breakage and leakage. Different designs can be formed with this material. Polyethylene (PE), Polypropylene (PP), Polyvinyl Chloride (PVC), Polystyrene, Polycarbonate and Polyethylene terephthalate (PET) materials are used to manufacture the plastic containers. Plastics are used to make the closures, bottles, bags, tubes, laminates with paper or foil etc. [78,83]. The limitation of the plastics are due to the migration problem of toxic additives and unreacted monomers and recyclability problem.

- **Rubber:**

Rubber composed of several ingredients, one of which is elastomer. Modern rubber compounds used in pharmaceuticals packaging include only a limited number of ingredients, which are very difficult to extract. Closures manufactured from these materials usually do not cause any concerns and are suitable for use with a wide variety of

pharmaceutical preparations. Migration problem is often important for this substrate.

- **Metal:**

Metal containers are preferred solely for medicinal products for non-parenteral administration. As metal is strong, impermeable to gases and shatterproof, it is the suitable packaging material for pressurized containers. It is used to manufacture the tubes, packs made from foil or blisters, cans, and aerosol and gas cylinders. Aluminium and stainless steel are widely used for both primary and secondary packaging for medicinal products. Aluminium is light weight material and provides excellent tamper-evident resistance [78,80,84]. It is most preferred by pharmaceutical industry for its inertness, flexibility, light weight and less migration factors. However, cost may be a limiting factor in some cases.

### **3.3 Blister Substrate used for Medicine packaging Printing**

- **Aluminium Blister Foil:**

Securing products from counterfeiters is a crucial aspect of packaging. Aluminium blister foil is a suitable option for packaging pharmaceuticals. It is commonly used to package various medical products like pills, capsules, and tablets. The typical thickness of aluminium foil ranges from 25 to 28 microns. The foil's properties, such as its ability to provide barrier protection against light, gas, and liquids, make it highly suitable for packaging medicines and food. One significant advantage of aluminium foil as a packaging material is its inertness, which means it does not react with chemicals found in medications, food, and beverages, and it does not produce any toxic residues [85-87]. When exposed to air, a thin layer forms on the surface of the aluminium, protecting it from oxidation. Blister foil, a flexible substrate, is widely utilized for packaging medicines and food. It creates a bubble or pocket that safeguards the product against external factors like moisture, humidity, temperature, and contamination for extended periods. Consequently, blister foil's resistance properties make it an ideal choice for pharmaceutical packaging. Furthermore, blister foil offers tamper-evident features, allowing each unit of medicine to be individually sealed. After each dosage is used, the remaining doses remain securely sealed [82]. If there is any tampering, replacement, or separation of the blister or strip pack materials, evidence of entry will be apparent. Once the blister packaging is broken, it cannot be repaired or resealed at the tampered location. In order to provide maximum protection for the product, the cold form aluminium blister format is also employed for medicine packaging purposes.



Fig 3.1: Blister Pack medicines

➤ **Types of pharmaceutical blister packaging:**

Two basic types of pharmaceutical packaging exist:

- ✓ One variation involves creating the cavity using transparent thermoformed blister foils, while the lid is fashioned using transparent plastic or a combination of plastic, paper, or foil.
- ✓ The alternative type of packaging includes foil as a crucial element in both the webs, and its cavity is created through cold stretching.

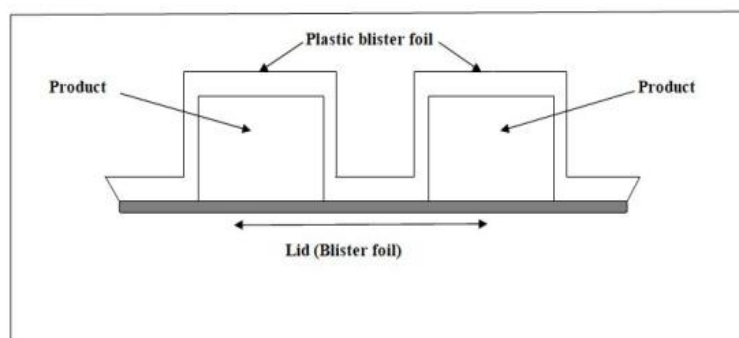


Fig 3.2: The basic configuration of blister packaging [82]

➤ **Pharmaceutical blister Packaging Components:**

The following are the four primary components of pharmaceutical blister packaging [82,84]:

- **The forming film** (About 80%–85% of blister packages are made of forming films) Forming film is a crucial part of packaging because it places the products in deeply drawn pockets. An essential aspect of effective packaging is the careful choice of the appropriate plastic film or material for the blisters, taking into account its specific properties, thickness, and quality. Furthermore, factors such as the product's dimensions, weight, the presence of sharp or protruding edges in the final package, as well as the film's ability to withstand impact, aging, migration, and cost are all taken into consideration when determining the

suitable forming film for pharmaceutical blister packaging.

- **The Lidding material** (lidding materials make up 15-20% of the total weight of the packaging)

The base or main structural material on which the final blister packaging has been made is considered as lidding material. The selection of lidding material is done according to the size, shape, or design of the package to be produced, weight of the product, types of medicine etc. The thickness of the lidding material from 0.36mm to 0.76mm. In blister packaging, both heat-sealing and printability are vital factors to consider, and the lidding material must offer an optimal balance that is suitable for practical use.

- **Heat seal coating**

Heat sealing coating is an essential component to produce final medicine package with blister substrate. The overall look and structural integrity of the blister package rely on the quality of the heat-seal coating. Due to the different printing processes and use of different coatings (water based or solvent based), it is very important to apply the heat-sealing coating on lidding material to protect the material and printing. An effective heat-sealing coating on a blister package demonstrates desirable qualities such as excellent gloss, clarity, resistance to abrasion, and strong hot tack properties.

- **Printing ink**

Printing inks offer the graphics and aesthetic appeal of the final medicine package product. By using different printing processes such as letterpress, gravure, flexography, printing inks (cyan, magenta, yellow and black) are used to print the detail information of medicine on the lidding material. Printing inks must be resistant to heat-sealing temperatures 300°C. without showing any discoloration or tackiness (blocking). Moreover, the application of heat-sealing coating on different materials has been resist abrasion, bending, fading the printing and also keep them safe until it is used. Printing inks should not have excessive amounts of hydrocarbon lubricants, greases, oils, or release agents.

The application of heat-sealing coating on different materials has been resist abrasion, bending, fading the printing and also keep them safe until it is used.



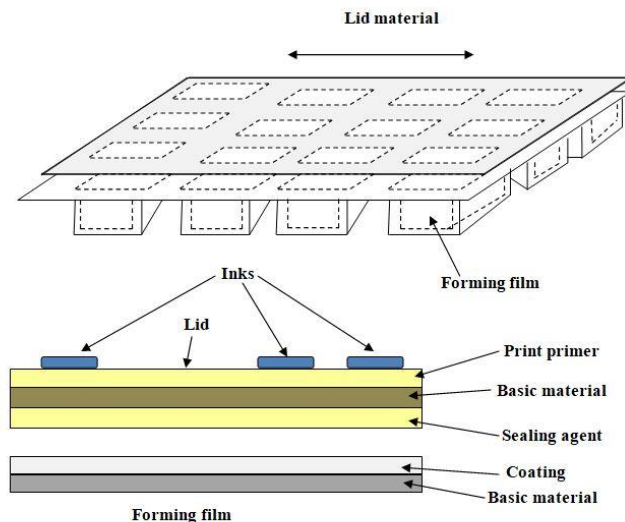


Fig 3.3: The basic components of blister packaging [82]

➤ **Advantages of Blister Packaging:**

✓ **Individual Packaging:**

Blister packaging provides a convenient way to pack separately each unit of medicines as an individual dose. Each dose is specified by product name, lot no and expiration date. So, the quality of the content through containment has been maintained in separate cavity or pockets by this type of packaging. If any part of packaging material is damaged due to some external conditions, it will not affect the whole packaging.

✓ **Maintaining Product Integrity:**

The use of blister packaging helps preserve the quality of the product by safeguarding drugs that are prepackaged in blisters from external environmental factors such as moisture, oxygen, and light etc. The preparation of forming films and lidding structures is customized based on the product's susceptibility to external environmental factors. The packaging components can be laminated with barriers that help to prevent them from contamination. The product degradation through UV radiation must be blocked for using opaque materials (aluminium) as medicine packaging.

✓ **Tamper Protection:**

Another significant advantage of blister packaging is its ability to provide clear indications of tampering. The package must be designed so that one cannot reshape the original form the package after usage of blister pack and it is impossible to separate the lidding or backing material from the blister for the inherent tamper-evident mechanism of blister packaging without causing visible damage. This type of characteristics of blister

packs could help to deter package pilferage in pharmaceuticals industry.

✓ **Preventing Accidental Drug Misuse:**

Blister packaging can be designed as child resistant packaging. Most child resistant blister package contains a film/paper wrapper with a peelable adhesive. As per the design of child resistant blisters packs and lidding structures of the packaging it could not be opened easily without instructions specified by a manufacturer. Thus, it helps to prevent children, and even old patients, from taking wrong medicine accidentally.

✓ **Visibility of Product:**

Blister packaging provides a notable display benefit, allowing customers to easily view the pharmaceutical products, thereby assisting in their purchasing decision. Additionally, the lid or backing material is intentionally colored and designed to attract potential customers.

✓ **Minimal Movement Within Packaging:**

Blister packs can easily be mold according to the shape of the product. A computer-aided machining program is used to control and to prepare the mold according to the shape of products (medicines). Therefore, this type of mold can be made for minimal movement of product within packaging.

➤ **Blister Packaging Process:**

The essential parts and functions of intermittently operating of blister foil packaging machine include the following steps [82,85,86]:

- ✓ The unwinding station: The forming films and the lidding materials are supplied to the unwinding unit of the blister packaging machine at a rate corresponding to the speed of packaging machine.
- ✓ The heating station: The heating station raises the suitable temperature to the forming film for deep drawing and provides the temperature according to the requirement of the materials used for medicine blister packaging. Heating station is present only in thermoform and thermos-cold blister pack machine.
- ✓ The forming station: It helps to form blister cavity via compressed air or die plates.
- ✓ The cooling station: After the forming process, the cooling station helps to cool the material.
- ✓ The feeding machine: In this unit blister cavities are loaded with products (medicines). The feeding machines can be linked to package the products (medicines) into the blisters.
- ✓ The sealing station: After product loading into the cavities of blister packs the sealing station heat seals the lidding material to the forming film for blister packaging. The

sealing temperature typically varies between 140 and 340-8 °C based on the type of machine.

- ✓ Mini Guide Rail: It helps to guide the sealed foil towards the printing station.
- ✓ The printing station: The detail product information like expiry date, manufacturing date, formulation etc. is printed on substrate in the printing station.
- ✓ Perforation Station: It uses to perforate the blister strips.
- ✓ The trimming station: In the trimming station blister are cut into specific and individual unit as per requirement.

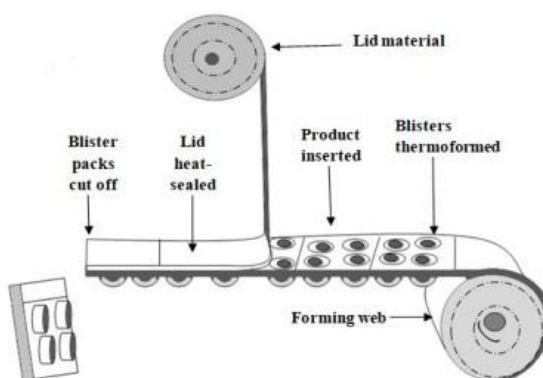


Fig 3.4: A common method for assembling blister packaging [82]

In this study, blister foil is considered as medicine packaging substrate due to its inertness and non-reactivity properties. The metallic luster and lightweight are additional advantages of the blister foil. In this work, the reference input color chart has been printed on the foil by the gravure printing process. The scanned same reference input color chart has also been reprinted by gravure printing process. Therefore, the gravure cylinder has been prepared by electromechanical engraving process for the artwork. Cyan, Magenta, Yellow and Black (CMYK) foil inks have been used to print (original sample) and to reprint (simulated counterfeited sample) the desired color artwork on the foil substrate. Blister foil has two different sides, one is matt side and another is glossy side. The bright side and the matte side of it are heat seal and print-treat coated respectively. To print (original sample) and to reprint (simulated counterfeited sample) with different gravure printing machines, the same matt side of blister foils has been taken for this experiment.

# Chapter 4

## ANTICOUNTERFEITING TECHNIQUES USED FOR PACKAGE PRINTING

### 4. Anticounterfeiting techniques

#### 4.1 Anticounterfeiting techniques used for package printing

Anticounterfeiting refers to measures taken to prevent or minimize the production, distribution and sale of counterfeited or fake goods. Counterfeited products are unapproved replicas or duplicates that are designed to mislead buyers into thinking that they are real. Counterfeiting is a serious problem that affects various industries, including pharmaceuticals and food products. The sale of counterfeit goods not only hurts the legitimate businesses but also creates significant health and safety risks to consumers. It is possible to make food or medicine items with fake or substandard materials and then pack it in a counterfeited package well printed that looks similar by external getup of the package. These products may not undergo the same safety testing as genuine products, potentially leading to health hazard or even death. By incorporating security measures in the packaging, not only the potential harm to consumers can be avoided, but also the financial loss as well as loss of reputation and brand names of original manufacturers can be protected. Technologies are advancing in rapid pace to ensure that packaged items are authentic and not imitated before they reach the end consumer [88-91].

##### 4.1.1 Anticounterfeiting of medicine and food packaging

Anticounterfeiting measures for medicine and food packaging are critical to protecting consumers and maintaining the integrity of the pharmaceutical supply chain. To prevent the production and distribution of counterfeited medicines, various anticounterfeiting measures can be implemented in medicine packaging. Secure packaging has a variety of safety features to meet the needs of high-value products and their supply chains, such as food, pharmaceuticals. Some anti-counterfeiting techniques are used on their packaging, such as Braille embossing, UV inks, color-changing ink, serial number identification, holograms, and watermarking [88-92].

To keep the integrity of the pharmaceutical product, the packaging has overt and covert security features. It is anticipated that overt features will help consumers to verify a pack's authenticity. Examples of overt features are holograms, color-shifting inks, tamper-evident seals, serial numbers and barcodes. A covert feature is intended to help the brand owner spot a product that has been copied. Covert security features are Invisible Ink, Microprinting, Watermarks, Security Threads or Fibers.

Some of these measures include-

**Tamper-evident packaging:** Incorporating tamper-evident features into the packaging helps ensure that any attempt to open or tamper with the product is noticeable. Examples include seals, holographic stickers, or shrink wrap that shows signs of tampering upon removal.

**Authentication technologies (Unique Serial Numbers or QR Codes):** Assigning unique serial numbers or QR codes to each package enables easy verification and tracking of individual products. Consumers can scan these codes using their smartphones or use online databases to confirm the authenticity of a product.

**Track and trace systems:** Track and trace systems use unique serial numbers or codes to track the movement of medicines throughout the supply chain, from manufacturing to dispensing. This helps identifying any counterfeit medicines and allows for timely intervention. Example is barcode.

**RFID Tags:** Radio Frequency Identification (RFID) tags can be embedded in packaging to track and authenticate products throughout the supply chain. RFID technology enables real-time tracking and helps detect counterfeit products by comparing their tag information with genuine ones [89,91,92].

**Overt (visible) features:** Incorporating visible features into the packaging, such as color-shifting inks or micro-printing, can make it more difficult for counterfeiters to produce identical copies of the packaging [88-92].

**Covert (hidden) features:** In the context of anti-counterfeiting typically refer to concealed security measures incorporated into products or documents to help detect and prevent counterfeiting. These features are intentionally hidden or difficult to replicate, making it harder for counterfeiters to produce fake versions of the original item.

Implementing these anticounterfeiting measures in medicine and food or any packaging can help protect consumers from potentially harmful counterfeit products and maintain the integrity of the pharmaceutical supply chain.

Anti-counterfeiting packaging security measures that involve watermarking and microscopic dot analysis can be effective in combating counterfeiting. Here's an overview of these techniques:

**Watermarking:** Watermarking involves embedding a unique, invisible mark or pattern into the packaging material or design. It can be achieved through various techniques, such as using specialized inks, holograms, or microtext. Watermarks are difficult to replicate, and they can be verified using specific devices or techniques. By incorporating watermarks into the packaging, it becomes easier to identify genuine products from counterfeit ones.

**Microscopic Dot Analysis:** Microscopic dot analysis is a technique that involves adding tiny, unique dots or particles to the packaging material. These dots are invisible to the naked eye but can be detected and analysed using specialized equipment like microscope. The arrangement and composition of these dots create a unique identifier for each package. By

comparing the dot patterns on a suspicious package with a genuine one, it becomes possible to determine its authenticity.

In this study, watermarking and microscopic dot analysis have been used to enhance the security of anti-counterfeiting packaging.

## **4.2. Watermarking process as security feature in anti-counterfeiting**

Counterfeit and tampered high-value items pose significant safety risks and can harm the reputation of a company [23].

### **4.2.1 Watermarking as anticounterfeiting technique**

Watermarking is a technique used to embed a hidden message or identifier into a document to provide copyright protection or to authenticate the document. It is usually embedded in a way that is not easily visible to the human eye but can be detected and decoded using specialized software or devices. In the case of anticounterfeiting, watermarking can be used to embed a unique identifier into a product image, label or packaging, which can be used to authenticate the product and prevent counterfeiting. To ensure the effectiveness of watermarking in anticounterfeiting, the watermark should be designed to be robust against counterfeiting, meaning it should be resistant to intentional and unintentional attacks that may attempt to remove or modify the watermark for counterfeiting purpose. The watermark should also be imperceptible, meaning it should not affect the quality or usability of the documents or packaging content.

### **4.2.2 Type of Watermarking process**

Watermarks come in a variety of forms, including visible and invisible. Visible watermarks are easily seen and indicate who owns the content, while invisible watermarks are imperceptible and not observable. Any secret information, signature or logo can be an invisible watermark.

A watermark is a signal or pattern that is added to a digital document, such as text, images or multimedia that carries information specific to the copyright holder, the document's author or the document's authorised user.

Watermarks come in a variety of forms including:

- a) Visible watermarks: Visible watermarks are those that can easily be seen by the viewer and indicate who owns the content. But the watermark must not take away from the image's actual substance.
- b) Invisible watermarks: These watermarks are made to imperceptible in with the background. Without image or data degradation, this form of watermark is not observable in the watermark image. The majority of current research focuses on invisible watermark to the naked eye.

c) Digital Watermarking: This refers to the process of embedding a digital watermark into a digital file. Digital watermarks can be visible or invisible and are used to track manipulation, identify the source of the item and limit unauthorised copying.

d) Analog Watermarking: Analog watermarking is the process of embedding a watermark into an analog-signal, such as an audio or video recording. Analog watermarking is often used to prevent unauthorized copying or distribution of copyrighted material.

### **4.3 Watermarking security and its vulnerability**

Watermark security means that unauthorised users can't take out, find, estimate, write or change the secrete information which make the watermark. Specifically, watermark security is not concerned with the semantics of the watermarking information but only with the physical existence of the watermarking information, meaning that it must presume that the attacker is familiar with the watermark embedding and detection methods. The goal of an attacker is to identify and copy the usefulness of the watermark, disable the detector or target the watermarking application's basic concept. An attack is continual improvement if the attacker disrupts any stage of the watermarked process; therefore, the content owner and the watermarking technology must guarantee that each stage is protected from such manipulations [15-26].

Watermarking systems are vulnerable to a number of attacks, including basic, geometric, cryptographic, protocol, and Print-Scan attack.

Basic attacks exploit the constraints of embedding techniques, such as amplitude distortion and noise addition, synchronisation of the chip signal and the ability to adjust the duration of audio without altering its pitch.

Geometric attacks alter the watermark detector's synchronisation with the embedded information, allowing the detector to recover the embedded watermark information when complete synchronisation is recovered, however the procedure is impractical due to its complexity.

The objective of cryptographic attacks is to eliminate watermark information or install misleading watermarks.

The entire application of watermarking is targeted by various attacks. The idea of inversion, when the attacker removes the owner watermark from the data and represents themselves as the owner, is the foundation of invertible watermarks. Copy attacks are used to transfer estimated watermarks to target data from watermarked data. Watermarks that depend on the signal can be immune to the copy attack.

Print-n-Scan (scan-and-reproduce) attack is consisting on scanning the source watermarked document using this scanner or photographing and reproduces the watermarked document for counterfeit the source documents [2,10].



In this study we have concentrated on the Print-n-Scan (scan-and-reproduce) attack on the packaging of the pharmaceuticals and food products.

#### **4.3.1 Properties of watermarking methods**

Although watermarking techniques can be characterised by a number of qualities, only four are often used: hiding capacity, perceptual transparency, robustness and security aspects. The effectiveness of a watermarking technique is often assessed based on three factors: fidelity, capacity and robustness.

Fidelity is related to the visibility of image artefacts created by the watermarking technique.

- Aliwa M. et. al. [27,28] described fidelity as the degree of "perceptual similarity" between a watermarked version and its unwatermarked counterpart.
- Capacity relates to the quantity of information that may be embedded in an image by the watermarking process.
- Robustness refers to the capacity of the watermarking process to survive passive distortions that do not render the image unsuitable for its intended purpose. Standard image processing, transmission distortion and storage distortion fall under this group. Moreover, robustness refers to the watermark's capacity to endure active attempts at unlawful removal. This group of operations contains statistical analysis and nonlinear geometric distortions.

#### **4.3.2 Applications of Watermarking**

Watermarks have the potential to be beneficial in several applications, including:

Ownership Assertion, Fingerprinting, Copy Control, Fraud and Tamper Detection, ID Card Security, Intellectual Property Right (IPR) Protection.

##### **a) Ownership Assertion**

The use of watermarks to show ownership of a work requires a watermarking algorithm that guarantees the inevitability of the watermark. Often, this is accomplished by introducing a Trusted Third Party (TTP) that issues an unambiguous registration code to the work's owner in order to prove ownership of the registered asset.

##### **b) Fingerprinting**

To prevent unlawful copying and distribution, the owner of multimedia material should encode a different watermark (or fingerprint) in each copy of the data. The watermark must be undetectable, impervious to purposeful attempts to fabricate, delete or invalidate it and resistant to user collusion.

##### **c) Copy Control**

Watermarks can be employed in closed systems, such as the Digital Versatile Disc, for copy protection and control (DVD). Standardization is being investigated for a copy



protection technique that involves digital watermarking and DVD players of the second generation may be able to read watermarks and respond based on their presence or absence.

#### d) Fraud and Tamper Detection

When using multimedia material for legal purposes, medical applications, journalistic reporting or business transactions, it is crucial to guarantee that the content originated from a certain source and has not been altered or distorted. This can be accomplished by embedding a watermark into the data, which is extracted using a source-specific key. The watermark may also contain information from the original image that may be used to reverse any changes and restore the original. Watermarks should not degrade the quality of an image and be counterfeit-resistant. The removal of the watermark renders the content invalid and unusable.

#### e) ID Card Security

By retrieving the encoded information and comparing it to the printed text, digital watermarking may be used to validate the legitimacy of a passport or identification card. This adds an additional layer of protection to the application, as if the ID card is taken and the photo is changed with a fake, the difficulty to remove the watermark will render the ID card invalid. Digital watermarking techniques must be created within the context of the complete system in which they will be used and each application imposes distinct criteria and would necessitate a different form of invisible or visible watermarking scheme.

#### f) Invisible Marking on Paper

Watermarks can be used to identify the originator, validate the legitimacy of the document content and expire the document. They are particularly valuable for formal documents, such as contracts, in which they can encode the lawyer's identity or vital information, such as essential monetary amounts. A method for invisibly marking white blank paper with normal and visible ink, which is currently known as Crypto-glyph.

#### g) Intellectual Property Right (IPR)

IPR protection is the first focused application of digital watermarking, safeguarding the creator's rights, the rightful owner's rights, copyright rights and moral rights. In IPR protection, proving ownership in legal disputes, fingerprinting and copy control are the three most important jobs.

### **4.4 Watermarking by Histogram**

Watermarking by histogram is a technique used in digital image processing to embed a watermark into an image by modifying its histogram. The watermark is a signal or pattern that is added to an image to indicate its ownership or authenticity. The watermark can be extracted from the watermarked image by analysing the histogram of the image. The extraction process involves identifying the modifications made to the histogram and then using them to extract the watermark signal. Watermarking histogram is one of the many

techniques used in digital image watermarking. It is a popular technique because it is simple and effective and it does not require a lot of computational resources [11,12].

#### **4.4.1 Histogram watermarking for package authentication**

Histogram watermarking is a technique used to embed hidden information within the statistical distribution of an image or a signal. This technique can be used for package authentication, where the histogram of the image of the package is used to embed a unique watermark that can be verified to ensure the authenticity of the package.

The process of histogram watermarking involves first selecting a region of interest (ROI) in the package image, such as the logo or barcode, secret information. The histogram of this ROI is then modified by adding a unique watermark signal. This watermark signal can be a random pattern or a predetermined sequence of bits. To verify the authenticity of the package, the histogram of the ROI is extracted and analysed to detect the presence of the watermark signal. The verification process involves comparing the extracted histogram with the original histogram and if the watermark signal is present, the package is considered authentic. Histogram watermarking is a robust and secure technique for package authentication, as it is resistant to various attacks such as cropping, rotation and compression. However, it requires careful selection of the ROI and the watermark signal to ensure that the embedded watermark is not perceptible and does not affect the quality of the image.

#### **4.5 Anti-counterfeiting measures microscopic dot analysis**

Microscopic Dot Analysis, also known as microdot technology, is one of the methods used for anti-counterfeiting measures on packaging and products. It involves the application of microscopic dots of prints on a packaged product, which are then examined under a microscope for authentication purposes. Here's how it typically works:

**Dot application:** Microscopic dots, usually smaller in size, are printed on a packaged product using specialized equipment. These dots are typically invisible to the naked eye and require magnification to be observed.

**Dot composition:** The microscopic dots may contain various materials, such as unique identifiers, special inks, or markers, which can be used to authenticate the product. These identifiers are often difficult to replicate and serve as a distinguishing feature.

**Dot examination:** To verify the authenticity of the product, trained inspectors or experts examine the microscopic dots using a microscope or other magnification tools. The dots may be inspected for specific patterns, codes, or other characteristics that indicate genuine products.

**Authentication process:** The examination of the microscopic dots helps determine whether the product is genuine or counterfeit. If the dots exhibit the expected features, it indicates authenticity. Conversely, the absence of dots, irregular patterns, or signs of tampering may suggest counterfeit or compromised products.

Microscopic Dot Analysis is just one of many techniques used in anti-counterfeiting measures [30-34].

In this study anti-counterfeiting medicine/food packaging has been introduced a method that uses variable image watermarking to ensure the authenticity of the product. This type of watermarking is dynamic in nature which will depend on the batch number and expiry date of the products embedded into the packaging material itself. The watermark may contain information such as the product code, batch number and manufacturing date, which can be verified by the manufacturer or regulatory authorities to ensure that the product is genuine. This helps to prevent the distribution of counterfeit or substandard medicines, which can be a serious threat to public health. In this study, specific combination of watermarking technologies and microscale dot pattern features have been used for anti-counterfeiting purposes to develop a secure packaging method.

# Chapter 5

## GRAVURE PRINTING PROCESS

### 5. GRAVURE PRINTING PROCESS

Gravure printing is one of the major printing processes which is characterized by its simplicity, high quality, and ability to print on flexible packages and at very high speeds. The advantageous features of gravure printing make it a very promising process for the flexible package printing industry. This is the major printing process used for food, medicine, confectionary and other packaging industry. Gravure printing also named as rotogravure printing or Intaglio printing is principally long-run or high-quality printing method suitable to print on many kinds packaging substrates, especially paper, paper board, film, and metal foil. Package printing plays a key role to attract the consumer and promote the sales appeal of a package. Package printing is defined by any reproduction activity of text and/or images in which, with the use of an image carrier like printing cylinder or plate for transfer of ink on paper or film or foil substrate. Modern gravure process includes ink fountain, an engraved gravure cylinder as an image carrier, impression roller, and the doctor blade as basic components. It can print with the widest range of substrate and ink formulations. These advantages also enable the gravure printing process to compete against other printing processes such as flexography, letterpress, lithography, and screen printing etc. The research and developments in this field are helping to fulfil the demands of the customers. Fig. 5.1 shows a schematic of a typical gravure printing process.

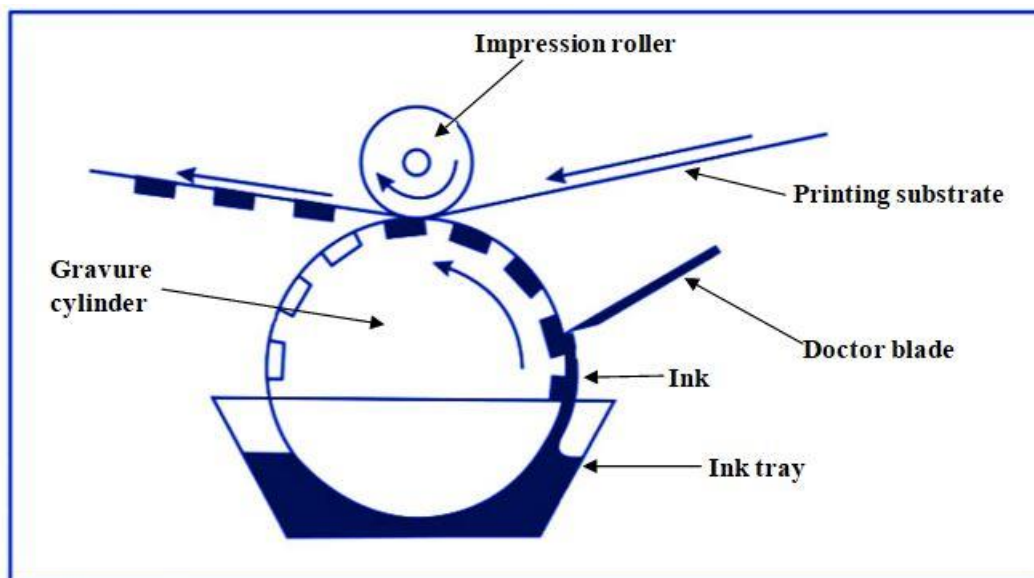


Fig 5.1: Gravure Printing Process

The gravure printing process is a recess process which means that the image carrier has the image etched below the surface of the non-image area. The image carrier is a cylinder with engravings that is partially dipped and rotated in an ink duct, effectively transferring the ink onto the cylinder's surface. The excess ink on the cylinder is wiped off by a doctor blade without

affecting the ink in the recessed image cell. An impression roller that is covered with an elastomer material, applies pressure to the substrate on the cylinder and transfers the ink from the cells to the substrate by capillary action [94]. Subsequently, the substrate is routed through a dryer unit to ensure it is dried before proceeding to the next color unit and absorbing an additional layer of ink.

## **5.1 GRAVURE CYLINDER MAKING:**

One of the most important features of the gravure printing process is the engraved cylinder that is used as an image carrier. Gravure cylinders are usually made of steel and electroplated with the copper or zinc and then images are engraved on this cylinder by chemical etching or with a diamond tool and laser beam [93-95]. Before the engraving process, a color separation process must be required from the original artwork. Electromechanical engraving is extensively used in gravure cylinder imaging.

The strength and benefits of gravure printing process is governed by the three main characteristics of Gravure cylinder – cylinder base, cylinder preparation and cylinder engraving.

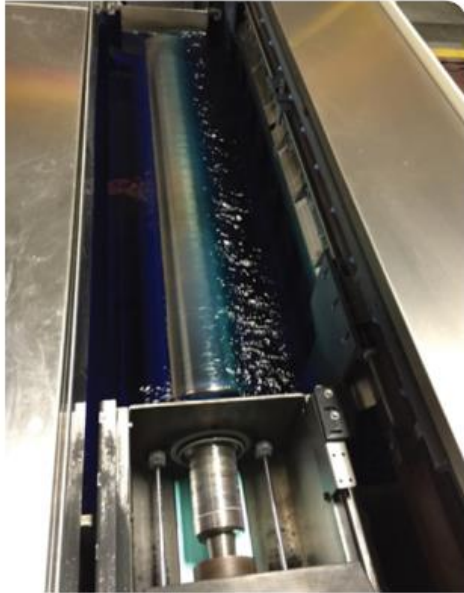
### **Cylinder Base:**

Gravure cylinder is essentially a steel roller that undergoes electroplating to deposit a layer of copper on its surface. Steel Bases are extremely durable and stable. The design of the task is etched onto the copper surface, which is subsequently coated with chromium to minimize cylinder wear and improve ink transfer. The procurement of fresh bases for a printing task results in a substantial increase in expenses. The advantage of engraved cylinder, when the cylinder requires to be re-engraved either with same design (if wear is excessive), or another design the outer layer is just torn and peeled off and replaced by another image artwork which can be engraved or etched, instead of the expensive and time-consuming process of manufacturing a new cylinder by building up a copper surface on a steel base.

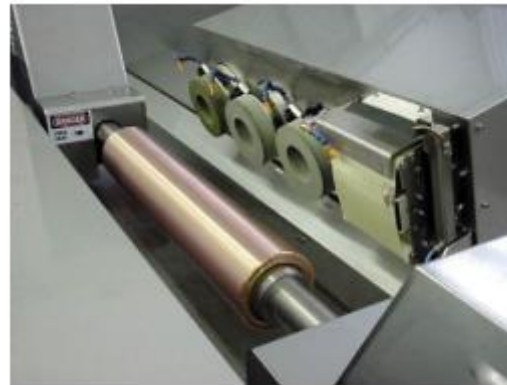
### **Copper Plating and Polishing:**

Copper has long been the preferred substrate for engraving cylinder due to its readily available, readily recyclable and more economical. During the preparation of the cylinder, it is important to have a clean surface free from oxides and grease for proper adhesion of copper. Therefore, chemicals are applied to remove grease and deoxidize the surface before the plating process. For a steel base-shell, an intermediate layer (nickel or alkaline copper) has to be plated onto the steel surface prior to copperplating in the acidic solutions used. The thickness of electro-plated nickel layer varies in the range of 150–200  $\mu\text{m}$  and is designed protects the steel from erosion caused by the Sulfuric acid used in the final plating process, which would result in the plate not adhering properly. A copper layer of thickness of about 50  $\mu\text{m}$  has been polished to get a typical uniform standard surface with surface roughness (Rz) ranging between 0.2 and 0.4  $\mu\text{m}$ . The diamond stylus of the engraving machine plays a crucial role in cleanly cutting through the copper, ensuring a smooth surface. It is essential

for the copper-plated cylinder to be free from imperfections and have accurate dimensions. The accuracy and smoothness of the copper plating reduce the need for extensive machining. Brighteners are incorporated into the plating solution to facilitate the process.



(a) Copper Plating



(b) Polishing Copper Plated Cylinder

Fig. 5.2: (a) Copper Plating (b) Polishing Copper Plated Cylinder [98]

Gravure cylinder imaging can be done by chemical etching, electromechanical engraving or laser engraving. A brief discussion of the processes is given below.

#### a. Chemical Etching:

The process of chemical etching has been developed in the 19th century and is now have only restricted use. The proposed technique includes two methods: the first method requires exposing a screen and a positive to carbon tissue that has been coated with gelatin-coated paper, while the second involves directly exposing screened images onto a photosensitive coating on a copper cylinder [94]. This engraving process is mainly done on using strong acid or mordant (e.g. ferric chloride) to remove the copper metal layer from a designated area of the unprotected parts of a metal surface to create a layout of the job in the gravure cylinder on the plated and polished copper metal as per required graphic design. Ferric chloride is used to etch the metal at different depths. However, direct exposure can lead to uneven etching and may require subsequent revisions. This method is the manual method and variable factors like strength of chemical, non-uniformity, etching perfection are having the major drawbacks of cell variation so later on, this process has been replaced by EME.

The basic stages of the process are listed below: Cylinder Preparation: The cylinder is first cleaned and polished to remove any impurities and roughness. Coating: A thin layer of light-sensitive photoresist is applied to the cylinder. The photoresist layer is exposed to UV light

through a film mask that contains the desired pattern. Developing: The cylinder is then washed in a developing solution that removes the unexposed photoresist, leaving behind the patterned photoresist layer. Etching: The cylinder is immersed in an etching solution that dissolves the exposed areas of the metal surface. The depth of the etched areas determines the ink volume that the cylinder can hold. Cleaning: After etching, the cylinder is thoroughly cleaned to remove any remaining photoresist and etching solution. Finishing: The cylinder is finished with a protective layer that helps to prevent wear and tear. The process of gravure cylinder chemical etching is preferable for cost effective high-quality printing.

### Engraving:

#### b. Electromechanical engraving

Electromechanical engraving (EME) is the process, where tiny cells are engraved on the surface of hard copper plated cylinder by a fully automatic process. The depth of the cylinder cells ranges from approximately 20 to 50  $\mu\text{m}$ , and these are engraved with high precision and consistency [98]. Fig. 5.2 shows the flow chart of the cylinder making by EME processes.

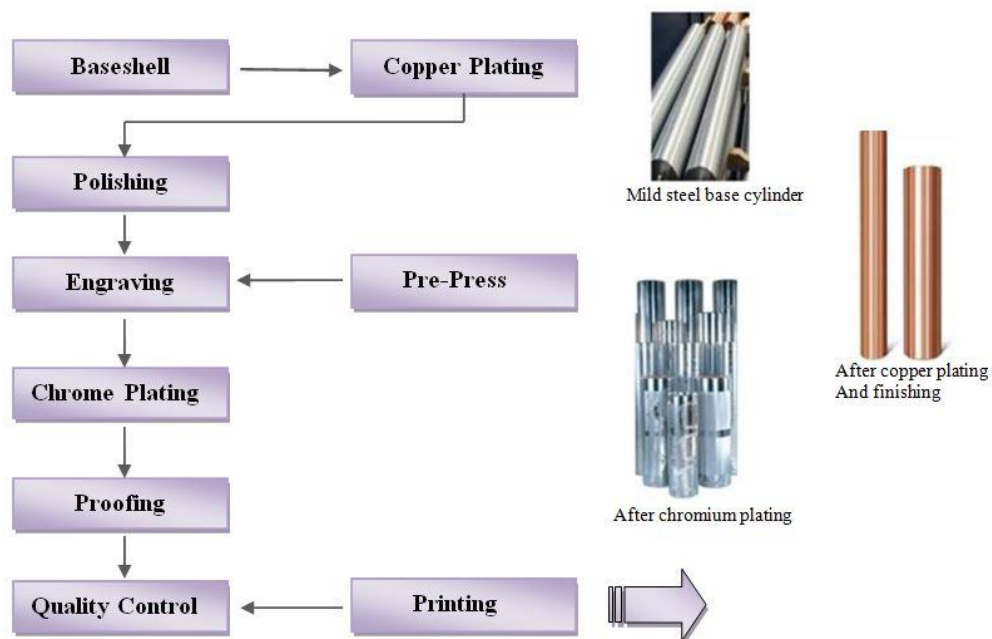


Fig 5.3: Flow chart showing the EME cylinders making processes [97]

Electromechanical engraving process has become popular in the packaging industry as it has brought consistency and predictability to the gravure process. In this particular electromechanical engraving technique, a diamond-stylus under electronic control is employed to create the cells on the copper-plated surface of the gravure cylinder, utilizing an oscillating motion. A stylus is composed of multiple angles at its cutting tip, and these angles, when measured, result in different depths of cells for a given cell width. Therefore, a fine screen that is chosen for detail can be prepared to deliver the cell volume required for



color density by selecting a more acute engraving stylus angle. The stylus is sharpened from  $110^\circ$  to  $130^\circ$ . In a typical engraving setup, a diamond stylus is selected with a specified geometry. The geometry is typically considered by the stylus angle and the relative shape of the engraved cell. In general, the lower the stylus angle, the sharper the stylus, and therefore a deeper cell will be engraved shown in Fig. 5.4. For non-image areas and light tone areas, the stylus either does not engrave or only cuts into the surface very lightly [98].

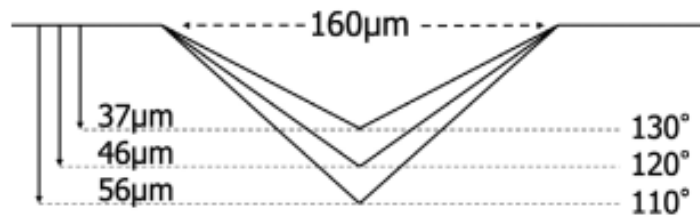


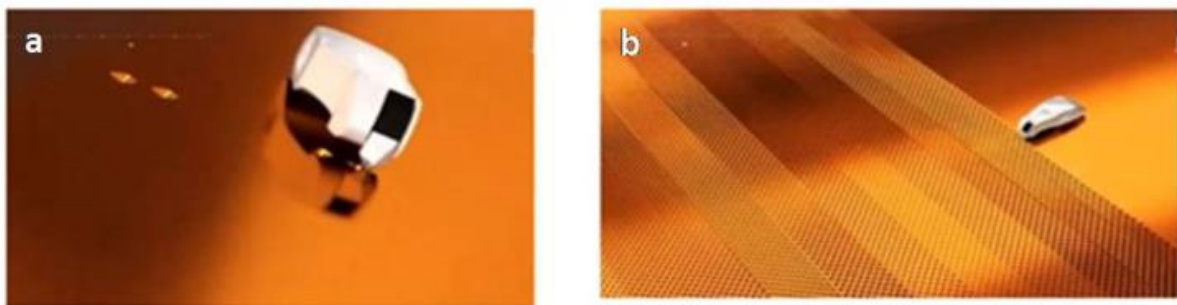
Fig.5.4: Different Stylus angels [98]

### Prepress:

The original artwork is scanned into a computer and digitized so that each scanned and digitized image can have an electronic signal. The different angled diamond-stylus is guided by an engraving system that moves across and around the cylinder. The computer controls the engraving head by which the diamond engraves cells at different depths. The thickness of the cell wall also can be varied in this method. It may produce elongated or compressed diamond-shaped cells based on the cell angle. The cell geometry controls the amount of ink transfer.



Fig. 5.5: Engraving Head [97]



(a)

(b)

Fig. 5.6. Images show (a) EME engraving process, (b) EME engraved cell on Cu plated cylinder [98]



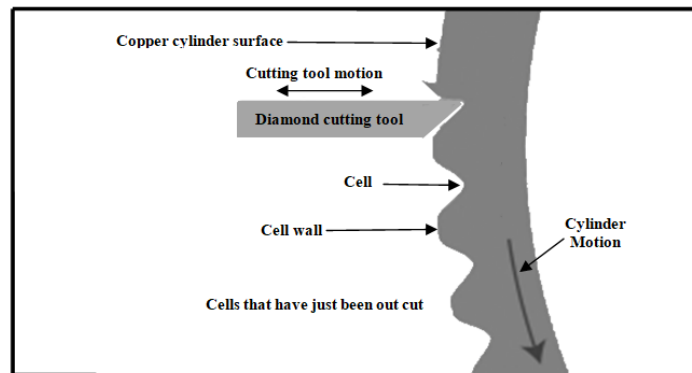


Fig. 5.7: Electromechanical Engraving of Cylinder [97]

The cells are etched in rows, and when larger cells are present, they are often linked by narrow channels because the stylus remains in contact with the surface. To enable the cells in adjacent rows to fit closely together, each subsequent row is shifted by half a cell. This allows for a nesting effect between the cells in adjacent rows. The spacing between rows of cells is typically kept constant, so that the only way to change the tone or size of the cells is to control the cutting depth. The spacing of the rows is called the line screen, and is typically specified in lines/inch or lines/centimetre. The tone is defined as the proportion of engraved area relative to the total surface area and ranges from 0 to 100 %. In theory, cells at 100% tone would have no space between the edges of adjacent cells, while 0% tone would represent a smooth surface, with no cells engraved. In practice, cells specified at 100% tone must have at least some areas between cells in order to support the doctor blade during doctoring. It is also very difficult to control the spacing with such small cells, so even cells specified at 100% tone may have up to 20% of “bridge” area, i.e. non-engraved areas between cells. This is also called the cell wall.



Fig. 5.8: Electromechanical engraving Machine

### c. Laser Engraving Process

Laser engraving is considered as a highly advanced technology. The laser engraved cell has several advantages over EME. Because of the “bucket” shaped cell, as opposed to the inverted

pyramid cells produced by a diamond stylus, Laser has the ability to transfer the ink in a more uniform and economical fashion. The laser engraving method has ability to deliver very precise shapes that conform to the outline of the desired image, therefore creating extremely fine detail pattern in small font text or vignettes, for example. LE cylinders minimize the transfer of high ink volume with the improved cell geometry because the depth of engraving cells is reduced by this engraving process. The smoother ink-layer leads to a uniform and high-quality ink application to the substrate, and half-tones are reproduced with better nuance and contrast. This latest method is capable to engrave in the speed of 70 kHz [99,100]. Therefore, laser-engraved cylinders are increasingly in demand for high-quality packaging. However, the process is still very expensive.

A laser beam is used to remove material from the surface of the cylinder, creating recessed areas that will hold ink. The laser used in the engraving process is typically a carbon dioxide (CO<sub>2</sub>) laser, which produces a focused beam of infrared light that is powerful enough to vaporise the metal on the surface of the cylinder. The laser beam is controlled by a computer, which directs it to create the desired pattern on the cylinder. The cylinder is rotated as the laser beam moves across its surface, creating a continuous pattern that may be used to print images onto paper or other materials. The depth and width of the engraved areas are carefully controlled to ensure that the ink will be applied evenly and consistently during the printing process. Once the engraving is complete, the cylinder is typically coated with a layer of chrome or nickel to protect the engraved pattern and improve its durability. The finished cylinder is then ready to be used in a printing press, where it will transfer ink onto paper or other materials to create the final printed image. The indirect laser engraving process uses a light-sensitive black layer applied to the surface of the copper layer of the gravure cylinder for engraving purposes.

In gravure cylinder manufacturing companies, the cylinders are washed and the chrome or copper layers are removed for reuse in engraving and printing. After the layers are removed, a thin layer of chrome is applied to the engraved copper-based cylinder to protect the etched surface during the printing process. Gravure cylinders are long-lasting and can be reused after printing, but only after the chrome and copper layers are removed and replated. The steel base can be reused when the cylinder is no longer required for the printing process. This study has followed EME method for cylinder preparation.

## **5.2 The Gravure printing Unit**

### **○ Gravure Cylinder:**

The first step of this printing process is to prepare a cylinder with an image or design for each color using a diamond stylus or laser. This cylinder is a type of tube manufactured from steel and coated with copper to create an engraved design. The circumference of the cylinder is measured depending on the layout of the job. The quantity of ink that flows or is transmitted to the substrate during printing is influenced by the depth and size of the etched or engraved cells. These cylinders can be reused by removing the copper layers and then applying a fresh layer of plating and polishing the surface.

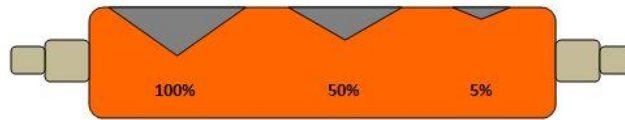


Fig. 5.9: Gravure cylinder

○ **Ink Metering:**

As the cylinder starts to rotate, the engraved cylinder is flooded with ink. The doctor blade acts as a squeegee removing excess ink from the non-printing areas of the cylinder before it makes contact with the substrate. It helps to transfer the right amount of ink to the cells. The doctor blade is a simple device made by stainless steel, plastic or nylon or composite materials. The thickness of the doctor blade is usually between 0.15-0.25 mm [93]. The blades must be positioned at an angle, but pressure and angle must be carefully adjusted to protect the cylinder surface. The doctor blade also helps to control the thickness of the ink film applied to the cylinder. This is important to maintain print density and to achieve high-quality prints.

Impression roller that is covered by rubber material, helps to bring the substrate in contact with the engraved cylinder, resulting in proper ink transfer. The pressure and speed of the printing press determine the right amount of ink that is transferred to the engraved cells. At suitable nip pressure and doctor blade pressure, reduction in viscosity results in reduction of ink thickness on the gravure cylinder and hence less volume of ink is transferred to the substrate.

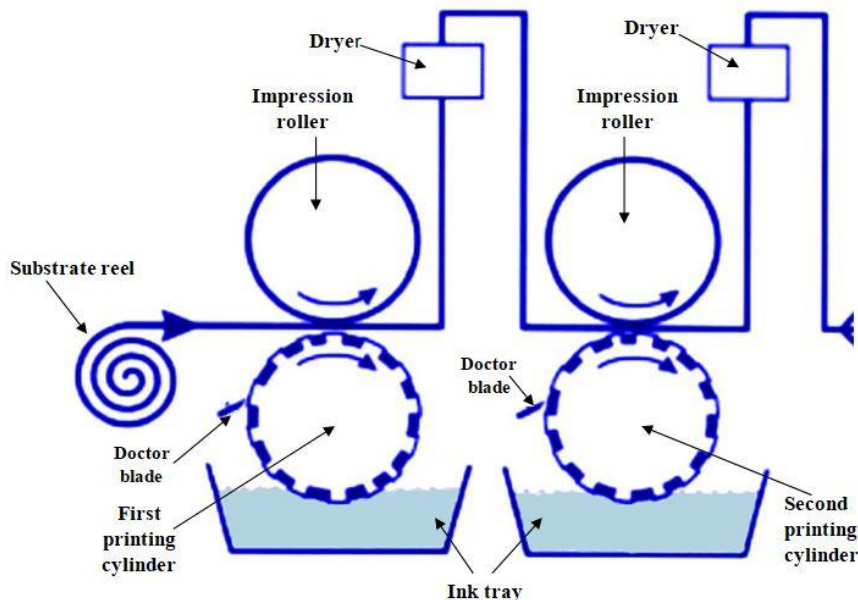


Fig 5.10: Gravure printing unit

○ **Drying System:**

In the gravure printing process, a drying system is essential to ensure that the ink on the

substrate is dried quickly and efficiently. The drying system is typically comprised of two main components: the dryer and the exhaust system. The dryer is responsible for providing the sufficient heat to the substrate and evaporating the solvents in the ink. The most commonly used dryer in gravure printing is the hot air dryer, which uses a series of fans and heaters to circulate hot air over the substrate. The temperature and speed of the hot air can be adjusted to suit the particular requirements of the printing job. The exhaust system is responsible for removing the evaporated solvents and fumes from the printing area. This is important for the health and safety of workers as well as for maintaining the quality of the printed product. The exhaust system typically consists of a series of fans and ducts that remove the solvents and fumes from the printing area and vent them outside the building. Overall, the drying system in gravure printing plays a crucial role in ensuring that the ink is dried quickly and achieving high quality job. The drying chamber is utilized to dry the ink on the substrate before it moves on to the next printing unit. The capacity of the dryer is determined by factors such as the printing speed, ink type, and printing sample volume. For low-speed gravure machines, a cold air blower is typically used as a drying system. Alternatively, a steam-heated dryer can be used to heat the substrate, followed by cooling with a cold chill roller at the machine's exit.

### 5.3 GRAVURE PRINT PARAMETERS

The gravure printing process has attracted great attention recently because of its high resolution, large throughput, and low cost. This is a versatile printing process used for printing graphics on products ranging from magazines and packaging to wallpaper. Print quality plays a major role in the product sale in packaging industry. Many factors affect the final printed product. These factors can be classified in five main categories as prepress, cylinder engraving, substrate properties, ink and process. The control parameters may include cell geometry, ink viscosity, press speed, impression pressure, hardness and doctor blade etc.

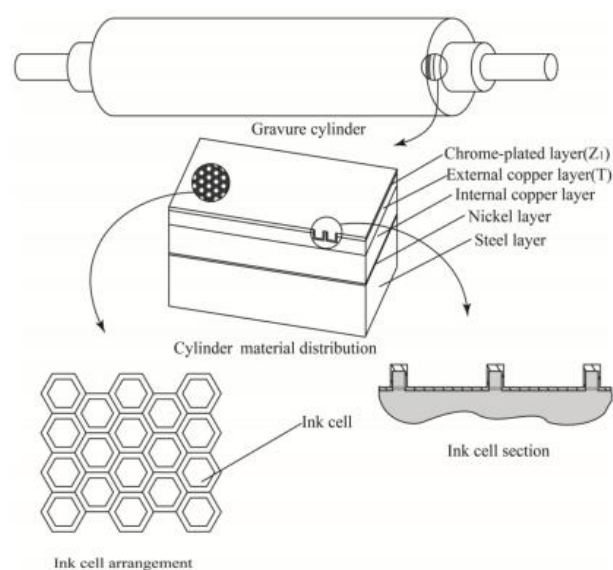


Fig 5.11: Microstructure of Gravure Cell [97]

### ❖ Cell Geometry:

Gravure printing is a printing process that uses a cylindrical printing plate with recessed cells or dots that are filled with ink and transferred to the substrate. The cell geometry determines the quality of printed quality and pattern. The optimization of the ink release is determined by the cell geometry which includes the cell shape, depth, opening, cell wall, cell channel, screen ruling etc. Hence the cell geometry plays a vital role in right amount of ink transfer [96,101,102]. A cell is comprised of two walls, one channel and one opening. The cells are further divided into three types - the conventional cells (constant opening and varying depth), the auto-typical cells (constant depth and varying openings) and half auto-typical cells (varying opening and depth with constant aspect ratio as per the application) [96].

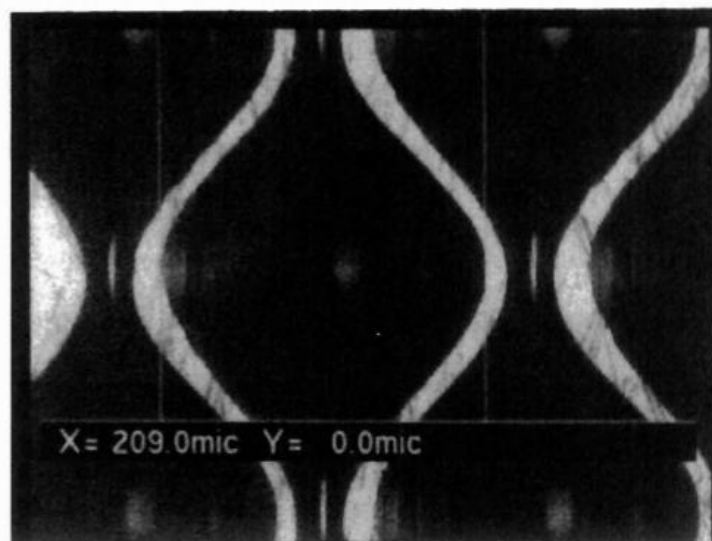


Fig 5.12: Cell and Cell wall [101]

### ❖ Line screen:

The screen rulings are defined as the number of rows of cells per linear inch, or centimetre. The choice of line screen is determined by the type of artwork to be printed along with the ink, or coating and the substrate. The more rows, or lines per inch/cm results the higher the resolution of the printed image [101].

### ❖ Cell Angle and Cell Shape:

Electromechanical engraving process is used to engrave the cells with a diamond stylus. The basic shape of the cells is determined by the geometry of the stylus. Generally, the cells are formed in pyramid shape by EME. The cells are made of different cell angles like 30°, 45° and 60° [103]. The cell angles control the cell shape and cell depth. At a cell angle of 30°, the vertical width of the cell is less than its horizontal width. At a cell angle of 45°, the vertical

width is equal to the horizontal width, while at a cell angle of  $60^\circ$ , the vertical width is greater than the horizontal width [101]. Fig. 5.5 shows the cell angles and the cell shapes formed.

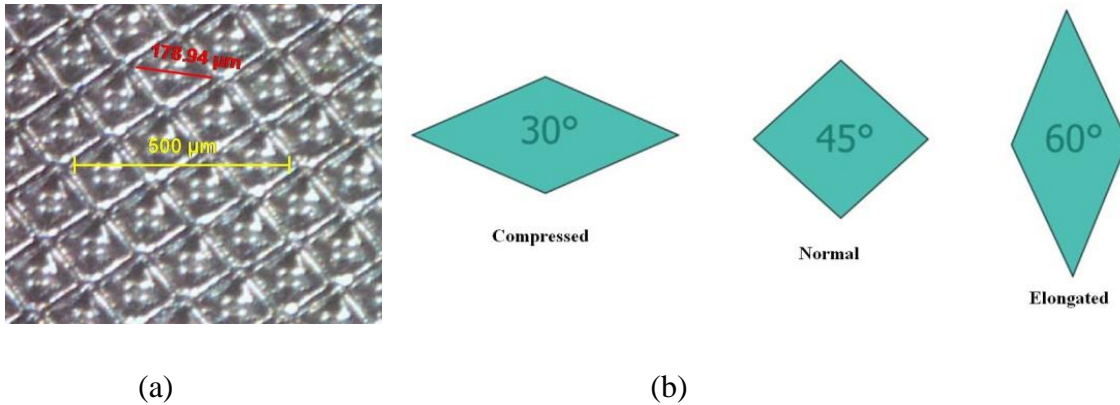


Fig. 5.13: (a)Pyramidal Electronic Engraved Cells [98] (b) Cell angle of compression [101]

#### ❖ Cell Depth:

In the EMA process, the gravure cells are engraved with a diamond stylus, giving the cells an approximately pyramidal shape. As shown in Fig. 5.6, the angle of the stylus is used to engrave a variety of angular depths. As the angle of the stylus decreases, the cell depth increases [101].

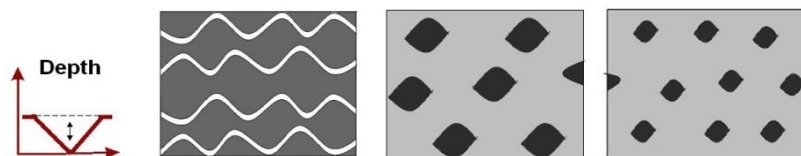


Fig. 5.14: Varying Cell Depth for Highlight, Middle-tone and Shadow [96]

#### ❖ Cell Size:

Cell size is also defined to as cell opening. The opening for round cells is expressed in diameter while diagonal for square cell. Cell units can be varied in size, shape and cell depth not in amount per square inch. Cell size has a great impact on ink release capacity of gravure cylinder. Range of tonal gradation also depends on the cell size variation from 0 to 100%. In half auto typical engraving cylinder, larger opening with shallower depth leads to minimize ink transfer from a cell. The larger cell opening transfer the higher volume ink coverage on the substrate while smaller cell opening are responsible for adequate ink fill and release. Besides, too large opening of a cell may affect its capacity to hold ink resulting in dirty printing [102,104].



### ❖ Cell Wall:

A gravure cylinder consists of many tiny cells. These cells are separated from each other by a border known as cell wall. Cell walls are considered as the non-printing areas that provide a plane surface for the doctor blade. The doctor blade rides on the cell walls to wipe the excess ink from the surface of the gravure cylinder. The amount of ink film thickness on the substrate is determined by the thickness of the cell wall [105,106]. In highlight areas of an image, the cells are shallow and the cells are separated from the neighbouring cell by a thick cell wall. Shadows or dark regions of an image comprises of many deep, wide cells which are surrounded by thin cell walls. For example, cells with 200 microns wide may have wall thickness of only 5 to 10 microns. Depending on the form of the cells and the engraving process the cell walls can vary a lot. The cell walls and the other non-printing areas together are defined as the gravure cylinder's land area [98].

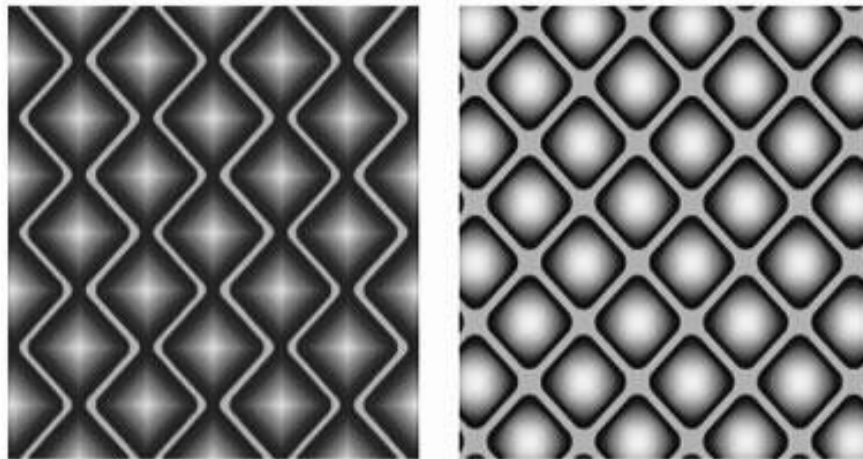


Fig. 5.15: Thin cell walls for shadows (L) and thick cell walls for highlights (R) [105]

### Aspect Ratio:

In gravure printing, the aspect ratio of the cell depth refers to the ratio of the depth of the cells to their width. The cell depth is the depth of the engraved recesses on the surface of the gravure cylinder, which hold the ink that is transferred to the printing substrate. The aspect ratio is an important parameter in gravure printing, as it determines the amount of ink that can be held by the cells and transferred to the substrate. A higher aspect ratio results in deeper cells that can hold more ink, which can lead to a higher ink transfer and a higher image quality. However, higher aspect ratios can also lead to increased dot gain and difficulty in controlling ink transfer, which can result in lower print quality. The ideal aspect ratio for a particular printing application depends on various factors, such as the substrate, ink, and desired print quality. Typically, aspect ratios in gravure printing range from 1:1 to 2:1, with higher ratios being used for printing on absorbent substrates and lower ratios for printing on non-absorbent substrates. The ratio of a cell's depth to its diameter, known as the aspect ratio (AR), plays a crucial role in how ink, cell, and substrate interact with each other.

The ability to release and fill ink is determined by the aspect ratio. When printing on low-quality substrates, a shallow cell with an  $AR < 0.1$  can lead to issues such as uneven ink transfer, skipping of dots, ink drying, and a doughnut effect on the print. On the other hand, for high-grade paper or foils, an  $AR < 0.5$  can result in similar problems. Therefore, the ink release increases with the aspect ratio. However, if the aspect ratio exceeds 0.5, capillary forces prevent the ink from being released, and the cell remains empty due to excessive depth. To control the aspect ratio, it is necessary to maintain a self-sufficient relationship between the cell's depth and diameter by adjusting the type, angle, and distance travelled by the engraving stylus [94].

### 5.3.1 GRAVURE INKS

Different types of printing inks are used for different printing processes starting from paste ink to liquid ink options. The formulation of a printing ink must take into account the type of the printing process, press speed, the type and characteristics of the substrate, the end use and desired appearance of the final printed image. It also varies according to the properties of ink like gloss, chemical resistance, heat resistance etc. Printing inks are made of three basic types of ingredients: colorants (pigments/dye), vehicles and additives. Colorants determine the desired color of the ink, including its hue (color shade) and strength, and also affect physical properties, such as fluidity (rheology), opacity or transparency, fastness and different resistance. Solvent and resin-based vehicles serve as carriers for the pigment in the printing process and ensure its adherence to the substrate. Additives, which encompass a wide range of ingredients such as waxes, plasticizers, antioxidants, lubricants, rheological agents, driers, and curing agents, are incorporated into the ink to provide specific characteristics. Gravure printing involves the transfer of ink from the engraved cylinders onto the substrate, creating an embossed effect. The gravure ink and flexo ink are liquid in nature having lower viscosities with respect to offset inks. Inks are formulated with different resins and additives for different substrates even though printed with the same process [93,94].

#### ❖ **Ingredients of Ink**

Gravure inks can be categorized as solvent-based or water-based inks. Solvent based inks contain organic solvents which can dissolve wide range of resins. Gravure inks also are differentiated according to the printed product like: 'Publication gravure' (magazines, catalogues) and Packaging gravure. Mostly the solvents such as ethanol (ethyl alcohol), isopropanol, ethyl acetate, acetone and water (also in combination with an organic solvent, generally alcohol) are used for gravure package printing. Hydrocarbon solvents are not used in packaging gravure but esters and alcohols are widely preferred. Water-based gravure ink offers less fire hazards in the press room and the special requirement is required to achieve for fluidity. However, solvent based inks are used for films and foil for providing suitable adherence. Gravure inks are generally viscose in nature and reduced down to the press viscosity by adding appropriate solvents. Viscosity is important factor



while using solvent based inks and needs to be constantly monitored and controlled. The viscosity is controlled by adding a compatible solvent in to the ink whose composition may change according to the press speed.

The typical gravure liquid ink is manufactured by the following ingredients: [94]

- i) Pigment - 4-12%
- ii) Extender pigment-0-8%
- iii) Resin-10-30%
- iv) Solvents-40-60%
- v) Additives-2-10%

➤ **Colorant:**

The colorant or pigments absorbs a specific range of wavelength of white light and reflects other wavelengths. Pigments are made in different sizes and shapes. The pigments are of two types i.e. organic and inorganic. Phthalocyanine blue, such as Pigment Blue 15, is the most common organic blue pigments in inks. The pigments like Lithol Rubine 4B, lithol reds (e.g. Pigment Red 57: 1) are most important magenta colorant in inks. Diarylide yellows and lake yellows are used as the principal yellow pigments in gravure inks.

➤ **Resins:**

Resin is the ingredient of ink that helps to bind the ink to substrate forming a uniform layer. It is also used for improvement of dispersion process by increasing pigment wetting. When varnish is laid on substrate, resin should form an even thin layer after evaporation of solvent. Resins imparts the properties of adhesion, flexibility, gloss and resistance characteristics. A typical ink may contain more than one resin for fulfilment of the properties and the selection of particular resin is a function of substrate, products use, type of solvent, printing factors and cost. The ideal resin would have a low molecular weight, high softening point, a rubbery or plastic transition state and a flexible and adhesive film property. For different packaging substrates, resins may include maleic resin, cellulose nitrate, acrylic resins, polyurethane resins and polyamide resins. But Nitrocellulose (NC) is the most important and most widely used vehicle for blister foil gravure printing.

➤ **Solvent:**

Solvent is used as the major component in liquid inks contributing to almost 70% of ink's volume. The solvents in gravure process have very low boiling points in the range of 70<sup>0</sup>C to 120<sup>0</sup>C. The selection of solvent depends on pigment type, resin system, substrate, press speed and end use properties needed. The hydrocarbon solvents such as Toluene and Xylene are generally used that give good print quality for publication. But these are avoided for packaging, specially for food or medicine packaging. The solvents also function as a lubricant which avoids wear of printing cylinder [94]. Food and

pharmaceutical packaging in particular use ester, alcohol, ketones or their combinations as cosolvent. Flammability of the solvents used needs special attention for gravure inks.

➤ **Additives:**

A wide variety of different chemicals are used in the ink mixture to solve specific printing and end user problems. Some additives provide essential properties such as stability by improving wetting or decreasing flocculation and additional end use properties. Dispersion and surface-active agent are incorporated for easier pigment wetting [94]. The additive increases the ink's wettability factor on plastic films and reduces the chances of pin-holing.

❖ **Properties of Ink:**

a) **Viscosity**

Viscosity is the resistance to flow of a liquid. Viscosity has the major impact on print quality. Generally, the gravure ink is typically lower viscous ink. The viscosity of the ink typically falls within the range of 15 to 25s Zahn Cup No.2 at 25<sup>0</sup>C, but may vary depending on various factors such as the press conditions, the speed of evaporation, the rheological characteristics, the depth and shape of the cell, the type of substrate used, and the design parameters, all of which can influence the viscosity of the ink [94].

Viscosity is the characteristic which affects the most in gravure printing and needs to be constantly monitored and controlled by the press operator. Viscosity depends on solid to solvent ratio of an ink. When the solvent is reduced, solid content of an ink increases, the viscosity increases. Moreover, solvent acts as a lubricant between the doctor blade and gravure cylinder thus minimizing cylinder wear on these components. An ink with high solid content can also damage doctor blade. The solid contents used in ink formulations remain constant while solvent causes the change in viscosity. When the viscosity is low, the lower force has to be applied to the blade that helps to reduce wear rate. The solvents used in gravure ink have very low boiling point. The evaporation rate of solvent is high due to heat from the dryer that result in increased viscosity. The change in viscosity affects the fluidity of ink and resists the flow of ink. This resistance to flow generates problem while filling and emptying of cells leading to cell clogging and missing print. Also, high-viscosity ink fills the engraved cell of the gravure cylinder and forms a concave meniscus, which leaves air space between the ink and substrate. Trapped air prevents ink from spreading evenly, causing it to spread outward and creating a "doughnut" effect. This effect deforms the dots, resulting in a larger dot perimeter [94,98,107]. On the flip side, if the viscosity is low, ink comes out of cell very easily and spreads on the substrate which results in dot deformation and crawly pattern. Gravure printing inks are generally supplied at higher viscosities than those used for printing. It allows the printer to adjust the viscosity and solvent balance according to press application. Moreover, the low viscosities used for gravure printing press can give rise to pigment settling on storage. Thus, higher viscosity ink supply will minimize this property [94].

### **b) Dispersion:**

The dispersion of ink is an important characteristic of the ink that affects flow properties and mottle of inks. The processing of dispersion refers to a considerable influence and interdependence between the pigments, binders, and other components of the ink throughout the liquid medium. Therefore, dispersion of pigment into vehicle during ink manufacturing is crucial. Level of dispersion depends on desired end use and affects properties such as gloss, color strength, thixotropy, and transparency [94].

The ink must have good dispersion properties for even transfer and production of a consistent image. The dispersion process includes breaking down the pigment particles to a small size and dispersing them uniformly throughout the liquid medium. This is typically done by the use of milling equipment, such as a three-roll mill, high-speed stirring or a bead mill. For pigment chip manufacture, the initial premixing of pigments and resins may be done in z-blade mixers. Then the materials are transferred in a two-roll mill. A plastic sheet is produced which is then cooled and the dried sheeted dispersion becomes very brittle. The chips are prepared by high output cutting mill with special care as nitrocellulose dispersion is explosive in nature. Then the chips are added to resin and solvents in high-speed disintegrating head disperser. The alternative way to produce pigment chip dispersion is to use Banburry mixer. The goal is to achieve a uniform particle size distribution and prevent agglomeration, which can lead to good print quality. To ensure proper dispersion, ink manufacturers often use a combination of milling techniques and additives such as dispersants to achieve the desired particle size and distribution. By carefully controlling the dispersion process, manufacturers can produce inks that provide consistent performance and high-quality printing results. The dispersion technique is selected based on the intended usage characteristics and demands of the ink [94].

### **c) Drying Speed:**

The drying speed of an ink is a most important factor to achieve desire print quality. The gravure printers run at higher speed that demands quick drying of an ink. The ink which is slow drying speed may lead to trapping, pick-offs, dot skips, patterns on machine rollers, retaining solvent in the final print and set off etc. Alternatively, too fast drying speed may give cell clogging, screening, skinning and other printability problems. The drying speed of gravure ink depends on the choice of solvent, resin system, substrate, and efficiency of dryers [93,94]. In case of multi-color printing, the first ink printed must be dried fast before the second ink is printed over it. To avoid rewetting problem, careful selection of resins and solvents are needed.

#### **5.3.1.1 Foil Ink**

Blister foil ink refers to the type of ink that is used to print on blister packaging material. Blister foil is extensively used in packaging both unsupported and as a laminate to paper and paper board. Blister foil packaging is a type of packaging

commonly used in the pharmaceutical industry to package tablets, capsules, and other small items. Blister foil ink is highly suitable for surface printing on aluminium foil. This foil ink is specially designed to be attached to the surface of blister packaging material, which is often made of aluminum foil or plastic. The ink is also designed to be resistant to water, chemicals, and other substances that the blister packaging may come into contact with during transportation or storage. Blister foil ink is typically formulated with high-quality pigments and resins that provide excellent adhesion and durability. Some formulations of blister foil ink may also include additives that provide additional properties, such as anti-microbial or anti-static properties. Overall, blister foil ink is an essential component in the production of high-quality blister packaging, as it ensures that the packaging material is clearly labelled and that the information remains legible throughout the packaging and transportation processes.

To make foil ink for gravure printing, nitrocellulose is altered using melamine resin to create properties that resist heat and promote adhesion. Another method for achieving adhesion to the surface is by using plasticized nitrocellulose that has been modified with polyvinyl butyral. The ingredients for making ink for aluminium foil consist of pigmented chip (60% nitrocellulose), maleic or shellac varnish, alcohol-soluble polyamide, nitrocellulose varnish, micronized polyethylene wax, plasticizer, n-propyl alcohol, and ethanol n-propyl acetate. This information on foil ink formulation is from a source [94]:

50% of pigmented nitrocellulose chip:	25.0
Polyvinyl butyral:	4.0
Dioctyl phthalate:	4.0
Wax dispersion:	3.0
Ethanol:	54.0
Isopropyl acetate:	10.0
	-----
	100.0

To achieve stable color printing on blister foil substrate for medicine packaging, it is necessary to use the gravure printing process and foil ink. The printed portion on blister foil is not easily removable by external factors such as air, water, or heat, making print stability crucial. Print stability factors need special consideration as medicine packages can be easily stored in deep freezers/ dark conditions etc.

### **Characteristics and type of substrates.**

Gravure is a printing process that involves etching an image onto a metal cylinder, which is then used to transfer ink onto a substrate. The characteristics and type of substrate used in gravure printing can vary depending on the specific application and desired results.

Characteristics of Substrate:

The substrate used in gravure printing should ideally have a smooth surface, which will ensure that the ink is evenly distributed across the surface. The substrate should also be able to absorb the ink well and prevent any smudging or bleeding of the ink. The color, texture, and weight of the substrate may also be important factors to consider, depending on the specific application.

#### Type of Substrate:

Gravure can be used to print on a wide range of substrates, including paper, plastic, metal, and fabric. Some of the most common substrates used in gravure printing include:

**Paper:** Gravure is commonly used to print high-quality images on paper, such as in magazines, catalogs, and packaging.

**Plastic:** Gravure can be used to print on a variety of plastic materials, including polyethylene, polypropylene, and PVC. This makes it a popular choice for printing on plastic bags, labels, and packaging.

**Metal:** Gravure can be used to print on metal substrates such as aluminum foil, which is often used for packaging and labels.

**Fabric:** Gravure can be used to print on fabric materials such as cotton, silk, and polyester. This makes it a popular choice for printing on clothing, textiles, and other fabric-based products.

**Blister Foil:** Blister foil is a type of packaging material that is commonly used to package pharmaceuticals, foods, and other consumer goods. It consists of aluminium foil often laminated with plastic film or sheet, usually made of PVC, PET, that is coated with a layer of heat-sealable cover. The cover layer provides a barrier against moisture, oxygen, and other environmental factors that could damage the contents of the package. Blister foil can be printed using the gravure printing technique to add branding or other graphics to the packaging material. The printing is typically done on the coated layer of the foil, which provides a smooth and even surface for the ink to adhere to. Gravure printing is a high-quality printing process that can produce sharp, clear images with fine detail and vibrant colors. Blister foils are preferred for pharmaceutical package printing for its chemical resistance, impermeability to air and water, light weight, flexibility and other characteristics.

Overall, blister foil and gravure printing are popular combinations for creating high-quality, visually appealing packaging for a wide range of products. The choice of substrate in gravure printing will depend on the specific application, desired results, and capabilities of the printing equipment. Hence, in order to achieve desirable color printing intensity and variation in color dots on blister foil substrate for medical packaging, it is essential to utilise the gravure printing process and foil ink. Unlike other printing methods, the printed portion on blister foil cannot be easily erased by external factors such as air, water, or heat. Due to the reliable print stability of blister foil, medicine packages can be stored in the deep freezer or in any other required location.

# Chapter 6

## CLASSIFICATION THROUGH SUPPORT VECTOR MACHINE (SVM)

### 6.1 Support Vector Machine

A Support Vector Machine (SVM) is a supervised learning model based on the principle of structural risk minimization, as defined by Cortes and Vapnik in 1995 [108]. It is particularly effective for solving binary classification problems, but it can also be extended to handle multi-class classification. Fig. 6.1 shows a schematic diagram of SVM. The basic idea behind SVM is to find an optimal hyperplane that best separates the different classes in the input data. The hyperplane is determined by maximizing the margin, which is the distance between the hyperplane and the closest data points from each class, known as support vectors. The support vectors are the important data points that affect where and how the hyperplane is positioned.

SVMs can handle both linearly separable and non-linearly separable data. In the case of linearly separable data, a linear SVM finds a hyperplane that completely separates the classes. For non-linearly separable data, SVMs use a technique called the kernel trick. The kernel trick transforms the input data into a higher-dimensional feature space, where it becomes easier to find a linear separating hyperplane. Popular kernel functions used in SVMs include linear, polynomial, Gaussian/radial basis function (RBF), and sigmoid.

Training an SVM involves finding the optimal hyperplane that maximizes the margin while minimizing the classification error. This is formulated as an optimization problem, where the objective is to minimize a cost function that penalizes misclassifications and maximizes the margin. The optimization process often involves solving a quadratic programming problem. Once trained, SVMs can be used to predict the class labels of new, unseen data points. The decision boundary of the hyperplane is used to make these predictions. SVMs have the advantage of being memory efficient and effective in high-dimensional spaces. They can handle datasets with a small number of training examples but a large number of features. SVMs have been widely used in various applications, including image classification, text classification, bioinformatics, and financial prediction. They are known for their ability to generalize well to new data and have good resistance to overfitting.

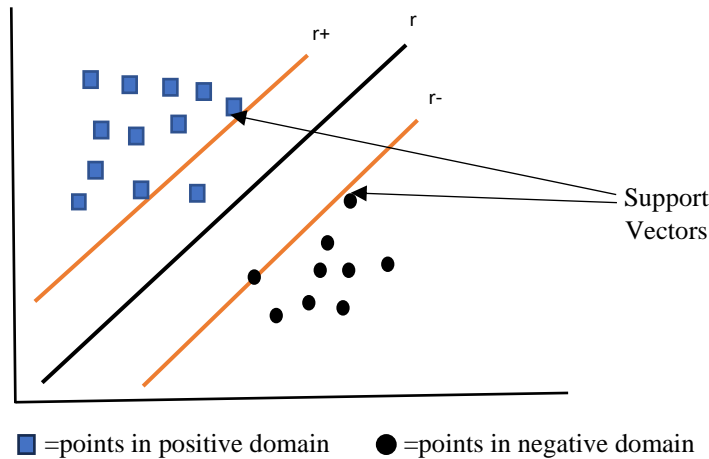


Fig 6.1: Schematic diagram image of SVM

### 6.1.1 Multiclass classification in SVM

Multi-class classification is a type of supervised machine learning task where the goal is to assign input data points to one of multiple possible classes. In this scenario, the problem involves distinguishing between more than two classes, unlike binary classification which involves only two classes [109].

To solve a multi-class classification problem, various algorithms can be used. Methods such as the following are examples of those that are regularly used:

**Logistic Regression:** Although logistic regression is primarily a binary classification algorithm, it can be extended to handle multi-class classification using techniques like one-vs-rest.

**Decision Trees:** Decision tree algorithms, such as CART (Classification and Regression Trees) or Random Forests, can be adapted to handle multi-class classification by making decisions based on hierarchical tree structures.

**Naive Bayes:** Naive Bayes classifiers, known for their simplicity and efficiency, can be applied to multi-class problems by using appropriate probability distributions and assumptions.

**Neural Networks:** Deep learning models, particularly neural networks with multiple output nodes, can be trained for multi-class classification and the multiple nodes representing as class. Techniques like soft-max activation function is commonly used to produce class probabilities.

**Support Vector Machines:** Support Vector Machines can handle multi-class classification by using strategies like one-vs-all, one-vs-one. These methods transform the problem into multiple binary classification tasks and combine the results.

There are several approaches to solve multi-class classification problems. [108]. Out of that, One-vs-One (OvO) is one of the popular techniques which is applied in this study.

**One-vs-One (OvO):** This strategy used in multi-class classification problems to train binary classifiers for each pair of classes. If there are  $N$  classes,  $N(N-1)/2$  binary classifiers



are trained. Each classifier is trained on a subset of the data that consists of only two classes, one as the positive class and the other as the negative class. During training, the data points belonging to these two classes are used to train the classifier, while the data points from other classes are ignored. To classify a new data point using the trained OvO classifiers, each classifier predicts the class label for the input. The class label that receives most votes across all the classifiers is selected as the final prediction. One advantage of the OvO strategy is that it can handle multi-class classification even when the base binary classifier is designed specifically for binary problems. Additionally, it can provide more refined information about the relationships between classes since it trains classifiers for all possible pairwise combinations.

Evaluation of multi-class classification models is typically done using metrics such as accuracy, precision, recall, F1 score, and confusion matrix, which provide insights into the model's performance across different classes.

Multi-class classification problems arise in various real-world applications, such as image recognition, text categorization, sentiment analysis, and medical diagnosis. The choice of algorithm and approach depends on the specific problem and the characteristics of the dataset. Fig. 6.2 shows a scatter plot of a binary classification and a multi-class classification. In this study one-vs-one approach has been used in multi-class classification.

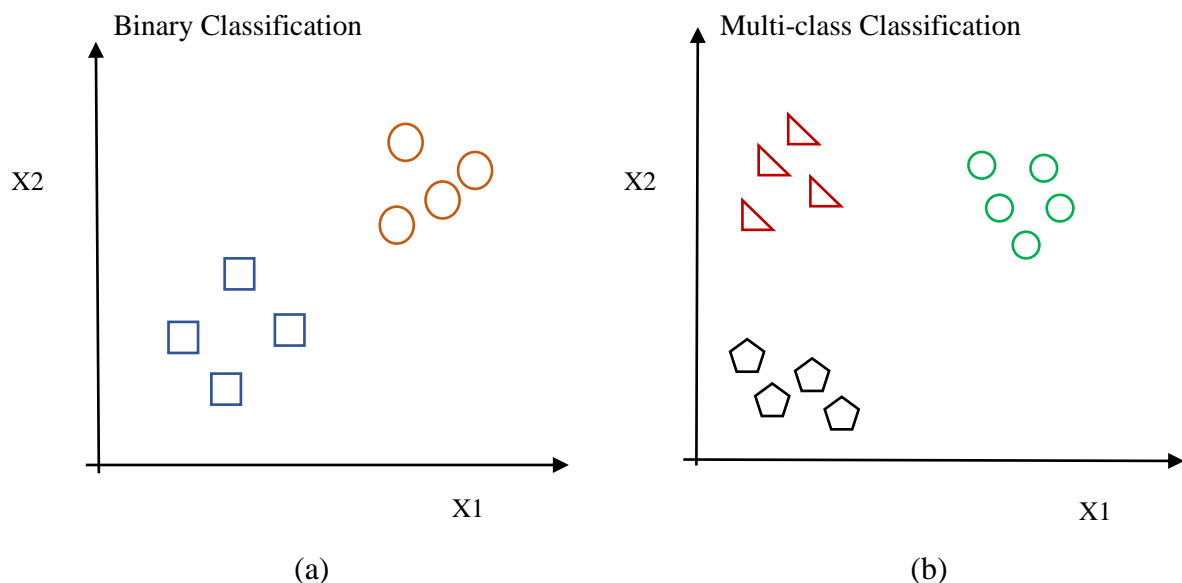


Fig 6.2: (a) Binary Classification (b) Multi- class Classification [109]

### 6.1.2 Type of SVM kernels

SVMs work by finding the best separating hyperplane that maximises the margin between the two or more classes. In cases where the data is not linearly separable, SVMs use kernel functions to transform the data into a higher-dimensional feature space where the data can be linearly separated.

Here are some of the most commonly used SVM kernels [110]:

The objective of SVM algorithm is to transform input data into a higher dimensional space and to construct an optimal line or decision boundary that can divide a n-dimensional space into classes, allowing to quickly classify new samples into the classification process.

Support vectors (SVM) labeled the training dataset explaining as [34,109]:

$$\{(x_1, y_1), \dots, (x_n, y_n)\} \in X \times \mathbb{R} \quad \text{Eq. (6.1)}$$

Where  $X$  represents the vector of input features. The output class labels ( $y_i$ ) belong to  $\{-1, 1\}$ . The input data for a non-linear SVM are transferred to a higher-dimensional space where the discriminating hyperplane can be generated linearly. A hyperplane is determined by solving the following optimization problem:

$$\underset{w, \xi}{\text{minimize}} \frac{1}{2} \|w\|^2 + C \sum_{i=1}^n \xi_i \quad \text{Eq. (6.2)}$$

with

$$\begin{cases} y_i((w, x_i) + b) \geq 1 \text{ with } b \in \mathbb{R} \\ \xi_i \geq 0 \end{cases} \quad \text{Eq. (6.3)}$$

Where:

- $\xi_i$  denotes the distance to the correct margin (find the max-margin classifier that perfectly separates the training data) with  $\xi_i \geq 0, i=1, \dots, n$ .
- $C$  indicates a regularization parameter (controls the trade-off of how well separated the data).
- $\|w\|^2$  represents the normal vector (hyperplane's slope).
- $x_i$  represents the transformed input space vector (dot product of training data).
- $b$  denotes a bias parameter.
- $y_i$  represents the  $i^{\text{th}}$  target value.

A kernel function might be used to add more dimensions to the raw data in a non-linear situation, making it linear in the resulting higher dimensional space. In the high-dimensional space, a kernel function  $k$  replaces the dot product in the nonlinear problem.

- Gaussian/Radial Basis Function (RBF) Kernel: The Gaussian/RBF kernel is a popular kernel used when the data is not linearly separable. This kernel allows SVMs to handle data that is not linearly separable by mapping the input data into a higher-dimensional feature space [34], where the data becomes linearly separable.

For kernels, like the Gaussian,  $K_{RBF}(x_i, x_j) = \left(-\gamma \|x_i - x_j\|^2\right)$  with  $x_i, x_j \in X$ , the corresponding feature vector is infinite dimensional. Gamma ( $\gamma$ ), which is determined by cross validation, scales the squared distance and it scales the influence on classification. In SVM the cross-validation consists to randomly split the set of observations into  $C$  number

of groups of equal size as per selected fold for cross-validation, in which the first fold treated as a validation set and the remaining C-1 groups being used to fit the algorithm. The gamma parameter controls the shape of the decision boundary and influences the flexibility of the SVM model. A small value of gamma makes the decision boundary smoother and leads to a more globalized model, while a large value of gamma leads to a more complex and localized decision boundary, potentially overfitting the training data. Selecting appropriate values for the hyperparameters, including gamma, is crucial for effective SVM classification. The optimal values depend on the specific dataset and problem at hand. Techniques such as cross-validation and grid search can be used to search for the best combination of hyperparameters.

- **Polynomial Kernel:** The polynomial kernel is used when the data has polynomial boundaries. It is defined as  $K(x_i, x_j) = (x_i^T x_j + c)^d$ , where  $c$  is a constant and  $d$  is the degree of the polynomial.
- **Sigmoid Kernel:** The sigmoid kernel is a non-symmetric kernel that is used when the data has a sigmoid boundary. It is defined as  $K(x_i, x_j) = \tanh(\alpha x_i^T x_j + c)$ , where  $\alpha$  and  $c$  are constants.

These are just a few of the most commonly used examples of the many SVM kernels available. The choice of kernel depends on the problem at hand and the properties of the data.

### 6.1.3 Validation Techniques for Multi-class classification SVM Model

Validation of Support Vector Machine highly depends on the training data and test data. Every time a SVM learning model is created, it needs to be fed with initial data to be trained. To determine how effectively the model operates and generalises over unknown data, it must subsequently be fed some unknown data (test data). The model is stable if it predicts accurately and consistently across a wide range of input data and performs well on untested data.

Cross-validation is a technique used in machine learning and statistics to assess the performance and generalization ability of a predictive model. It involves splitting the available data into multiple subsets or folds and iteratively training and testing the model on different combinations of these folds.

In general, this is how cross-validation works:

**Splitting the Data:** The original dataset is divided into  $K$  equal-sized folds, where  $K$  is typically chosen to be a value between 5 and 10. Each fold contains a roughly equal distribution of data points from the entire dataset.

**Iterative Training and Testing:** The model is trained on  $K-1$  folds (the training set) and evaluated on the remaining fold (the validation set). This process is repeated  $K$  times, with each fold serving as the validation set in each iteration. The goal is to ensure that all data points are used for both training and testing, providing a more robust evaluation.

Performance Evaluation: The performance of the model is measured using appropriate metrics (confusion matrix), such as accuracy, precision, recall, or mean squared error, depending on the specific problem. The evaluation results from each iteration are typically averaged or aggregated to obtain an overall performance estimate for the model.

k-Fold Cross-validation: This is performed by dividing the dataset into k equally sized folds. The model is trained and tested k times, with each fold serving as the validation set once and the remaining folds used for training.

Cross-validation is a valuable technique for model evaluation and selection, helping to assess the generalization performance of models and improve their reliability on unseen data.

#### 6.1.4 Confusion Matrix

A confusion matrix is a table-based tool for displaying the effectiveness of the prediction model. Each row in a confusion matrix indicates the number of predictions produced by the model. The confusion matrix compares actual and predicted values. A confusion matrix has dimensions N x N, where N represents the total number of classes or outputs. The diagonal elements indicate the number of points where the predicted label/data matches the actual label/data, whereas the off-diagonal elements represent the labels/data assigned incorrectly by the classifier. The confusion matrix's diagonal values should be greater, which denotes several accurate predictions [31-34].

The confusion matrix enables to compare the real (actual) target values with those predicted values by the SVM model to evaluate the model's performance and prediction errors.

Table 6.1- Confusion matrix		
	Predicted positives	Predicted negatives
Real positives	True Positive (TP)	False Negative (FN)
Real negatives	False Positive (FP)	True Negative (TN)

The formulas for P, R, and F<sub>1</sub> for each print samples are defined as:

$$P = \frac{TP}{TP+FP} \quad \text{Eq. (6.4)}$$

$$R = \frac{TP}{TP+FN} \quad \text{Eq. (6.5)}$$

$$F_1 = \frac{2}{1/P+1/R} \quad \text{Eq. (6.6)}$$

Where TP denotes the number of prints correctly assigned to the positive class, TN is defined as the number of prints correctly assigned to the negative class. FP represents the number of prints incorrectly assigned to the positive class (which is considered as a Type 1 error), and FN represents the number of prints wrongly assigned to the positive class (i.e

a Type 2 error). Precision shows what percentage of positive predictions turned out to be true. Recall shows what percentage of all positive samples the classifier correctly predicted as positive. It's also called True Positive Rate (TPR), Sensitivity, and Probability of Detection. For all data points, the accuracy score (Acc) is determined by dividing the number of true positives by the sum of true positives and false positives. The harmonic score  $F_h$  corresponds to the average value of the  $F_1$  score, as defined below:

$$A_{cc} = \frac{\sum_{i=1}^{N_p} TP_i}{\sum_{i=1}^{N_p} (TP_i + FP_i)} \quad \text{Eq. (6.7)}$$

$$F_h = \frac{1}{N_p} \sum_{i=1}^{N_p} F_{1,i} \quad \text{Eq. (6.8)}$$

Where,  $F_{1,i}$  is the  $F_1$  score of the  $i^{\text{th}}$  print sample, and  $N_p$  is the number of print samples.

### 6.1.5 SVM step by step process

Support Vector Machine (SVM) is a machine learning algorithm used for classification and regression analysis. It works by finding the optimal hyperplane that separates the data into different classes with the maximum margin. Here is a brief overview of how SVM works:

✓ Data Preparation:

The first step is to prepare the data for training the SVM algorithm. The data should be cleaned and pre-processed by removing any outliers, filling in missing values, and scaling the features to have a similar range of values.

✓ Feature Selection:

The next step is to select the most important features that can help to classify the data into different classes. This step is optional, but it can help to improve the accuracy and speed of the SVM algorithm.

✓ Training the Model:

The SVM algorithm tries to find the optimal hyperplane that maximizes the margin between the closest points from each class. The support vectors are the closest points from each class, and the margin refers to the distance between these points and the hyperplane.

The SVM algorithm works by finding the best values of the hyperplane parameters that minimize the classification error while maximizing the margin. There are several types of SVM algorithms, such as the linear SVM, polynomial SVM, and Gaussian Kernel /radial basis function (RBF) SVM.

✓ Testing and Evaluation:

Once the SVM model is trained, it can be used to predict the class of new data points. The SVM algorithm classifies the new data points by checking on which side of the hyperplane

they fall. The predicted class is then compared with the actual class to calculate the accuracy of the model.

✓ Tuning the Parameters:

SVM has several parameters that can affect the performance of the model, such as the kernel type, regularization parameter, and gamma parameter. Tuning these parameters can help to improve the accuracy of the SVM algorithm.

To put it briefly, SVM operates by identifying the best possible hyperplane that can divide the data into distinct classes while keeping the largest possible gap/margin between them. The SVM algorithm uses the support vectors to find the best hyperplane parameters that minimize the classification error while maximizing the margin. SVM can be used for classification and regression tasks, and it has several parameters that can be tuned to improve its performance.

## 6.2 Multiclass classification (M-SVM) model development to classify the Print sample on blister foil

### 6.2.1 Generate a classification model to differentiate print and reprint samples using SVM Multi-class classification model

- Feature Selection for our model

In this work, the cyan, magenta, yellow and black color tint dots have been examined under a microscope to provide microscale images of the specific dot percentage from color chart IT 8.7/3. Moreover, the dot descriptor index parameters of the dot patterns from printed and reprinted samples have been obtained using these printed microscale pictures of the specific dots. In chapter 8, the specific experimental findings have been given. The dot descriptor index parameters, eg. area, perimeter, circularity, eccentricity, solidity, major axis, and minor axis, are utilised as features input in our multi-class suggested model.

In the proposed study, two distinct types of samples—original print samples (P1, P2, P3) and reprint (simulated counterfeited) samples (R1, R2, R3)—have been classified using this model. Fig 6.4 shows the block diagram of multi-class classification SVM Input-Output.

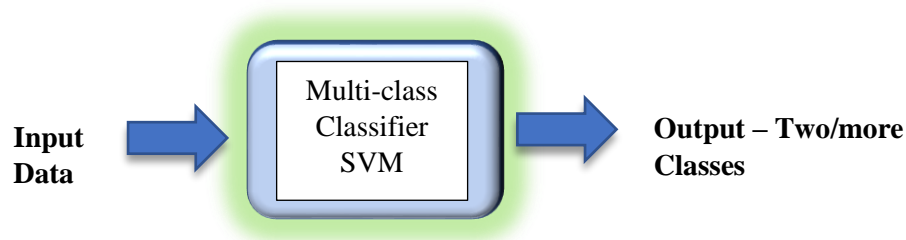


Fig 6.3: Block diagram of Multiclass classification SVM Input-Output

## 6.2.2 Cross – validation for training and testing the model

- Input Parameters:

In this study, the SVM model used six features as input parameters for each patch. The input features of area, perimeter, circularity, eccentricity, solidity, major axis, and minor axis have been used to create a multi-class classification model.

- Output Parameters:

The model classifies the print and reprint samples as two classes, for print samples (P1, P2, and P3) and reprint samples (R1, R2, and R3) as outputs for microscopic dots percentage on the basis of input feature parameters. The model classifies the print and reprint samples as two classes, for print machine P1, P2, and P3, and reprint machine R1, R2, and R3, as outputs for microscopic dots percentage on the basis of input feature parameters.

- Training and testing our model:

In this study, the ratio between the training and test sets has been set at 3:2, and selected from each color dot features. In this experiment, 6-fold cross-validation was utilised to evaluate kernels with gaussian and radical basis functions. For kernel selection in this proposed model, the Gaussian or Radial Basis Function (RBF) kernel (mentioned in Eq.6.1) is used for the input data as the corresponding feature vectors [34].

Here, the cross-validation process involves some steps in which the dataset is divided into 6 equally sized subsets, or "folds." The model is then trained on 6–1 fold and validated on the remaining fold.

Experimentally determined ideal cross-validation values are  $C = 6$ . Gamma ( $\gamma$ ), which is determined by cross-validation, scales the squared distance and it scales the influence on classification. Fig 6.5 shows Six-fold cross validation for Dataset – Print (P1, P2, P3) and Reprint (R1, R2, R3).



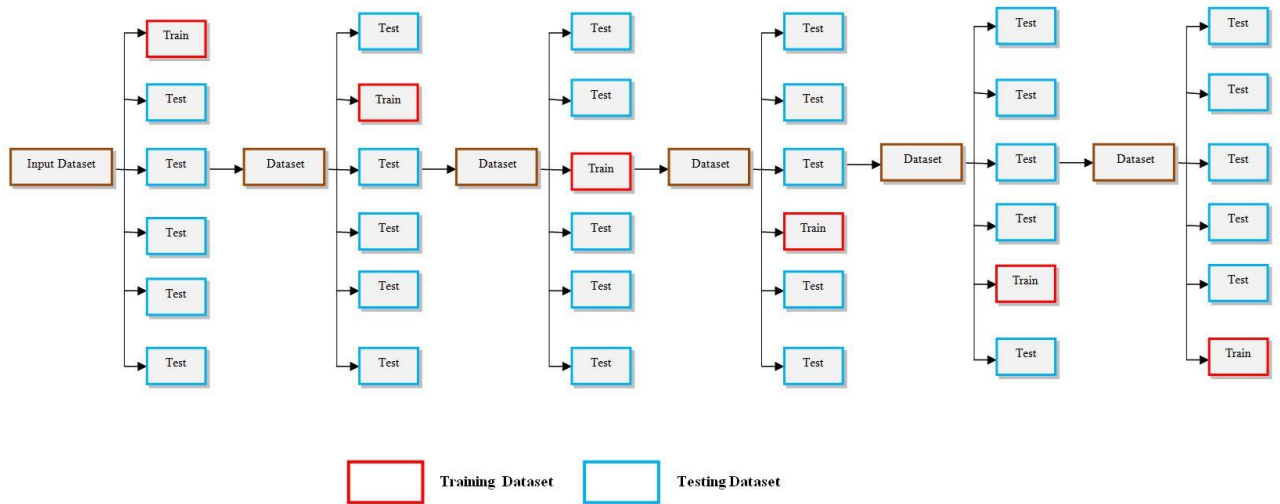


Fig 6.4: Six-fold cross validation for Dataset – Print (P1, P2, P3) and Reprint (R1, R2, R3)

### 6.2.3 Evaluation of proposed model

After the process of training, testing, and validation of the network, the obtained data have been evaluated by using confusion matrix. The confusion matrix then allows us to evaluate the performance and prediction errors of the SVM model by comparing the actual (real) target values to those predicted by the model. For the F1 score, we computed the harmonic mean between precision and recall, which both depend on false positive and false negative values. Precision P and recall R were used to determine the classifier's effectiveness.

### 6.2.4 Implementation

In this study, SVM multi-class classification model has been used to classify the dot structure parameters of printed sample to identify the print sample and reprint sample (shown in Fig 6.6). This study examines the dot patterns of printing at a microscopic size for gravure printing on foils substrate for three print machine P1, P2, P3. The purpose of this experiment is to distinguish an original print from a reprint sample (simulated counterfeit) printed on a blister foil using gravure printing process (the same gravure machine has been used; for clear understanding reprint sample named as R1, R2, R3). The methods, based on Support Vector Machine, is built using shape descriptor indexes of microscopic dots (print and reprint), with shape descriptor indexes serving as features in the model. For the classification purpose in this study, the SVM Toolbox of MATLAB (R2018a) software is used to design the proposed model. The model developed in this work consists of a multiclass classification (one vs. one) approach with a Gaussian kernel and cross-validation to evaluate the validation technique. This work presents the confusion matrices for the SVM-based categorization of print and reprint data from its dot shape descriptors index features parameter. In the Fig 6.6 shows a Block diagram of Multi-class SVM model in this study.

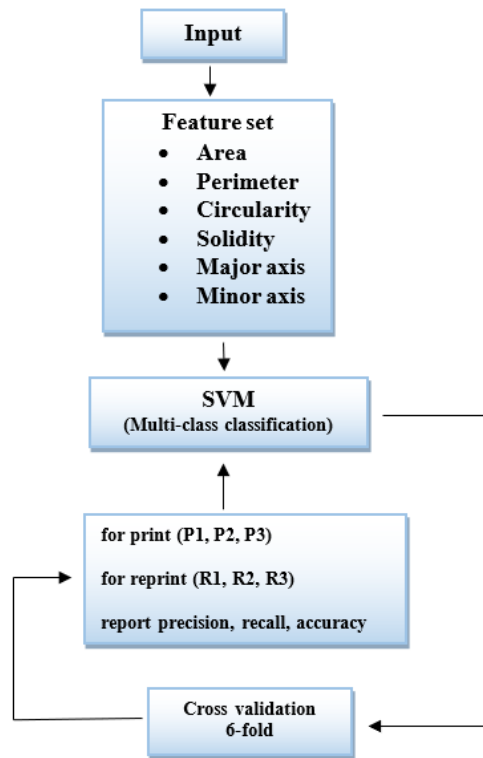


Fig 6.5: Block diagram of Multi-class SVM model in this study

In this study, MATLAB(R2018a) has been used for multiclass classification by SVM to classify the printed and reprinted samples. The scatter plot shows the decision boundary and explores the classification results visually. Once the training and testing has been completed, we evaluated the performance of the model using the "confusion matrix" and "accuracy" metrics.

In chapter 8, all experimental result images are shown for better understanding.

# Chapter 7

## EXPERIMENTAL PROCEDURE

### 7. Experimental Procedure

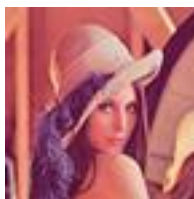
Various experimental techniques and data collection procedures related to this study have been outlined. The goal of the study has to assess the anti-counterfeiting security features using variable image watermarking and microscale dots on the blister foil using gravure printing, which is commonly utilized for medicine/food packaging.

In this study, blister foils are printed in Gravure printing process which are given as follows:

#### ❖ Source Artwork

- Images for Variable Image Watermark

In this study Four Host Images (HI) sizes of 1 inch x 1 inch with 600dpi resolutions (Lena, Baboon, Avion, Peppers) have been taken for the watermarking. Each of the images have been selected as host image one by one for the experiment. After embedding the information into these images, all watermarked images (HIW) have been engraved on cylinder using electro-mechanical engraving process. The experimental artwork has been shown in Fig 7.1



(a) Lena



(b) Baboon



(c) Avion



(d) Peppers

Fig 7.1: Source Images ((a)Lena, (b) Baboon, (c) Avion, (d) Peppers)

- IT8.7/3 color chart for Microscopic Dot Shape analysis

In this second part of this work, the study has focused on microscopic dot analysis print and reprint sample. In this study the artwork IT8.7/3 color target chart has been engraved as a reference image on the gravure cylinder by Electro-Mechanical engraving process. The reference image artwork IT8.7/3 is shown in Fig 7.2.

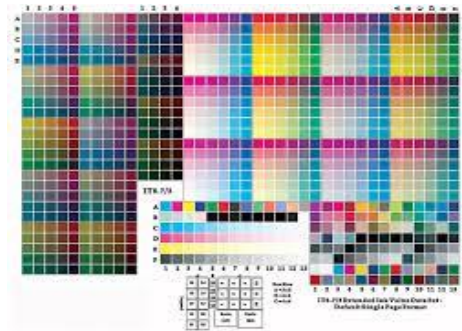


Fig 7.2: Reference image IT8.7/3 Color Chart [60]

The process involved taking the source images (depicted in Fig 7.1) and incorporating hidden information (watermarks) into them. These watermarked images have been then combined with a color chart (shown in Fig 7.2) to create the final artwork. The combined artwork for variable image watermark and microscopic dot shape analysis engraved on cylinder has been shown in the Fig 7.3

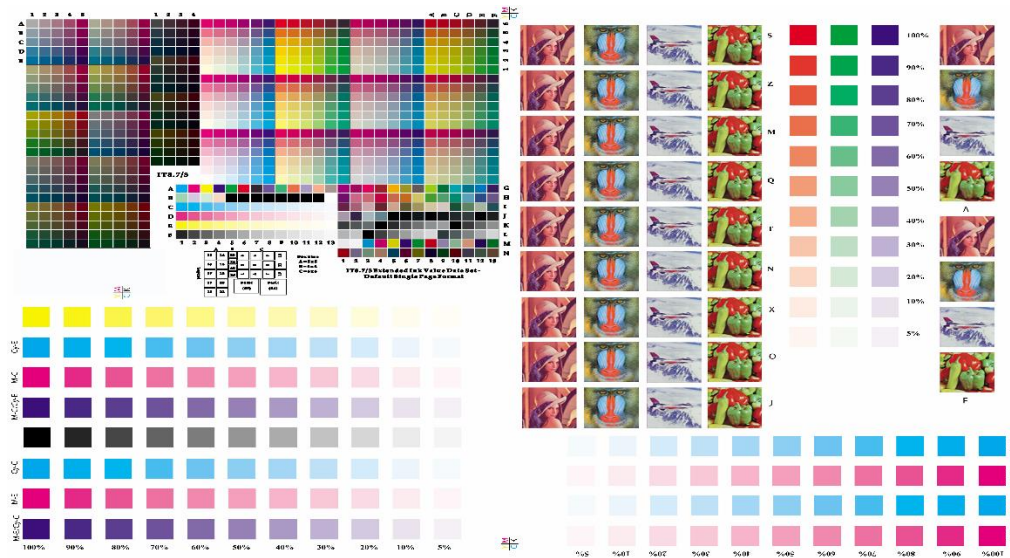


Fig 7.3: Combined artwork for variable image watermark and microscopic dot shape analysis engraved on cylinder

❖ **Engraving the Cylinder Pre-press parameters for the artwork**

For printing purpose four gravure cylinders have been taken for each four color (C, M, Y, K) and the final combined artwork has been engraved on the cylinders by electro-mechanical engraving process at specific LPI screen ruling, stylus angle and cell angle shown in Table 7.1. Before the gravure cylinder preparation (size: 300x534 mm) some parameters for the cylinder engraving have been set at the pre-press unit using Art-Pro software (shown in the Fig 7.4).

Table 7.1: Set parameters for engraving on Gravure cylinder

Color	LPI	Angle	Stylus	Channel	Wall	Volume
Magenta	150	30°	130	35	8	12.2bcm
Cyan	150	60°	110	4	8	12.0bcm
Yellow	150	45°	130	27	8	12.4bcm
Black	150	30°	110	30	8	11.2bcm

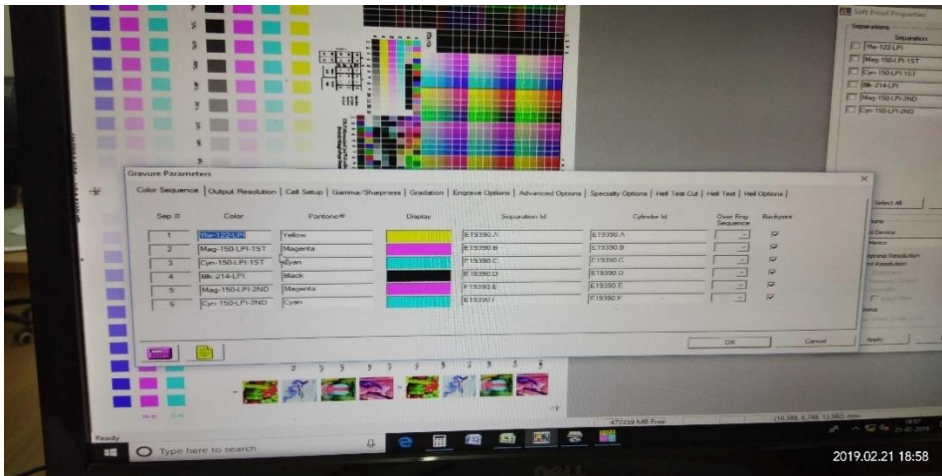


Fig 7.4: Gravure cylinder engraving parameters set in the pre-press using Art-Pro software

### ❖ Gravure cylinder engraving process

After setting the pre-press (Fig 7.4) parameters for engraving, the four cylinders (size 300x534 mm) have been engraved for four colors (cyan, magenta, yellow, black). The electro-mechanical engraving has been used to engrave the final combined artwork on the gravure cylinders (Shown in chapter 5 sec 5.1(b)). The Hell engraving machine shown in Fig 7.5 has been used to engraved the four cylinders with set of specific parameters.



Fig 7.5: HELL machine for cylinder engraving (electromechanical)

### ❖ Gravure machine unit in the printing press

During the printing of the samples, the printing speed, printing pressure, and doctor blade pressure have been kept constant (Shown in Table 7.2). And all the equipment, press, pre-press setup, software has been used same for the print sample and reprint sample (simulated counterfeited samples) analysis. Gravure machine unit has been shown in Fig. 7.6.

Table 7.2: Set parameters for Gravure printing

Parameters	Specification
Cylinder size:	300X534 mm
Gravure speed:	17MPM
Angle of doctor blade:	30°
Rubber roller pressure:	2.5 kg/cm <sup>2</sup> (for each unit)
Doctor's blade pressure:	1kg/cm <sup>2</sup> (for each unit)
Drying temperature:	50°C to 60° C

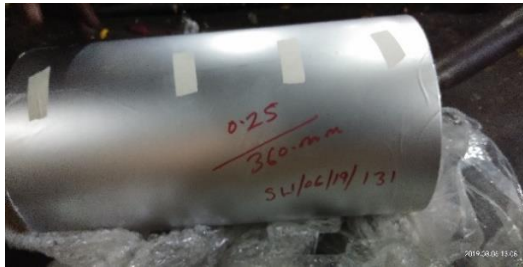


Fig 7.6: Gravure Printing press



❖ **Print substrate and ink**

- **Substrate:** The experiment has been carried out on the blister foil substrate, which is extensively used in the medicine and food packaging industry. The thickness of the foil is 25 $\mu$ . shown in Fig 7.7(a). It has two sides, matte and glossy. The matte side has been used to print the artwork for this study.



(a)

(b)

Fig 7.7: (a) Substrate blister foil (b) Printing on blister foil using engraved cylinder

- **Ink:** The solvent-based foil ink cyan, magenta, yellow, black have been used to produce the image on the blister foil. The specifications for the foil inks have been shown in Table 7.3. The detail composition of the foil ink has been shown in Chapter 5(section 5.3.1).

Table 7.3: Set parameters for foil ink

SAP Code	Description	Viscosity, Ford Cup 4@30°C	Unit of Measure
120000003560	DK0020-GR. FOIL BLUE	27 $\pm$ 5	Second
120000003587	DK0020-AL GV NEW MAGENTA	32 $\pm$ 5	Second
120000003599	DK0020-AL GV FOIL YELLOW	28 $\pm$ 5	Second
120000003538	DK0020-GR. FOIL BLACK	25 $\pm$ 5	Second

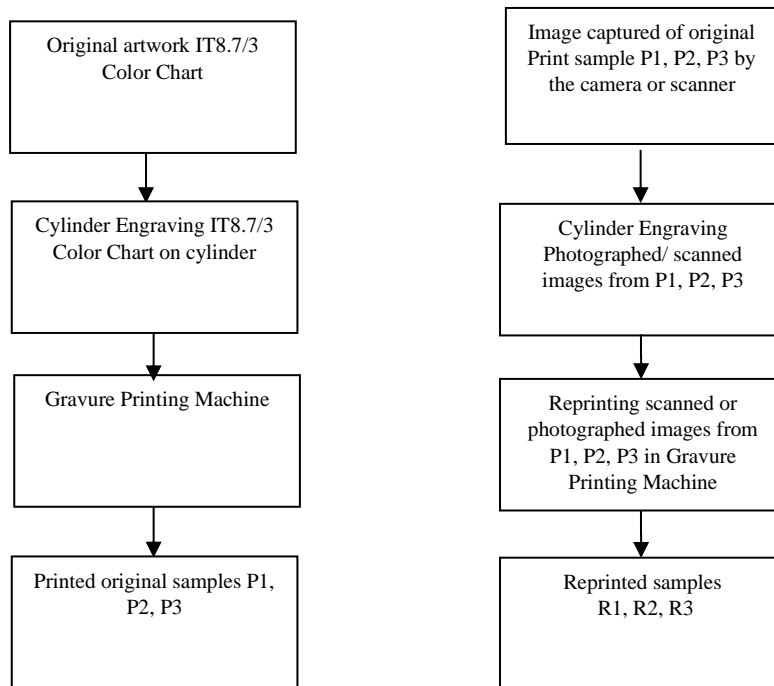
❖ **Capture/Scan and Engrave Reprint Cylinder for Simulate the counterfeiting process**

The printing and reprinting (simulated counterfeiting) process has been conducted under the same conditions to eliminate any impact of parameter changes on the output samples. The reference combo final art work image has been printed on blister foils utilizing CMYK colors, and the four images have been analyzed for variable watermarking to protect the expiry date (ED) and batch number (BN) from counterfeiting and using the color chart a series of color patches have been



examined for microscopic dot shape analysis. To ensure accuracy, each patch has been measured five times for the samples. To simulate the counterfeiting process of the print samples, different input devices, such as a digital camera, mobile camera, or scanner, have been unitized to capture an image of each print sample, which has been reproduce (reprint samples) from the three different gravure printing machines. The samples have been captured under controlled illumination conditions using various cameras in a lighting booth.

In the experiment, the process of printing and simulating counterfeiting has been depicted in Fig 7.8, where the print samples (original samples) have been denoted as P1, P2, and P3, while the reprinted samples (simulated samples) have been represented as R1, R2, and R3.



Flowchart of Printing Process

Flowchart of Simulated Counterfeiting Process

Fig 7.8: Flow Chart Original Print Process and Simulated Counterfeiting Process

### ❖ Collection of sample data

In this study, data samples have been obtained from both printed samples and reprinted samples for a two-way analysis. The collected data samples have been then subjected to two distinct modes of analysis: soft copy analysis and hard copy analysis. The step-by-step process of data has been collected shown in Fig 7.9 which illustrated the experimental procedure's overall structure.

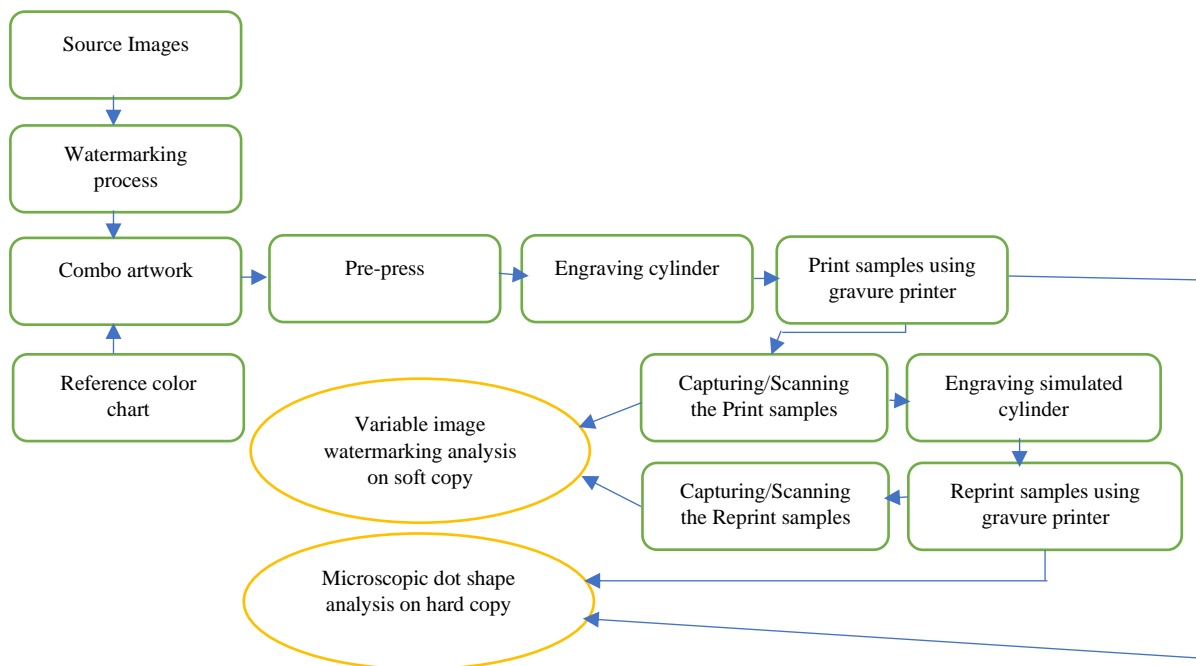


Fig.7.9: Experimental procedure (step by step process) for data collection

**In this study, four different methods have been used to authenticate original print from its copied/scanned reprints which are as follows:**

1. Method for Introducing Variable Image Watermark on Different Packaged Products and System Thereof
2. Characterization of Prints Based on Microscale Image Analysis of Dot Patterns
3. Identification of A Fake Medicine Packaging Print From its Dot Sizes and Shape
4. Identification of fake printed medicine packaging from a SVM approach and dots shape features

**The details of experimental procedures of the above methods have been discussed in details as follows:**

- 7.1 Method for Introducing Variable Image Watermark on Different Packaged Products and System Thereof
- 7.2 Characterization of Prints Based on Microscale Image Analysis of Dot Patterns
- 7.3 Identification of A Fake Medicine Packaging Print From its Dot Sizes and Shape
- 7.4 Identification of fake printed medicine packaging from a SVM approach and dots shape features

## 7.1 Method for Introducing Variable Image Watermark on Different Packaged Products and System Thereof

### 7.1.1 Source Artwork for watermarking process

This study has been used four different host images (Lena, Baboon, Avion, Peppers- shown in Fig. 7.1) as the host images for watermarking. Fig 7.3 displayed the experimental artwork in the section 7.

### 7.1.2 Preparing watermarked image using the MATLAB

The process involved taking four host images (HI), and then utilizing MATLAB(R2018a) to embed secret information, including the expiry date (ED) and batch number (BN), into the host image. This process resulted in the creation of watermarked host images (HIW), which have been utilized in the development of the experimental study's artwork.

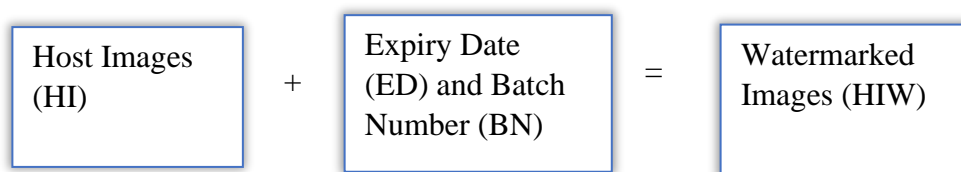


Fig.7.10: Preparing watermarked image (HIW)

The secret information (ED and BN of the product) has been converted into binary data and store in a 16-bit buffer which has been refer as watermark in this study. Then adding the said 16 bits of watermark into different spatial intensity in a specific channel of Host Image (HI). Fig. 7.10 shown a block diagram of preparing watermarked images for experiments.

The software photoshop CS4 has been used to observed the Histograms of the host images (HI), host images watermarked (HIW), original watermarked print samples refer as Printed and Scanned Watermarked Image (PS-WI) and reprint (simulated counterfeit) samples refer as RePrinted and ReScanned Watermarked Image (RPRS-WI). In Fig.7.11 shown the data collection for analysis. In this part of analysis, the histogram helped to shown exact intensity bins of the images.

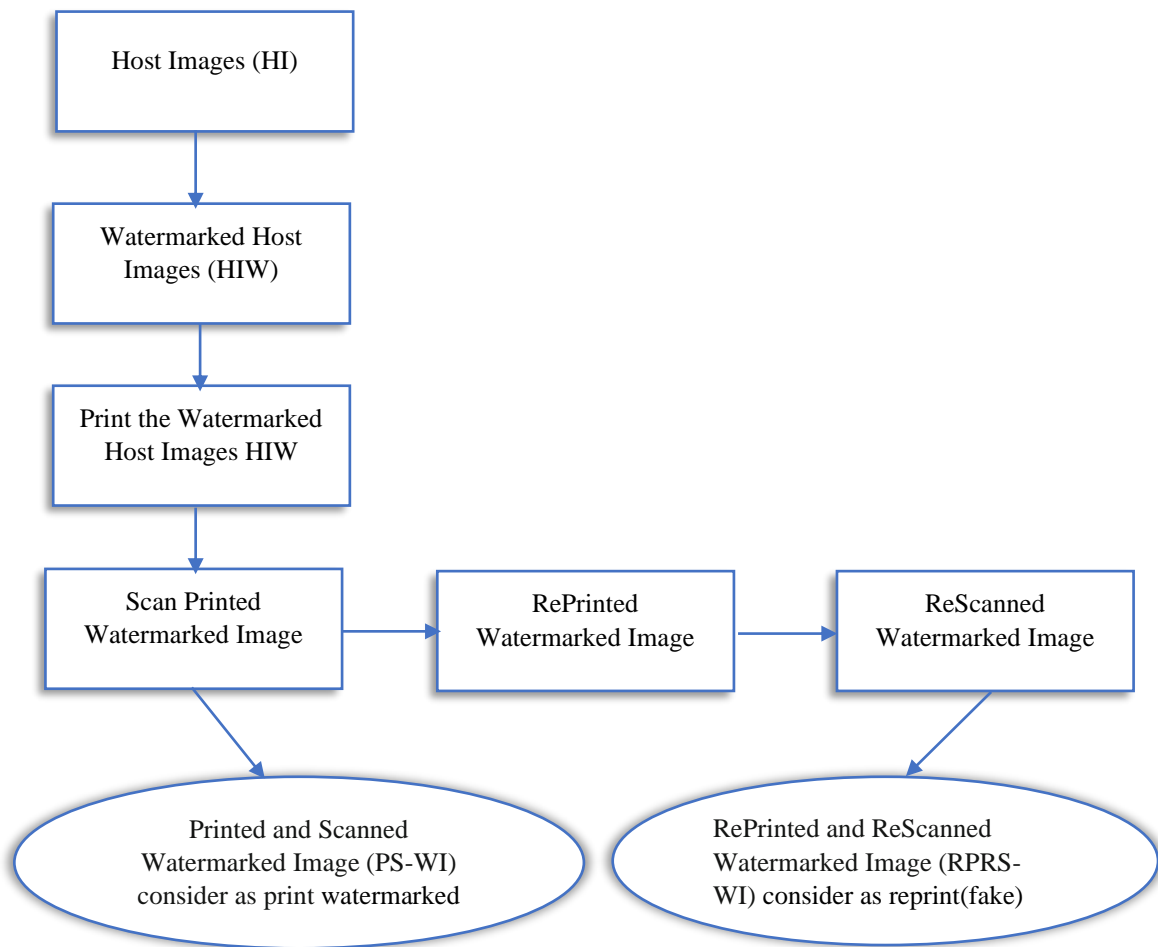


Fig.7.11: Data collection for variable image watermarking analysis

### 7.1.3 Proposed Watermarking Scheme

In this proposed watermarking scheme, Batch Number (BN) and Expiry Date (ED) have been embedded as Watermark or Secret information into the Host Image (HI). The comparison of the Host Image Softcopy with Host Image with Watermark softcopy (HIW) has been done to prove the imperceptibility of the watermark. The watermarked images have been printed and scanned. Then, the scanned images have been reprinted and rescanned without any other processing with different printers. The scanned image of the first print (PS-WI) and the second print or reprint (RPRS-WI) has been compared with the Host Image with Watermark softcopy (HIW). It has been observed that the unique histogram patterns and difference in co-relation co-efficient values for the second print are significantly

different from the first print, which ensures that if the original print is rescanned and reprinted for counterfeiting, it would have lower co-relation co-efficient values than the standard print. Hence, by comparing statistical analysed values and observing histograms patterns of print, the authenticity of the product may be detected.

### ❖ Proposed Watermark Design

To incorporate a watermark, the initial step involved converting the decimal values of the Batch Number (BN) and Expiry Date (ED) into binary data. Subsequently, these binary values have been stored within a 16-bit buffer. The next phase consisted of embedding the 16-bit watermark into various intensity values within the Host Image (HI). The selection of these intensity values has been predetermined based on their intensity values, which included 16, 32, 48, 64, 80, 96, 112, 128, 144, 160, 170, 192, 208, 224, 240, and 256.

Preparing watermark: In this study, the Batch Number begins with an alphabetical character ranging from A to Z and ends with a numeric value. Each alphabet is assigned a corresponding decimal value, where A represents 1, B represents 2, C represents 3, and so on, until Z, which represents 26. Additionally, the Batch Number concludes with a decimal value at the end falling within the range of 0 to 9. Like this, the decimal value for month is within 1 to 12 and for year is within 17 to 99. According to this Z,9 and 12/99 are the maximum values and A,0 and 1/17 are the minimum values.

Table 7.4: Set range for the expiry date and batch number

Data	Decimal value		Number of Binary bits Value	
	Min.	Max.	Min.	Max.
Batch no.	1	26	1 bit	5 bits
	0	9	1 bit	4 bits
Month	1	12	1 bit	4 bits
Year	17	99	5 bits	7 bits

Now for example a Batch No. has been selected as refer to Z\_\_\_\_\_9 and Expiry Date 12/99 (MM/YY). In between Z and 9 any number can be placed. Here, Z is represented as 26 (Decimal value) then converted into binary value 11010. Next 9 has represented as 1001, same way 12 has represented as 1100 and 99 has represented as 1100011. After getting the Z's binary and 9's binary value, the binary value of 9 has been subtracted from Z's binary value. After subtraction the value becomes 10001 for Z9. Table 7.5. represents the Expiry date and Batch number in binary.

Table 7.5: Representation Expiry date and Batch number in binary

Data	Decimal	Binary	Buffer
Batch No	Z9	10001	5 bit
Month	12	1100	4 bit
Year	99	1100011	7 bit

The 16-bit buffer has been utilized to store the binary watermark, consisting of the expiry date and batch number (represented as 1000111001100011 in binary format), for the purpose of embedding it into the host image.

### ❖ Watermark Embedding Scheme

Here is the detail diagram of embedding watermark process has been shown Fig 7.12:

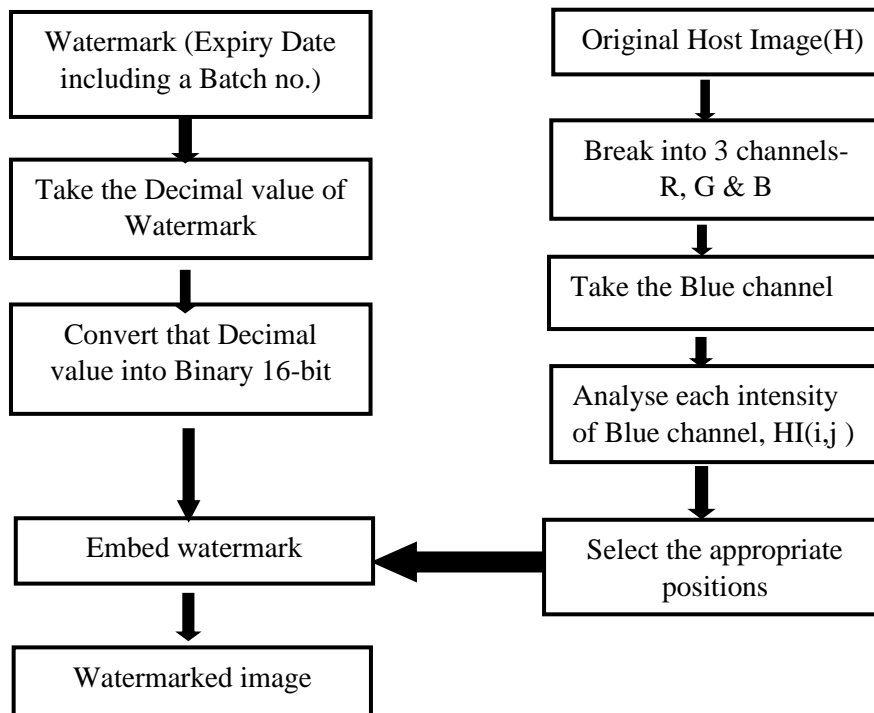


Fig 7.12: Flow diagram of embedding watermark process

In this proposed work consider 64-bit image as a host image for embedding data into it. This host image (HI) has RGB channels and each channel has Gray level values 0-255 (for Red, Green and Blue). If bit depth increases then the grey level intensity values range will increase for each channel. According to the intensity of each pixel, have selected some intensity into the image in a particular channel Blue.

The idea has been to embed the information (Expiry date and Batch number) into host image and after watermarking one comparison has been done to prove the imperceptibility of the watermark. Again, second comparison has been done after print and scan to calculate the distortion level to set a threshold value for the print and scan attack from inkjet printer and gravure printer.

### 7.1.4 Steps of the Embedding Watermark into the Host Image

One by one binary watermark bit, has been embedded, into the blue channel, in one of the selected positions  $HI(i, j)$  sequentially. The watermarked image  $HIW^{\wedge}$  has been then obtained by embedding all the 16 binary watermark bits into the intensity values of the selected pixels of the host image (HI). The step-by-step process of watermarking shown in Fig 7.13.

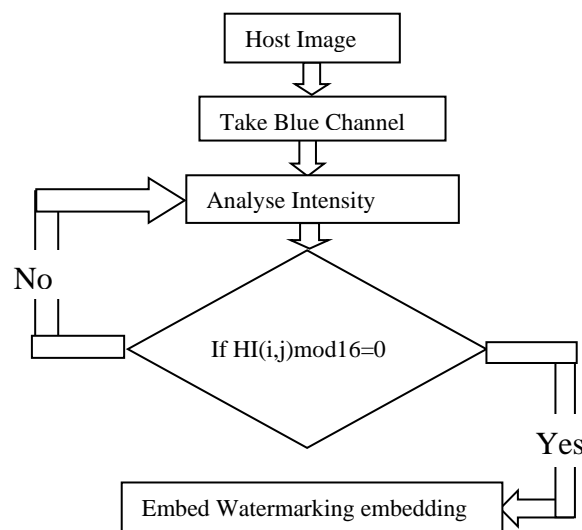


Fig 7.13: Step by step process of watermarking

The watermarked image (HIW) is obtained by embedding all the 16 bits into the intensity values of the selected pixels of the host image (HI).

#### ✓ Detail steps of embedding watermark

- **Step 1:** Choose the host image HI whose size is  $M \times N$ .
- **Step 2:** Then break those chromatic components into 3 channels i.e. Red, Green and Blue.
- **Step 3:** Take the Blue channel and posterized the blue channel.
- **Step 4:** Analysed each intensity of blue channel i.e.,  $HI(i, j)$ . The analysis has been done as follows,

$$0 < HI(i, j) \leq 255$$

$$HI(i, j) \bmod 16 \text{ is equals to } 0.$$

- **Step 5:** Select those positions where the modulo operation values come zero (0).
- **Step 6:** Embedding watermark into the intensity.



**Example:** The 1<sup>st</sup> binary watermark bit i.e. **B(1)** have been embedded into the 1<sup>st</sup> selected intensity of host image i.e. **HI(i, j)=16**. Then the 2<sup>nd</sup> binary watermark bit **B(2)** have embedded into 2<sup>nd</sup> selected intensity **HI(i, j)=32**. By repeating this procedure each binary watermark bit of 16 bit have been embedded into 16 different intensity of host image sequentially to get the watermarked image.

### 7.1.5 Quality measures (MSE, PSNR, SSIM) for host images (HI), host images watermarked (HIW), original watermarked print samples (PS-WI) and reprint (simulated counterfeit) samples (RPRS-WI) on A4 paper media

Measurement of image quality is a challenging problem in huge range of application. The quality measures can be classified into two groups: Objective and subjective. There are different type number of objective measures. Here have been mentioned some of these measures such as MSE, PSNR and SSIM by which measure the degradation of two images between before watermarking and after watermarking [1].

Mean Square Error (MSE): It is one of the earliest tests that has been performed to test if two pictures are similar. MSE denotes the power of the distortion, i.e., the difference between the reference and test images. In this study the reference images have been referred as HI (host image) and test images have been referred as HIW' (host image with watermark) [1].

-MSE value has been calculated using the following equation (Eq. 7.1):

$$MSE = \frac{1}{M \times N} \sum_{x=1}^M \sum_{y=1}^N [HI(x, y) - HIW'(x, y)]^2 \quad \text{Eq. (7.1)}$$

Where, M, N =Dimensions of the image and x, y =co-ordinates of the given image. HI(x,y)= Host or Original image and HIW'(x,y)=Watermarked image.

MSE has only lower bound and it has no upper bound, if the comparison result come out which is closes to zero that mean output result take as a good result. If the comparison result come out is greater than zero then this outcome would be considered as not good.

In this part the blue component of the Host image (HI) and watermarked image (HIW)has been compared. PSNR (Peak signal-to-noise ratio) values has been taken to measure the similarity degree between these two images as in equation (Eq.7.2). HI represents as Host or Source image and HIW' represents as Watermarked image.

$$PSNR = 10 \log_{10} \frac{M \times N \times \max\{[HI(x, y)]^2\}}{\sum_{x=1}^M [HI(x, y) - HIW'(x, y)]^2} \quad \text{Eq. (7.2)}$$

Where HI(x,y) and HIW'(x,y) present the value of pixel (x,y) in two dimensional host image and watermarked image and M and N denote the width and height respectively. Here PSNR has two bounds, one is lower boundary as zero and other is upper boundary 99. If the comparison result has come out nearer to zero then the result will be considered as not good, if the result has come out nearer to 99 that mean the comparison result is good.

The Structural similarity (SSIM) index measurement proposed by Wang et al. (2004) [27] is used to correlate the quality perception of the human visual system (HVS) with the predicted result. The SSIM has been designed by modelling image distortion that combines three factors: loss of correlation, luminance distortion and contrast distortion, and it is defined as in equation (Eq.7.3):

$$SSIM(HI, HIW') = l(HI, HIW') \cdot c(HI, HIW') \cdot s(HI, HIW') \quad \text{Eq. (7.3)}$$

Where,

$$l(HI, HIW') = ((2\mu_{HI}\mu_{HIW'} + C1))/(\mu^2_{HI} + \mu^2_{HIW'} + C1) \dots\dots\dots 1^{st} \text{ term}$$

$$c(HI, HIW') = (2\sigma_{HI}\sigma_{HIW'} + C2)/(\sigma^2_{HI} + \sigma^2_{HIW'} + C2) \dots\dots\dots 2^{nd} \text{ term}$$

$$s(HI, HIW') = (\sigma_{HI HIW'} + C3)/(\sigma_{HI}\sigma_{HIW'} + C3) \dots\dots\dots 3^{rd} \text{ term}$$

The first term measures the closeness of the two images' mean luminance ( $\mu_{HI}$  and  $\mu_{HIW'}$ ). The second term measures the closeness of the contrast of the two images, and the contrast is measured by the standard deviation  $\sigma_{HI}$  and  $\sigma_{HIW'}$ . The third term is the structure comparison function which measures the correlation coefficient between the two images HI and HIW'.

Note that  $\sigma_{HIHIW'}$  is the covariance between HI and HIW'. The positive constants C1, C2 and C3 are used to avoid a null denominator.

By default,

- $C1 = (0.01 * L)^2$ , where L is the specified Dynamic Range value of image, default L=255
- $C2 = (0.03 * L)^2$ , where L is the specified Dynamic Range value of image.
- $C3 = C2/2$

SSIM has a lower bound and an upper bound. It is always between -1 and 1.

$$-1 \leq SSIM \leq 1$$

SSIM value could be varies from -1 to 1.

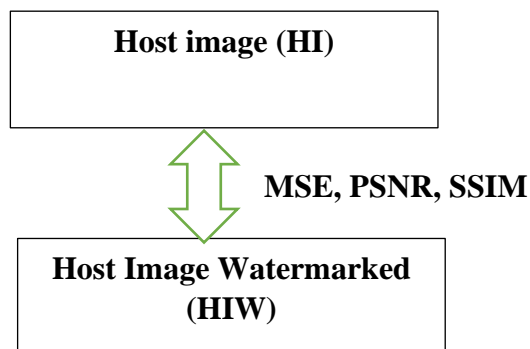


Fig 7.14: Statistical Analysis Flow Chart of comparison for MSE, PSNR, SSIM

### 7.1.6 Quality Measures (by co-relation co-efficient) for host images watermarked (HIW), original watermarked print samples (PS-WI) and reprint (simulated counterfeit) samples (RPRS-WI) on Paper and Foil Media

In a wide variety of applications, measuring picture quality has proven to be a difficult task. The two categories of quality measurements are objective and subjective have been mentioned earlier. Here, the co-relation co-efficient has been used as objective measures to evaluate the difference between Host Image (HI) with Watermark soft copy (HIW), Print sample (PS-WI) and Reprint sample (RPRS-WI).

Pearson's correlation coefficient,  $r$ , has been widely used in statistical analysis, pattern recognition, and image processing. Applications for include comparing two images for the purposes of image registration, object recognition, and disparity measurement. When the value of  $r$  is 1, it indicates that the two images are identical, and when it is 0, it means that there is no correlation between the images. On the other hand, if  $r$  is -1, it implies complete anti-correlation between the images, such as when one image is the negative of the other.

For monochrome digital images, the Pearson correlation coefficient is defined as follows:

$$r = \frac{\sum_i(x_i - x_m)(y_i - y_m)}{\sqrt{\sum_i(x_i - x_m)^2} \sqrt{\sum_i(y_i - y_m)^2}} \quad \text{Eq. (7.4)}$$

For first statistical analysis in equation (Eq.7.4),  $x_i$  defines the intensity of  $i$ -th pixel in image 1 (Host Image with Watermark soft copy (HIW)),  $y_i$  defines the intensity of the  $i$ -th pixel in image 2 (Print sample (PS-WI)),  $x_m$  defines the mean intensity of image 1 (Host Image with Watermark soft copy (HIW)), and  $y_m$  defines the intensity of image 2 (Print sample (PS-WI)).

For second statistical analysis in equation 7.4,  $x_i$  defines the intensity of  $i$ -th pixel in image 1 (Host Image with Watermark soft copy (HIW)),  $y_i$  defines the intensity of the  $i$ -th pixel in image 2 (Reprint sample (RPRS-WI)),  $x_m$  defines the mean intensity of image 1 (Host Image with Watermark soft copy (HIW)), and  $y_m$  defines the intensity of image 2 (Reprint sample (RPRS-WI)).

Now in the third statistical analysis in the equation 7.4,  $x_i$  defines the intensity of  $i$ -th pixel in image 1 (Print sample (PS-WI)),  $y_i$  defines the intensity of the  $i$ th pixel in image 2 (Reprint sample (RPRS-WI)),  $x_m$  defines the mean intensity of image 1(Print sample (PS-WI)), and  $y_m$  defines the intensity of image 2 (Reprint sample (RPRS-WI)).

Depending on image and watermark embedding the values for  $r$  range varies in between same range in this process, so that using this range authenticate the image watermarking. This is the uniqueness of this proposed work. In the Fig 7.15 shows the flow chart comparative statistical analysis for the correlation coefficient.

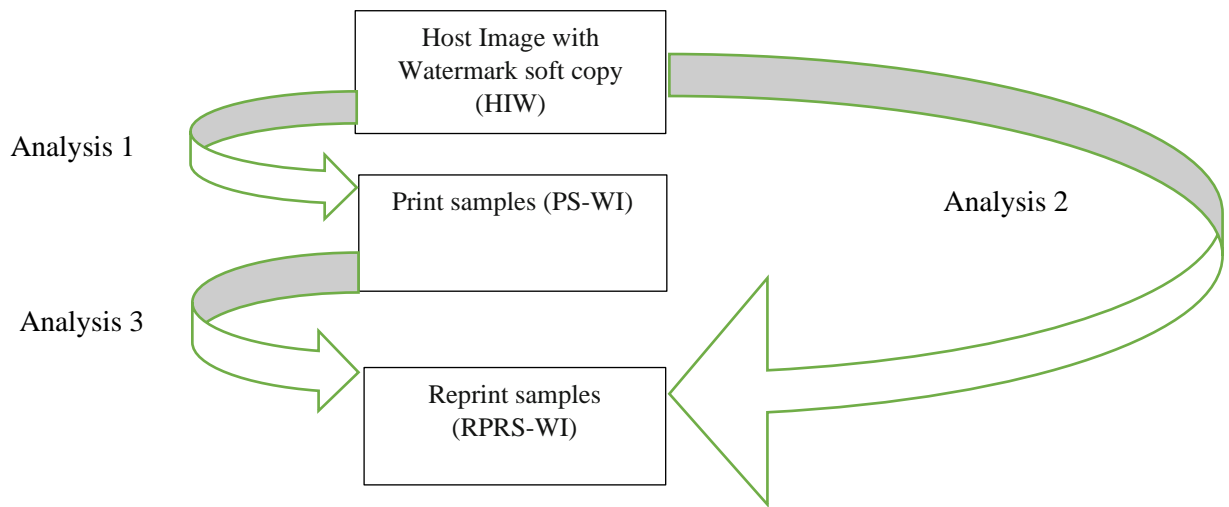


Fig 7.15: Flow Chart of Comparative statistical analysis for the correlation coefficient

The result of the statistical analysis has been explained in details in the next chapter 8 for this experimental procedure of watermarking process for this study.

Now in the next part 7.2 has been explained the experimental procedure on dot shape structure analysis of this study.

## 7.2 Characterization of Prints Based on Microscale Image Analysis of Dot Patterns

### 7.2.1 Source Artwork

In this part of study mainly concentrated on microscopic dot analysis of print and reprint sample. As it has been mentioned in section 7, gravure printing press has been used to print the IT8.7/3 standard color target chart with Cyan, Magenta, Yellow, and Black foil inks on a blister foil substrate. The reference image artwork IT8.7/3, after print and reprint have been observed under microscope shown in Fig 7.16.

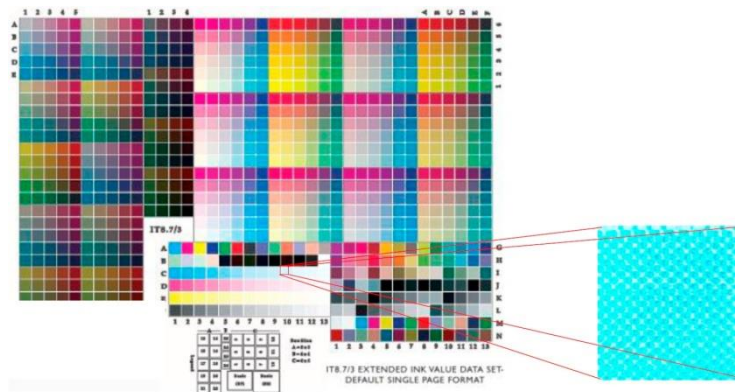


Fig 7.16:(a) Selected samples from the IT8.7/3 Color Chart: sample C10—Cyan with 20% ink coverage; sample D10—Magenta with 20% ink coverage, sample E10—Yellow

with 20% ink coverage, (b)cropped image of a Rotogravure printed cyan sample magnified  $\times 4$ .

## 7.2.2 Cylinder Engraving for the artwork

Pre-press parameter: The desired parameters for the cylinder have been set in this experimental analysis using Art-Pro software in the pre-press. All the detail shown in section 7. The set cylinder engraving parameters have been shown in Table 7.1.

❖ Cylinder Engraving machine has been shown in Fig 7.5.

## 7.2.3 Microscope instrument and function

Several color print and reprint samples (monochromatic (e.g., C, M, or Y); bi-chromatic (e.g., CM); tri-chromatic (CMY); or quadri-chromatic (CMYK)) were gathered for analysis. These color samples correspond to chosen samples from the IT8.7/3 color chart, which is often used to define CMYK printers (see example in Fig 7.15(a)).

The dots of printed (P1, P2, P3) and reprinted samples (R1, R2, R3) have been analysed using a microscopic camera (model HDCE-X3) attached with Lawrence & Mayo microscope (shown in Fig 7.17). It has been used to capture each color patch from print samples and reprint samples with 4x zoom magnification (step 1). The microscopic captured images have been processed with the ScopeImage 9.0 microscopy software. This work has examined the analysis of color tints, specifically from lower dot percentages to higher dot percentages. The observations reveal that as the dot percentage increases, there is an increase in dot bridging and dot kissing between the dots. Consequently, the proper separation of the dot structure becomes challenging when a higher percentage of dots is present. As a result, the primary focus of this study was on analysing dot structures within the lower dot percentages to mid-tone dot percentages range.



Fig 7.17: Lawrence & mayo Microscope.

ScopeImage 9.0, a robust software bundled with the microscope, serves the purpose of capturing and examining sample images at a microscopic level. It facilitates image analysis

and processing tasks. This software offers a range of helpful image button functions, including the Angle Measure function, enabling the measurement of angle orientations of the dots, and the Polygon function, designed specifically for measuring dot structures. Subsequently, MATLAB was employed to conduct an analysis of the microscopic dot structure found in the samples.

The following experimental analysis focused on examining the dot structure of color tints in each sample, specifically for cyan, magenta, and yellow colors.

### 7.2.4 Measurement, Modelling and Analysis at the Microscale of Printed Dots for three colors (CMY) using MATLAB

The image processing pipeline that has proposed in this study is illustrated in Fig 7.18 and detailed in the following section.

#### (i) Separation of Ink Colors (Step1)

After taking the print image it has separate the channel for the experimental analysis. Same procedure has been applied on reprint samples. Separating ink colors can be challenging due to the frequent occurrence of mis-registration between the printed color channels. Fig 7.19 shows an example a printed cyan, magenta and yellow dot shifted in position.

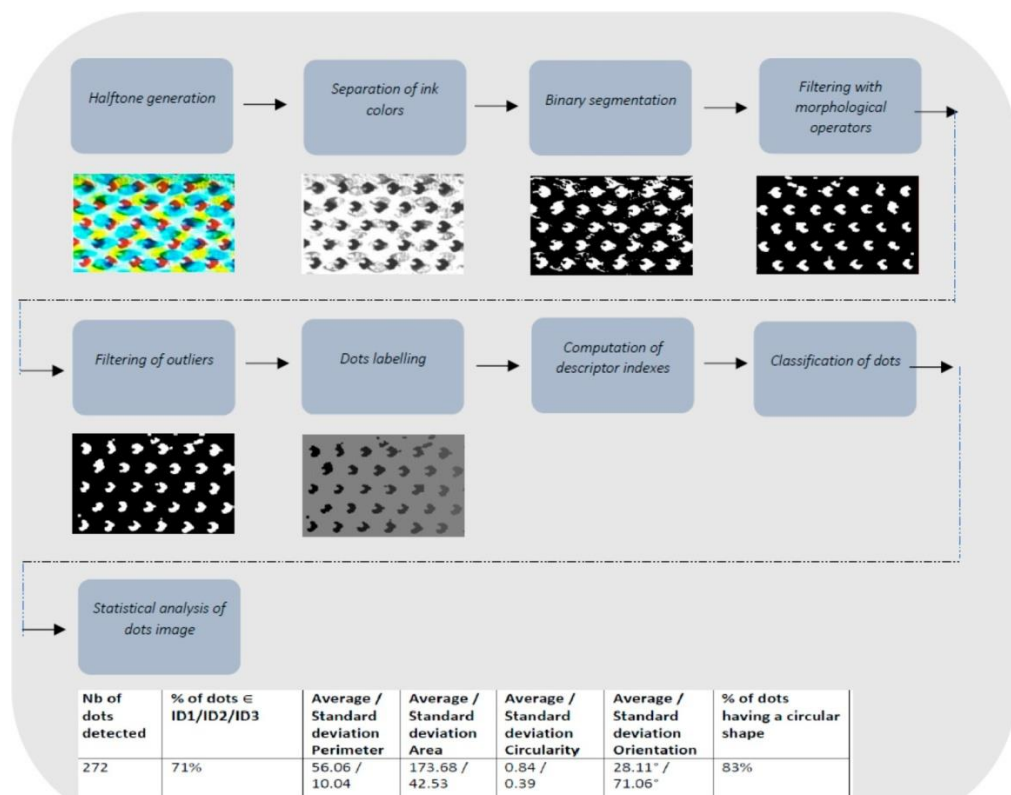


Fig 7.18: Framework of the proposed image processing pipeline.

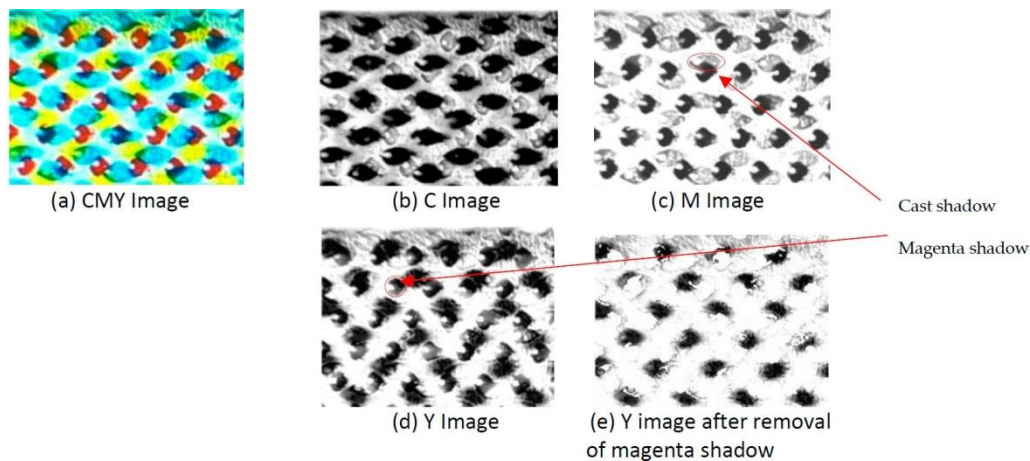


Fig 7.19: (a) Example of halftone misregistration for a CMY image with 20% of ink coverage for each channel. (b) cyan separation. (c) The contrast between the magenta dots and the background is enough to distinguish them even if the cyan dots are visible in the magenta image. (d) Separating magenta dots from yellow dots is not possible in the yellow image. (e) In order to correctly identify yellow dots, magenta dots that have been segmented in the magenta image are excluded from the yellow image.

The issue of halftone misregistration has been investigated in [30]. Fig 7.19a shows an example of a halftoning scheme with different screen angles for cyan, magenta, yellow and black channels. NAMEDANIAN [30] stated that the color black, which has the most prominent contrast, is half-toned and positioned at a  $45^\circ$  angle because the eye is less sensitive at this angle meanwhile, yellow, the weakest color, is halftoned at  $0^\circ$ , where the human eye is most sensitive. NAMEDANIAN [30] states that utilizing distinct angles for each channel can decrease the impact of misregistration. Nevertheless, this technique brings about a particular pattern, referred to as a rosette pattern, which is highly visible at a microscopic level. The issue of halftone misregistration has been proposed in [30]. Fig 7.20a has been shown an example of the halftoning scheme with different screen angles for cyan, magenta, yellow and black channels. The study involved examining samples where black, the color known for its highest contrast, was halftoned and positioned at a  $45^\circ$  angle. This choice was made considering the relatively reduced sensitivity of the human eye to stimuli at this particular angle. On the other hand, yellow, the color with the least contrast, was halftoned at a  $0^\circ$  angle, which corresponds to the angle where the human eye is most sensitive [30]. By employing different angles for each channel, the negative influence of misregistration is diminished. However, this approach introduces noticeable rosette patterns that are clearly visible at the microscale.



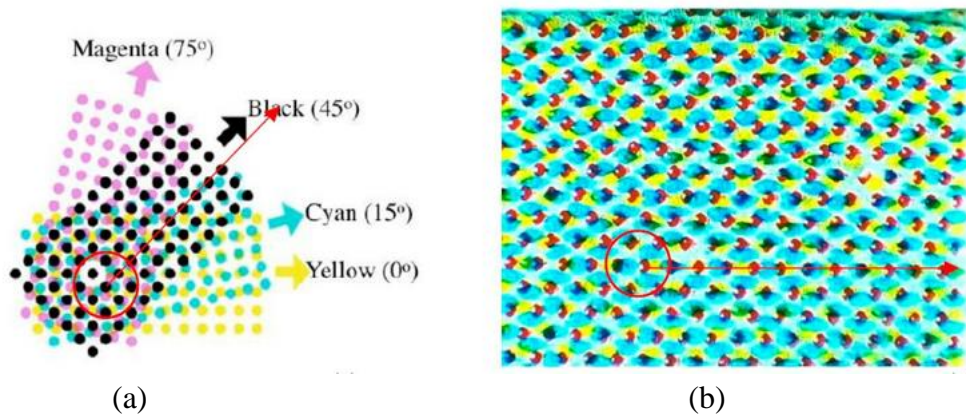


Fig 7.20:(a) Typical halftoning scheme for yellow ( $0^\circ$ ), cyan ( $15^\circ$ ), black ( $45^\circ$ ) and magenta ( $75^\circ$ ) ([1]). (b) An example of a rosette pattern that can occur with a different color halftoning method is shown, with CMYK at  $0^\circ$  and a slight shift  $\mu\text{m}$  along the X and Y axis.

Namedanian suggested in [30] using various wavelengths to differentiate colors, but the proposed technique has limited to only two colors of ink. Additionally, this approach is limited by the availability of suitable wavelengths, and it can be difficult to find appropriate wavelengths for separating more than two colors of ink. When printing color dots on top of each other (known as dot-on-dot), the primary problem is that separating the ink colors completely is difficult. This leads to a shadow effect because the impact of one ink cannot be entirely eliminated when transmitting light at the absorbing wavelength band of the other ink. The term "shadow effect" of an ink means to how that ink contributes to the reflectance spectra of other inks, as described in [30].

In this study, it has been not a problem to detect dots in both the cyan and magenta channels, even if cyan dots have been printed on the magenta layer. We independently process these two channels from the others because of their misregistration or lack of alignment. In contrast, because the yellow dots have been printed above the cyan layer and there is an issue with detecting dots on the yellow channel due to the misregistration of these two channels, then we have made the choice to mask the dots that were identified in the cyan image on the yellow image. This is so that we can proceed with processing the yellow channel separately from the other channels in the next step. Images corresponding to samples number 7, 8, 9, 10, 14, 15, 16 and 18 in Tables 8.8–8.10 (Chapter 8) have shown a similar misregistration problem. This study has been exclusively dealt with CMY images, do not include CMYK images in this part.

The knowledge that has been acquired in this study about the printing process used enables us to propose an ad hoc solution to separate color dots from color channels. In future study, we will study if this approach could be extended to CMYK images.

## ii) Binarization of Color Images (Step2)

In Fig 7.21(b), there is a depiction of how the quality of the printed images studied is low, due to a high signal-to-noise ratio. Consequently, neither edge-based methods nor

region-based methods have been adapted to this type of images. Alternatively, the global thresholding approach suggested by Otsu [35] has been adapted. There are two primary reasons for this:

Firstly, it relies on an unsupervised technique for histogram thresholding that minimizes the variance of intensity within each class. Secondly, it has excellent results in distinguishing areas of ink coverage from paper regions [36], as demonstrated in prior proposed work. Nevertheless, this approach has a limitation whereby it underperforms compared to local threshold methods when the background is not homogeneous. We suggest filtering the segmented image after the fact to make up for local variations caused by the background and to make the Otsu segmentation method work better.

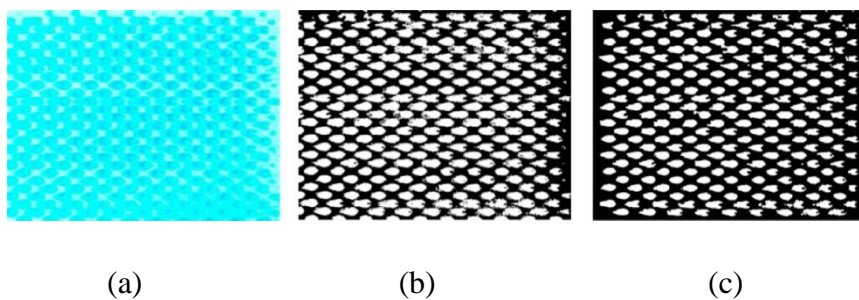


Fig 7.21:(a) Cyan dots; (b) binary image (with physical dot gain); (c) binary image after removal of dots connected to the borders and noise around dots. The physical dot gain causes printed dots to deform, affecting their shape and size. This deformation produces light cyan elliptical regions due to physical dot gain, while printed dots are represented by dark cyan circular regions.

### iii)Filtering of Color Channels (Step3)

Multiple techniques of morphological analysis were utilized to decrease the level of noise present in the image. These treatments consist of:

1. A removal of dots connected to the image border.
2. An erosion with a disk-shaped structuring element of one-pixel radius. This erosion removes isolated pixels (punctual noise) and reduces the border effects due to the physical dot gain on the size of the dots (Fig 7.21).
3. An opening (erosion followed by a dilation) with a disk-shaped structuring element of one-pixel radius. This opening remove noise and removes small objects from the foreground.
4. A removal of small holes in foreground areas with a disk-shaped structuring element of radius 1.
5. A transformation of a watershed that utilizes the Euclidean distance as its basis. By dividing continuous areas into individual objects, this transformation enhances the separation of linked dots. Fig 7.21c, 7.22e, 7.23d and 7.24e illustrates some results obtained with these operations.

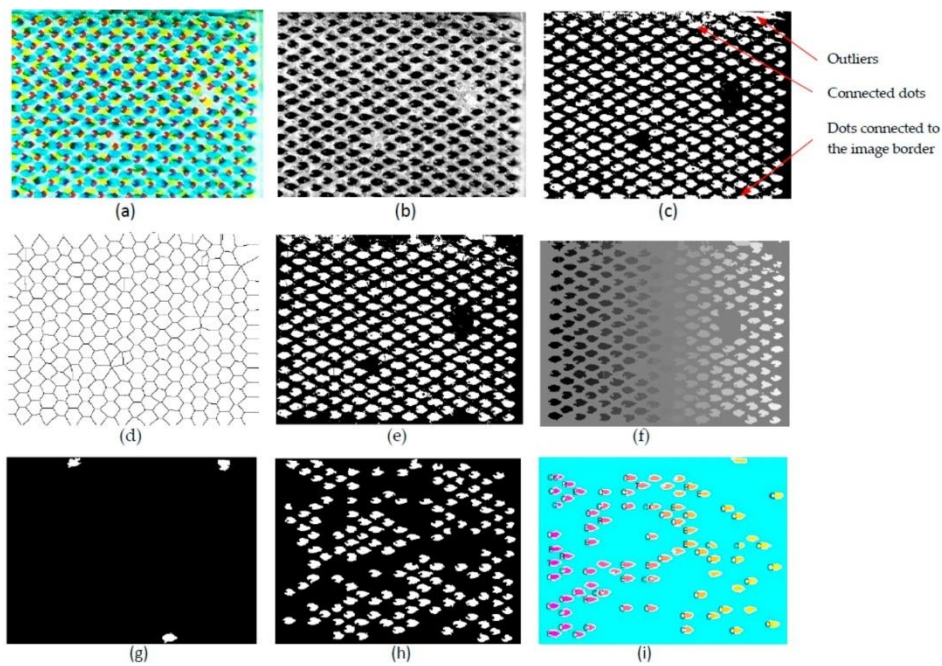


Fig 7.22: Displays a depiction of the step-by-step results obtained. In this example, cyan dots are extracted, measured and analysed. (a)CMY image, (b)Step1: extraction of C channel, (c)Step2: binarization,(d) Step 3.5: isosurface of distance transform, (e) Steps 3.1 to 3.4:removal of noise and irrelevant areas.(f) Step 4:labelling of regions of interest, (g) Step 5: removal of outliers, (h) Step 7: extraction of dots with concavity (ID1/ID2/ID3)or an irregular shape (ID4) defined by a solidity upper than 0.75, (i) extraction of dots with a convex shape (ID5) with a circular equivalent shape, or an elliptic equivalent shape, or another pattern shape.

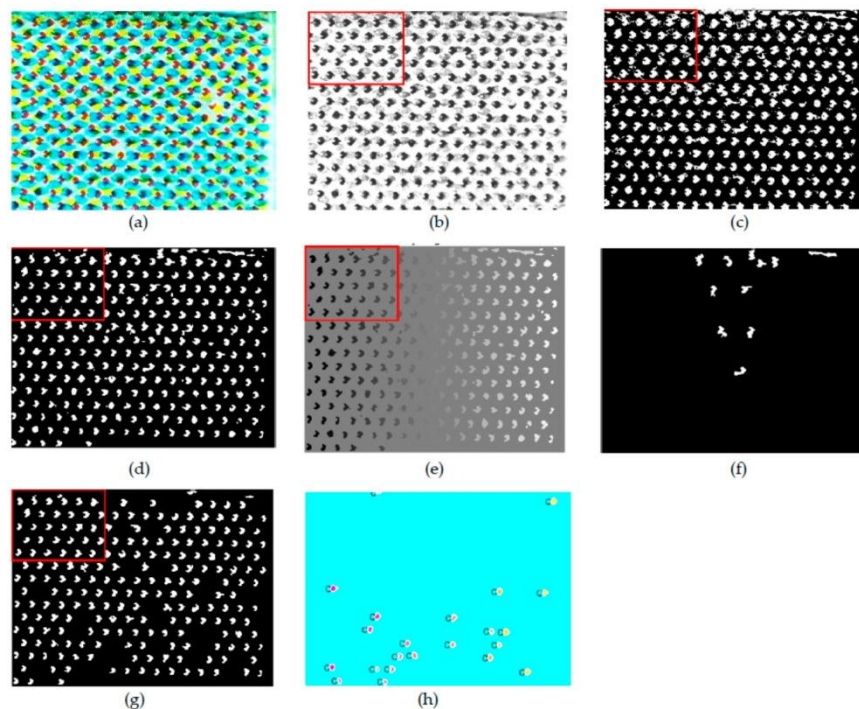


Fig 7.23: Illustration of the results obtained step by step. In this example magenta dots are extracted, measured and analysed. The red windows correspond to the image areas shown in Fig 7.18. (a) CMY



image, (b) Step 1: extraction of Magenta channel, (c) Step 2: binarization, (d) Steps 3.1 to 3.4: removal of noise and irrelevant areas, (e) Step 4: labelling of regions of interest, (f) Step 5: removal of outliers, (g) Step 7: extraction of dots with a concavity (ID1/ID2/ID3) or an irregular shape (ID4) defined by a solidity upper than 0.75, (h) extraction of dots with a convex shape (ID5) with a circular equivalent shape, or an elliptic equivalent shape, or another pattern shape.

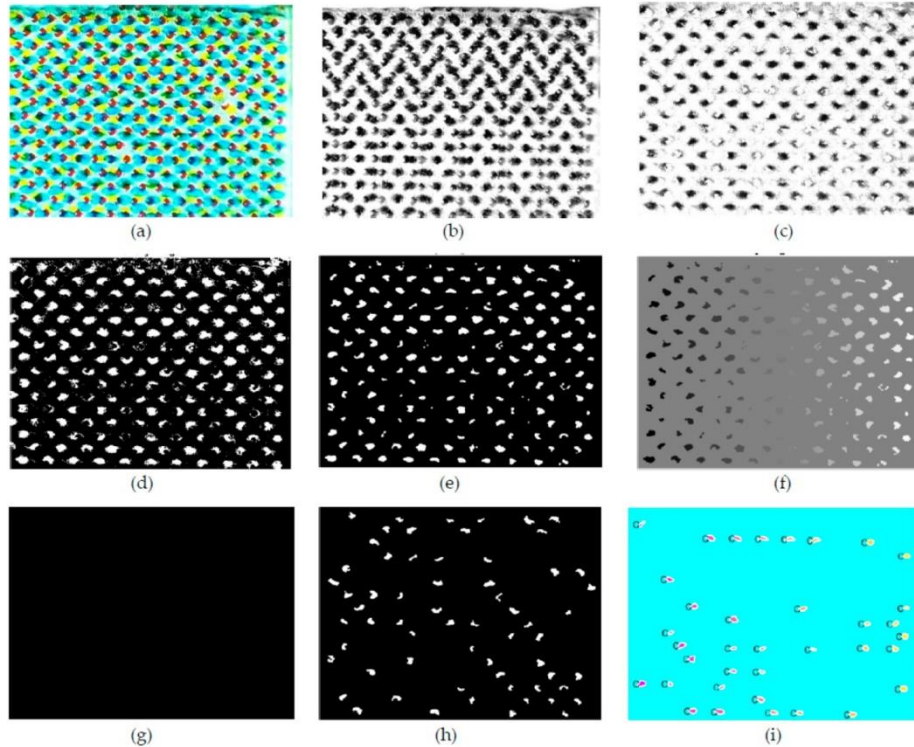


Fig 7.24: (a) CMY image, (b) Step 1: extraction of the Yellow channel, (c) Step 1: Y image after removal of Magenta shadow, (d) Step 2: binarization, (e) Steps 3.1 to 3.4: removal of noise and irrelevant areas, (f) Step 4: labelling of regions of interest, (g) Step 5: removal of outliers, (h) Step 7: extraction of dots with concavity (ID1/ID2/ID3) or an irregular shape (ID4) defined by a solidity upper than 0.75, (i): extraction of dots with a convex shape (ID5) with a circular equivalent shape, or an elliptic equivalent shape, or another pattern shape.

#### iv) Labelling of Regions of Interest (Step 4)

Connected pixels belonging to a region of interest of the foreground has been labelled as dots. If the area of a region of interest is too large in comparison with the average area of the other dots, then this region is considered an outlier. When two dots overlap, it becomes very challenging to separate them, given their statistical significance in terms of the overall number of dots. Therefore, our proposition involves excluding these regions from our analysis procedure. When two dots are adjacent, it is possible to disconnect them using the watershed transform (refer to step v). Thus, pixels belonging to the frontier of the two dots (defined by the isosurface of their distance transform) are removed from the foreground in order to separately label each of these two dots.

On the other hand, if the area of a region of interest is too small in comparison with the average area of the other dots, then this region is considered an outlier.

#### v) Filtering of Outliers (Step5)

If the area of a region of interest is larger than 1.5x the average area of all dots or smaller than 0.5x the average area of all dots, then it is removed from the foreground (refer in Fig 7.22g, 7.23f and 7.24f). The process can be divided into two smaller steps: the initial elimination of two tiny dots and the adjustment of the average size of the remaining foreground objects, followed by the elimination of two larger dots.

#### vi) Computation of Dot Descriptors (Step 6)

In this step this study has defined six categories of dot patterns, which has been computed as Dot descriptors (shown in Fig 7.25):

ID1 refers to a symmetrical doughnut shape with a hole located inside the convex hull of the dot;

ID2 describes a shape that is symmetrical and has a convex hull, with a relatively large hole;

ID3 refers to a shape that is concave in nature, with a hole located inside the convex hull of the dot, and is an asymmetric or not symmetrical;

ID4 refers to a shape that is either circular/elliptical and has a hole situated in the center of the dot;

ID5 refers to a shape which is elliptic/circular shape;

ID6 refers to random shape;

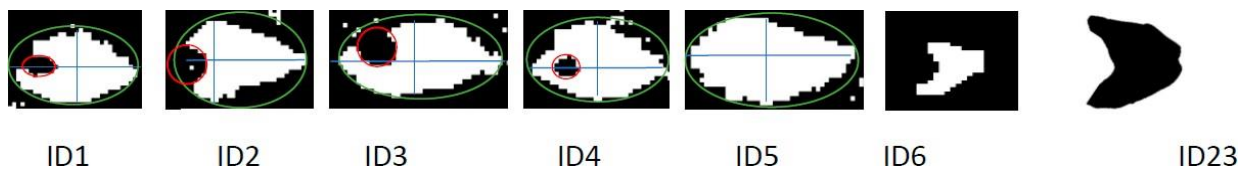


Fig 7.25: Categories of dot patterns (convex hulls of dots are highlighted in green, major/minor axis are highlighted in blue, convex hulls of holes are highlighted in red).

The pattern ID6 is comparable to the ID23 pattern that has been specified in [36].

To analysed each individual dot, this study has proposed computing the following shape descriptors:

- Centroid (X, Y coordinates in  $\mu\text{m}$ );
- 'A' value represents the area of the dot's surface in square micrometers ( $\mu\text{m}^2$ );
- $A_h$  refers to the area of the hole within the dot in square micrometers ( $\mu\text{m}^2$ );
- $A_c$  refers to the size of the convex hull area of the dot measured in micrometers squared ( $\mu\text{m}^2$ );
- $A_e$  denoted as area of the elliptical shape that encloses the dot is given in square micrometers ( $\mu\text{m}^2$ );
- Solidity =  $A/A_c$ ;

- Perimeter of the dot's surface is measured in micrometers ( $\mu\text{m}$ );
- $P_c$  value represents the perimeter of the convex hull of the dot in micrometers ( $\mu\text{m}$ );
- $P_e$  is the perimeter of the elliptical shape that bounds the dot, also measured in micrometers ( $\mu\text{m}$ );
- Convexity =  $P_c/P$ ;
- Circularity =  $\sqrt{4\pi A/P^2}$ ;
- Roundness =  $\sqrt{4\pi A/P_e^2}$ ;
- $DF_{\min \max}$  Feret diameters in  $\mu\text{m}$ ;
- Aspect ratio =  $DF_{\min}/DF_{\max}$ ;
- Orientation = refers to the measurement of the angle formed between the major axis of an ellipse that has the same second-moments as the region and the x-axis.;
- Major and minor axis;
- $A^{x1}$  is the area of the dot located upper the major axis;
- $A^{x2}$  is the area of the dot located lower the major axis;
- $A^{y1}$  refers to the area of the dot situated to the left of the minor axis;
- $A^{y2}$  represents the area of the dot situated to the right of the minor axis;
- Eccentricity =  $\frac{\text{distance from center to the foci or focal}}{\text{length of semi - major axis}}$
- Elongation in the X direction= is equal to the width of the elliptical bounding box divided by the width of the largest inscribed ellipse.;
- Symmetry with respect to the X and Y axes is determined by the ratios of  $A^{x1}$  to  $A^{x2}$  and  $A^{y1}$  to  $A^{y2}$ , respectively.

A few of these descriptors has been utilized by Valla and Olson in their work [36,37].

In order to assign a dot into one of the six categories of dot patterns, this study has established the following set of rules:

- For concave shapes, those belonging to category ID1 must have an elongation greater than 1.75, a symmetry value  $A^{x1}/A^{x2}$  between 0.85 and 1.15, and a solidity greater than 0.8.
- Category ID2 concave shapes must have a solidity greater than 0.75 and a symmetry value  $A^{x1}/A^{x2}$  between 0.85 and 1.15.
- Category ID3 concave shapes must have a solidity greater than 0.75 and a ratio  $A^{ij}/A$  greater than 0.15 in the region  $R^{ij}$ .
- Category ID4 dots must have a ratio  $A_h/A$  greater than 0.15. Below this value, holes are insignificant.
- Category ID5 circular equivalent dots must have a roundness value higher than 0.90 and an eccentricity greater than 0.85(see example shown in Fig 7.26).
- Elliptic equivalent dots must have a roundness value between 0.8 and 0.9 and an eccentricity between 0.6 and 0.85.(see example shown in Fig 7.26)
- Elongated dots (category ID6) must have an eccentricity lower than 0.6, a roundness value lower than 0.8, and an elongation greater than 1.3.
- Any other shape which does not satisfy any of the above rules belongs to category ID6.

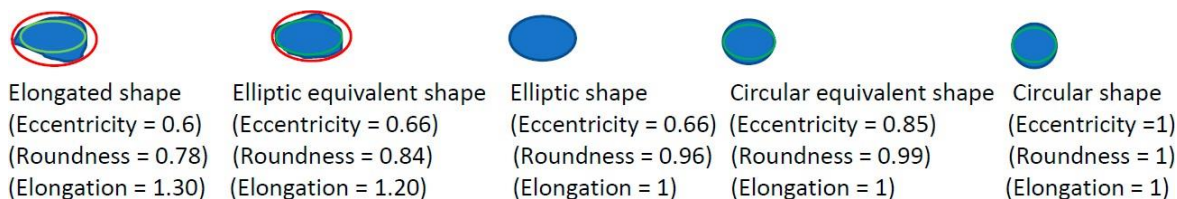
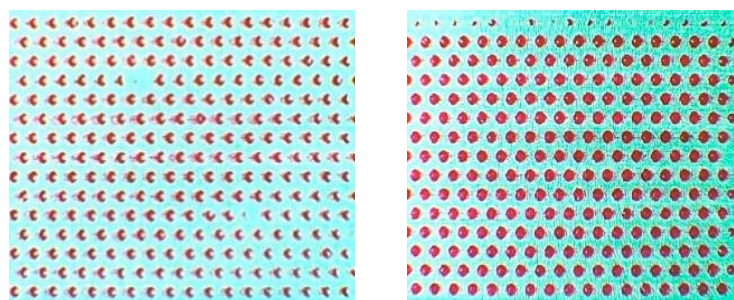


Fig 7.26: Examples of descriptor values for various patterns. The elliptic bounding box corresponds to the red ellipse. The inscription corresponds to the green ellipse.

These rules have been based on threshold values experimentally set from a statistical analysis of 4467 dots from 18 print samples. The thresholds provided in this study case are applicable only to the test samples that were analysed. It is necessary to adjust the rules and threshold values to suit each specific case being studied. Certain patterns such as ID1, ID2, ID3, and ID4 may be observed only in limited cases, such as when the ink viscosity is low. This can be seen in the images for samples numbered 1, 2, 3, 4, and 5 (shown in Fig 7.27 and 7.28 and chapter 8, Table 8.8). The quality thresholds are influenced by various factors such as print quality, noise, contrast, physical dot gain, ink coverage rate, and ink overlap. As a result, printing parameters such as ink viscosity and temperature affect these thresholds. Setting these parameters involves balancing between the accuracy of the descriptors and their ability to withstand (robustness against) print noise from one dot to another.



(a) Magenta print (Sample 1)      (b) Magenta print (Sample 2)

Fig 7.27: Example of results for two print samples printed with a cell angle of 60°. (a) % of dots belonging to category ID1 (0%), ID2 (92%), ID3 (2%), ID4 (less than 1%), ID5 (0%), ID6 (5%, most of them are at right of the figure). In total, 92% of dots have a circular shape—see statistical values report in (shown in chapter 8, Table 8.10). (b) % of dots belonging to category ID1 (less than 1%), ID2 (0%), ID3 (less than 1%), ID4 (40%), ID5 (49%, all have a circular shape), ID6 (6%, most of them are the top of the figure). The circular shape is present in 94% of all dots.



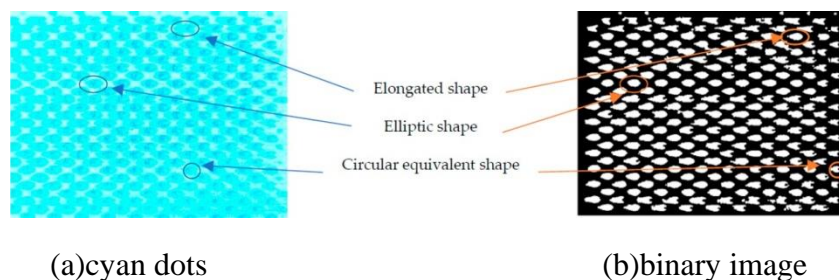


Fig 7.28: Illustrate example of results for a cyan print with a cell angle of  $60^\circ$  % of dots belonging to category ID1 (34%), ID2 (0%), ID3 (0%), ID4 (0%), ID5 (55%), ID6 (11%, most of them are at the border of the figure). In total, 62% of dots have an elliptic shape, while 25% of dots have an elongated shape (less than 1% has a circular shape).

From this study it has been claimed that: several dot descriptors must be used to properly evaluate the shape of the dots printed; several dot descriptors must be analyzed conjointly to classify properly the dots in predefined dot patterns; the robustness of these thresholds and rules greatly depends on the print parameters.

#### (vii) Global Analysis vs. Individual Analysis (Step 7)

Considering the varying dot patterns (like heterogeneity of dot patterns) and their randomly distributed nature on printed samples, as depicted in Figure 7.28, it has been proposed that in order to accurately characterize and identify a print, a global level analysis is required. This entails statistically analysing the distribution of dots printed on these samples. The experimental results presented in Tables 8.8-8.10 of Chapter 8 provide statistical findings for 18 print samples.

The next section, 7.3, provides an explanation of the experimental process conducted in the third phase of the study, focusing on the analysis of dot structure. This analysis involves incorporating additional dot parameters and expanding the sample size to include CMYK samples.

### 7.3 Identification of A Fake Medicine Packaging Print From its Dot Sizes and Shape

In the next part of the study, has been analysed the same artwork IT8.7/3 standard color target chart as a reference image shown in Fig 7.16(section 7.2.1). This part of experiment the Cyan, Magenta, Yellow and black color patches have been analysed for print and reprint samples using the same gravure printing press on blister foil substrate.

As we have mention that the same artwork has been analysed so the other technical parameters like cylinder making parameters at pre-press, cylinder size, parameters at the time of engraving the cylinder, press parameters at time of print and reprint sample printing from the press, the same three printing press with same gravure machine has been used. For print purpose the substrate blister foil has been used mentioned in the section 7. The four-color solvent – based foil ink has been used for printing and reprinting (shown in section 7, Table 7.3).

After getting the samples it has been analysed under same microscope Lawrence & mayo Microscope and it has used for dot structure analysis (mentioned in Fig 7.16 and 7.17).

### 7.3.1 Measurement at the Microscale of Print and Reprint Dots for colors (CMY) MATLAB function

This third part of study has focused to distinguish the print sample and reprint sample depending on parameters like dot area, major and minor axis of dots, eccentricity of the observed dots. Three distinct gravure printers have been used to print the reference image (P1, P2, P3). The images of print samples are then captured (Scanned) using selected input devices camera. The images have been then printed again in those three printers, the samples have been referred to as reprint or counterfeited prints (R1, R2, R3).

- The Lawrence & Mayo microscope with a 4x magnification (shown in Fig 7.17) has been used to examine the intricate features of print and reprint dot samples. The ScopeImage 9.0 microscopy software has been utilized to analyze the samples. The study involved observing, various dot areas of cyan, magenta, yellow and colors have been examined. The utilization of dot area, major axis, minor axis, and eccentricity as parameters has been applied to differentiate between print and reprint dots. In order to assess the consistency, the experiment has been carried out on multiple prints and replicated samples. The Murray-Davies Equation [30] has been used to compute the parameter dot area.
- The study implemented edge detection to quantify the number of dots present in printed samples with a particular patch or tint percentage. Images of the dot samples have been captured for analysis using the microscopic camera model HDCE-X3. These images have been converted to grayscale or binary format, and canny edge detection has been subsequently applied to them. The edges of the dot sample images have been determined based on noticeable changes in pixel intensity from the foreground to the background. The next stage of the analysis involves taking the contours of the detected edges of the dots in the samples. The outlines of all the dots have been drawn in white and set against a black background. In this study, the circular Hough transform, which is a modified version of the Hough transform, has been employed to detect the contours of objects or dots that are more or less circular in shape. The objective of using this contour detection method is to count the dot objects regardless of their shape. The MATLAB functions have been utilized to compute the major axis, minor axis, and eccentricity parameters of the observed dots. First, the 'Centroid' has been located and then the 'MajorAxisLength' and 'MinorAxisLength' have been determined. For every dot object, the eccentricity parameter has been computed, which is determined by the ratio of the distance between its center and its foci or focal point to the length of its long (major) axis.:

$$\text{Eccentricity} = c/a \qquad \text{Eq. (7.5)}$$

Where,  $c$ = distance from center to the foci or focal,  $a$ =length of semi-major axis

A range of object eccentricity from 0 to 1 is obtained as the output. Typically, an eccentricity value nearing 0 denotes that the shape is like to a circle, while an eccentricity value nearing 1 indicates that the shape is more similar to an ellipse.

### Theories

The present study has been used the Murray-Davies Equation to estimate the area of the dots [30],

$$A = \frac{1-R_{ht}}{1-R_s} \quad \text{Eq. (7.6)}$$

The given equation involves three variables:  $A$ , which represents the size of the dot area for a specific tint, which is a patch of halftone color; and which represents the amount of light reflected by a patch of solid color,

This equation (Eq.7.6) has been modified for our present study and the modified equation is Eq. 7.7,

$$D_A = \frac{(1-10^{-D_{ht}})}{(1-10^{-D_s})} \quad \text{Eq. (7.7)}$$

Where,  $D_A$ denotes Area of the particular tint percentage,  $D_{ht}$ is half tone color density and  $D_s$ is the density of solid color patch.

$$\text{Area of single dot}(D_{AS}) = \frac{D_A}{N_D} \quad \text{Eq. (7.8)}$$

The area of individual dots has been determined using equation Eq.7.8, which uses  $D_{AS}$  to represent the area of a single dot with a certain tint percentage,  $D_A$  to represent the total area of all dots with that tint percentage,  $N_D$  is to represent the number of dots with that tint percentage. Statistical analysis has been conducted by calculating the mean and standard deviation of the dot areas, major axis, minor axis, and eccentricity parameters.

In the Fig 7.29 illustrated flowchart of experimental process.

- **Flowchart of Experimental process:**

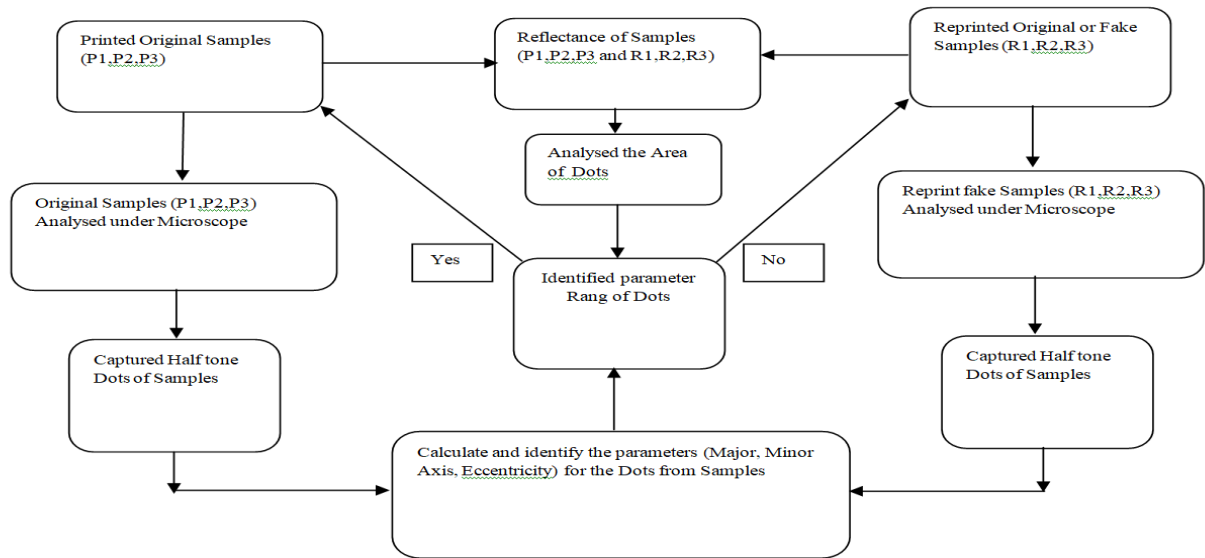


Fig 7.29: Print sample dot parameters compared with reprint dot parameters

In the next part of experimental procedure different shape descriptors index parameters such dot area, perimeter, circularity, eccentricity, solidity, major and minor axis of dots have been used for classification between the print sample and reprint sample. The study demonstrated that print and reprint dot shape descriptor index parameters might be utilized to distinguish at a microscopic scale. A multi-classification-based method Support Vector Machine have been utilized using shape descriptor index features for print and reprint source identification.

#### 7.4 Identification of fake printed medicine packaging from a SVM approach and dots shape features

The dots of print (P1, P2, P3) and reprint samples (R1, R2, R3) have been analysed using a microscopic camera (model HDCE-X3) attached with Lawrence & Mayo microscope (shown in Fig 7.17, section 7.2.3).

To analyse the microscopic images of print and reprint samples for cyan and magenta tint, each image was firstly converted to a binary image (step 2), then the canny edge detection algorithm was applied on these binary images (step 3) using MATLAB R2018a generic functions. Edge detection was performed to determine the number of dots in print samples for a given percentage of dots. The edges of the dot sample images were computed from the intensity contrast between the foreground and background pixel. For the next stage of analysis, the contours of the edge dots found in the samples were extracted. The circular Hough transform, which is a modification of the conventional Hough transform, has been used to detect dot contours (step 4). This transform has been used to detect the dots irrespective of their shape. Then, seven dots shape descriptor indexes have been computed (step 5). The shape descriptor indexes of dot patterns

have been computed using MATLAB(R2018a) generic functions. The dots descriptor indexes were then used as features vector to classify the dots in the samples (step 6).

To distinguish between print and reprint samples, feature parameters such as dot area, parameter, circularity, eccentricity, solidity, major axis, and minor axis, have been used to classify the printed dots using a multi-class SVM classification model, with the objective to differentiate the printed dots from the reprinted dots. To check the repeatability of our statistical analysis, the measurements have been carried out 5 times for each press and 10 samples have been taken for each print and reprint sample. In this study, cyan, magenta, yellow and black color dot percentages have been considered for analysis of print and reprint samples. In Fig 7.30 has been shown some samples of dots structures used in this study, with 20% of cyan print (represented as P1C20), 20% of magenta print (represented as P1M20) printed using the printing press P1. Similarly, for two other gravure printing presses (P2 and P3) the print samples are represented as P2C20, P2M20 and P3C20, P3M20. The reprint samples have been referred as R1C20, R1M20, R2C20, R2M20, R3C20, R3M20, for three printers respectively (R1, R2 and R3). For 40% of cyan and magenta tints the same representation has been used shown in the Fig 7.31.

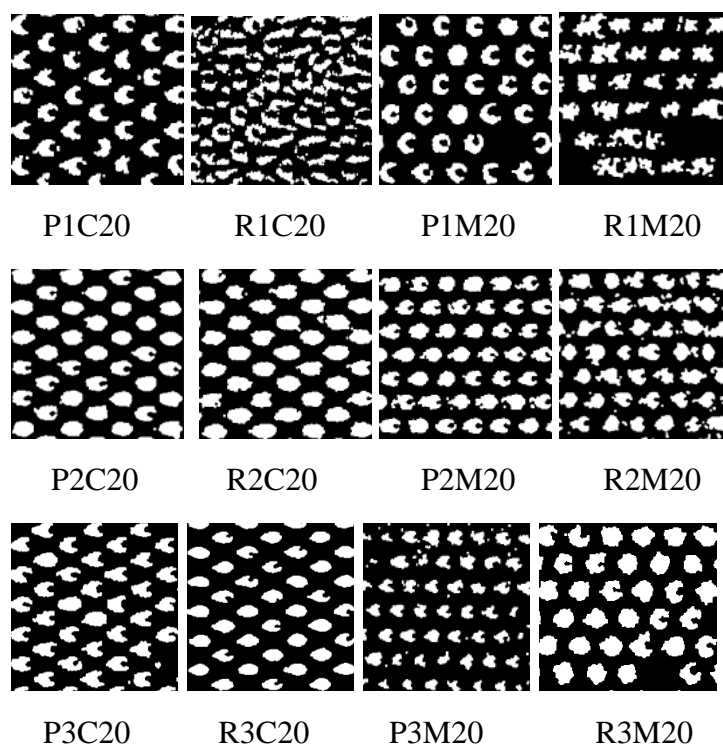
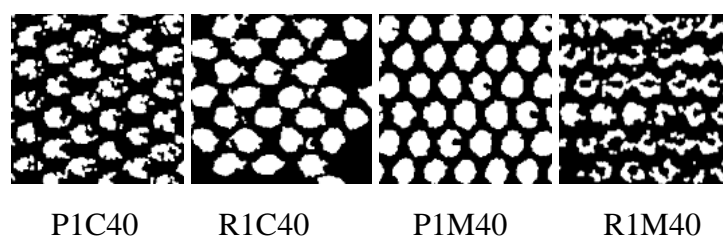


Fig 7.30: Binary images with several dot patterns corresponding to 20% of Cyan and Magenta tints (for Print samples - P1, P2, P3, for Reprint samples - R1, R2, R3).



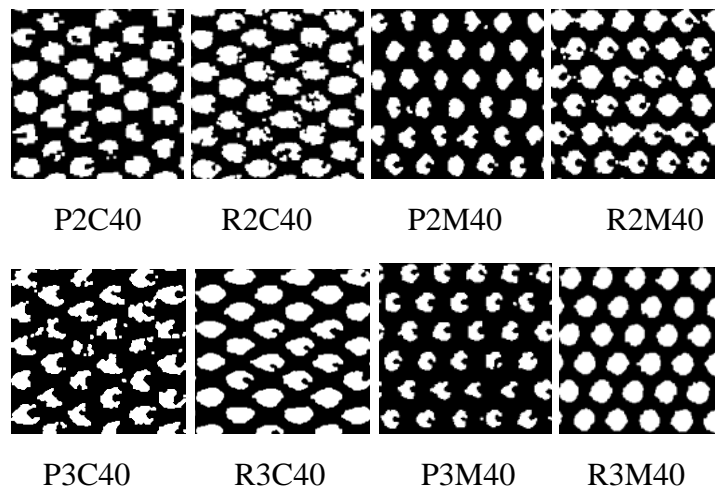


Fig 7.31: Binary images with several dot patterns corresponding of 40% of Cyan and Magenta tints (for Print samples - P1, P2, P3; for Reprint samples - R1, R2, R3).

#### 7.4.1 Classification process

In this section, the classification process that has been applied to detect and distinguish authentic print samples from reprint samples, based on a machine learning method using several dots shape descriptor indexes. In this study, a Support Vector Machine (SVM) method has been applied as a multi-class classification process to differentiate original print samples from simulated counterfeit (scanned reprint samples), using seven 2D shape features such as area, perimeter, circularity, eccentricity, solidity, major axis and minor axis.

##### 7.4.1.1 Support Vector Machine multi-class for classification

In the proposed experiment, six distinct types of samples -original print samples and -reprint (simulated counterfeited) samples have been classified using SVM. The training dataset and testing dataset ratio has been set to 3:2 for each percentage of dots for print and reprint samples (i.e. for 20%, 40% and 50%) of dots. Different shape descriptors index parameters such dot area, perimeter, circularity, eccentricity, solidity, major and minor axis of dots for different print and reprint options have been measured and used for classification between the print sample and scanned reprint sample. The Gaussian kernel function have been tested using 6-fold cross-validation for this experiment. The optimal parameters for cross-validation, experimentally defined correspond to  $C=6$ , gamma set to  $\gamma=0.06$  and plug it in the dataset from the observations are relatively close to each other or far to each other. In chapter 8 (Fig 8.46-8.69) represent the model prediction plot of the dots features for gravure printers P1, P2, P3 and for reprints R1, R2, R3, for cyan, magenta, yellow and black dots.

Then, the confusion matrix enables us to compare the real (actual) target values with those predicted values by the SVM model to evaluate the model's performance and prediction errors (shown in chapter 8 Tables 8.11,8.12, 8.13). For the  $F_1$  score, we

computed the harmonic mean between precision and recall, which both depend on false positives and false negatives values. The efficiency of the classifier was evaluated based on Precision P and Recall R (shown in chapter 8, Tables 8.14, 8.15, 8.16).

The original print samples identify using different methods for gravure printing process on foil:

**1.** The idea of this watermarking is to imperceptibly embed a small amount of secret information (i.e. Batch Number (BN) and Expiry Date (ED)) as Watermark into the Host Image (HI), in the packaging system so that it can be detected later to make an assertion about the host image. The image with the watermark (HIW) was printed and scanned. The scanned image was again printed and rescanned using three gravure printers without any additional processing. The first print's scanned image (PS-WI) and the second print's scanned image (RPRS-WI) have been compared to the softcopy of the host image with a watermark (HIW). It has been observed that the difference in SSIM, PSNR and Co-Relation Co-Efficient values for the second print are significantly different from the first print, which ensures that if the original print is rescanned and reprinted for counterfeiting, it would have lower co-relation co-efficient values than the standard print. Hence, by comparing those values and observing histograms of print, the authenticity of the product may be detected.

**2.** The goal of this second section of the experiment is to distinguish printed samples that have been replicated (counterfeited) by utilizing a gravure printing machine that uses CMYK (Cyan Magenta Yellow Black) colors data and microscopic examination. The production of counterfeit packaging on blister foils through the gravure printing process is usually caused by the utilization of forged cylinders and gravure presses.

Our initial study focused on exploring a potential solution for distinguishing between an original print document and a counterfeit using a pattern recognition process. Through our experiment, we were able to demonstrate that by analyzing the geometrical shape of printed dots at a microscopic level, we could distinguish between an original print and a reprint. To enhance the dot segmentation process, we proposed a new image processing pipeline. In addition, we created six different categories of dot patterns, including four variations of doughnut-shaped patterns, and created a new method for characterizing complex geometrical dot shapes. It has been shown through these results that the microscopic analysis of the geometric shape of printed dots can be utilized to distinguish an original print from a reprint, much like identifying a fingerprint. By conducting this analysis, it will be possible to recognize instances of counterfeit medicine packaging through printing.

**3.** In the third part of study, different dot structure parameters like dot area, major axis, minor axis and eccentricity have been calculated using MATLAB and Murray-Davies Equation. Microscopic studies of dot characteristics show that the reprint sample has a larger dot area than the print samples, as well as a larger dot's major axis, minor axis, and eccentricity. If a pharmaceutical package is printed by the original manufacturer or their authorized printer, it must be easy to determine if the packaging was made by counterfeiters or the real manufacturer.



4. The goal of the studies forth section is to differentiate between printed and reprinted dots utilizing shape descriptor index parameters as print features, such as dot area, perimeter, circularity, and eccentricity, and solidity, main and minor axis of the samples. The counterfeiter makes the reprint by scanning or capturing the original print and duplicating it. The major goal of this work is to categorize the print and reprint dot shape features using a multi-class Support Vector Machine (SVM) classification model in order to identify the characteristics of dot shape size variations. This study demonstrates the accuracy of the classification of printing dot patterns with 20%, 40% and 50% of cyan, magenta, yellow and black color for print samples. Relatively lower accuracy has been obtained with reprints, and the dot sizes and shapes for reprints have increased irregularly after imaging. The variation of accuracy and harmonic means they are wide apart and inevitable. SVM classification and its associated parameters may be effectively used for identifying counterfeited documents, and printing source may be established for authentication applications.

In the next Chapter 8 discusses the experimental findings from distinct experimental methods.

# Chapter 8

## EXPERIMENTAL RESULT AND DISCUSSION

### 8. Experimental Result and Discussion

In this chapter, results obtained from the four different anticounterfeiting methods have been provided in four parts.

#### 8.1 Experimental results and discussions for Variable Image Watermark Process

In this study, a non-blind dynamic watermark has been embedded into an image. The 16-bit watermark has been generated based on the product batch number and expiry date. The watermark has been kept in a 16-bit buffer. Each of the 16 bits of the watermark has been added to intensity values of some predefined intensities of the blue channel / specific channel. It has been investigated how robust is the printed watermarked image against the scan and print attacks. Comparison between Host Image (HI) without watermark, Host Image with Watermark (HIW), Print sample – ‘Printed and Scanned Watermarked Image (PS-WI)’ and Reprint sample – ‘RePrinted and ReScanned Watermarked Image (RPRS-WI)’ have been done. The proposed method successfully makes the watermark perceptually invisible and robust to print and scan attacks, according to experimental data [1,23].

In this study, the watermark (Batch Number (BN) and Expiry Date (ED)) has been embedded in the blue channel of the RGB image as the human visual system is much less sensitive to blue [1] in comparison to red and green channels. So, the watermarking can be done more effectively and imperceptibly.

This study has been done on two types of substrates:

- on paper media(substrate) (A4 paper 88gsm and 120gsm) printed in inkjet printer
- on blister foil media(substrate) printed in gravure process.

##### 8.1.1 Experimental results and discussions for watermarking process on A4 media

Four different 64-bit standard images have been chosen as the host images in this proposed work so that data can be embedded into them. In the experiment, the watermarks used for the study have the names Z, A, M, Q, T, J, F, O, X and N. Watermark Z refers to Z9-12/99 where Z9 is the code of Batch No. and 12/99 refers to the expiry date of December 2099. Similarly, watermark A refers to A0-1/17, where A0 indicates its batch number code and 1/17 indicates expiry date of January 2017. Similarly, M referring to M4-7/28, Q referring to Q6-9/45, T referring to T2-5/61, J referring to J7-6/70, F referring to F5-2/82, O referring to O4-4/35, X referring to X1-5/56, and N referring to N7-8/95 are various watermarks showing their batch number and expiry date. After embedding the watermark into the blue

component, the R, G, and Watermarked B channels of the image have been concatenated to get the RGB image, i.e, Host Image with Watermark soft copy (HIW). It has been observed that apparently there is no visual difference between the Host Image (HI) and Host Image with Watermark (HIW). The histograms of the blue channels of the host image (HI) and the host image with watermark (HIW) have been compared, and the results have been shown in Table 8.1. Fifteen observers reported that there was no visible difference between the host image (HI) and the watermarked host image (HIW). The watermarked images (HIW) have not been changed visibly. This indicates that the watermark's fidelity is maintained [28].

Table 8.1: Histogram of Host Image (HI) and Host Image with Watermark softcopy (HIW)


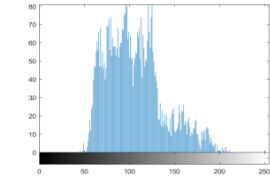

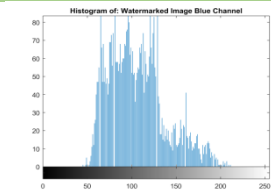

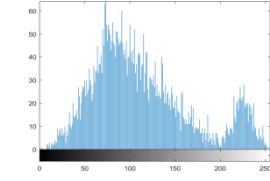

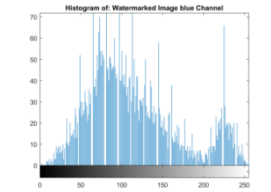

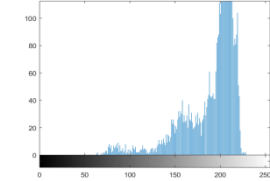

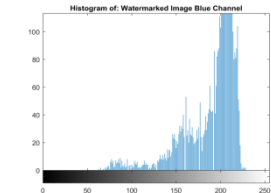

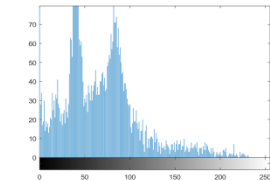

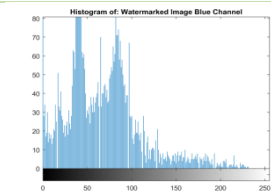
Host Image	Host Image Histogram(HI)	Watermarked Image	Watermarked Image Histogram(HIW)
			
			
			
			

Table 8.1 compares the blue channel histograms of the host image (HI) and the soft copy of the host image with the watermark (HIW) that indicates clear difference between histograms of HI and HIW. The histograms of the watermarked image have distinct peaks at select predetermined intensities, as shown by the sharp peaks at specific predefined intensities. The histogram's shape however, has been unchanged [11,12].

### 8.1.1.1 Testing the Fidelity of Embedded Data into Image

One of the most common property watermarking processes is fidelity. Fidelity is defined as the visible similarity between the watermarked image and the unwatermarked image. It has been observed, apparently there is no visual difference between the Host Image (HI) and Host Image with a watermark (HIW). Beside visual comparison, PSNR (peak signal-to-noise ratio) and SSIM (structural similarity index measurement) values between the Host Image (HI) and Host Image with Watermark (HIW) have been reported. Generally, a larger PSNR indicates that the watermarked image has a similar appearance to the host image. That means that the watermarking method makes embedded data more imperceptible. The SSIM characterises image degradation as perceived changes in structural information. The suggested watermark method has been compared with previously proposed watermark process, as shown in Tables 8.2 and 8.3. Table 8.2 has shown the comparison of PSNR results obtained by the proposed watermark method and other watermark methods: (Qingtang et al., 2017), (Das et al., 2014), and (Kalra et al., 2015) [1]. Table 8.3 has shown the comparison of SSIM results obtained by the proposed watermark method and other watermark methods: (Qingtang et al., 2017), (Das et al., 2014), and (Kalra et al., 2015). This study has calculated and compared the blue component's PSNR and SSIM values for the host image (HI) and the watermarked image (HIW). It has been established that PSNR values of about 36 dB and above are practically imperceptible to human sight (Afrakhteh et al., 2010) [5]. Therefore, it may be assumed that the difference between the host image (HI) and the watermarked image (HIW) is undetectable to the human eye for PSNR values greater than 36 dB. Tables 8.2 and 8.3 display a comparison of the suggested method's watermark invisibility results with those of (Qingtang et al. (2017), (Das et al., 2014), and (Kalra et al. (2015). These statistics show that the suggested method's PSNR and SSIM values are higher than those of (Qingtang et al., 2017), (Das et al., 2014), and (Kalra et al.,2015). This indicates that the proposed watermarking technique provides higher fidelity in comparison to the existing techniques.

Table 8.2: Comparison results between different methods using the PSNR (without any attacks)

Blue component	PSNR			
Image	Proposed Method	Qingtang Su et al. (2017)	Das et al. (2014)	Kalra et al. (2015)
Lena	<b>63.1015</b>	49.9898	41.7801	42.0109
Baboon	<b>65.3652</b>	49.8901	40.2446	36.1103
Avion	<b>69.6314</b>	49.8664	40.7932	39.7644
Peppers	<b>67.7913</b>	50.0839	41.0122	42.6843

Table 8.3: Comparison result between different methods using the SSIM (without any attacks)

Blue component	SSIM			
<b>Image</b>	Proposed method	Qingtang Su et al.(2017)	Das et al. (2014)	Kalra et al. (2015)
<b>Lena</b>	<b>0.99</b>	0.9872	0.9704	0.9787
<b>Baboon</b>	<b>0.99</b>	0.9957	0.9893	0.9754
<b>Avion</b>	<b>0.99</b>	0.9854	0.9872	0.9851
<b>Peppers</b>	<b>0.99</b>	0.9859	0.9733	0.9816

### 8.1.1.2 Robustness of Watermark Against Print and Scan attacks

The watermarked image (HIW) has been printed and subsequently scanned, and saved as Printed and Scanned Watermarked Image (PS-WI). The watermarked print image (PS-WI) has been reprinted and rescanned. It has been saved as RePrinted and ReScanned Watermarked Image (RPRS-WI). Comparison of the host image blue channels after Watermarked image (HIW) and Printed and Scanned Watermarked Image (PS-WI) and RePrinted and ReScanned Watermarked Image (RPRS-WI) showed a significant difference in MSE, PSNR, and SSIM. There has been observed a noticeable variation in MSE, PSNR, and SSIM between the blue channels of (HIW) and PS-WI and RPRS-WI that has been tabulated in Table 8.4-(a) and (b). The results show that it may be easily identified from such a comparison whether an unknown print sample has been printed by the original printer authorised by the manufact user or by the counterfeiter who tries to replicate it by scanning the original print and reprinting it.

Table 8.4(a). Experimental analysis the Print samples (HIW vs PS-WI) and Re-print samples (simulated counterfeited sample) (HIW vs RPRS-WI) in Canon E400 printer cum scanner

Sample	Print			Reprint		
	LENA			LENA		
WATER MARK	MSE	PSNR	SSIM	MSE	PSNR	SSIM
Z	2.0816e+03	31.24	0.97	5.5423e+03	11.73	0.92
A	1.9998e+03	32.52	0.97	5.3211e+03	12.22	0.94
M	1.9131e+03	33.99	0.97	5.3528e+03	12.15	0.93
Q	1.9791e+03	32.86	0.98	5.3312e+03	12.19	0.94
T	2.0605e+03	31.56	0.97	5.3201e+03	12.22	0.94
J	1.9767e+03	32.89	0.97	5.6245e+03	11.56	0.93
F	2.0858e+03	31.16	0.98	5.3501e+03	12.15	0.94
O	1.9733e+03	32.95	0.98	5.3993e+03	12.04	0.94
X	2.0926e+03	31.07	0.97	5.5551e+03	11.71	0.93
N	2.1584e+03	30.13	0.98	5.2743e+03	12.33	0.94
WATER MARK	BABOON			BABOON		
	MSE	PSNR	SSIM	MSE	PSNR	SSIM
Z	2.1097e+03	30.8217	0.97	5.6499e+03	11.51	0.92
A	1.9852e+03	32.7538	0.97	5.5041e+03	11.81	0.93
M	2.0449e+03	31.7985	0.97	5.5954e+03	11.62	0.93
Q	1.9779e+03	32.8744	0.97	5.4661e+03	11.62	0.93
T	2.0898e+03	31.1154	0.98	5.6991e+03	11.89	0.93
J	2.1263e+03	30.5803	0.97	5.5714e+03	11.41	0.93
F	1.9288e+03	33.712	0.97	4.4256e+03	11.67	0.93
O	2.0290e+03	32.044	0.97	5.5038e+03	11.82	0.93
X	1.9211e+03	33.8467	0.97	5.6242e+03	11.56	0.93
N	1.9887e+03	32.6965	0.97	5.5794e+03	11.65	0.93
WATER MARK	AVION			AVION		
	MSE	PSNR	SSIM	MSE	PSNR	SSIM
Z	2.0429e+03	31.8289	0.98	3.3801e+03	19.24	0.90
A	1.9874e+03	32.7185	0.98	3.2343e+03	20.10	0.92
M	2.1401e+03	30.3837	0.98	3.3533e+03	19.39	0.92
Q	1.9662e+03	33.0701	0.98	3.2602e+03	19.94	0.92
T	2.1924e+03	29.6587	0.97	3.1953e+03	20.35	0.92
J	1.9788e+03	32.8607	0.97	3.6495e+03	17.82	0.91
F	2.1604e+03	30.0976	0.97	3.2261e+03	20.16	0.91
O	2.0749e+03	31.3374	0.98	3.2925e+03	19.74	0.92
X	2.1091e+03	30.8296	0.98	3.3626e+03	19.34	0.90
N	2.1679e+03	29.9935	0.97	3.2850e+03	19.79	0.90
WATER MARK	PEPPERS			PEPPERS		
	MSE	PSNR	SSIM	MSE	PSNR	SSIM
Z	2.1833e+03	29.7817	0.96	7.3036e+03	8.90	0.75
A	2.1069e+03	30.8617	0.97	7.1962e+03	0.77	0.77
M	2.0858e+03	31.1745	0.96	7.1001e+03	9.16	0.77
Q	2.0342e+03	31.9655	0.98	7.1064e+03	9.15	0.77
T	2.2337e+03	29.1101	0.98	7.0655e+03	9.20	0.77
J	2.1476e+03	30.2772	0.97	7.4203e+03	8.76	0.76
F	1.9932e+03	32.6225	0.97	7.4090e+03	8.78	0.76
O	2.1832e+03	29.7868	0.97	7.3001e+03	8.91	0.77
X	2.1151e+03	30.7429	0.97	7.3444e+03	8.85	0.77
N	2.0581e+03	31.594	0.97	7.2245e+03	9.00	0.77

Table 8.4(b). Experimental analysis the Print samples (HIW vs PS-WI) and Re-print samples (simulated counterfeited sample) (HIW vs RPRS-WI) in Canon E610 printer cum scanner

Sample	Print			Reprint		
WATER MARK	LENA			LENA		
	MSE	PSNR	SSIM	MSE	PSNR	SSIM
Z	2.0591e+03	31.5789	0.96	6.9017e+03	9.4215	0.89
A	1.9946e+03	32.6002	0.95	6.9363e+03	9.3745	0.89
M	1.9205e+03	33.8581	0.95	6.8508e+03	9.4915	0.89
Q	2.0074e+03	32.3911	0.95	6.9480e+03	9.3588	0.87
T	1.9923e+03	32.637	0.95	6.9259e+03	9.3886	0.89
J	1.9996e+03	32.5176	0.95	6.8677e+03	9.4682	0.89
F	2.0606e+03	31.5553	0.96	6.9512e+03	9.3544	0.88
O	1.9942e+03	32.607	0.96	6.8646e+03	9.4724	0.89
X	1.9400e+03	33.5179	0.96	7.0166e+03	9.2672	0.87
N	1.9418e+03	33.4687	0.96	6.9153e+03	9.403	0.88
WATER MARK	BABOON			BABOON		
	MSE	PSNR	SSIM	MSE	PSNR	SSIM
Z	2.0188e+03	32.2202	0.95	6.0594e+03	10.7312	0.88
A	1.9003e+03	34.2173	0.95	6.0697e+03	10.713	0.88
M	2.0107e+03	32.3385	0.96	6.6783e+03	9.7367	0.89
Q	2.0139e+03	32.2874	0.96	6.0188e+03	10.8035	0.89
T	1.8880e+03	34.4407	0.96	6.6164e+03	9.8278	0.89
J	2.0679e+03	31.4449	0.96	6.0386e+03	10.7682	0.89
F	2.0105e+03	32.3426	0.95	6.0436e+03	10.7593	0.88
O	1.9866e+03	32.7309	0.95	5.5521e+03	11.7116	0.89
X	2.0294e+03	32.0414	0.94	6.6388e+03	9.7946	0.89
N	1.9454e+03	33.4243	0.95	6.0311e+03	10.7815	0.89
WATER MARK	AVION			AVION		
	MSE	PSNR	SSIM	MSE	PSNR	SSIM
Z	2.0167e+03	32.243	0.98	3.9466e+03	16.476	0.93
A	1.9933e+03	32.6202	0.98	3.9035e+03	16.658	0.94
M	1.8834e+03	34.5247	0.97	3.9357e+03	16.5216	0.94
Q	1.8180e+03	35.7663	0.98	3.9088e+03	16.6352	0.94
T	1.9445e+03	33.4402	0.98	3.9462e+03	16.4778	0.94
J	1.8639e+03	34.8855	0.98	3.938.1e+03	16.5117	0.94
F	1.8828e+03	34.5347	0.98	4.0021e+03	16.2475	0.94
O	1.9903e+03	32.6696	0.98	3.9947e+03	16.2776	0.93
X	1.9878e+03	32.7118	0.97	3.9754e+03	16.3565	0.93
N	1.9389e+03	33.5363	0.98	3.9336e+03	16.5303	0.94
WATER MARK	PEPPERS			PEPPERS		
	MSE	PSNR	SSIM	MSE	PSNR	SSIM
Z	2.0628e+03	31.5219	0.97	4.4752e+03	14.53	0.72
A	1.8796e+03	34.5951	0.95	4.8382e+03	13.44	0.71
M	1.8827e+03	34.5377	0.97	4.8180e+03	13.4961	0.72
Q	1.8249e+03	35.6307	0.96	5.2042e+03	12.4947	0.72
T	1.8323e+03	35.4873	0.98	4.8155e+03	13.5031	0.71
J	1.8781e+03	34.6226	0.97	4.4559e+03	14.5928	0.72
F	1.8809e+03	34.5702	0.97	5.8987e+03	12.5077	0.72
O	1.8734e+03	34.7092	0.97	6.1376e+03	10.5944	0.72
X	1.8279e+03	35.5725	0.97	5.6238e+03	11.5624	0.72
N	1.8730e+03	34.7155	0.97	5.1337e+03	12.6662	0.72



The results in Table 8.4-(a), (b) demonstrated that the MSE values of the print samples (HIW vs PS-WI) have been observed significantly lower than the MSE values of the reprint samples (HIW vs RPRS-WI), meanwhile the PSNR and SSIM values are higher. Prints from Canon E400 and Canon E610 printers both had shown similar behaviour. According to these findings have been observed the difference in statistical values of MSE, PSNR, SSIM between the image HIW and PS-WI is less than difference in values between HIW and RPRS-WI. Furthermore, image (PS-WI) appears to be visually more similar to the host image watermarked (HIW) in comparison to RPRS-WI. Therefore, whether a print sample is authenticated source or not, may be determined by the difference in values of MSE, PSNR and SSIM. The graphs in Figs. 8.1(a, b), 8.2(a, b), and 8.3(a, b, c, d, e, f, g, h), 8.4(a, b, c, d, e, f, g, h) show how the PSNR and SSIM values of print sample (PS-WI) and reprint sample (RPRS-WI) changed when printed on two different printers (Canon E400 and Canon E610). It has been observed that the PSNR and SSIM of each image fall within a predetermined range for PS-WI and HIW. However, the difference is much higher in case of RPRS and HIW. The range of values may be checked in order to verify the originality of printer. The print might not be regarded as original if the values of MSE are higher and PSNR are lower than the stipulated range. The results show that the suggested watermarking process is effective against the Print & Scan attack.

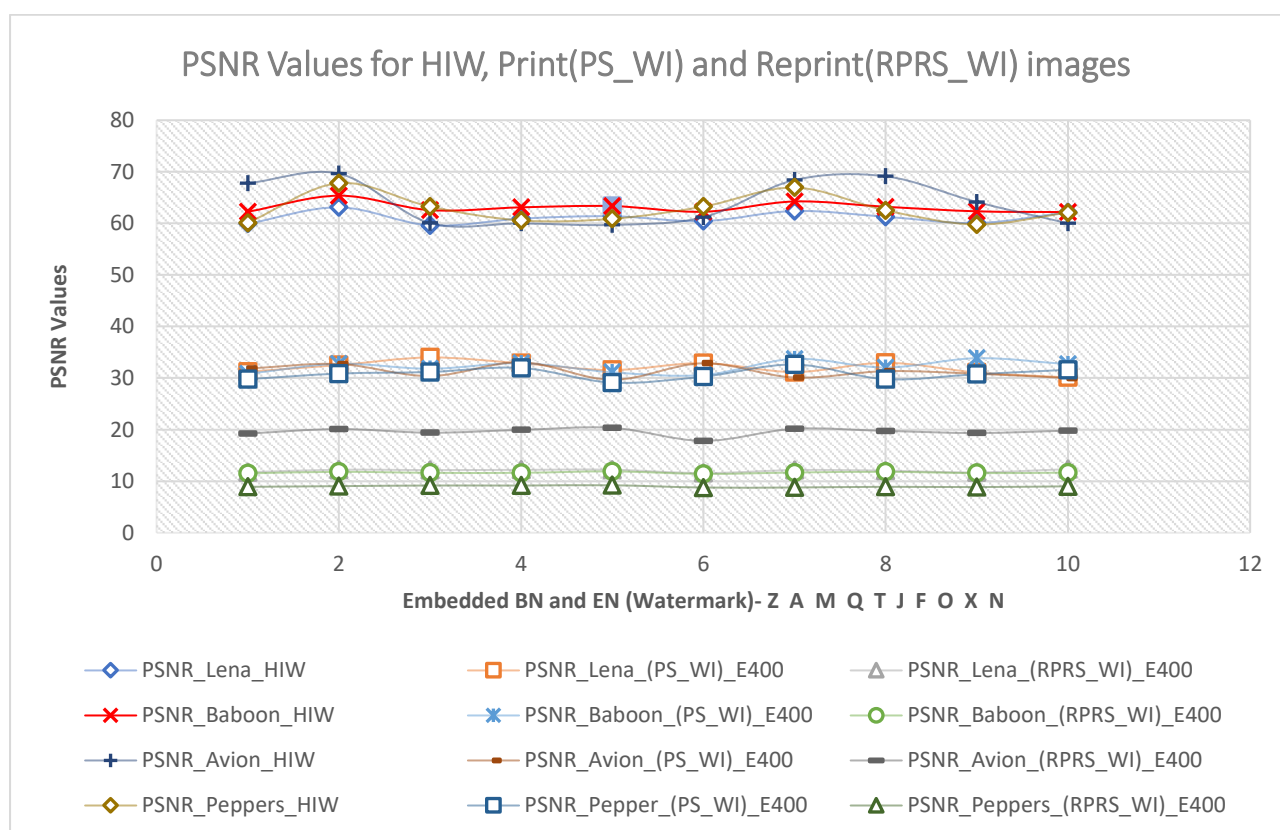
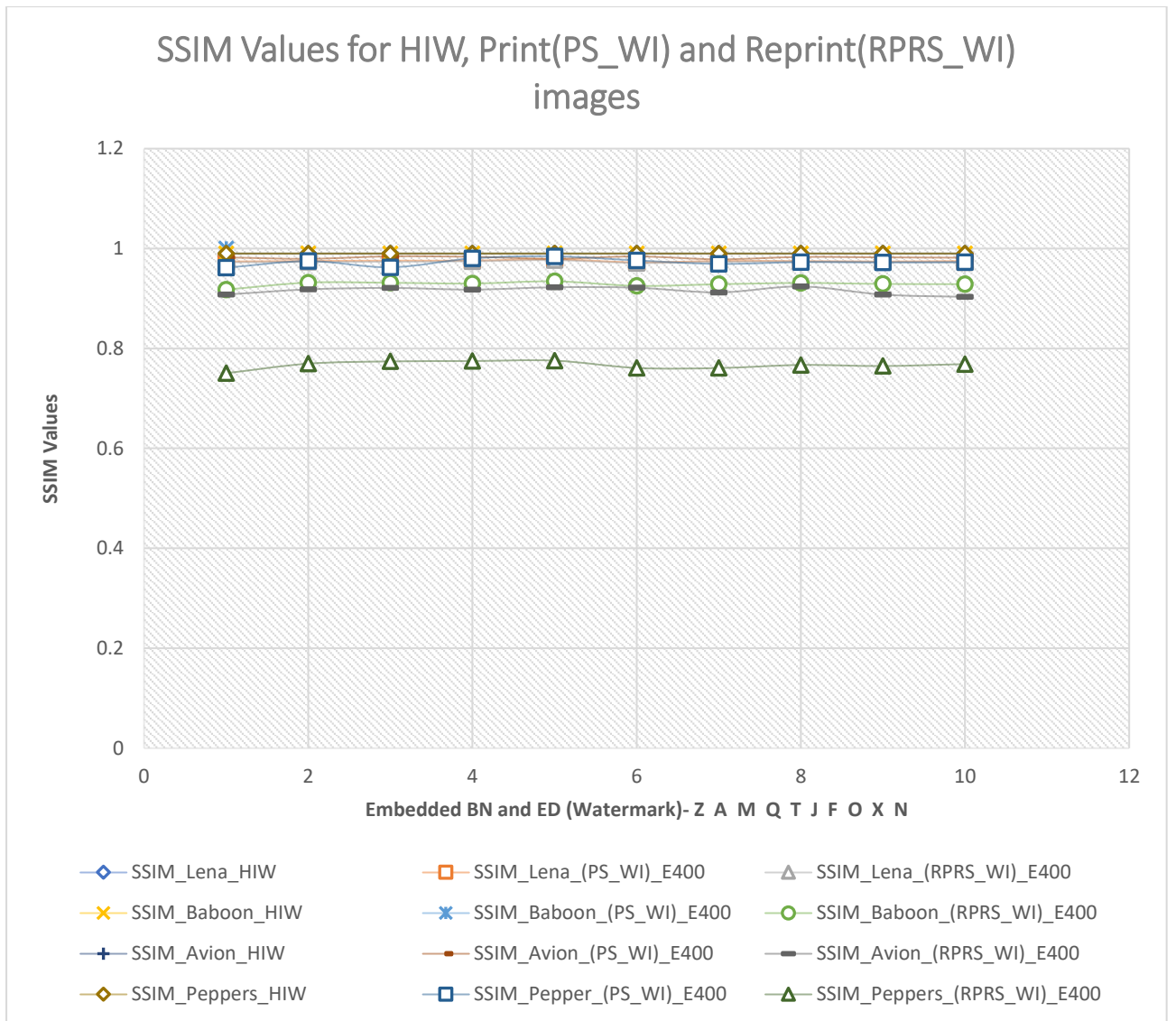


Fig: 8.1: (a)PSNR values for HIW, Print (PS-WI) and Reprint (RPRS-WI) for Canon E400



(b)

Fig: 8.1: (b)SSIM values for HIW, Print (PS-WI) and Reprint (RPRS-WI) for Canon E400

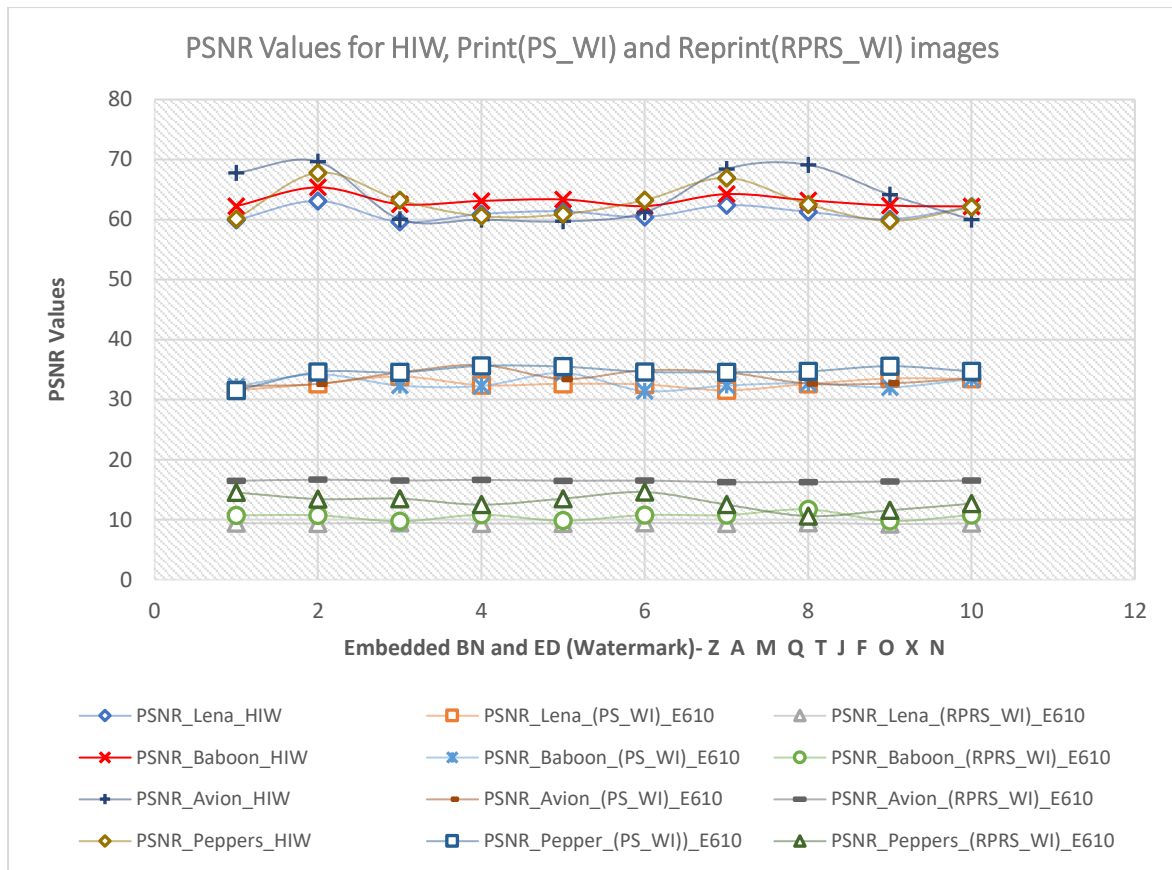
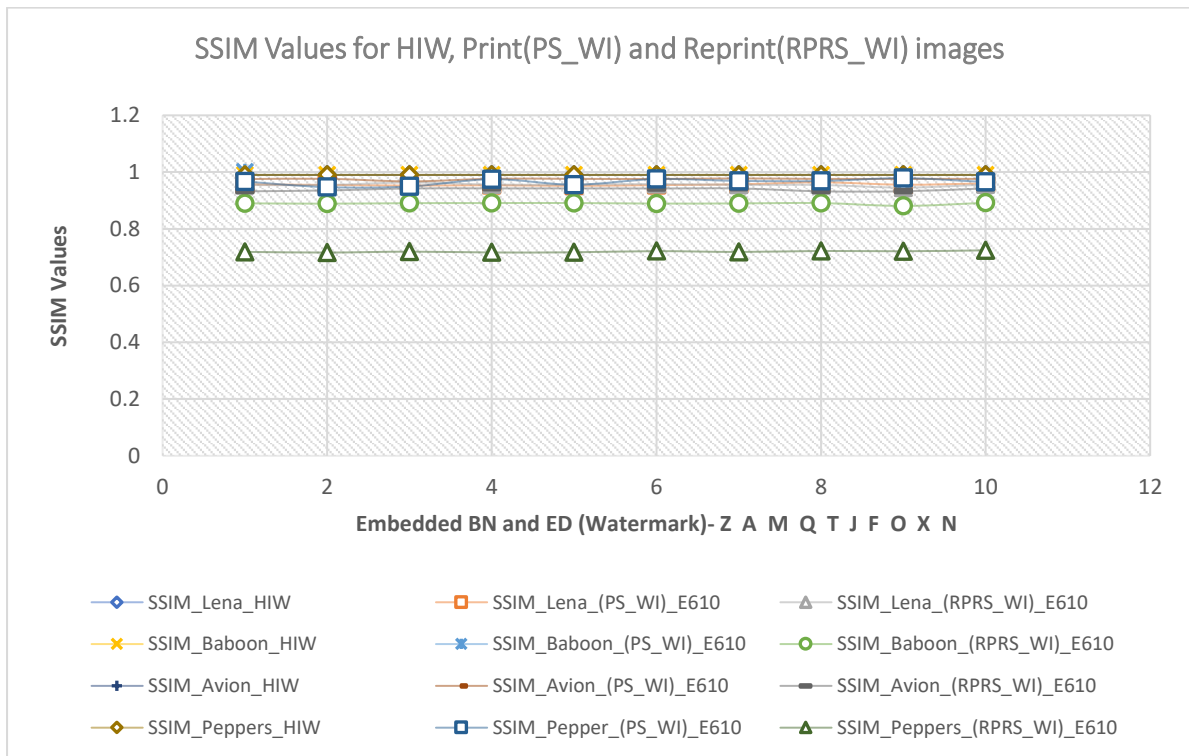
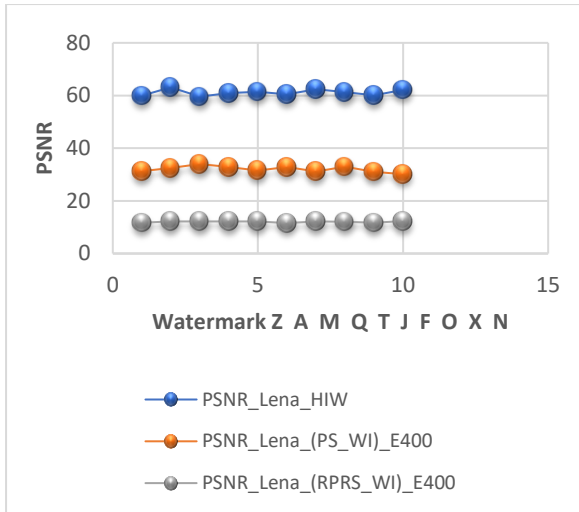


Fig 8.2: (a)PSNR values for HIW, Print (PS-WI) and Reprint (RPRS-WI) images for Canon E610

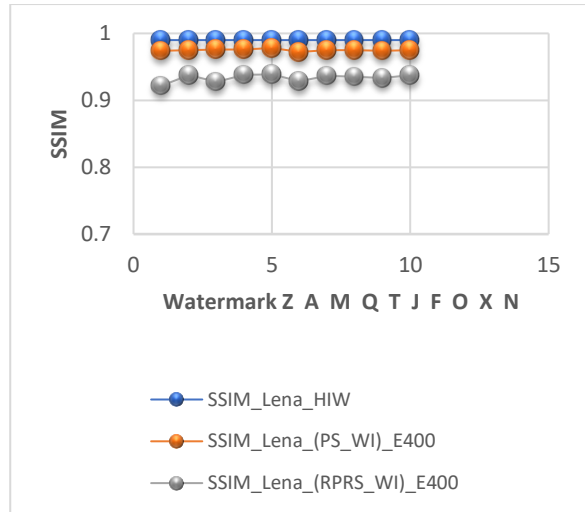


(b)

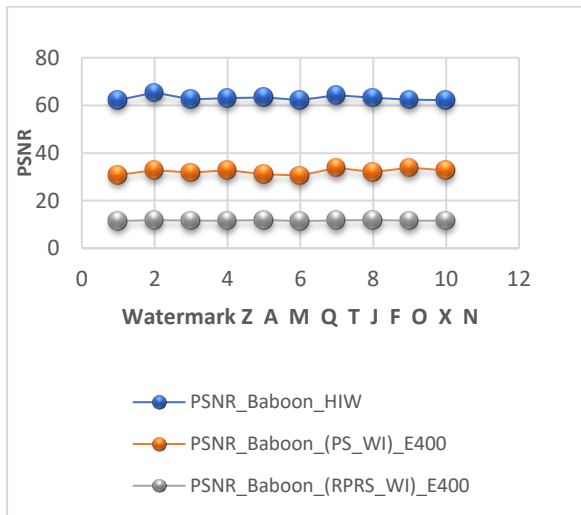
Fig 8.2: (b)SSIM values for HIW, Print (PS-WI) and Reprint (RPRS-WI) images for Canon E610



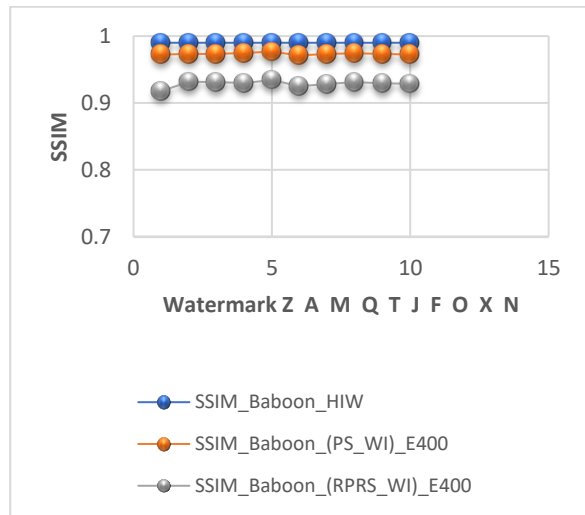
(a)



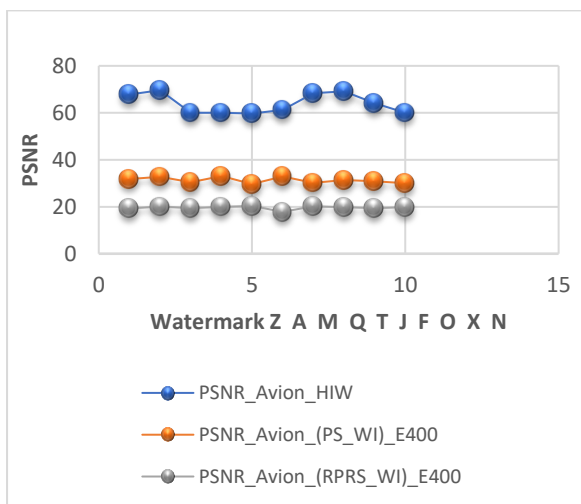
(e)



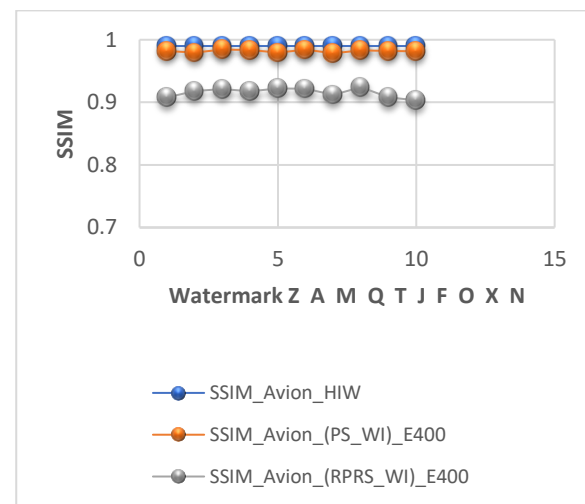
(b)



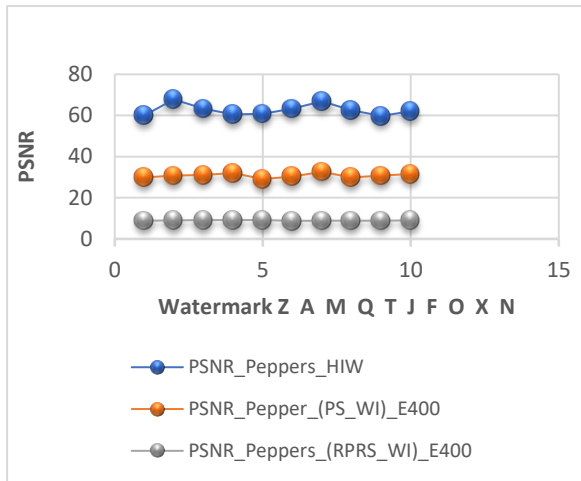
(f)



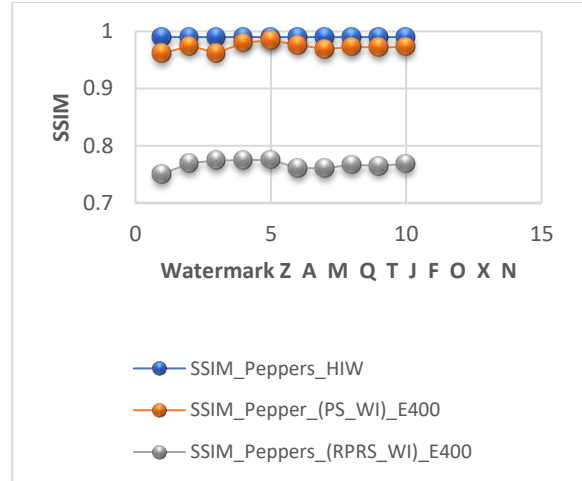
(c)



(g)

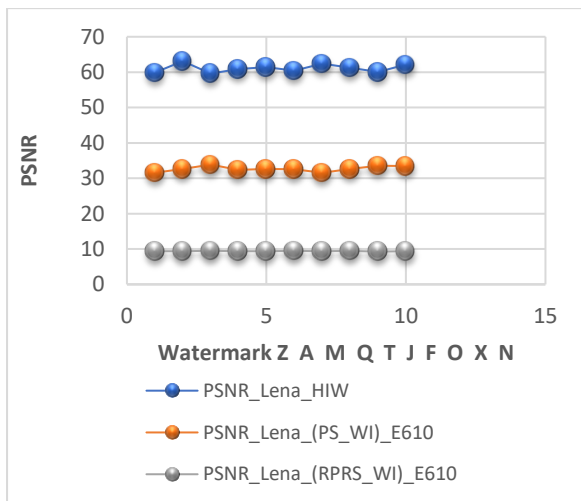


(d)

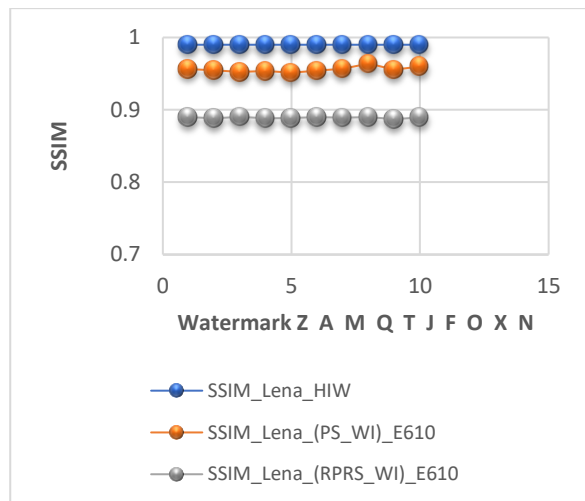


(h)

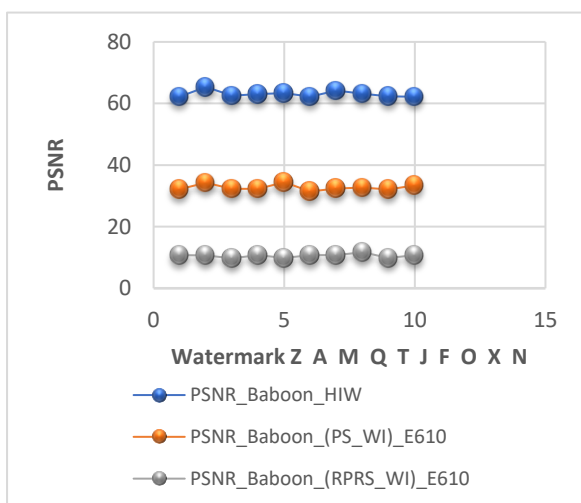
Fig 8.3: PSNR values for PS-WI and RPRS-WI of images-(a) Lena (b) Baboon (c) Avion (d) Peppers and SSIM values for PS-WI and RPRS-WI of images-(e) Lena (f) Baboon (g) Avion (h) Peppers using Canon E400



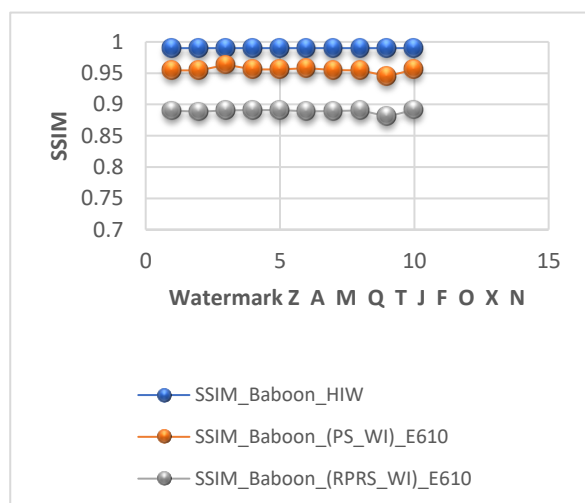
(a)



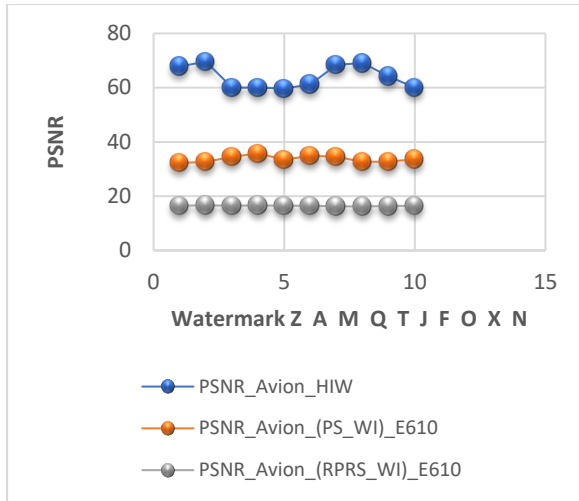
(e)



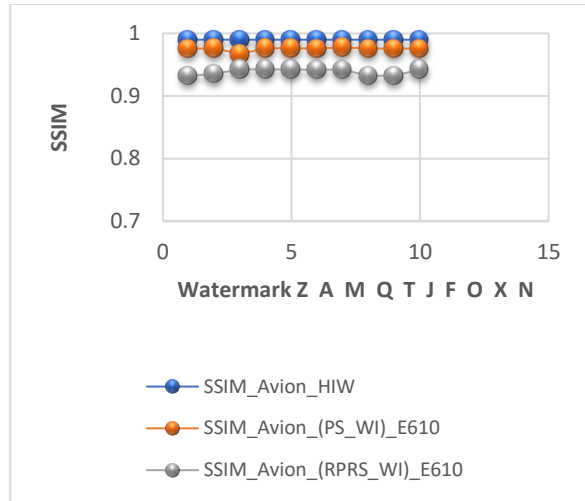
(b)



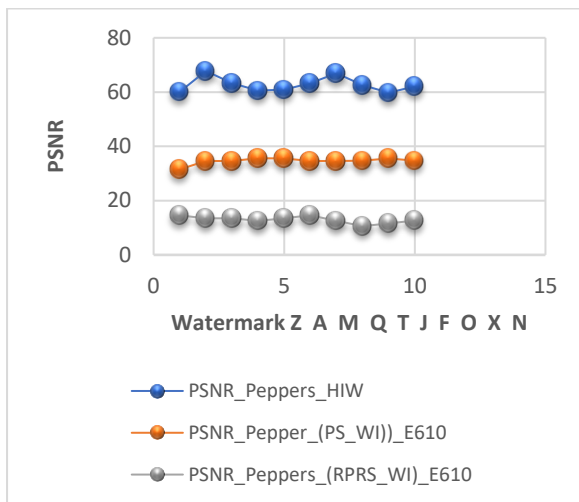
(f)



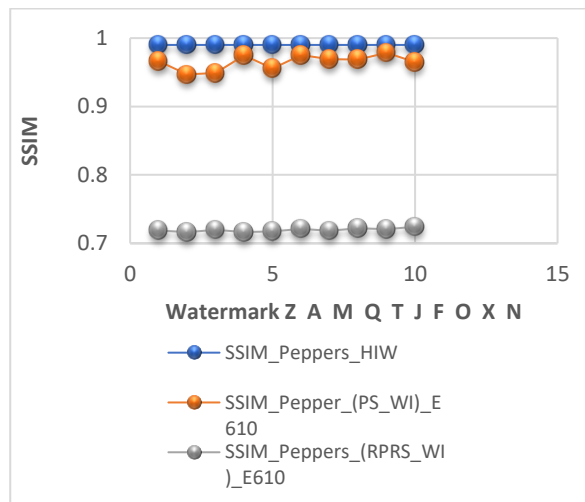
(c)



(g)



(d)



(h)

Fig 8.4: PSNR values for PS-WI and RPRS-WI of images-(a) Lena (b) Baboon (c) Avion (d) Peppers and SSIM values for PS-WI and RPRS-WI of images-(e) Lena (f) Baboon (g) Avion (h) Peppers using Canon E610

### 8.1.2 Experimental results and Discussion for A4 paper 120gsm and foil media

This experiment has been done on A4 paper (120 gsm) using a Canon E400 printer. Same experiment has been carried out on foil media using a gravure printing machine (P1). The following Tables 8.5 and 8.6 show the histograms of the Host Image with Watermark (HIW), Printed and Scanned Watermarked Image (PS-WI), RePrinted and ReScanned Watermarked Image (RPRS-WI) for two different printing media and two printing processes. Table 8.5 shows the experimental results done on A4 paper (120 gsm) using a Canon E400 printer.

Table 8.5: Histogram of Host Image with Watermark softcopy (HIW), Print sample image (PS-WI) and Reprint sample image (RPRS-WI) on A4 media (Scan using Canon E400(Scanner S1))

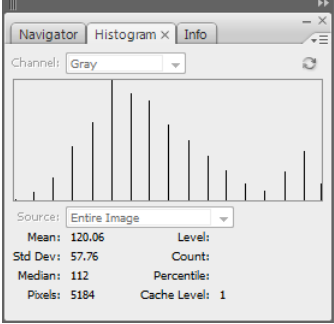
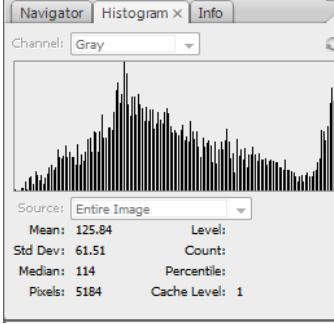
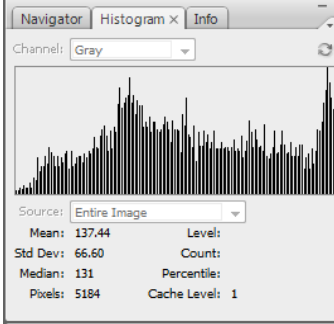
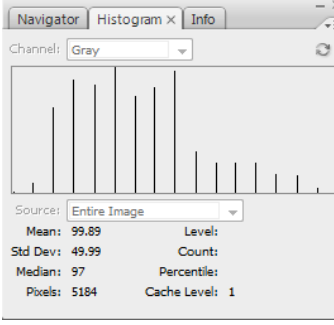
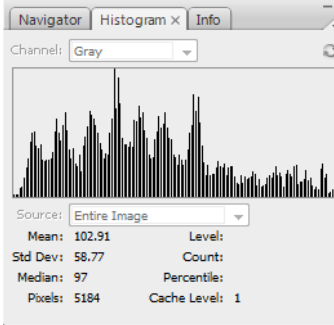
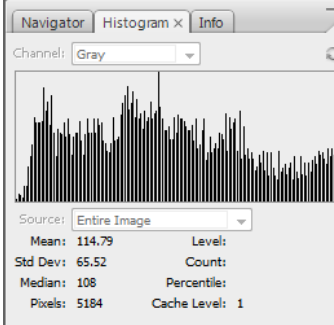
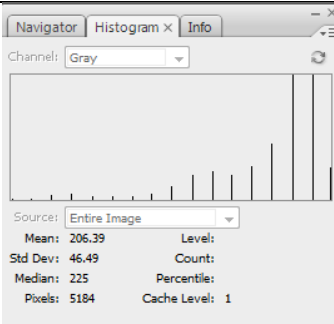
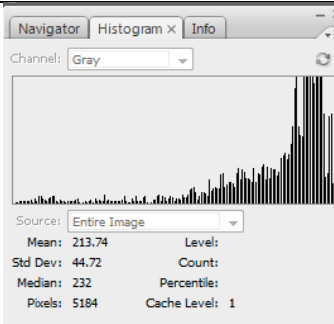
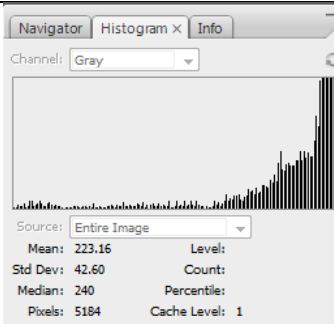
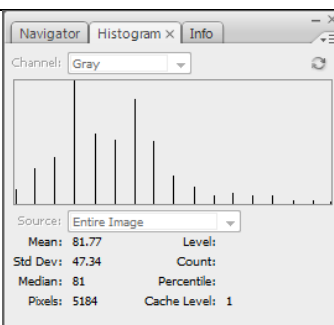
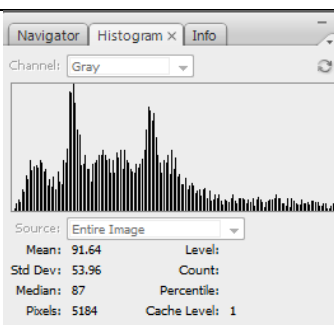
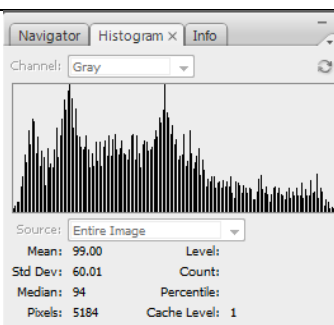
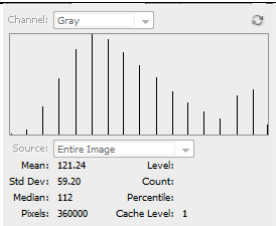
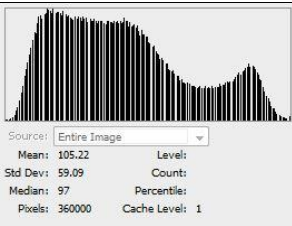
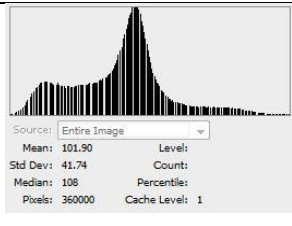
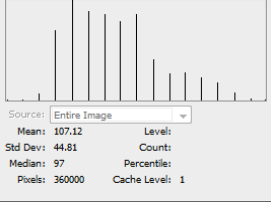
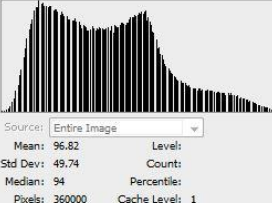
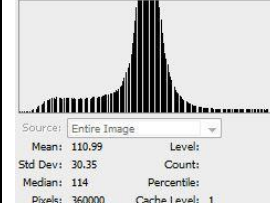
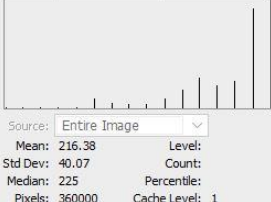
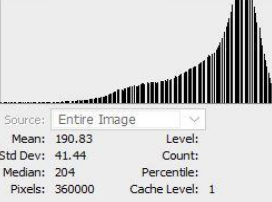
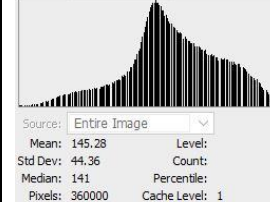
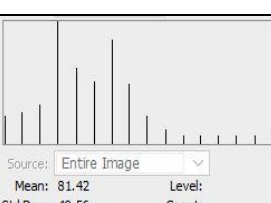

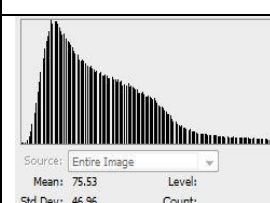
Images	Host Image with Watermark softcopy (HIW)	Printed and Scanned Watermarked Image (PS-WI) Print sample	RePrinted and ReScanned Watermarked Image (RPRS-WI) Reprint sample
Histogram Of Baboon	 <p>Channel: Gray</p> <p>Source: Entire Image</p> <p>Mean: 120.06    Level:   </p> <p>Std Dev: 57.76    Count:   </p> <p>Median: 112    Percentile:   </p> <p>Pixels: 5184    Cache Level: 1</p>	 <p>Channel: Gray</p> <p>Source: Entire Image</p> <p>Mean: 125.84    Level:   </p> <p>Std Dev: 61.51    Count:   </p> <p>Median: 114    Percentile:   </p> <p>Pixels: 5184    Cache Level: 1</p>	 <p>Channel: Gray</p> <p>Source: Entire Image</p> <p>Mean: 137.44    Level:   </p> <p>Std Dev: 66.60    Count:   </p> <p>Median: 131    Percentile:   </p> <p>Pixels: 5184    Cache Level: 1</p>
Histogram Of Lena	 <p>Channel: Gray</p> <p>Source: Entire Image</p> <p>Mean: 99.89    Level:   </p> <p>Std Dev: 49.99    Count:   </p> <p>Median: 97    Percentile:   </p> <p>Pixels: 5184    Cache Level: 1</p>	 <p>Channel: Gray</p> <p>Source: Entire Image</p> <p>Mean: 102.91    Level:   </p> <p>Std Dev: 58.77    Count:   </p> <p>Median: 97    Percentile:   </p> <p>Pixels: 5184    Cache Level: 1</p>	 <p>Channel: Gray</p> <p>Source: Entire Image</p> <p>Mean: 114.79    Level:   </p> <p>Std Dev: 65.52    Count:   </p> <p>Median: 108    Percentile:   </p> <p>Pixels: 5184    Cache Level: 1</p>
Histogram Of Airplan	 <p>Channel: Gray</p> <p>Source: Entire Image</p> <p>Mean: 206.39    Level:   </p> <p>Std Dev: 46.49    Count:   </p> <p>Median: 225    Percentile:   </p> <p>Pixels: 5184    Cache Level: 1</p>	 <p>Channel: Gray</p> <p>Source: Entire Image</p> <p>Mean: 213.74    Level:   </p> <p>Std Dev: 44.72    Count:   </p> <p>Median: 232    Percentile:   </p> <p>Pixels: 5184    Cache Level: 1</p>	 <p>Channel: Gray</p> <p>Source: Entire Image</p> <p>Mean: 223.16    Level:   </p> <p>Std Dev: 42.60    Count:   </p> <p>Median: 240    Percentile:   </p> <p>Pixels: 5184    Cache Level: 1</p>
Histogram Of Peppers	 <p>Channel: Gray</p> <p>Source: Entire Image</p> <p>Mean: 81.77    Level:   </p> <p>Std Dev: 47.34    Count:   </p> <p>Median: 81    Percentile:   </p> <p>Pixels: 5184    Cache Level: 1</p>	 <p>Channel: Gray</p> <p>Source: Entire Image</p> <p>Mean: 91.64    Level:   </p> <p>Std Dev: 53.96    Count:   </p> <p>Median: 87    Percentile:   </p> <p>Pixels: 5184    Cache Level: 1</p>	 <p>Channel: Gray</p> <p>Source: Entire Image</p> <p>Mean: 99.00    Level:   </p> <p>Std Dev: 60.01    Count:   </p> <p>Median: 94    Percentile:   </p> <p>Pixels: 5184    Cache Level: 1</p>



Table 8.6 shows the results on blister foil using a gravure printer (P1). The reprint has been done with the same printer with respect to the substrate, and all the process parameters have been the same and maintained for the print and reprint processes. In this part of the study, a scanner (S1) has been used to observe the difference in histogram pattern due to counterfeiting (print and scan attack). The results indicate that, by histogram analysis of a print, it may be identified whether it is printed by the original manufacturer or its authorised printers or has been counterfeited by scanning the printed image and reprinting it. The scanned images of the first print (PS-WI) and the second print or reprint (RPRS-WI) have been compared with the Host Image with Watermark softcopy (HIW). Experimental results have been shown that the histograms patterns are similar if it is printed in the original printer by observing print sample (PS-WI) histogram with Host Image with Watermark (HIW) image histogram. However, if it is printed in any other printer or printed from the scanned watermarked image, then the histogram patterns have been changed and quite different from histogram patterns of HIW image. It shows that the watermarked image cannot be easily scanned and printed on any other printer. By observing the histograms, it can be easily identified whether it has been printed by the original manufacturer or not. Thus, the proposed watermarking scheme successfully makes the watermark perceptually invisible and robust against print and scan attacks with inkjet printers on A4 paper and with gravure printing machines on blister foil media. Since the watermarked host image contains expiry date and batch number information, it varies according to the embedded information or watermark (Batch Number (BN) and Expiry Date (ED)). This changing of histogram patterns proved the watermarking process dynamic in nature. The authenticity of the printed samples can be checked by evaluating the correlation coefficient of the printed test image with the original image.

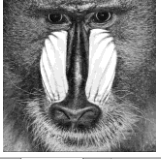
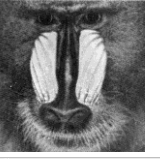

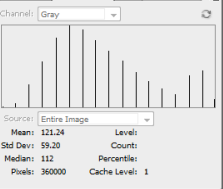
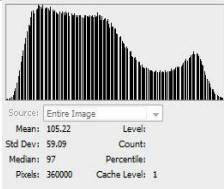
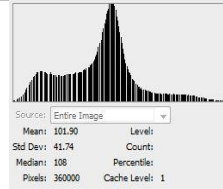
Table 8.6: Histogram of Host Image with Watermark softcopy (HIW), Printed and Scanned Watermarked Image (PS-WI) and RePrinted and ReScanned Watermarked Image (RPRS-WI) on foil from Printer P1 and scanner S1.



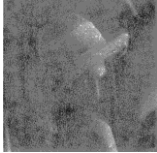
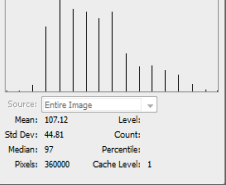
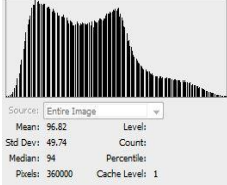
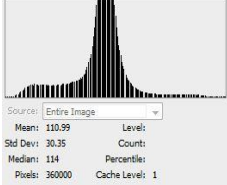


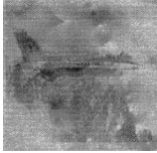
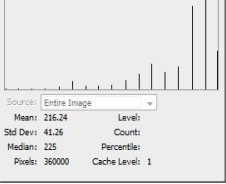
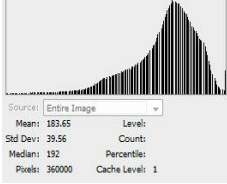
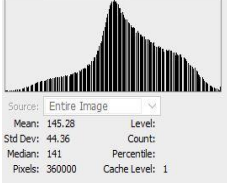



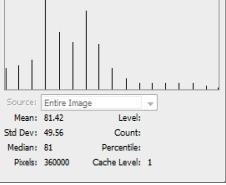
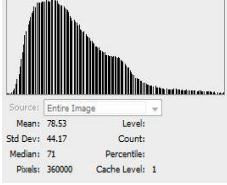
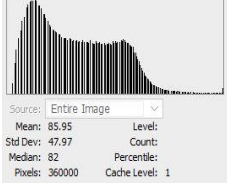
	Host Image with Watermark softcopy (HIW)	Histogram of Print and Scanned Watermarked Image (PS-WI)  Print samples  (Printer P1 scanner S1) on foil	Histogram of RePrinted and ReScanned Watermarked Image (RPRS-WI)  Reprint sample  (Printer P1 scanner S1) on foil
Histogram Of Baboon WZ	 <p>Channel: Gray</p> <p>Source: Entire Image</p> <p>Mean: 121.24    Level:   </p> <p>Std Dev: 59.20    Count:   </p> <p>Median: 112    Percentile:   </p> <p>Pixels: 360000    Cache Level: 1</p>	 <p>Source: Entire Image</p> <p>Mean: 105.22    Level:   </p> <p>Std Dev: 59.09    Count:   </p> <p>Median: 97    Percentile:   </p> <p>Pixels: 360000    Cache Level: 1</p>	 <p>Source: Entire Image</p> <p>Mean: 101.90    Level:   </p> <p>Std Dev: 41.74    Count:   </p> <p>Median: 108    Percentile:   </p> <p>Pixels: 360000    Cache Level: 1</p>

Histogram Of Lena WZ	 Source: Entire Image Mean: 107.12 Level: Std Dev: 44.81 Count: Median: 97 Percentile: Pixels: 360000 Cache Level: 1	 Source: Entire Image Mean: 96.82 Level: Std Dev: 49.74 Count: Median: 94 Percentile: Pixels: 360000 Cache Level: 1	 Source: Entire Image Mean: 110.99 Level: Std Dev: 30.35 Count: Median: 114 Percentile: Pixels: 360000 Cache Level: 1
Histogram Of Avion WZ	 Source: Entire Image Mean: 216.38 Level: Std Dev: 40.07 Count: Median: 225 Percentile: Pixels: 360000 Cache Level: 1	 Source: Entire Image Mean: 190.83 Level: Std Dev: 41.44 Count: Median: 204 Percentile: Pixels: 360000 Cache Level: 1	 Source: Entire Image Mean: 145.28 Level: Std Dev: 44.36 Count: Median: 141 Percentile: Pixels: 360000 Cache Level: 1
Histogram Of Peppers WZ	 Source: Entire Image Mean: 81.42 Level: Std Dev: 49.56 Count: Median: 81 Percentile: Pixels: 360000 Cache Level: 1	 Source: Entire Image Mean: 85.95 Level: Std Dev: 47.97 Count: Median: 82 Percentile: Pixels: 360000 Cache Level: 1	 Source: Entire Image Mean: 75.53 Level: Std Dev: 46.96 Count: Median: 67 Percentile: Pixels: 360000 Cache Level: 1

From these histograms, it has been observed that Print samples (PS-WI) histogram patterns are consistent with respect to the Host Image with Watermark (HIW) histograms. Whereas, Reprint samples (RPRS-WI) histogram patterns differ from the original Host Image with Watermark (HIW) histograms. From this, it can be inferred that image authentication has been achieved by this watermarking method.

Table 8.7: Histogram of different Host Images with Watermark softcopy (HIW), Print sample image (PS-WI) and Reprint sample image (RPRS-WI) on foil from Printer P1 and scanner S1 for verification.

	Watermarked Image (Blue channel)	Printed Watermark Image on foil (Blue channel) (Scanner S1)	Re-Printed Watermark Image on foil (Blue channel) (Scanner S1)
Baboon Image WZ			
Histogram Of Baboon	 Channel: Gray Source: Entire Image Mean: 121.24 Level: Std Dev: 59.20 Count: Median: 112 Percentile: Pixels: 360000 Cache Level: 1	 Source: Entire Image Mean: 105.22 Level: Std Dev: 59.09 Count: Median: 97 Percentile: Pixels: 360000 Cache Level: 1	 Source: Entire Image Mean: 101.90 Level: Std Dev: 41.74 Count: Median: 108 Percentile: Pixels: 360000 Cache Level: 1

Lena Image WZ			
Histogram Of Lena	 Source: Entire Image Mean: 107.12 Level: Std Dev: 44.81 Count: Median: 97 Percentile: Pixels: 360000 Cache Level: 1	 Source: Entire Image Mean: 96.82 Level: Std Dev: 49.74 Count: Median: 94 Percentile: Pixels: 360000 Cache Level: 1	 Source: Entire Image Mean: 110.99 Level: Std Dev: 30.35 Count: Median: 114 Percentile: Pixels: 360000 Cache Level: 1
Avion Image WZ			
Histogram Of Avion	 Source: Entire Image Mean: 216.24 Level: Std Dev: 41.26 Count: Median: 225 Percentile: Pixels: 360000 Cache Level: 1	 Source: Entire Image Mean: 183.65 Level: Std Dev: 39.56 Count: Median: 192 Percentile: Pixels: 360000 Cache Level: 1	 Source: Entire Image Mean: 145.28 Level: Std Dev: 44.36 Count: Median: 141 Percentile: Pixels: 360000 Cache Level: 1
Peppers Image WZ			
Histogram Of Peppers	 Source: Entire Image Mean: 81.42 Level: Std Dev: 49.56 Count: Median: 81 Percentile: Pixels: 360000 Cache Level: 1	 Source: Entire Image Mean: 76.53 Level: Std Dev: 44.17 Count: Median: 71 Percentile: Pixels: 360000 Cache Level: 1	 Source: Entire Image Mean: 85.95 Level: Std Dev: 47.97 Count: Median: 82 Percentile: Pixels: 360000 Cache Level: 1

It may be noted that the watermarks have been worked on the chrominance level and not on the spatial level. In this Table 8.7, the first row contains a baboon image with a watermark that has been characterised by WZ, and the second row contains the histogram of that image. Watermark Z defines one particular batch number (BN) and expiry date (ED). It has been observed that the histogram of Print sample image (PS-WI) (when it has been Printed using P1 gravure printing machine and scanned by S1 to observed the histogram) for watermark Z is quite different from the histogram of Reprint sample image (RPRS-WI) (Printer P1 scanner S1) watermark on foil. Similar results have been observed for other images.

In Figs. 8.5(a) and 8.5(b), there is a baboon image with two different watermarks, which have been characterised by WZ and WX that represent two different batch numbers and expiry dates. In Figs. 8.4(c) and 8.4(d), it has been observed that the histogram of Print sample (PS-WI) (Printer P1 scanner S1) for watermark Z is a little bit different from the histogram of Print sample image (PS-WI) (Printer P1 scanner S1) for watermark X on foil. The printer and the scanner processes have been unchanged. This change in the histogram pattern has been changed due to the different watermark. That means our proposed

watermarking process is dynamic in nature due to embedded information(watermark). This is the uniqueness of proposed watermarking process that can be varied time to time as batch number and expiry date changes. Hence it will be very difficult to counterfeit by the counterfeiters since the watermark is dynamic in nature.

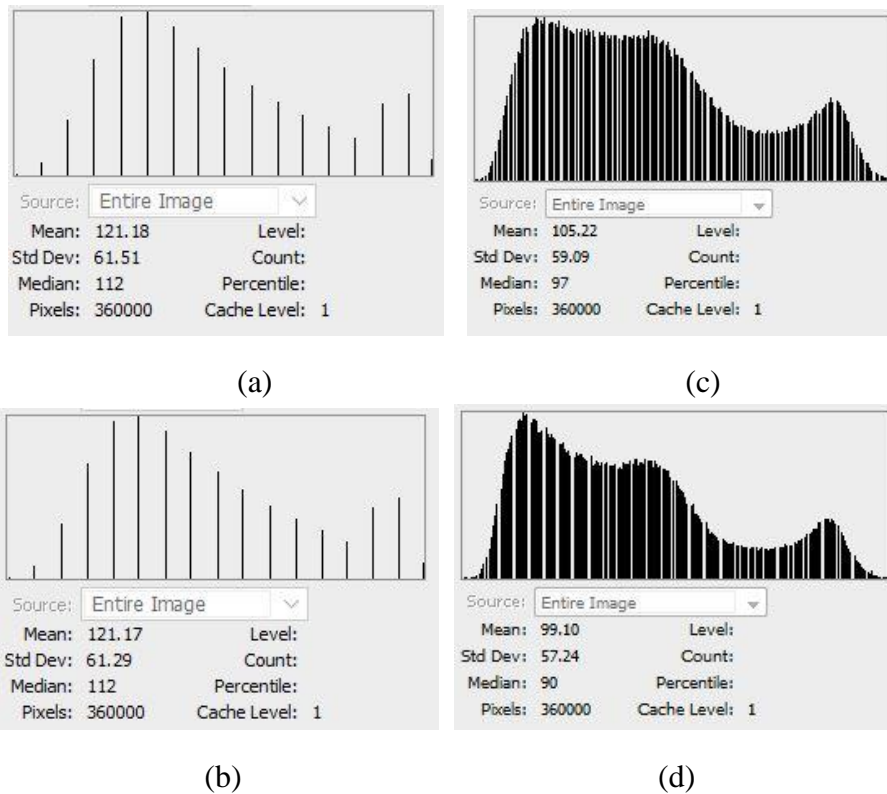


Fig 8.5 (a)Histogram of HIW with WZ (b) Histogram of HIW with WX  
(c)Histogram of PS-WI with WZ (d)Histogram of PS-WI with WX

### 8.1.2.1 Robustness of Watermark Against Print and Scan attacks

Comparison of the blue channels of Host Image with Watermark softcopy (HIW) with Print samples (PS-WI) and Host Image with Watermark softcopy (HIW) with Reprint samples (RPRS-WI) have been showed a significant difference in the co-relation coefficient. It may be shown from Fig. 8.6 that the correlation coefficients for image Lena using five different watermarks are always higher for print sample (PS-WI) in comparison to the reprint sample (RPRS-WI) with the Host Image with Watermark softcopy (HIW). It can be easily identified from such a comparison whether an unknown print sample has been printed from the original printer or from some other printer. The results in Figs. (8.6–8.13) show that when comparisons have been made between the print sample (PS-WI) and the reprint sample (RPRS-WI) with the Host Image with Watermark softcopy (HIW), the values of the co-relation coefficient of the print samples (PS-WI), are much higher than the values of the reprint samples (RPRS-WI) for different images with different watermarks representing different batch number and expiry dates. The results indicate that the print samples (PS- WI) are more similar to the (HIW) than the reprint samples (RPRS-WI). The difference in correlation values can therefore determine whether a print is authenticated or not.

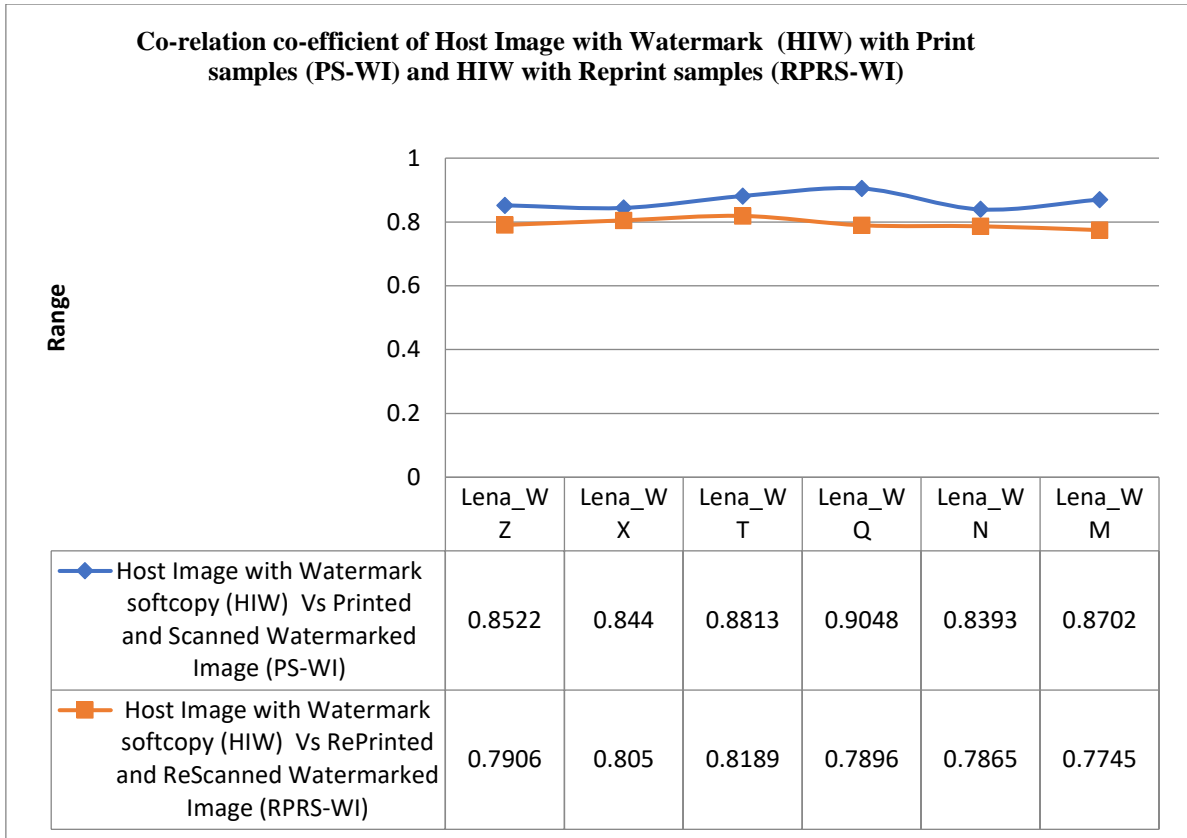


Fig 8.6:Co-relation co-efficient of Lena HIW with PS-WI and RPRS-WI on A4 paper

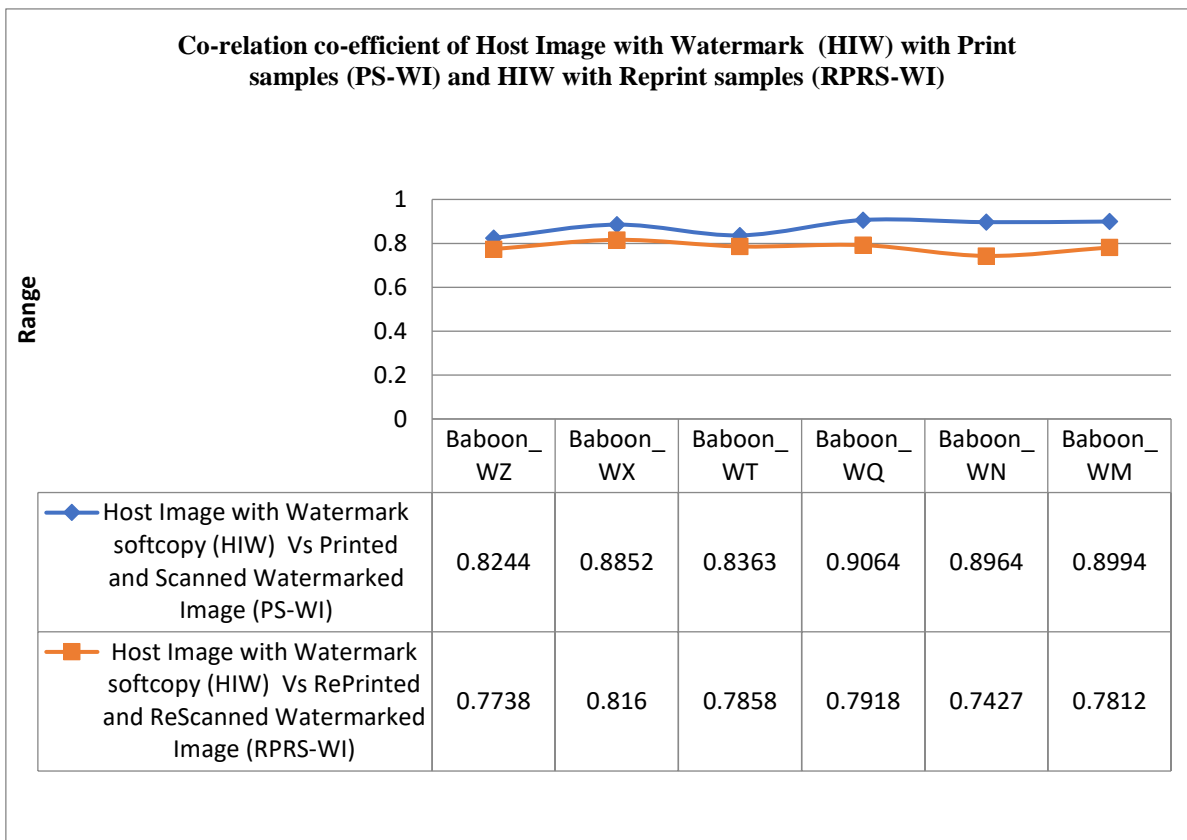


Fig 8.7:Co-relation co-efficient of Baboon HIW with PS-WI and RPRS-WI on A4 paper

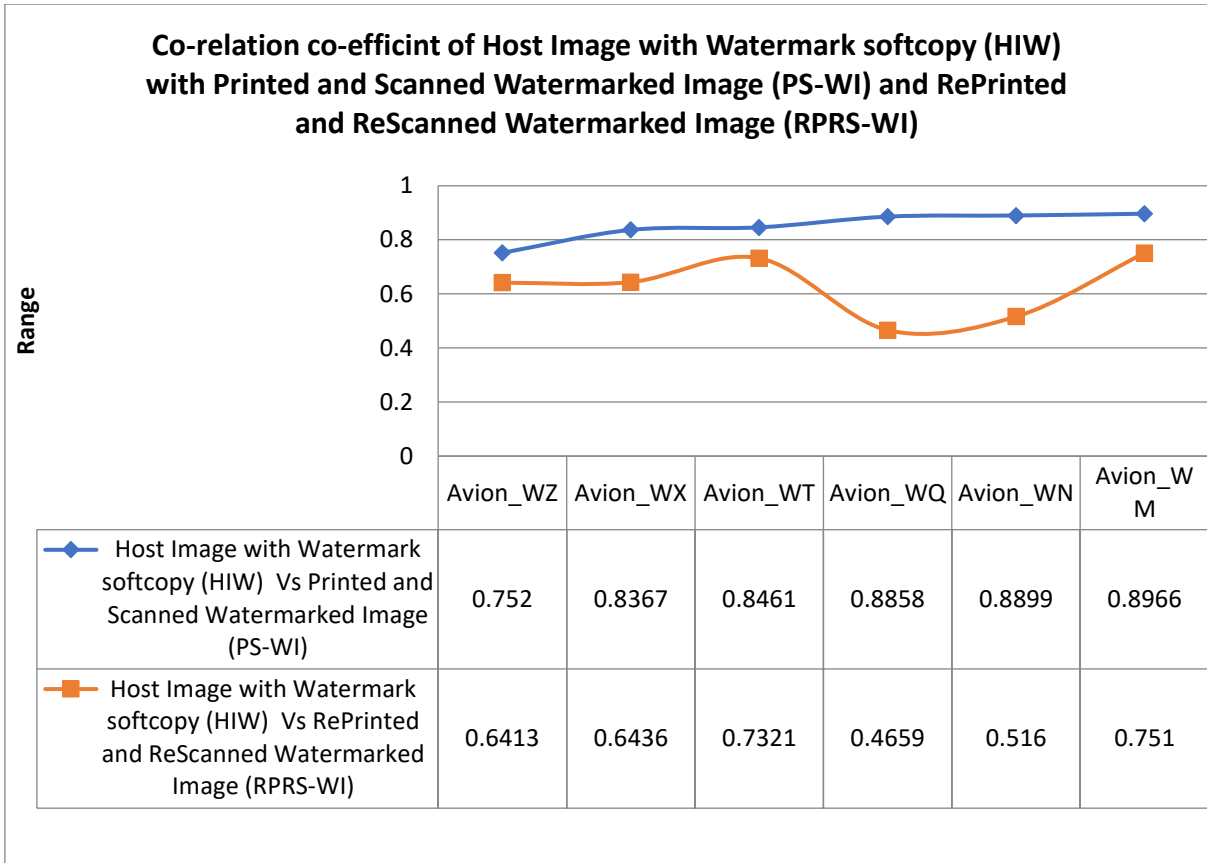


Fig 8.8:Co-relation co-efficient of Avion HIW with PS-WI and RPRS-WI on A4 paper

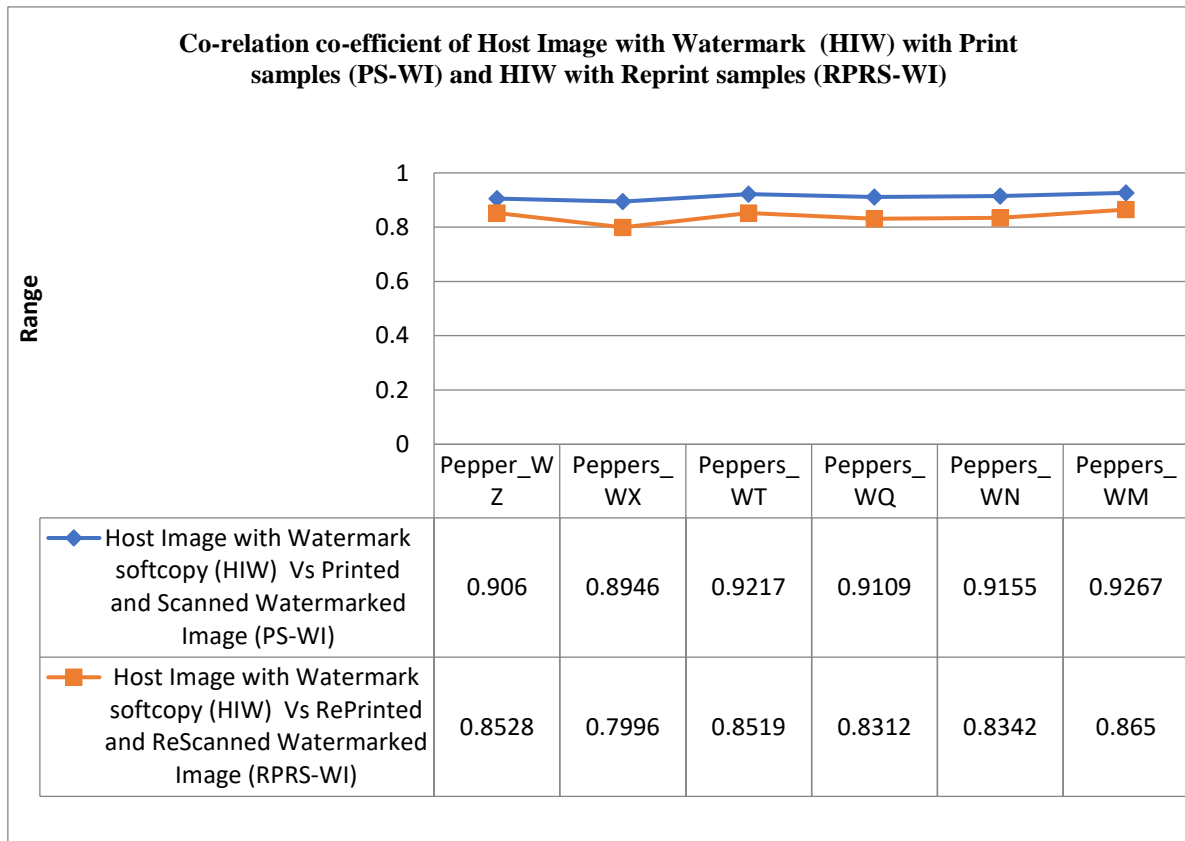


Fig 8.9:Co-relation co-efficient of Peppers HIW with PS-WI and RPRS-WI on A4 paper

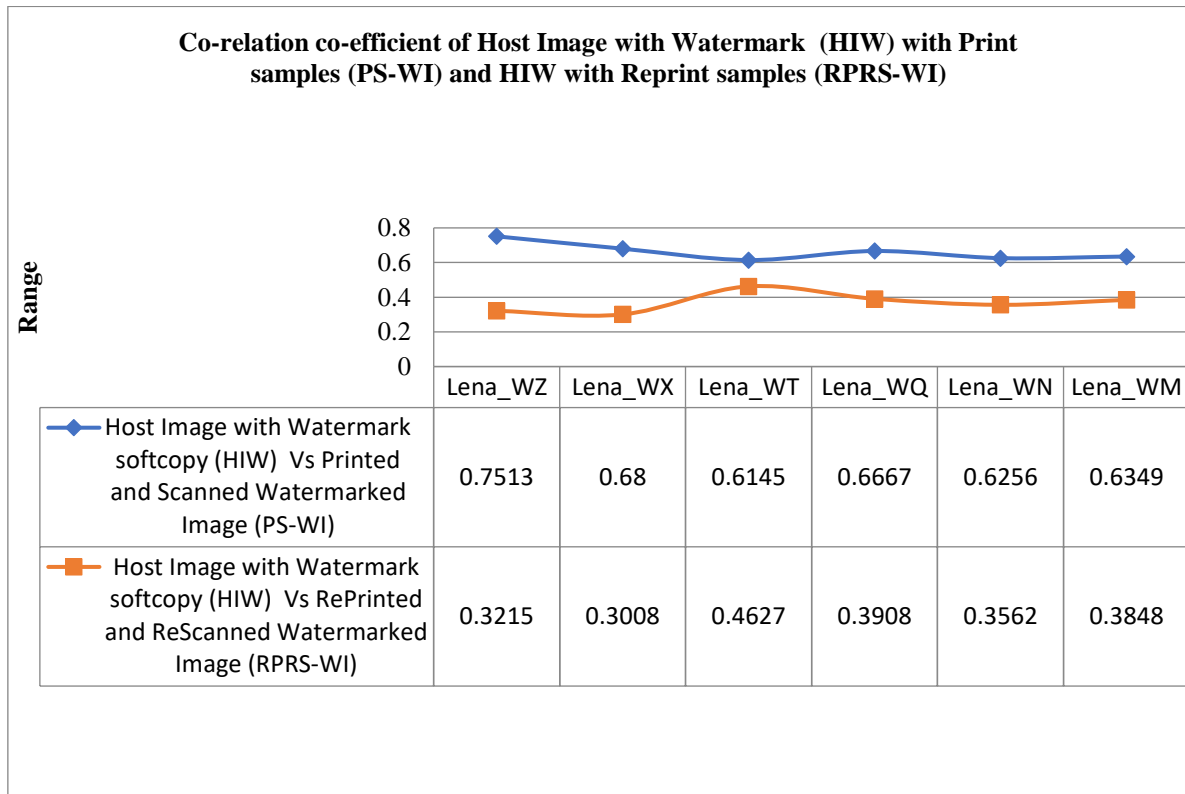


Fig 8.10:Co-relation co-efficient of Lena HIW with PS-WI and RPRS-WI on Foil media

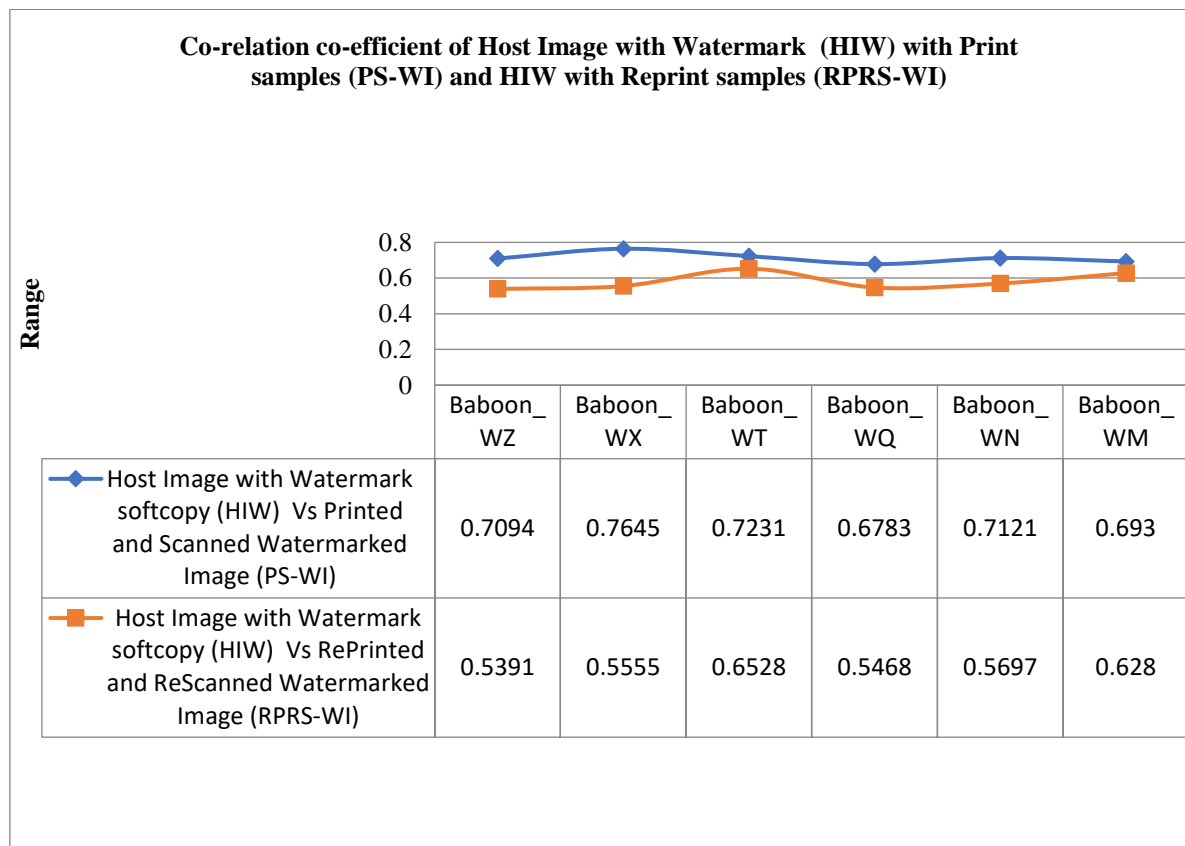


Fig 8.11:Co-relation co-efficient of Baboon HIW with PS-WI and RPRS-WI on Foil media



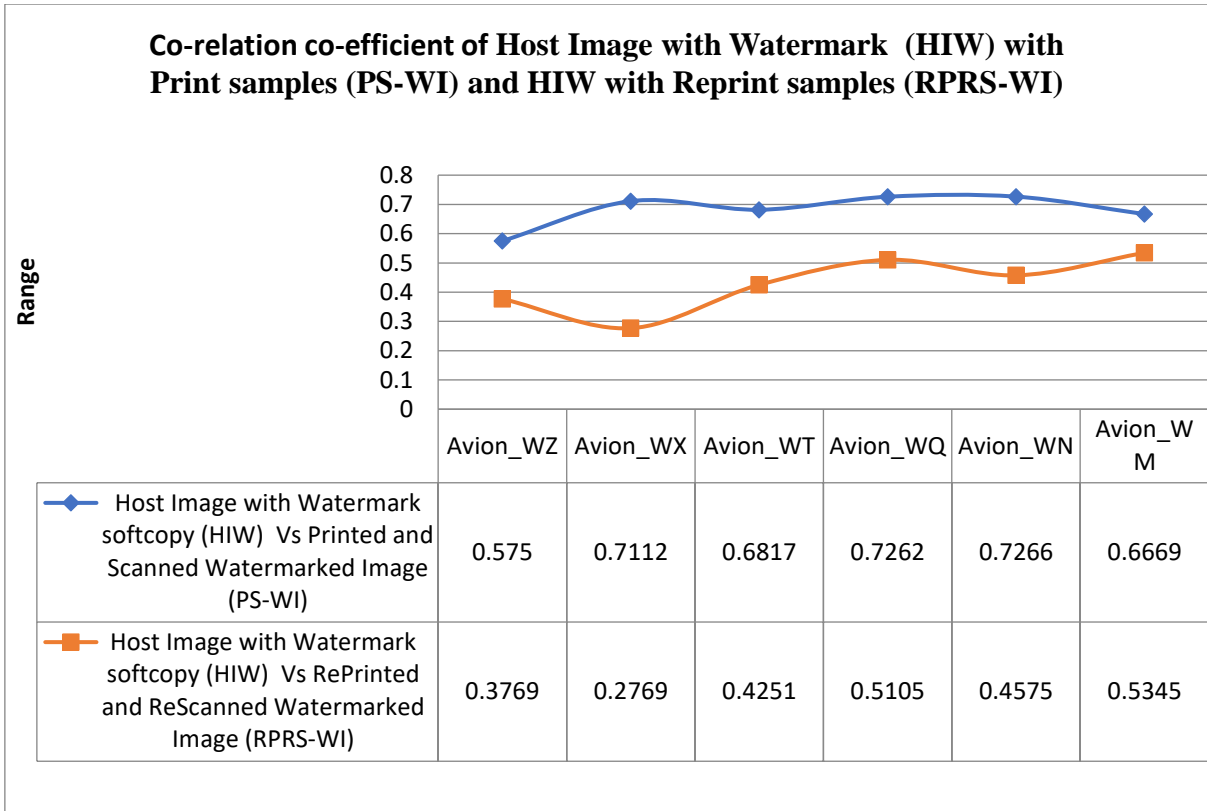


Fig 8.12:Co-relation co-efficient of Avion HIW with PS-WI and RPRS-WI on Foil media

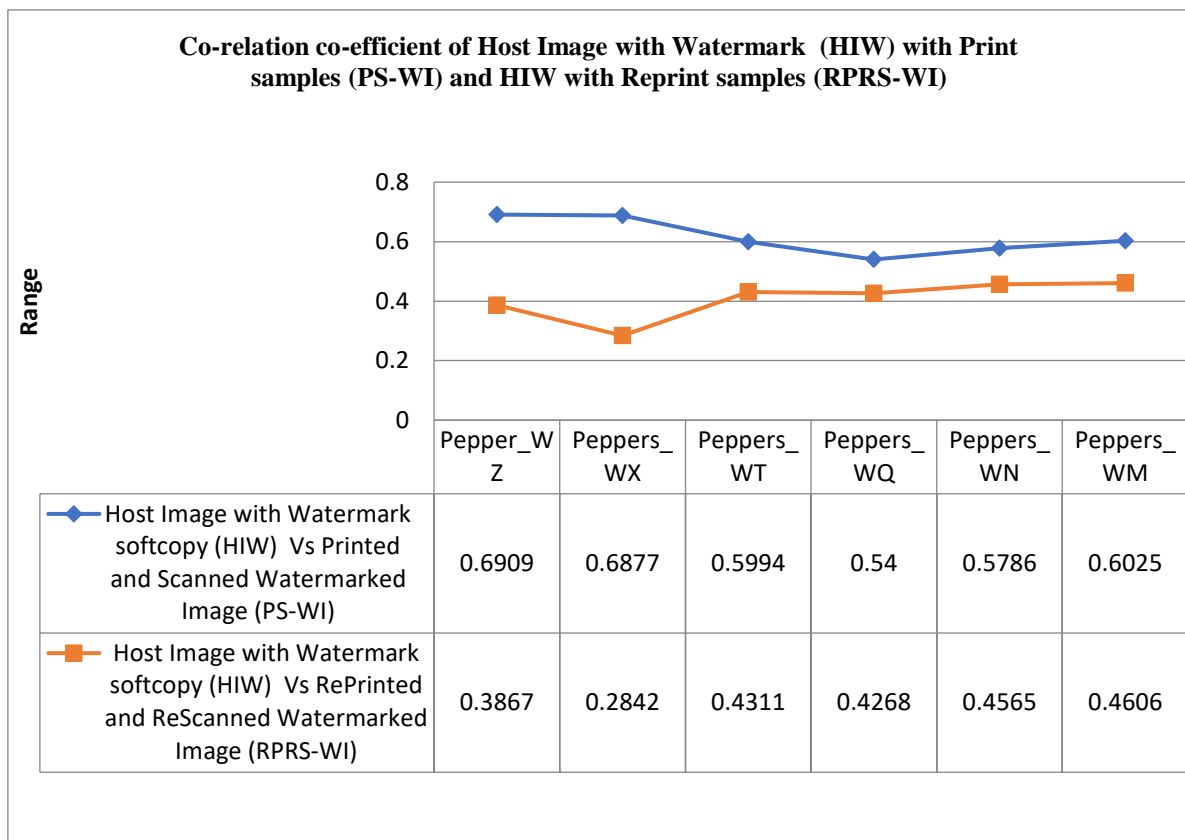


Fig 8.13:Co-relation co-efficient of Peppers HIW with PS-WI and RPRS-WI and RPRS-WI on Foil media

According to the findings in Figs 8.6-8.9, when the PS-WI and the RPRS-WI have been compared, the co-relation co-efficient of the PS-WI is significantly greater than the co-relation co-efficient of the RPRS-WI for A4 paper media. These statistical findings indicate that the Print samples (PS-WI) are less different from the HIW image but more different from the Reprint samples (RPRS-WI). Therefore, whether a print is authorised or not may be determined by the difference in values. Similar analysis has been done to check blister foil by gravure print. It may be identified whether the expiry date and batch numbers are tampered with or not. Thus, it might be helpful not only to identify whether the product is original or not but also to identify whether the product is outdated or not. This study of reprinted and rescanned images (simulated counterfeit samples) has been used to identify whether a blister medicine package print is counterfeited or not. The results in the Figs (8.10-8.13) show the comparisons between the PS-WI with HIW and the RPRS-WI with HIW for foil. It has been observed that the values of the co-relation coefficient of the Print samples (PS-WI) are much higher than the values of the Reprint samples (RPRS-WI). From these observed results, it has been inferred that the Print samples (PS-WI) are less different than the Reprint samples (RPRS-WI) in comparison with the Host Image watermarked (HIW). The difference in values can therefore determine whether a print is authenticated or not on the blister foil media.

### **8.1.3 Discussions**

In this proposed work, four different 64-bit images (a, b, c, d) as shown in Fig 7.1(chapter 7), have been taken as host images for embedding data into them. The watermark has been applied by taking 16-bit on the blue channel / specific channel only. Each of the 16 bits of the watermark has been added to intensity values of some predefined pixels coordinates of the blue channel / specific channel. In order to evaluate the performance of the proposed method, the host color image H of size 1 x 1 inch has been first separated into R, G and B component. The blue channel / specific channel of the images has been used for watermarking. Then, the binary bit for batch number with Batch Number (BN) and Expiry Date (ED) (e.g. the binary bit related to the Z watermark) has been embedded into the blue channel / specific channel of the image. Then this Host Image with Watermark soft copy (HIW) has been printed by CMYK colors on A4 paper using Canon E400 printer and the watermarked images have been engraved in gravure cylinder and then printed on blister foil media using gravure printing machine. The experiment has been carried out in inkjet printer as well as in gravure printer several times to check repeatability and consistent results are obtained. Experiments were made with different combinations of expiry date and batch number. The method for identification of counterfeited printed batch number and expiry dates can be identified for various kinds of printers with different types of substrates. The statistical results and histogram analysis has been utilized to identify the original print from scanned and reprint sample. The experiments are carried out for inkjet printers on paper and gravure printing on blister foils. However, it can be extended to any printing process with any substrates as it works well with paper and foil. It may be concluded that a simple variable watermark is necessary to protect the originality of batch number and expiry date of different types of packaged products, specially for food and medicine products. The experimental results for this study of print images could enable one to identify whether a printed package is counterfeited or not.

## **8.2 Experimental Results obtain from Prints Based on Microscale Image Analysis of Dot Patterns**

The analysis at microscopic scale of print documents shows that dot shapes depend on different printing process parameters. The dot patterns serve as a unique identifier to distinguish an original print from its scanned reprint. In this study, several dot shape indexes have been used to analyze print documents on aluminium foils using rotogravure printing process. This study includes three steps. First, a new image processing pipeline has been used to segment the dots. The second step involves characterizing dot patterns automatically using new dot pattern features. In this study six different dot (including four different doughnut patterns) patterns are proposed. A statistical analysis is used to characterize a printed sample based on its dot pattern. Results demonstrate the potential of this method to distinguish a scanned reprint from an original print.

### **8.2.1 Results obtain from Prints Based on Microscale Image Analysis of Dot Patterns**

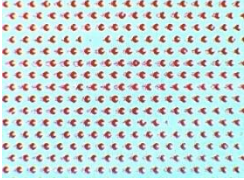
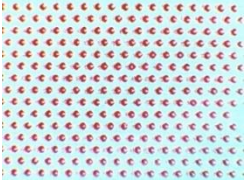
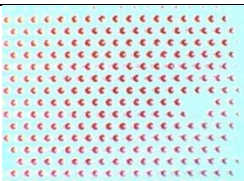
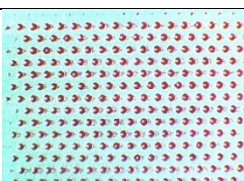
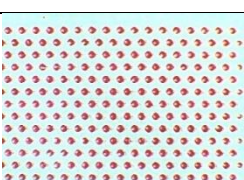
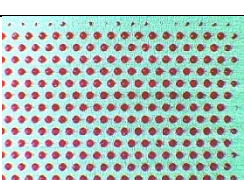
The effectiveness of the dot segmentation method has been assessed. The accuracy of computed values of the shape parameters such as major and minor axis sizes, area, and the radius of the circumscribed circle have been evaluated using the ScopeImage 9.0 software. The issue of evaluating and comparing threshold methods have been discussed [35], while [36] deals with the problem of calibrating measurements for shape. In this study, the objective was only to compare computed dot pattern values between prints.

From Table 8.8 it may be observed that samples number 1, 2, 3, 4 and 5 are very similar in terms of dots shape (high proportion of doughnuts), meanwhile sample corresponding to sample number 6 is unique (in comparison with these samples) which has low proportion of doughnuts.

The threshold separating circular shapes from elliptical shapes may be used to characterize the circularity of non-circle shapes such as the one  $\in$  (ID1/ID2/ID3).

The shape of the dots of print samples having number 1, 2, 3, 4, 5 and 6 are more or less homogeneous.

Table 8.8: Dot shape parameters values of Magenta dots

Ref	Features Print Image	Nb of dots detected	% of total dots having shape ID1/ID2/ID3	Average Perimeter	Average Area	Average Circularity	Average Orientation	% of dots with a circular shape
1	 Analysis of Magenta dots	258	<b>96%</b>	49.52	121.79	0.79	-23.04°	99%
2	 Analysis of Magenta dots	261	<b>96%</b>	51.6	120.96	0.76	12.40°	99%
3	 Analysis of Magenta dots	237	<b>84%</b> (10 % ∈ ID6)	42.05	90.34	0.80	-24.17°	90%
4	 Analysis of Magenta dots	242	<b>95%</b>	54.55	135.68	0.76	-6.32°	96%
5	 Analysis of Magenta dots	241	<b>94%</b>	54.98	143.34	0.77	40.56°	94%
6	 Analysis of Magenta dots	251	3% <b>(40 % ∈ ID4)</b>	62.48	247.12	<b>0.89</b>	22.13°	94%  (49 % ∈ ID5)

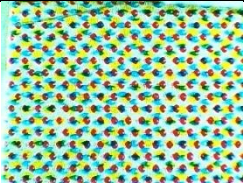
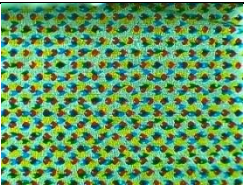
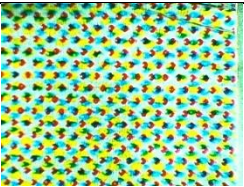
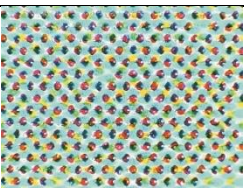
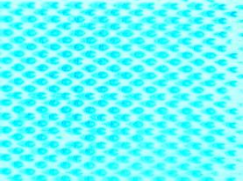
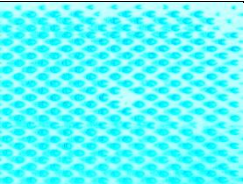
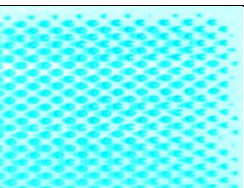
Ref	Features	Nb of dots detected	% of dots ∈ ID1/ID2/ID3	Average Perimeter	Average Area	Average Circularity	Average Orientation	% of dots with a circular shape
7	 Analysis of Magenta dots	272	71%	56.06	173.68	0.84	28.11°	83%
8	 Analysis of Magenta dots	278	76%	55.20	161.01	0.82	35.49°	82%
9	 Analysis of Magenta dots	287	66%	49.84	137.19	0.84	31.8°	72%
10	 Analysis of Magenta dots	258	32%  (42 % ∈ ID4)	63.95	199.48	0.79	10.7°	75%

Table 8.8 shows that the proportion of doughnuts nearby periphery of the dots in magenta prints for samples number 1,2,3,4,5 are much higher than sample number 6. As the doughnuts are more in sample number 1 to 5, their corresponding circularity are less in comparison to sample number 6. It may be noted that though sample number 6 has less doughnut shapes with respect to ID1,2 or 3, it contains more doughnuts of shape ID 4. Since ID 4 has circular doughnut almost at the centre, hence circularity of sample 6 is not affected by the doughnuts.

From Table 8.9, it has been observed that the samples corresponding to samples number 11, 12 and 13 are very similar in terms of cyan dots shape, most of the dots have a “elliptic equivalent” shape oriented in the direction of the print (shown in Fig. 8.14), which is coherent with the values computed for the parameter “orientation”. Similar observation was made in case of sample 17 of yellow dots as shown in Table 8.10.

Table 8.9: Dot shape parameters values of Cyan dots. The most significant values are in bold.

Ref	Print Image	Nb of dots detected	% of dots ∈ ID1/ID2/ID3	Average Perimeter	Average Area	Average Circularity	Average Orientation	% of dots with a elliptic shape
11	 Analysis of Cyan dots	267	34%	86.51	373.45	<b>0.81</b>	<b>-1.20°</b>	18%  (37% have a circular shape)  (55 % ∈ ID5)
12	 Analysis of Cyan dots	265	34%  (4% ∈ ID6)	94.78	487.83	0.84	<b>-2.00°</b>	35%  (10% have a circular shape)  (45 % ∈ ID5)
13	 Analysis of Cyan dots	249	8%	93.50	481.32	0.83	<b>1.81°</b>	24%  (31% have a circular shape)  (86 % ∈ ID5, among them 31% are nor circular nor elliptic)
Ref	Reprint Image	Nb of dots detected	% of dots ∈ ID1/ID2/ID3	Average Perimeter	Average Area	Average Circularity	Average Orientation	% of dots having a elliptic shape

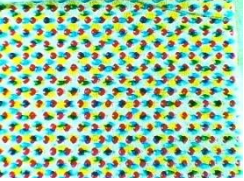
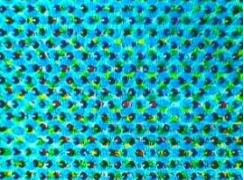



14	 Analysis of Cyan dots	246	5%	63.80	203.20	0.80	5.44°	21%  (25 % ∈ ID5)
15	 Analysis of Cyan dots	250	4%	86.79	483.47	<b>0.92</b>	3.63°	31%  (17% have a circular shape)  (53 % ∈ ID5)
16	 Analysis of Cyan dots	250	8%  (23% ∈ ID6)  (22% of connected dots not analysed)	87.84	464.39	<b>0.93</b>	4.23°	28%  (15% have a circular shape)  (47 % ∈ ID5)

Table 8.10: Dot shape parameters values of Yellow dots. The most significant values are in bold.

Ref	Print Image	Nb of dots detected	% of dots ∈ ID1/ID2/ID3	Average Perimeter	Average Area	Average Circularity	Average Orientation	% of dots with elliptic shape
17	 Analysis of Yellow dots	156	6%  (7% ∈ ID6)	91.04	484.19	<b>0.86</b>	<b>-1.01°</b>	75%  (80% ∈ ID5)
Ref	Reprint Image	Nb of dots detected	% of dots ∈ ID1/ID2/ID3	Average Perimeter	Average Area	Average Circularity	Average Orientation	% of dots having a elliptic shape



18		199	30% (30% ∈ ID6)	56.08	188.63	0.87	5.96°	32% (38% ∈ ID5)
	Analysis of Yellow dots							

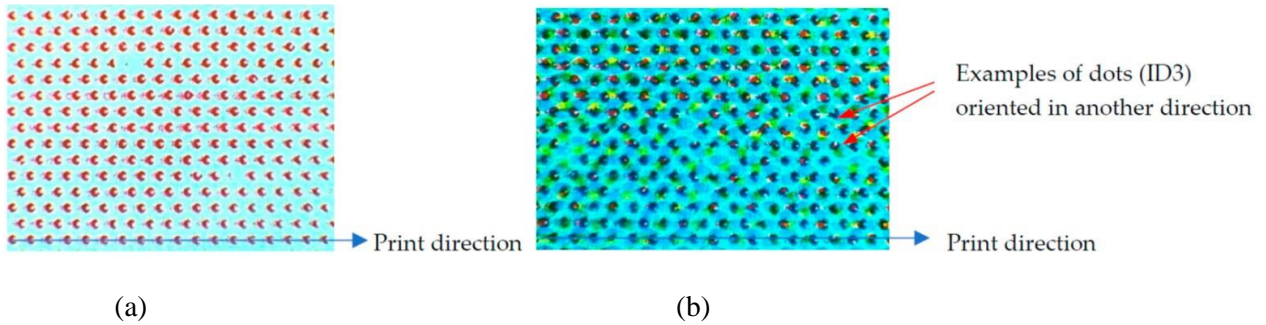


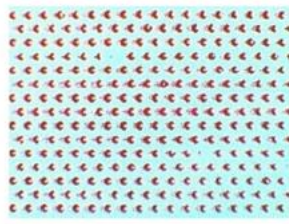
Fig 8.14: (a) Magenta dots with 95% of doughnuts oriented in the print direction; (b) Magenta dots with 85% of doughnuts oriented in the print direction. Orientation of the doughnuts vs. print direction.

In the next section, the robustness of these parameters versus different printing systems have been compared.

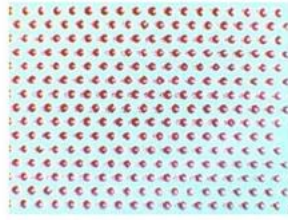
### 8.2.2 Prints vs. Reprints

As shown in Table 8.8 for samples number 1, 2 and 3, Fig 8.15(a) to (c) show that the dot distribution in these samples is statistically very similar. Nevertheless, it has been noticed that the proportion of doughnuts in sample number 3 (printed with printer P2) is lower than for the two other samples (both were printed with printer P1). This supports our hypothesis that the distortions of printed dots at a microscopic level, caused by the printing process, can serve as a unique identifier to distinguish between two prints.

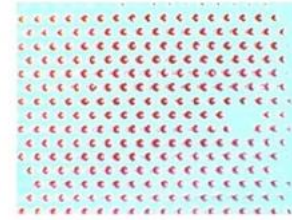
Table 8.9 samples number 11, 12 and 13 as shown in Fig 8.15(d) to (f) show that the dots distribution in these samples are statistically very similar (elliptic shape), nevertheless it has been noticed in previous section that the proportion of doughnuts in sample number 13 (printed with printer P2) is lower than for the two other samples (both were printed with printer P1).



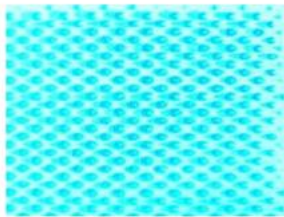
(a)Sample 1-magenta dots (printed with printer P1 and ink DIC (with cell angle of  $30^{\circ}$ )



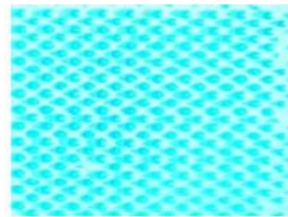
(b)Sample 2- magenta (printed with printer P1 and same ink (with cell angle of  $30^{\circ}$ )



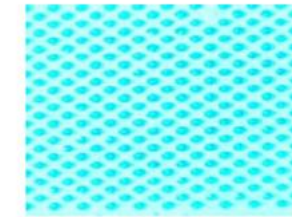
(c)Sample 3- magenta dots (printed with printer P2 and same ink (with cell angle of  $30^{\circ}$ )



(d)Sample 11-cyan dots (printed with printer P1 and same ink (with cell angle of  $60^{\circ}$ )



(e)Sample 12- cyan dots (printed with printer P1 and same ink (with cell angle of  $60^{\circ}$ )



(f)Sample 13-cyan dots (printed with printer P2 and same ink (with cell angle of  $60^{\circ}$ )

Fig 8.15. Robustness of the dot patterns detection method relative to the printing device.

Now this study has been proceeded with the comparison of three reprint samples of the same artwork. Images shown in Fig 8.16 demonstrated that the dot distribution in these samples is very similar, results shown in Fig 8.16d–f demonstrate the dot patterns detection process is quite robust against noise, non-uniformity of lighting field, dots connectivity, dot-on-dot misregistration, inks, etc. In this scenario, the accurate estimation of the Yellow dots' shape has been negatively affected by the overlapping of Cyan and Magenta dots on the top of Yellow dots. The arrangement of dots in these reprint samples does not match the dot arrangement of the scanned print sample (sample 11) due to the reflective nature of the substrate, which complicates the color calibration process and leads to an inaccurate color measurement of the dot distribution.

In this study samples have been compared that corresponding to (11–13) (printed samples) with samples corresponding to (14,15) (reprinted samples), it has been noticed a higher proportion of dots belong to (€) ID6 for (14,15) than for the three other samples (shown in Table 8.9). The fact can be explained that, for the reprint samples, it is more difficult to estimate properly the shape of the dots due to a higher statistical value of “area” and “circularity” parameters (and consequently a higher connectivity rate of dots). The hypothesis of this study that this is due to the scan process (as the density of Cyan dots was well estimated). Therefore, drawn the assumption that the deformations at microscopic scale of

reprinted dots (induced by the print and scan and reprint process) can be used as a fingerprint to differentiate a print from a reprint.

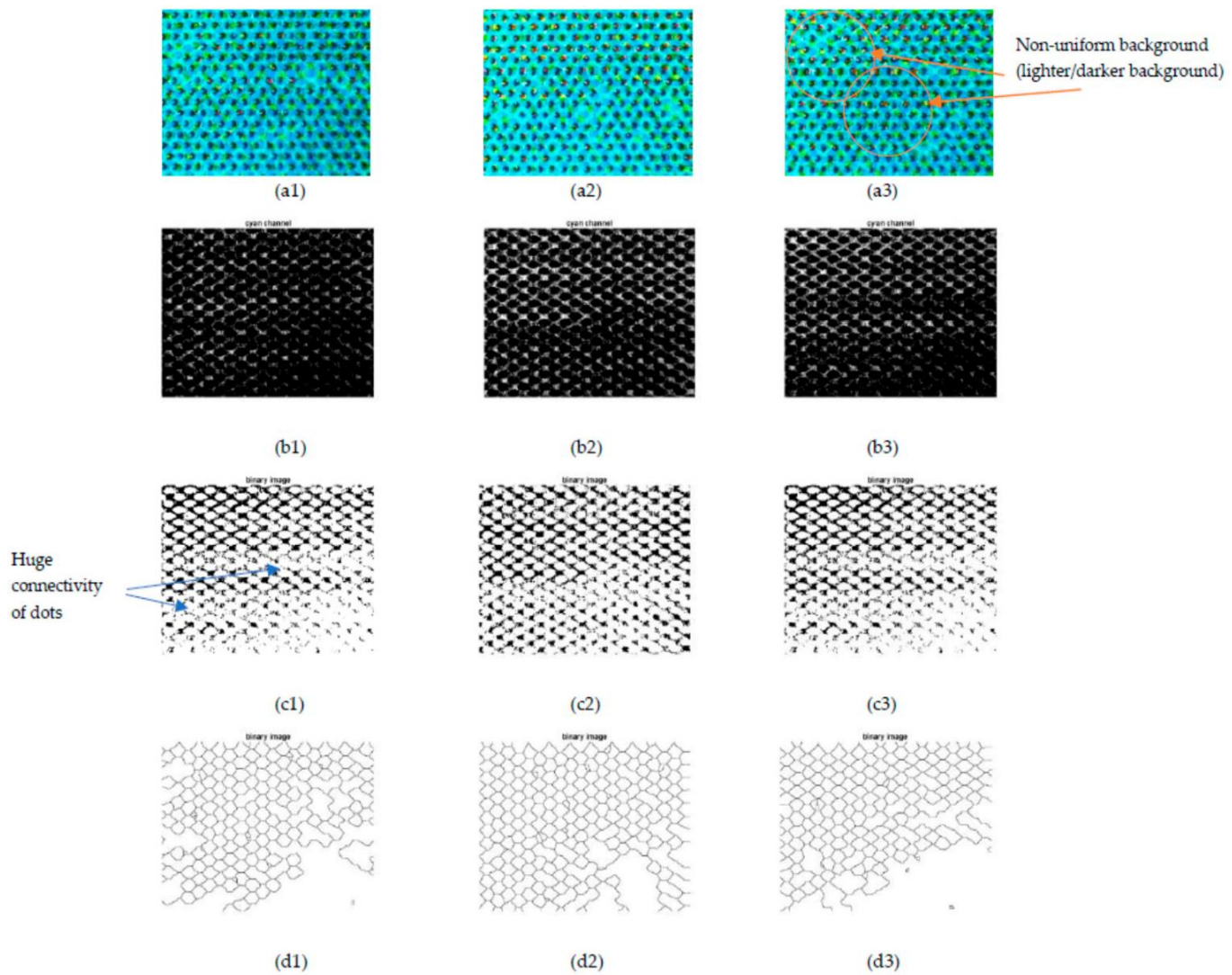


Fig 8.16. Cont.

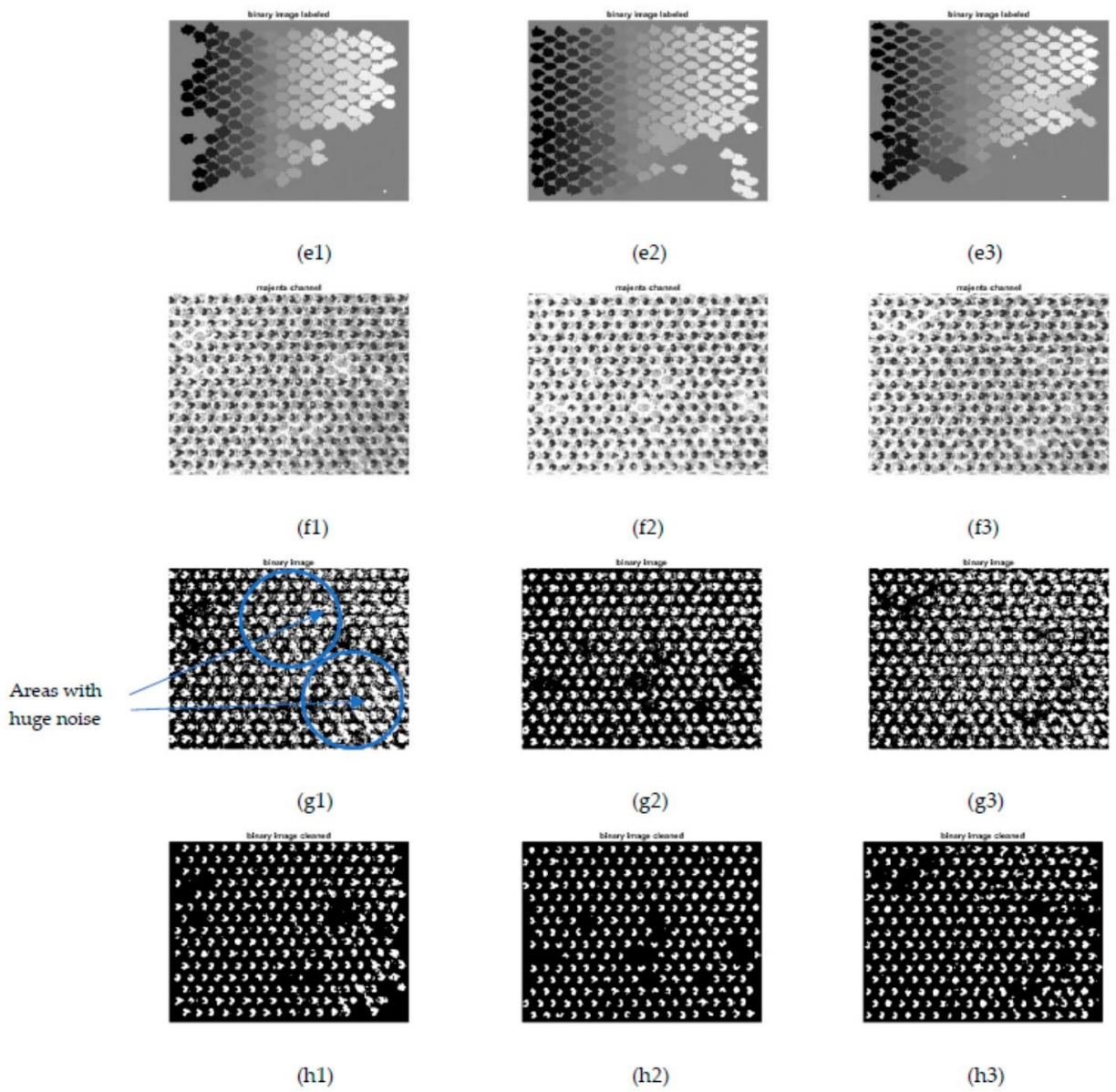


Fig 8.16. Cont.



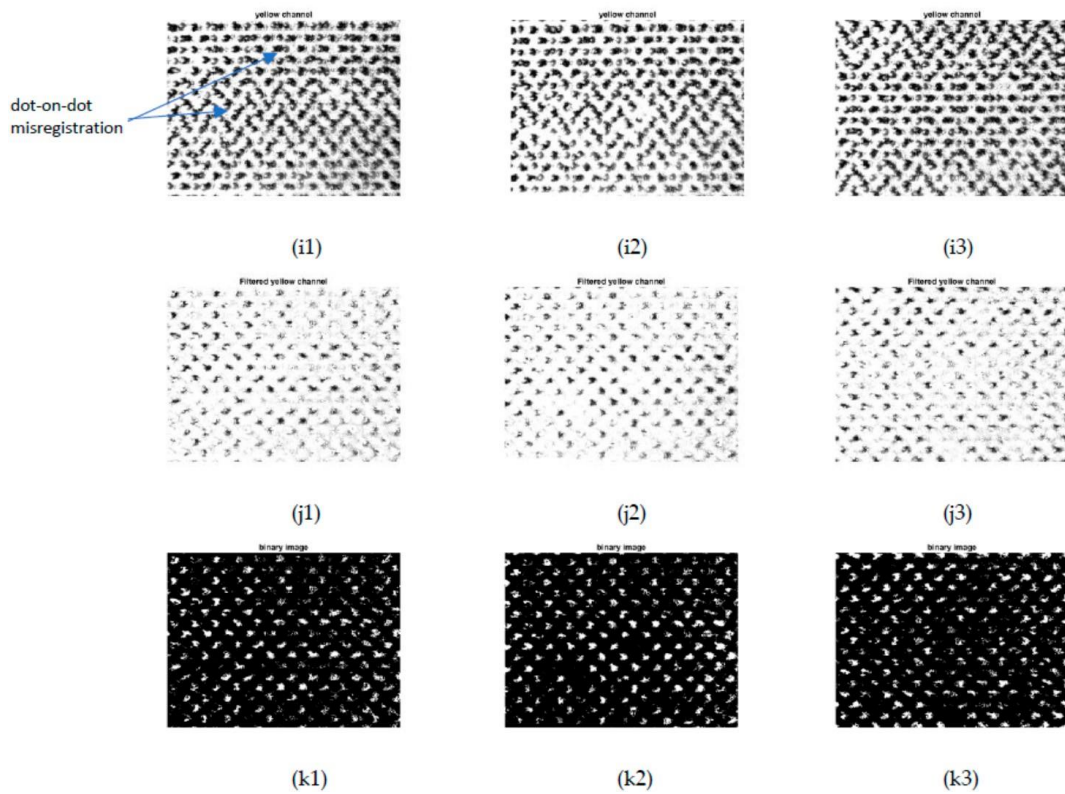


Fig. 8.16: Robustness of the dot pattern detection method relative to the printing device (a1) Cyan (reprint 1) Image (printed with printer P2 and ink DIC) (cyan dots have a cell angle of  $60^\circ$  and magenta dots have a cell angle of  $30^\circ$ ), (a2) Cyan (reprint 2) Image (cyan dots have a cell angle of  $60^\circ$  and magenta dots have a cell angle of  $30^\circ$ ), (a3) Cyan (reprint 3) Image (cyan dots have a cell angle of  $60^\circ$  and magenta dots have a cell angle of  $30^\circ$ ), (b1–e3) results step by step for C color channel, (f1–h3) results step by step for M color channel, (i1–k3) results step by step for Y color channels.

Fig 8.17 illustrates two examples of dots' deformation, one for Magenta print dots (shown in Fig 8.17c), another for Magenta reprint dots (depicted in Fig 8.17f). The overgrowth of dots caused by the printing process has been smoothed, and morphological procedures have been applied prior to computing shape indexes, but the overgrowth of dots can't be eliminated properly because it is inherent in the printing process. The "elongation" parameter enables these local deformations to be quantified (refer the examples highlighted with an orange arrow). The size of the Magenta dots is larger in Fig 8.17f than in Fig 8.17c; meanwhile, elongated dots with an overgrowth in the opposite direction of the print direction are more regularly distributed (shown the dot line highlighted with a blue arrow).

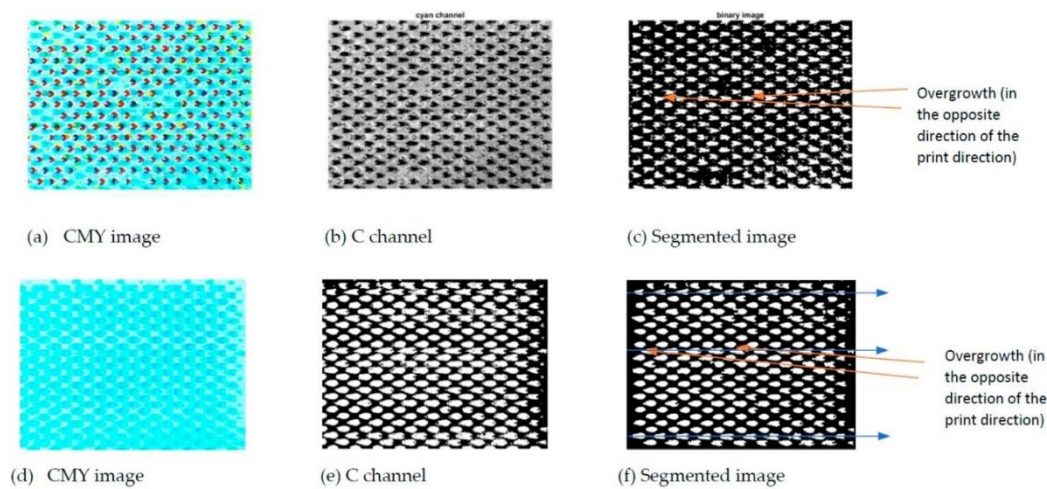


Fig 8.17: Examples of dot deformation.

### 8.2.3 Discussion

In this second part of study, observed method has not been compared the performance (nor the accuracy) of our thresholding method to other thresholding methods. Likewise, we have not compared the performance (nor the accuracy) of the samples dot size and shape indexes with other indexes of the state of the art. Our main objective has been to demonstrated that the use of size and shape indexes is not sufficient to properly characterize the shape of print dots (printed using a gravure process), and that the categorization of dots in predefined dot patterns combined with a statistical analysis of relevant shape indexes is more relevant to properly characterize a print from its dots' distribution. In Section 7.2.4(Chapter 7), it has been discussed the limitations of the different methods used for steps 1 to 7 of the framework that has been proposed and of the threshold values that has been used. Our objective has not to optimize the efficiency of each of these steps but to propose a relevant framework to our study case that could be extended to other study cases similar to the one studied. Several limitations pointed out in Section 8.2.1 would need improvements that could be obtained only with a higher number of print samples.

This second part of study has been done from a “limited” set of prints (with, in total, 4467 dots). To evaluate the accuracy and robustness of the pattern recognition process proposed, more tests should be done with annotated data. More samples should be analysed and also more printers (and printing parameters) should be compared. Similarly, in order to assess the effectiveness of our hypothesis based on the deformations of dots at a microscopic level, a larger number of prints and reprints (and printing parameters) should be compared. That is, the first results shown in this the study are very promising and demonstrate that the study parameters and the proposed methodology are relevant enough to support the hypothesis.

In further work of the study, more samples have been analysed and computed the confusion matrix (in %) of the proposed classification method and evaluated its robustness using Precision–Recall curves.

In the next section more samples have been analysed, results obtained from dot structure analysis of color tint for three different gravure printers are discussed.

### **8.3 Experimental Results and discussion obtain from print and reprint Dot Sizes and Shape**

In this study, a method has been introduced to study how the dot sizes and shapes of color prints can be used to identify the authenticity of the original printed package by the manufacturers or their authorized printers. The differentiation is done on the basis of different parameters such as dot area, major and minor axis of dots, eccentricity of the printed dots. The parameters like dot area, major axis, minor axis and eccentricity of cyan, magenta and yellow (20 %, 40%, 50%) tint for print and reprint samples are obtained by using MATLAB R2018a. For the edge detection, the canny edge detection algorithm has been applied on the microscopic images. The boundaries of the objects have been calculated by detecting the contours of the detected edge dots in the samples. The study shows that the dot shape parameters (Dot area, Major and Minor axis, Eccentricity) [36,37] may be used to distinguish the print sample from reprint sample.

#### **8.3.1 Results obtain from print and reprint Dot Sizes and Shape (CMYK)**

The dot structure parameters (dot areas, major axis, and minor axis) might be useful to distinguish the print samples from its scanned reprint samples (which may be treated as counterfeited samples). Using a microscope, the study captured the color dots of print and reprint samples of different dot areas and transformed them into binary images. The binary images were then analysed using MATLAB software to derive dot parameters for both the print and reprint samples. Figs. 8.18 and 8.19 showed the dot structure of print-reprint samples. The print quality for both original-print and reprint (simulated counterfeited) for different dot percentages for cyan and magenta color patches have been observed. Figs. 8.20 and 8.21 show similar results for yellow and black color patches.



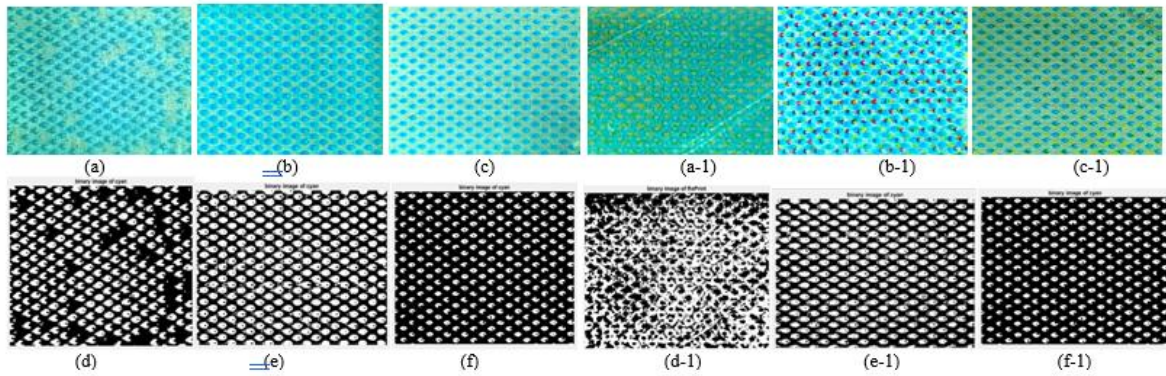


Fig 8.18: Analysed image of Print ((a)Cyan 20% patch of Printer 1(P1), (b)Cyan 20% patch of Printer 2(P2), (c)Cyan 20% patch of Printer 3(P3)), (d)Binary image of Cyan20% patch of Printer 1(P1) , (e)Binary image of Cyan20% patch of Printer 2(P2), (f)Binary image of Cyan20% patch of Printer 3(P3)) and Reprint ((a-1)Cyan 20% patch of Re-printer 1(R1), (b-1)Cyan 20% patch of Re-printer 2(R2), (c-1)Cyan 20% patch of Re-printer 3(R3)), (d-1)Binary image of Cyan20% patch of Re-printer 1(R1), (e-1)Binary image of Cyan20% patch of Re-printer 2(R2), (f-1)Binary image of Cyan20% patch of Re-printer 3(R3))

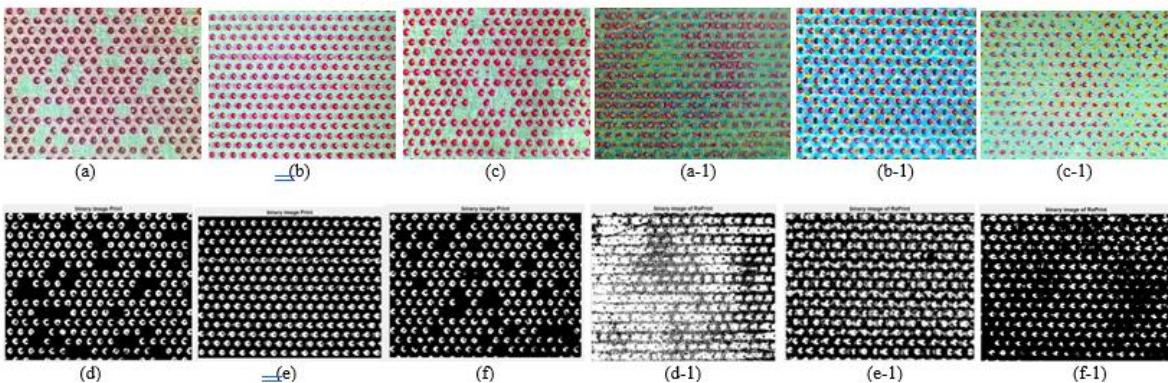


Fig 8.19: Analysed image of Print ((a)Magenta 20% patch of Printer 1(P1), (b)Magenta 20% patch of Printer 2(P2), (c)Magenta 20% patch of Printer 3(P3)), Binary images of Print ((d)Binary image of Magenta 20% patch of Printer 1(P1), (e)Binary image of Magenta 20% patch of Printer 2 (P2), (f)Binary image of Magenta 20% patch of Printer 3(P3)) and Re-print ((a-1) Magenta 20% patch of Printer 1(R1), (b-1) Magenta 20% patch of Printer 2 (R2), (c-1) Magenta 20% patch of Printer 3(R3)), Binary images of Re-print ((d-1)Binary image of Magenta 20% patch of Re-printer 1(R1) , (e-1)Binary image of Magenta 20% patch of Re-printer 2(R2) , (f-1)Binary image of Magenta 20% patch of Re-printer 3(R3))

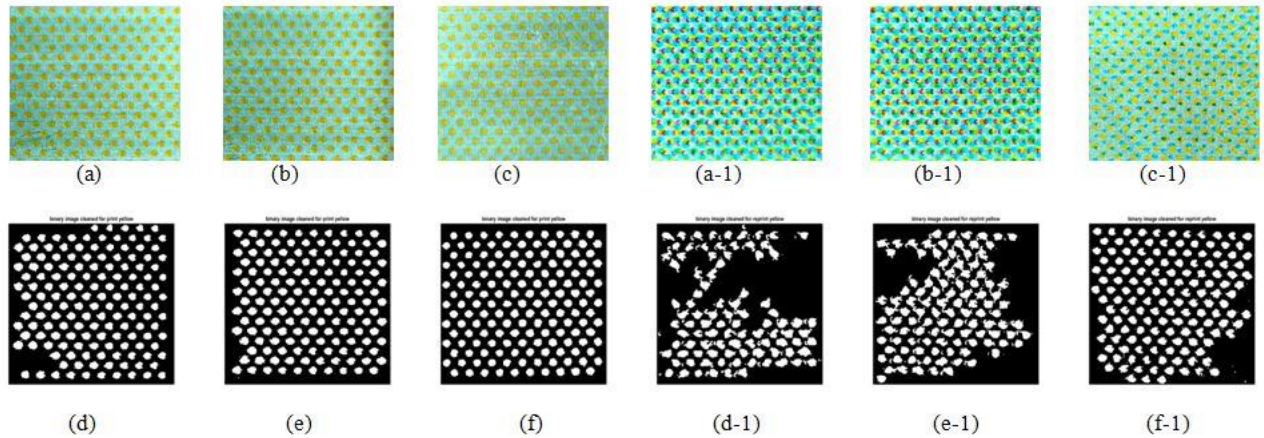


Fig 8.20 Analyzed image of Print ((a)Yellow 20% patch of Printer 1(P1), (b)Yellow 20% patch of Printer 2(P2), (c)Yellow 20% patch of Printer 3(P3)),Binary images of Print ((d)Binary image of Yellow 20% patch of Printer 1(P1), (e)Binary image of Yellow 20% patch of Printer 2 (P2), (f)Binary image of Yellow 20% patch of Printer 3(P3)) and Re-print ((a-1) Yellow 20% patch of Printer 1(R1), (b-1) Yellow 20% patch of Printer 2 (R2), (c-1) Yellow 20% patch of Printer 3(R3)),Binary images of Re-print ((d-1)Binary image of Yellow 20% patch of Re-printer 1(R1) , (e-1)Binary image of Yellow 20% patch of Re-printer 2(R2) , (f-1)Binary image of Yellow 20% patch of Re-printer 3(R3))

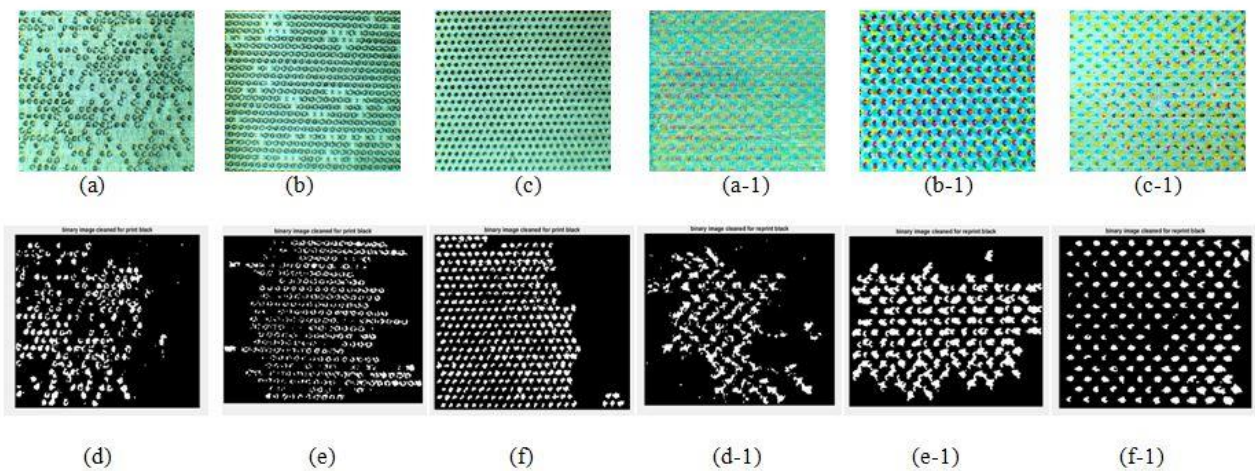


Fig 8.21 Analyzed image of Print ((a)Black 20% patch of Printer 1(P1), (b)Black 20% patch of Printer 2(P2), (c)Black 20% patch of Printer 3(P3)),Binary images of Print ((d)Binary image of Black 20% patch of Printer 1(P1), (e)Binary image of Black 20% patch of Printer 2 (P2), (f)Binary image of Black 20% patch of Printer 3(P3)) and Re-print ((a-1) Black 20% patch of Printer 1(R1), (b-1) Black 20% patch of Printer 2 (R2), (c-1) Black 20% patch of Printer 3(R3)) Binary images of Re-print ((d-1)Binary image of Black 20% patch of Re-printer 1(R1) , (e-1)Binary image of Black 20% patch of Re-printer 2(R2) , (f-1)Binary image of Black 20% patch of Re-printer 3(R3))

The experimental dot areas for print sample parameters are depicted in Figs 8.22, 8.23, and 8.24. In Fig. 8.22, the average dot area for printers P1, P2, and P3 and for reprints R1, R2, and R3 has been plotted for 20% cyan dots. It has been observed that the mean dot areas for scanned reprints are considerably larger than those for the original prints. Similar results are observed in Figs. 8.23 and 8.24 for 40% and 50% dot areas, respectively.

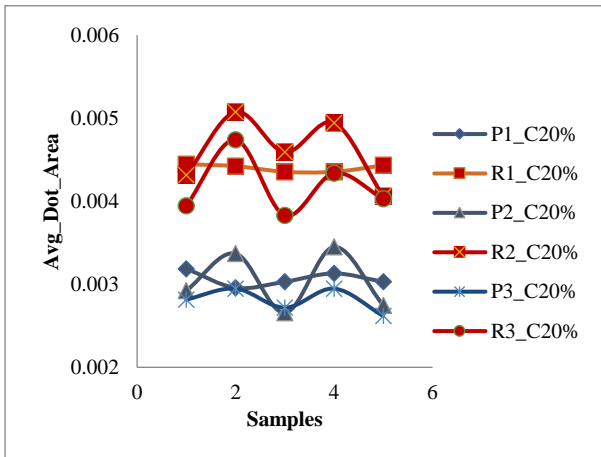


Fig 8.22: Cyan 20% patch Average Dot Area

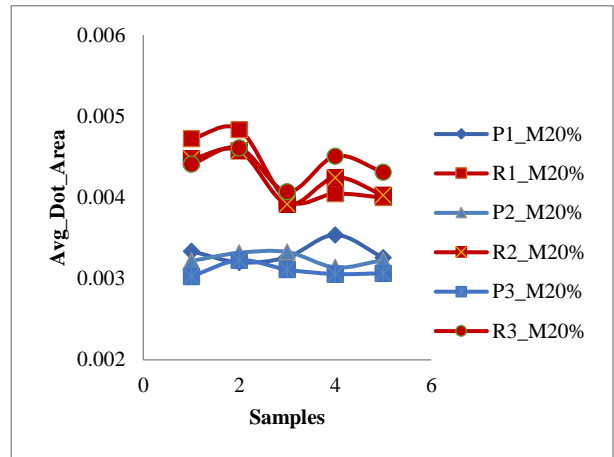


Fig 8.25: Magenta 20% patch Average Dot Area

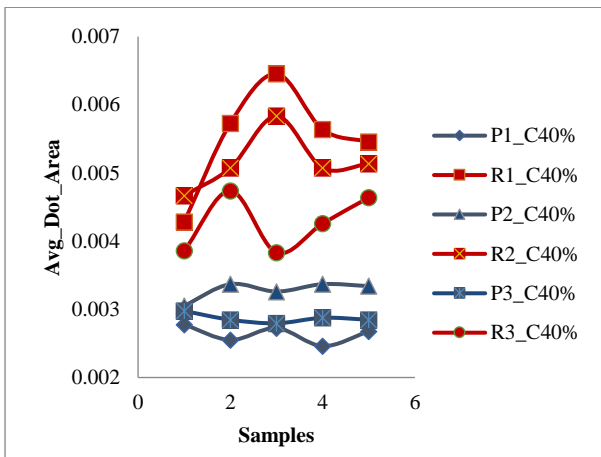


Fig 8.23: Cyan 40% patch Average Dot Area

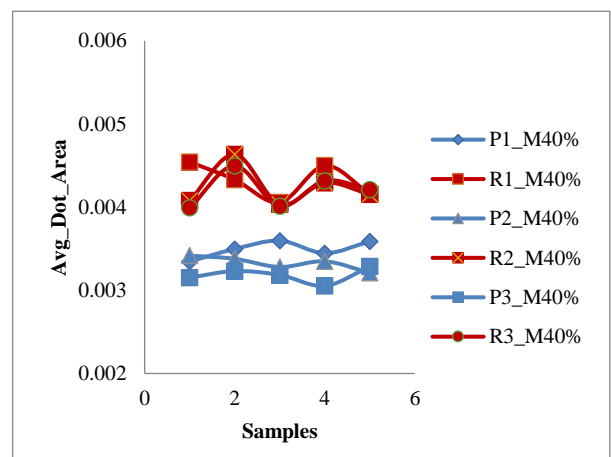


Fig 8.26: Magenta 40% patch Average Dot Area

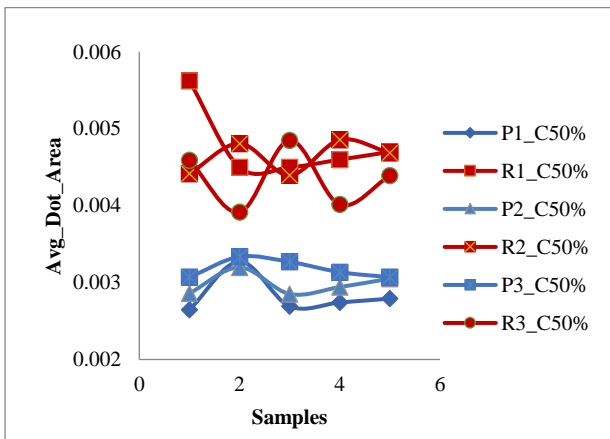


Fig 8.24: Cyan 50% patch Average Dot Area.

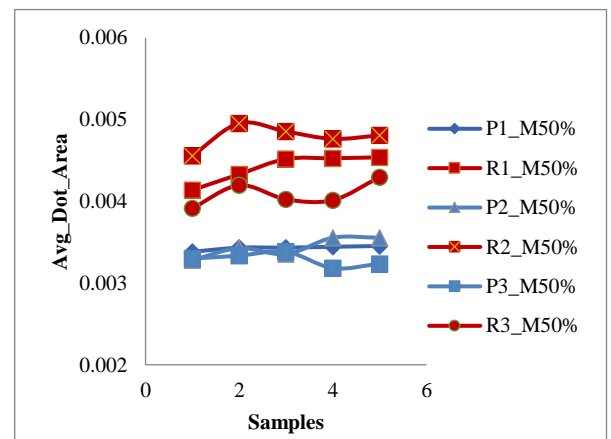


Fig 8.27: Magenta 50% patch Average Dot Area



Figs. 8.25, 8.26, and 8.27 indicate that the dot areas of reprints are significantly larger compared to the original prints across 20%, 40%, and 50% dot areas of magenta, respectively. Likewise, Figs 8.28, 8.29, and 8.30 illustrated a significant increase in dot areas for reprints compared to the original prints at 20%, 40%, and 50% dot areas of yellow, respectively. Similarly, Figs. 8.31, 8.32 and 8.33 showed that the dot areas for reprints are much higher than original prints for 20%, 40% and 50% dot areas of black respectively.

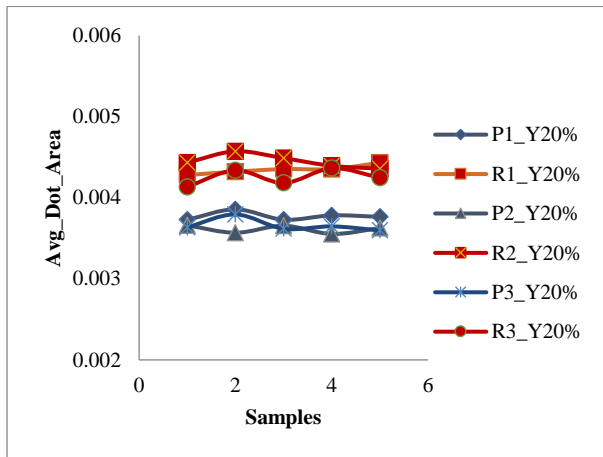


Fig 8.28: Yellow 20% patch Average Dot Area

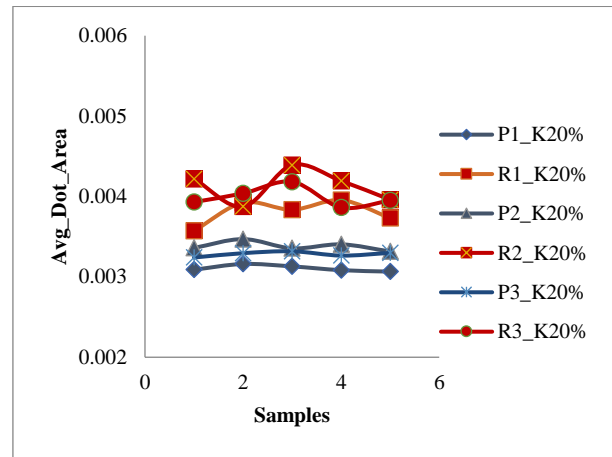


Fig 8.31: Black 20% patch Average Dot Area

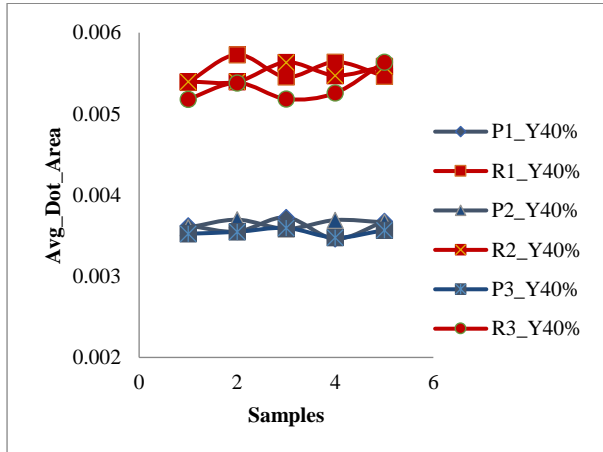


Fig 8.29: Yellow 40% patch Average Dot Area

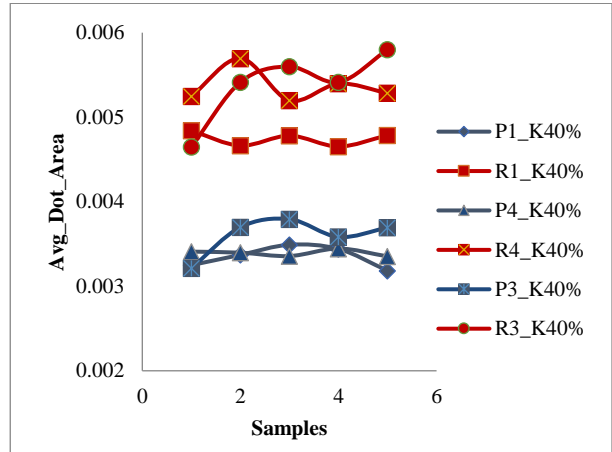


Fig 8.32: Black 40% patch Average Dot Area

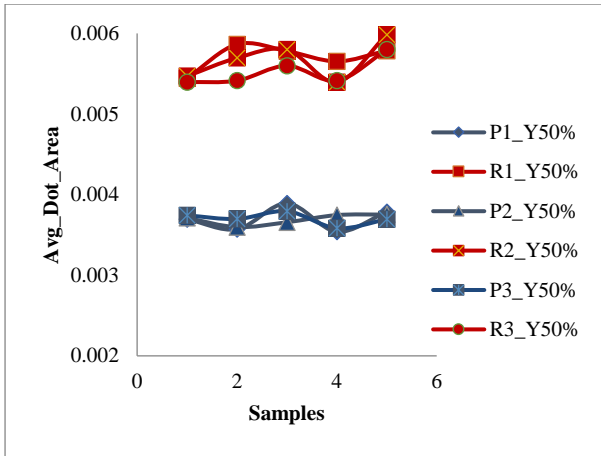


Fig 8.30: Yellow 50% patch Average Dot Area

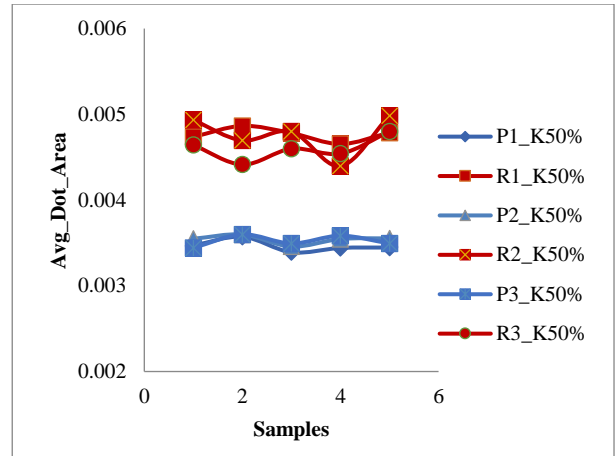
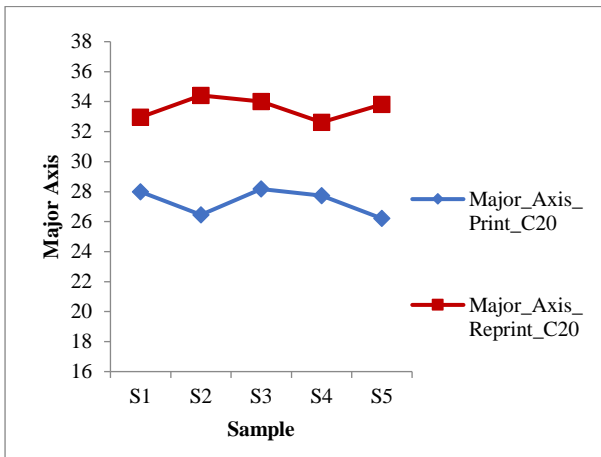
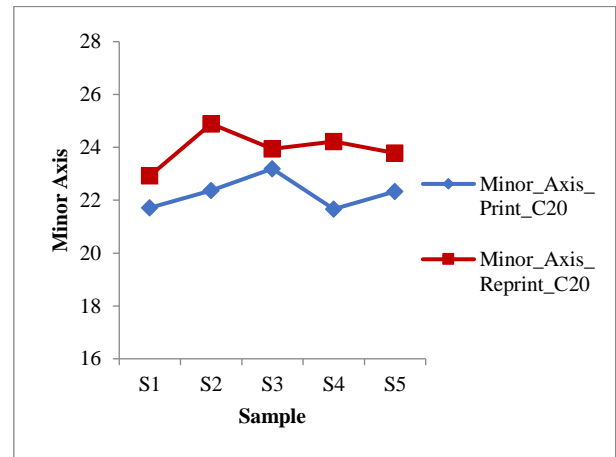


Fig 8.33: Black 50% patch Average Dot Area

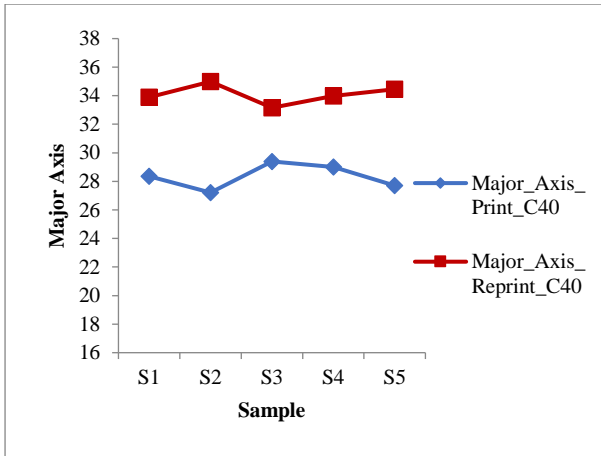
The major and minor axes, as well as eccentricity, have been examined for color patches with different dot areas for both print and reprint samples. Fig. 8.34(a, b, and c) showed that the major axis of reprints is much greater than the original prints for 20%, 40%, and 50% dot areas of cyan, respectively. Similar results have been shown for the minor axis in Fig 8.35(a, b, and c) for 20%, 40%, and 50% dot areas of cyan, respectively. In Fig. 8.36(a, b, and c), it is shown that the eccentricity of cyan reprint dots has increased over print dots. Results of a similar nature have been obtained for magenta, yellow and black prints. The mean value of the major and minor axes for the reprint dots are higher than those of the original prints.



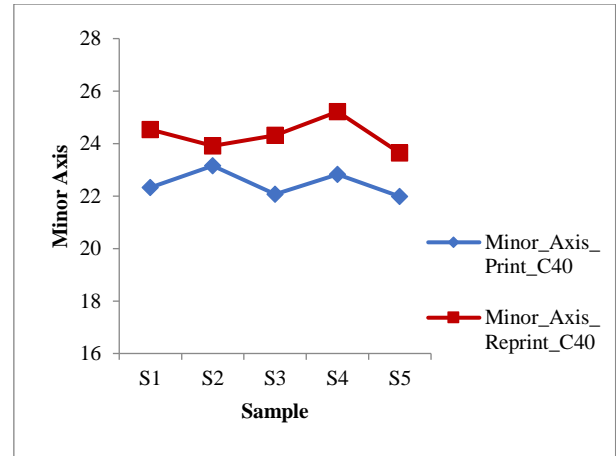
(a)



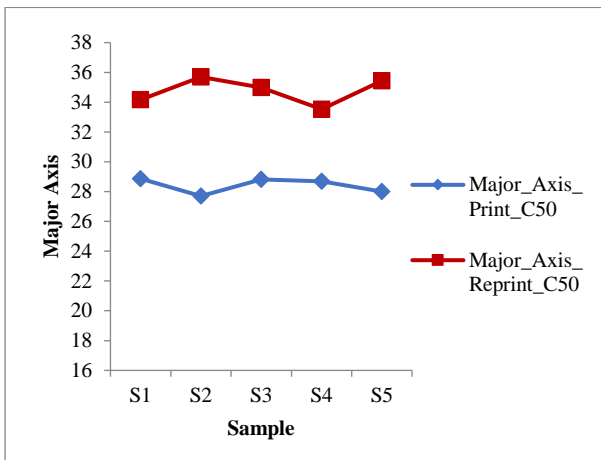
(a)



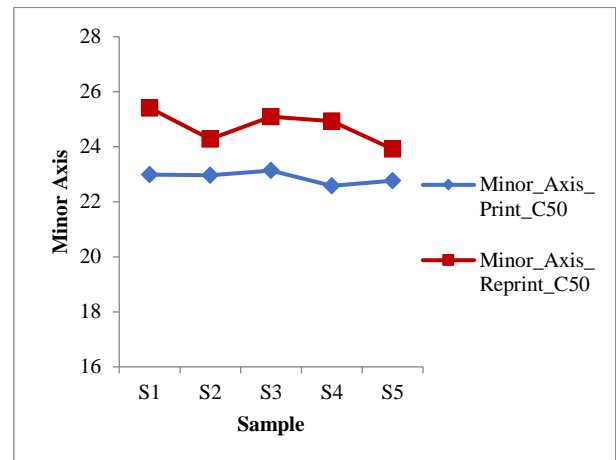
(b)



(b)

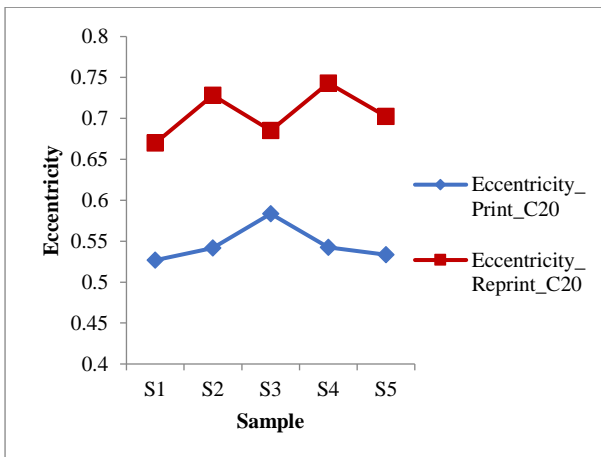


(c)

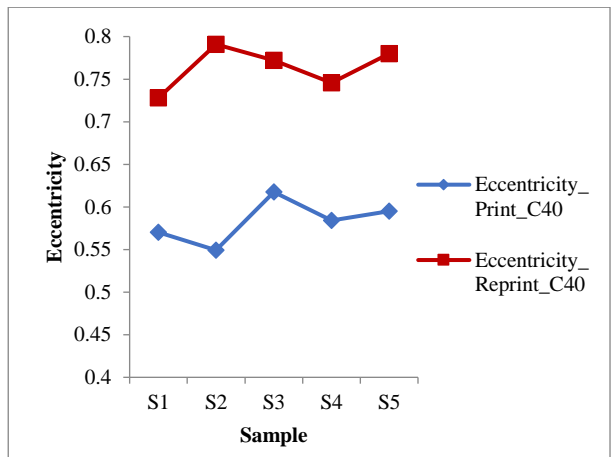


(c)

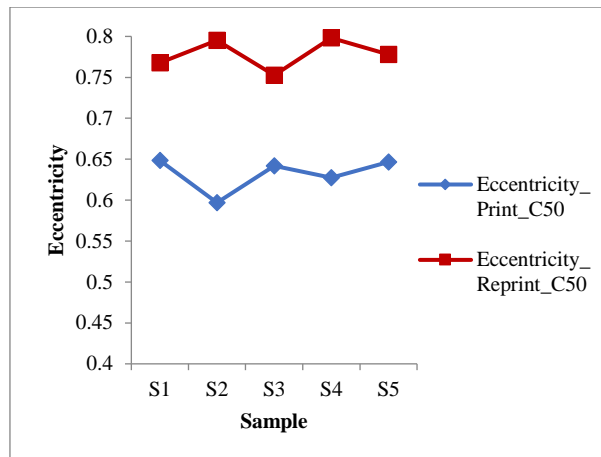
Fig 8.34(a, b, c): Major axis of cyan print and reprint Fig 8.35(a, b, c): Minor axis of cyan print and reprint



(a)



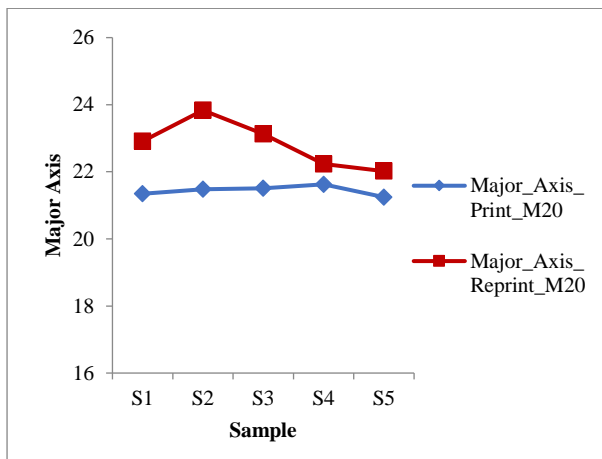
(b)



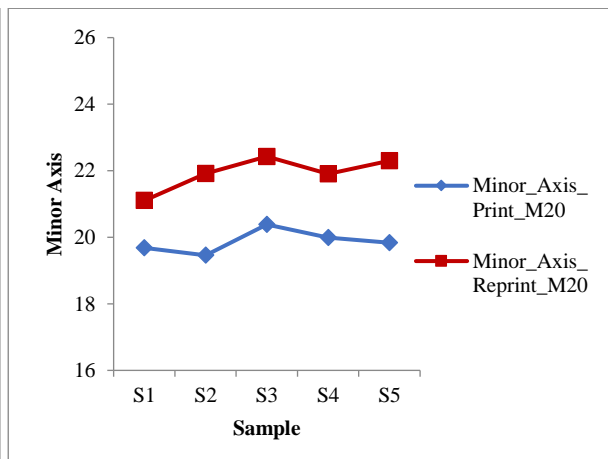
(c)

Fig 8.36(a, b, c): Eccentricity of cyan print and reprint

Similar to the cyan dots, the three parameters have been computed for magenta prints and reprint dots, which are depicted in Figs. 8.37 and 8.38 below. In Fig. 8.37 (a, b, and c), it has been observed that the major axis values of reprint samples are larger than that of print. Similarly, Fig. 8.38 (a, b, and c) show that the minor axis values are also higher for reprint samples compared to print samples.

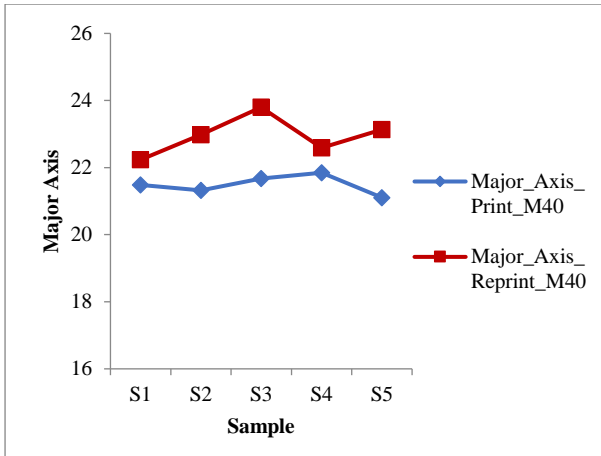


(a)

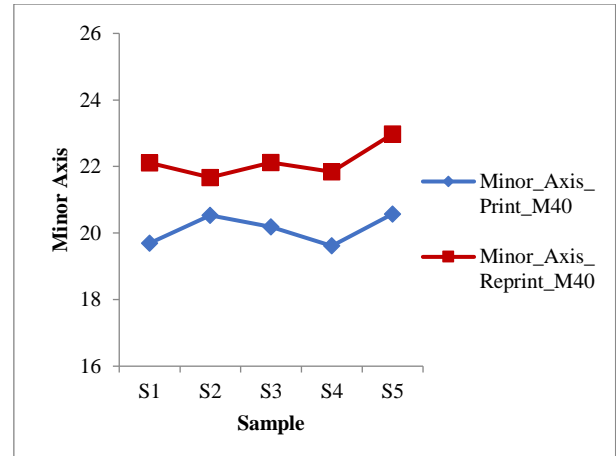


(a)

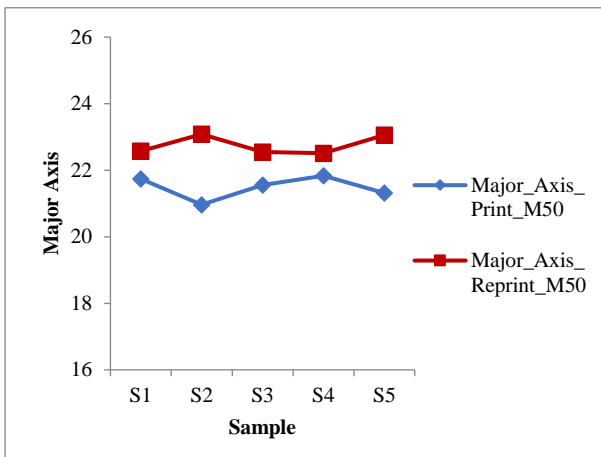




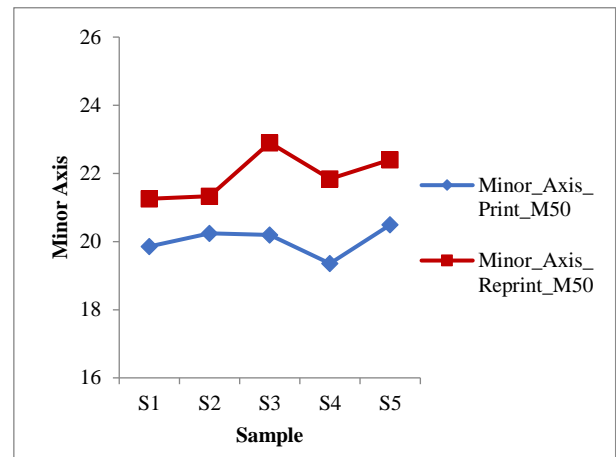
(b)



(b)

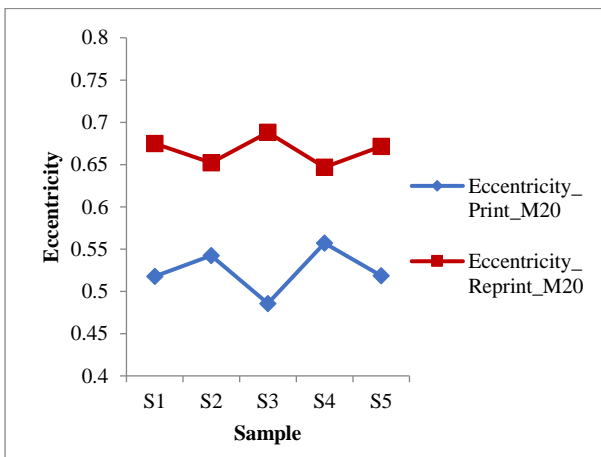


(c)

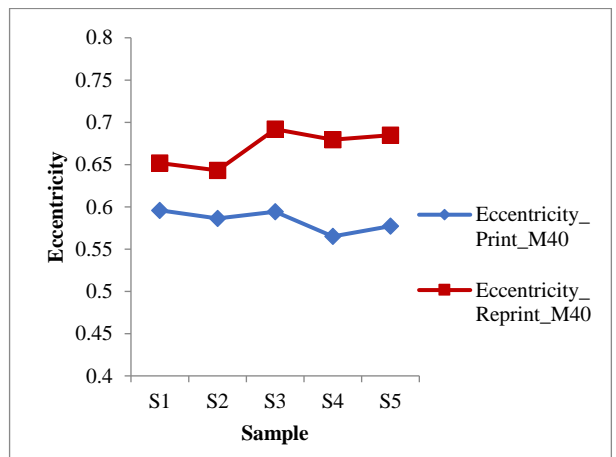


(c)

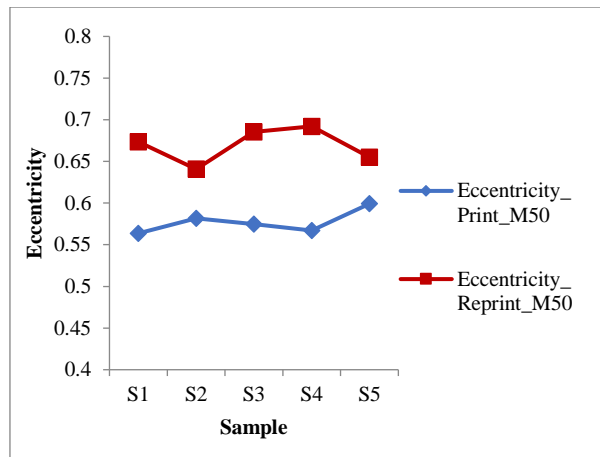
Fig 8.37(a, b, c): Major axis of magenta print and reprint Fig 8.38(a, b, c): Minor axis of magenta print and reprint



(a)



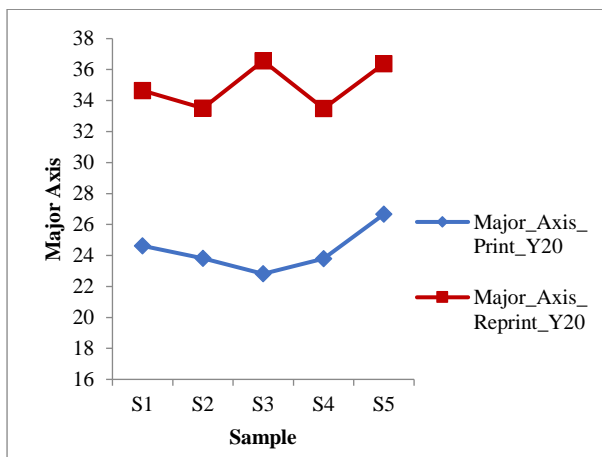
(b)



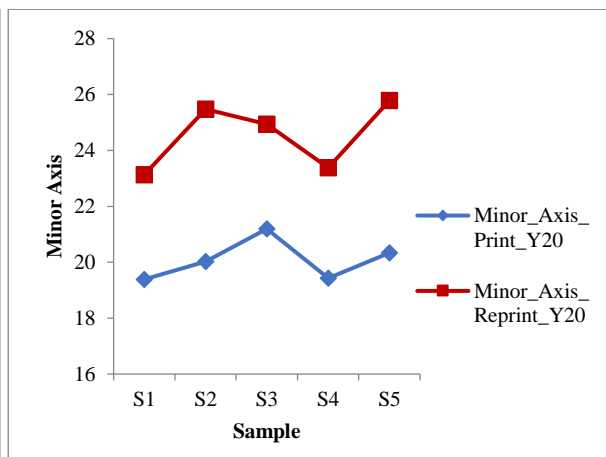
(c)

Fig 8.39(a, b, c): Eccentricity of magenta print and reprint

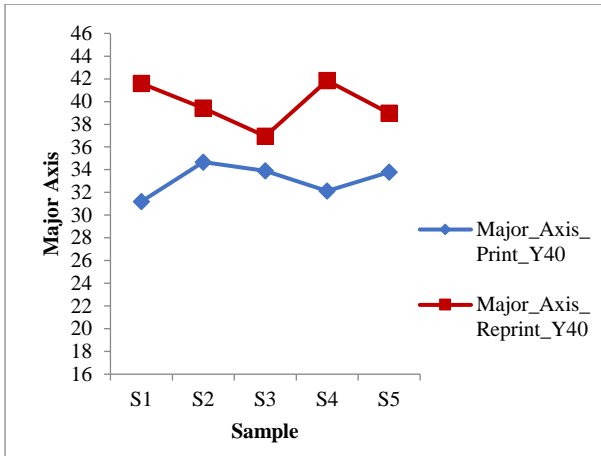
In general, the degree of eccentricity assists in determining the curvature of a shape. When the curvature decreases, the degree of eccentricity tends to rise. In Fig. 8.39 (a, b, and c), the eccentricity of print and reprint dot samples has been plotted for magenta. The dots in the reprint samples have a higher average eccentricity, which implies that the shape of the dots has been changed irregularly, for reprints in comparison to the dots in the print samples. The findings for yellow samples have been observed similar outcomes, as shown in Fig 8.40 (a, b, and c). It can be observed that the average major axis values of reprint samples have increased. Likewise, in Fig 8.41 (a, b, and c), the average minor axis values have also shown a rise for reprint samples when compared to print samples.



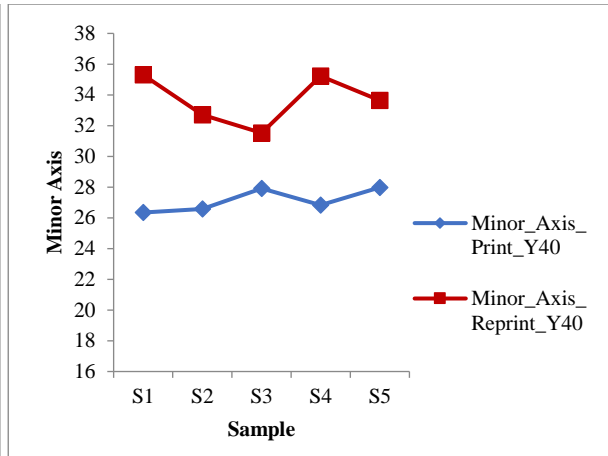
(a)



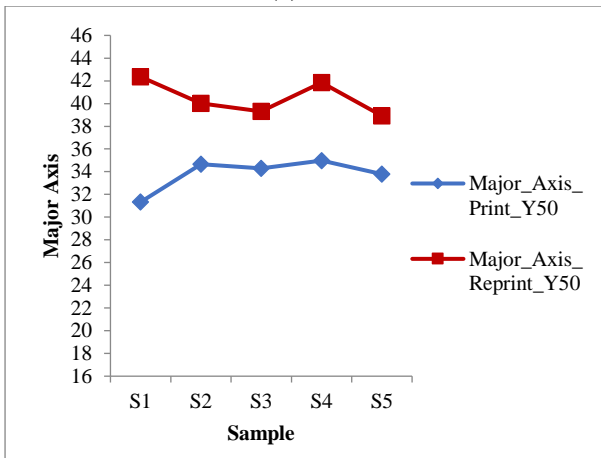
(a)



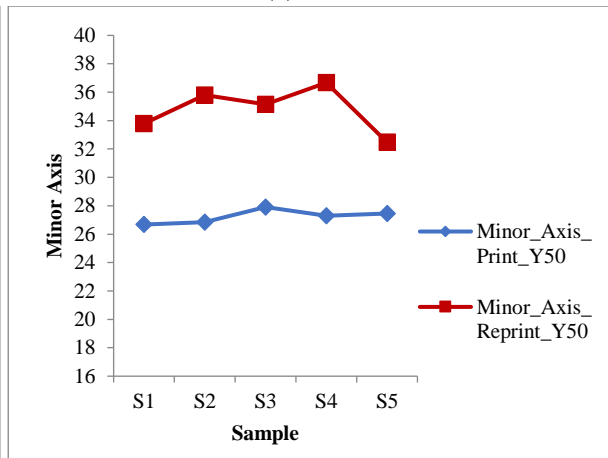
(b)



(b)



(c)

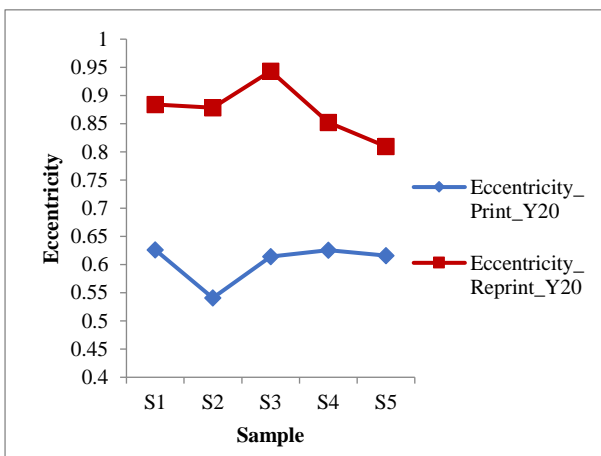


(c)

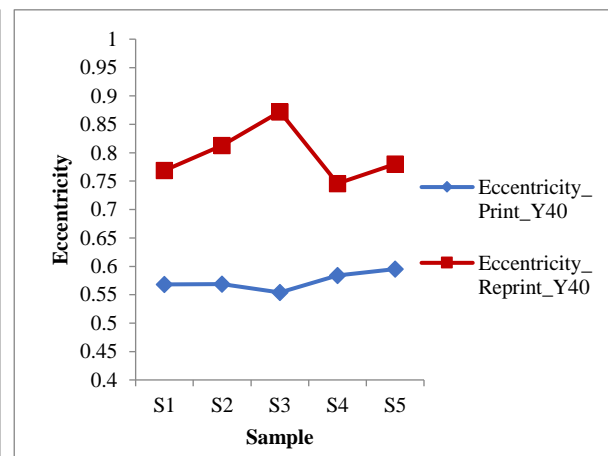
Fig 8.40(a, b, c): Major axis of yellow print and reprint

Fig 8.41(a, b, c): Minor axis of yellow print and reprint

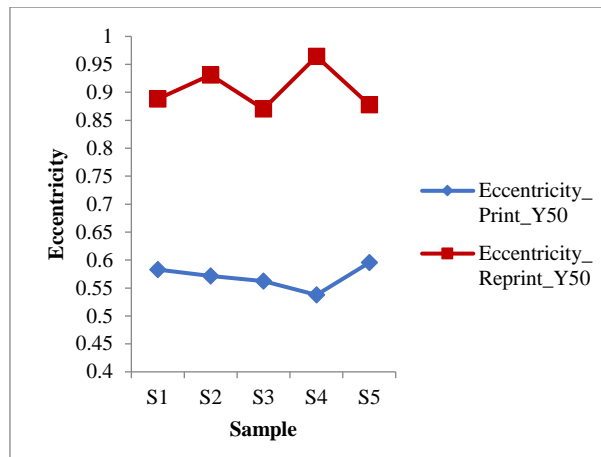
The eccentricity of print and reprint dot samples has been plotted in Fig 8.42(a, b, and c) for yellow print samples. The reprint dot samples have a higher average eccentricity of the dots compared to the original prints.



(a)



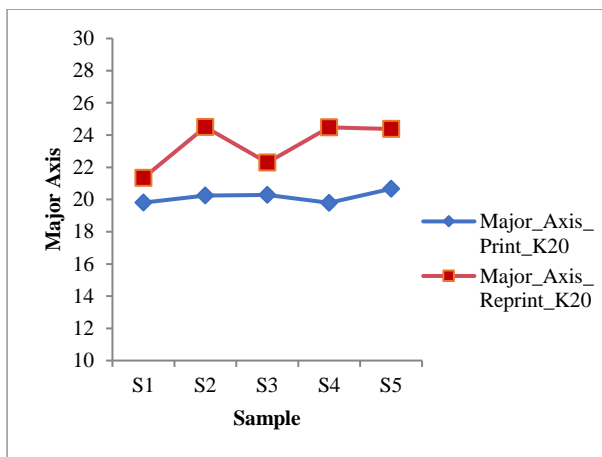
(b)



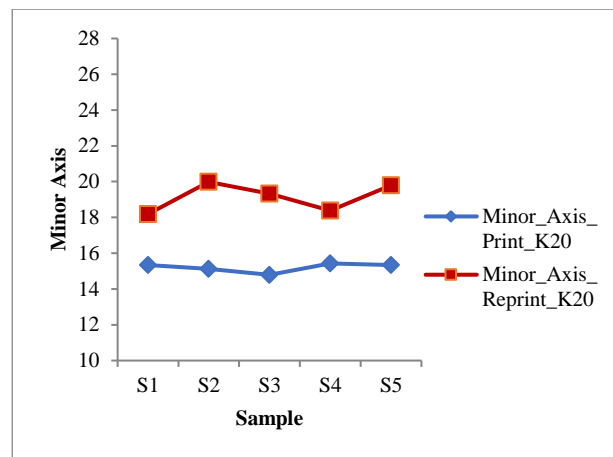
(c)

Fig 8.42(a, b, c): Eccentricity of yellow print and reprint

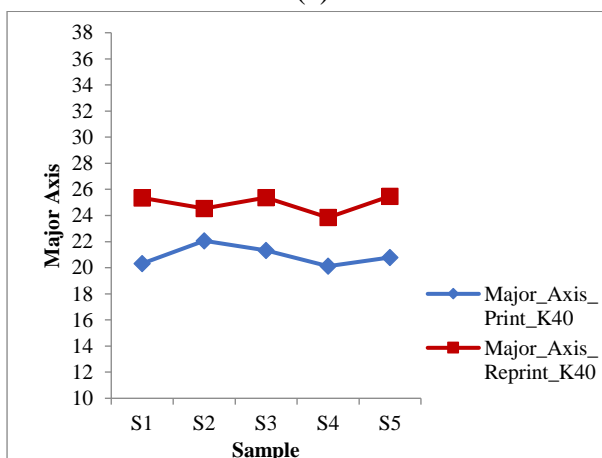
Similar results have been observed for black samples, as shown in Fig 8.43 (a, b, c), where the average of major axis values of reprint samples have increased, and in Fig 8.44 (a, b, c), where the average of minor axis values have also increased for reprint samples compared to print samples.



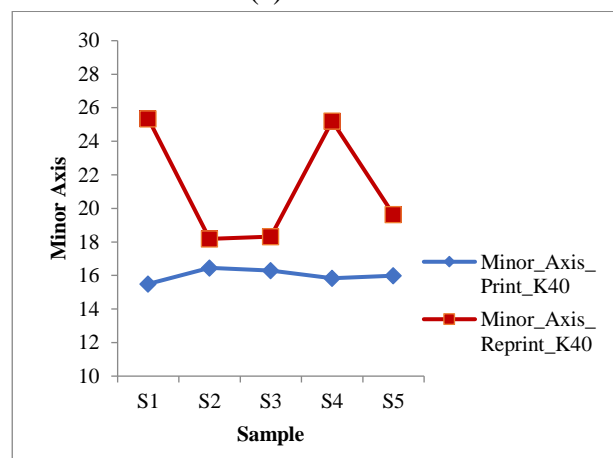
(a)



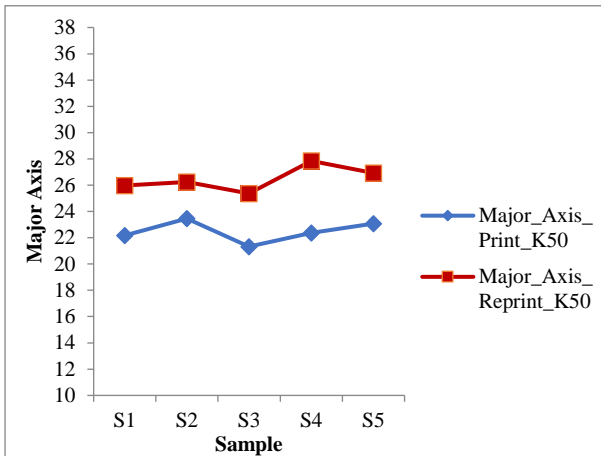
(a)



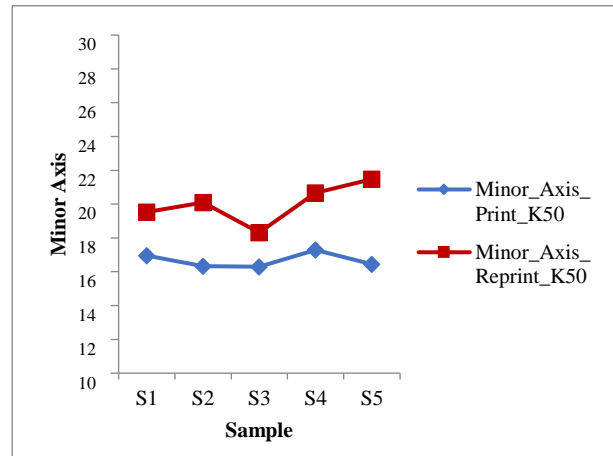
(b)



(b)



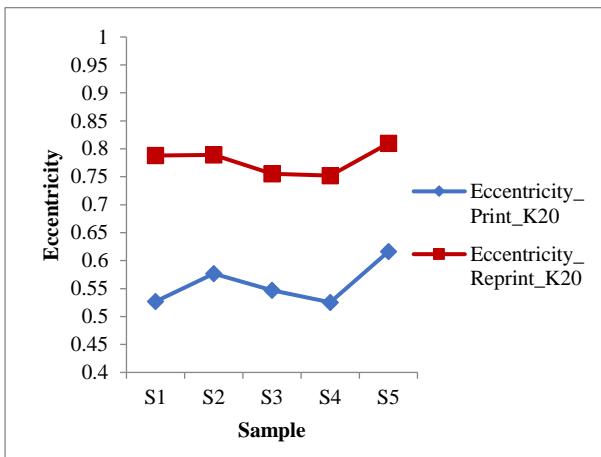
(c)



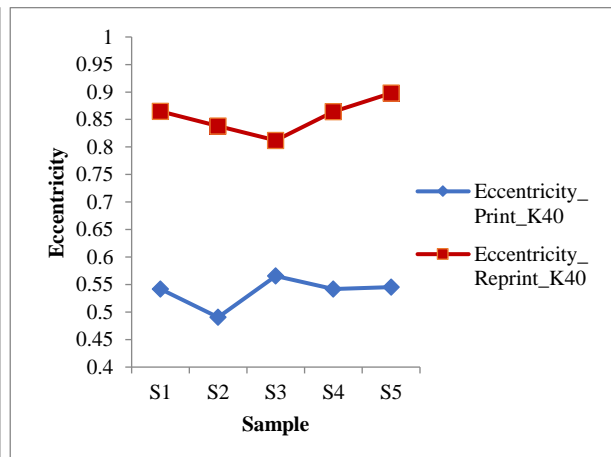
(c)

Fig 8.43(a,b,c): Major axis of black print and reprint Fig 8.44(a,b,c): Minor axis of black print and reprint

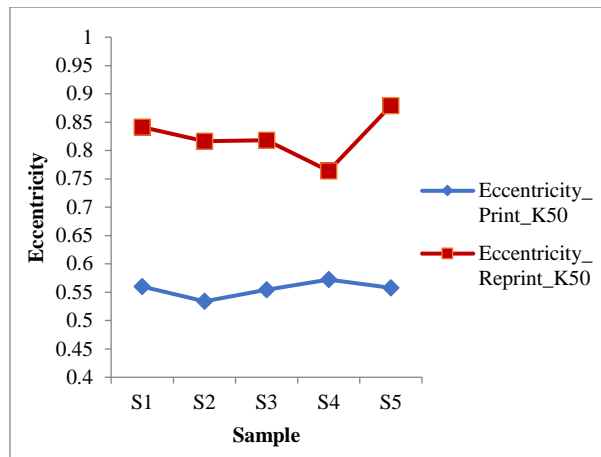
The eccentricity of print and reprint dot samples has been plotted in Fig 8.45(a, b, and c) for black dots. The reprint dot samples have a higher mean dot eccentricity, indicating an irregular change in dot shape compared to the original print samples.



(a)



(b)



(c)

Fig 8.45(a,b,c): Eccentricity of black print and reprint

Based on the analysis of all observed variations, it has been showed that the optical dot gain is unavoidable in case of reprints during imaging/copying the original prints. This implies that optical dot gain is an inevitable occurrence when copying and reproducing original prints, as indicated by all the observed variations [111]. Adjustments cannot fully eliminate dot gain due to light scatter. Foil is smoother than other substrates. Therefore, if the variation is noticeable in foil, it will naturally be greater in other materials, such as paper or plastic, that are used for packaging.

### 8.3.2 Discussion

In this part of the study, dot parameters like major, minor axis, and eccentricity, have been evaluated for different dot areas of color patches for print and reprint samples.

It has been observed that when the prints are copied/scanned and reprinted, the reprinted samples have dot gain, which is irregular and irreversible. The higher statistical values of dot areas, major or minor axes, and eccentricity show that the original artwork's dots won't remain the same after being copied.

The variations observed indicate that managing optical dot gain through adjustments is impractical due to substrate scattering. Foil, being smoother than other substrates, increases the effect. Therefore, if the effect is noticeable in foil, it will be even more prominent in other substrates such as paper or plastic packaging.

The subsequent part of the experiment involved the application of different shape descriptors, including dot area, perimeter, circularity, eccentricity, solidity, and major and minor axes, to differentiate between print and scanned reprint samples. The findings indicated that these shape descriptors can effectively distinguish between print and reprint dots when viewed under a microscope. To identify prints and reprints, a Support Vector

Machine (SVM) based multi-classification approach was used, which relied on the shape descriptor index properties.

#### **8.4 Experimental Results and discussion obtain from a Support Vector Machine approach and dots shape features**

In the fourth or last section of the study, several shape descriptors have been utilised, such as dot area, perimeter, circularity, eccentricity, solidity, and major and minor axes, to differentiate between print and scanned reprint samples. The findings indicated that these shape descriptors are useful for distinguishing between print and reprint dots at a microscopic level. To recognise print and reprint samples, a multi-classification strategy based on Support Vector Machine (SVM) has been used, utilising the characteristics of the shape descriptor index [31]. This approach achieved a high level of accuracy when categorising print and reprint samples at various dot percentages.

##### **8.4.1 Experimental Results obtain from a Support Vector Machine approach and dots shape features**

This experiment has been done to identify and differentiate an original print from a reprint sample (simulated counterfeit), both printed on the IT 8.7/3 target chart using gravure printing on a blister foil. In this study, 20%, 40% and 50% of cyan, magenta, yellow, and black dots have been taken into consideration. Different shape descriptor index parameters such as dot area, perimeter, circularity, eccentricity, solidity, and the major and minor axes of dots have been used for classification between the print sample and the scanned reprint sample. The dataset has been used for SVM classification in MATLAB using the median Gaussian kernel function with 6-fold cross validation. Figs. 8.46 (a) represents the scatter plot of the perimeter vs area of the original dots for gravure printers P1, P2, and P3 and for reprints R1, R2, and R3 for 20% of cyan. Figs. 8.46 (b) represents the scatter plot of the perimeter vs area of the dots for gravure prints and for reprints for 20% of cyan after SVM Classification. Similarly, Figs. 8.47 (a) and 8.47 (b) represent the scatter plot of the perimeter vs dot area for gravure printers P1, P2, and P3 and for reprints R1, R2, and R3, for 20% magenta for before and after SVM classification respectively. Figs. 8.48 (a) and 8.48 (b) display scatter plots of the dots' features of perimeter vs. dot area for gravure printers P1, P2, and P3 and reprints R1, R2, and R3, specifically for 20% yellow for before and after SVM classification respectively. The scatter plots in Fig 8.49 (a) and (b) display scatter plots of perimeter vs. dot area for printers and reprints for 20% black for before and after prediction.



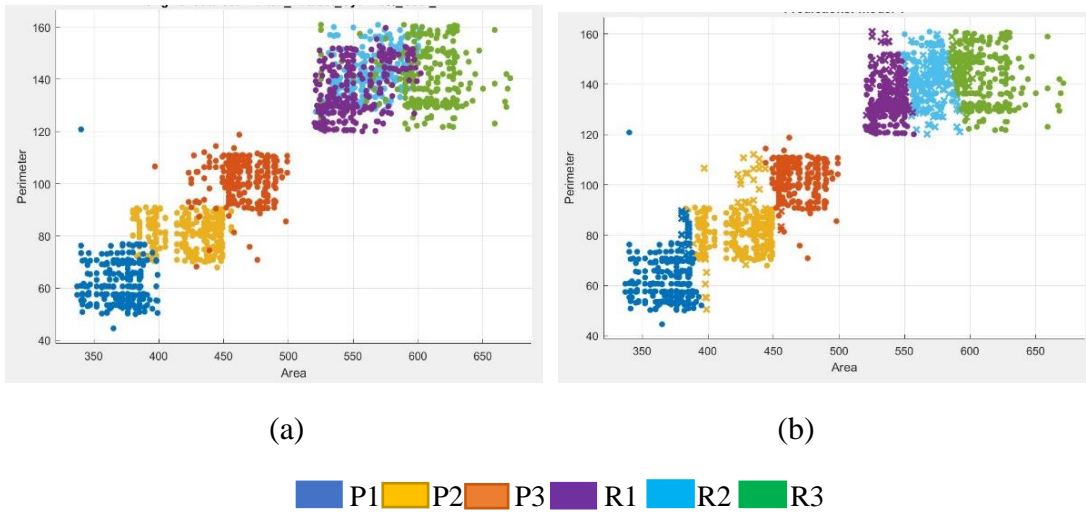


Fig 8.46: Scatter plots for 20% of Cyan for Print sample (P1, P2, P3) and Reprint sample (R1, R2, R3) (a) Original data Area vs. Perimeter before classification (b) Predicted data Area vs. Perimeter after SVM Classification,

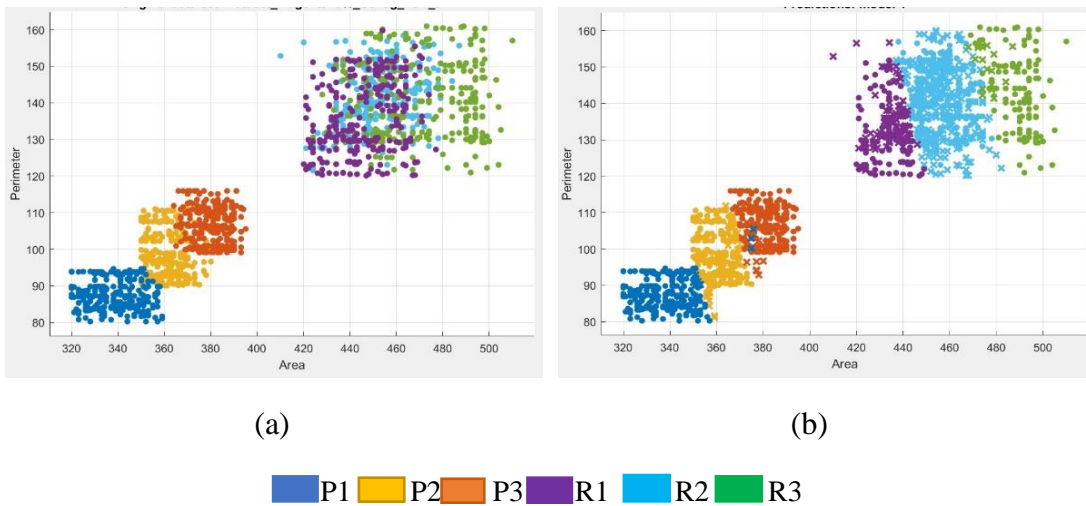


Fig 8.47: Scatter plots for 20% of Magenta for Print sample (P1, P2, P3) and Reprint sample (R1, R2, R3) (a) Original data Perimeter vs Area before classification (b) Predicted data Perimeter vs Area after classification.

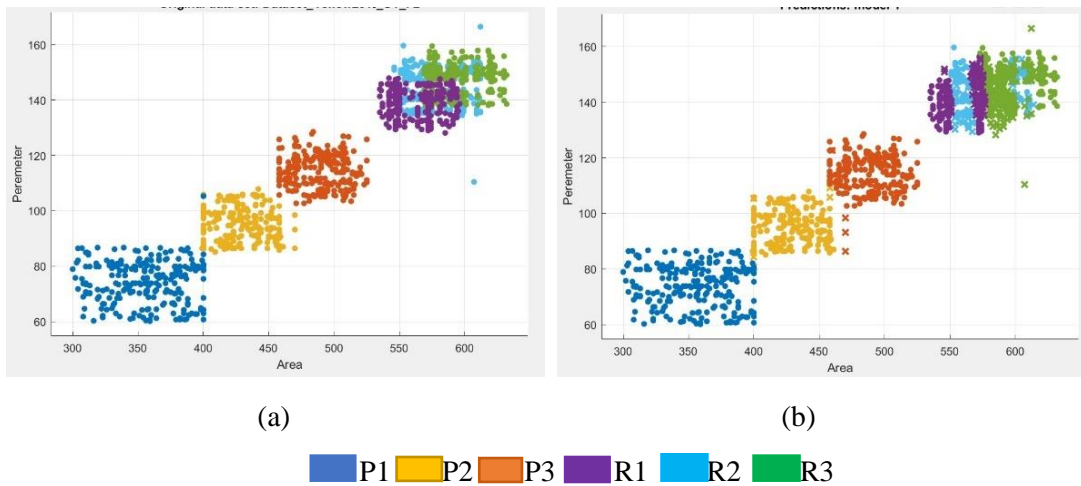


Fig 8.48: Scatter plots for 20% of Yellow for Print sample (P1, P2, P3) and Reprint sample (R1, R2, R3) (a) Original data Perimeter vs Area before classification (b) Predicted data Perimeter vs Area after classification.

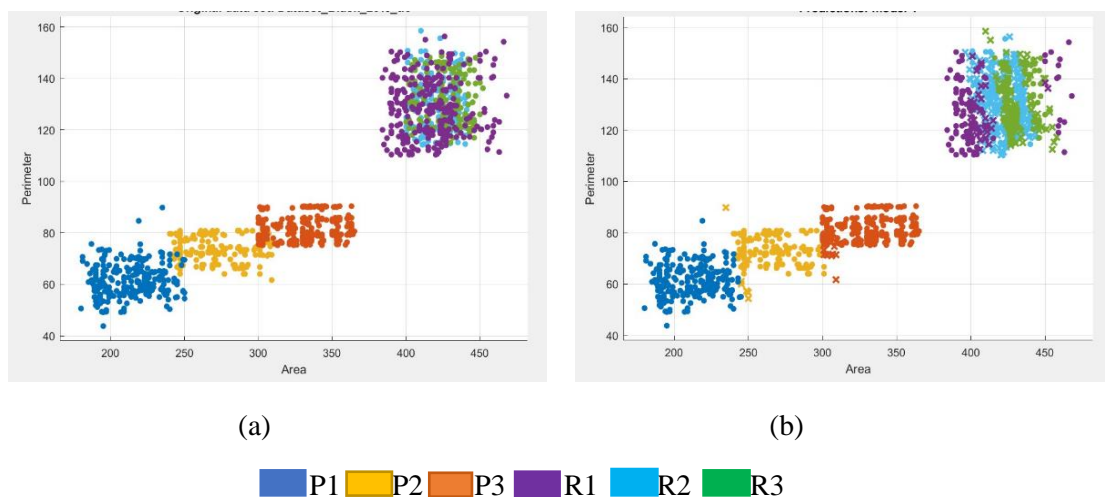


Fig 8.49: Scatter plots for 20% of Black for Print sample (P1, P2, P3) and Reprint sample (R1, R2, R3) (a) Original data Perimeter vs. Area before classification (b) Predicted data Perimeter vs. Area after classification.

Likewise, in, Fig. 8.50 (a) presents the scatter plot of the perimeter vs. area of the original dots for the printers P1, P2, P3 and for reprints R1, R2, R3 for 40% of cyan and Figs. 8.50 (b) represents the scatter plot of the perimeter vs area of the dots for gravure prints and for reprints for 40% of cyan after SVM Classification. Fig. 8.51 (a) and (b) display scatter plots of perimeter vs. dot area for gravure printers P1, P2, and P3 and reprints R1, R2, and R3, specifically for 40% magenta prints and reprints for before and after SVM classification respectively. Moving on to, Fig 8.52 (a) and(d) these figures exhibit the scatter plot of perimeter vs. dot area for original and predicted dot features for 40% yellow prints and reprints, and Fig 8.53 (a)–(d) depict corresponding the plots for 40% black prints and reprints similar fashion.

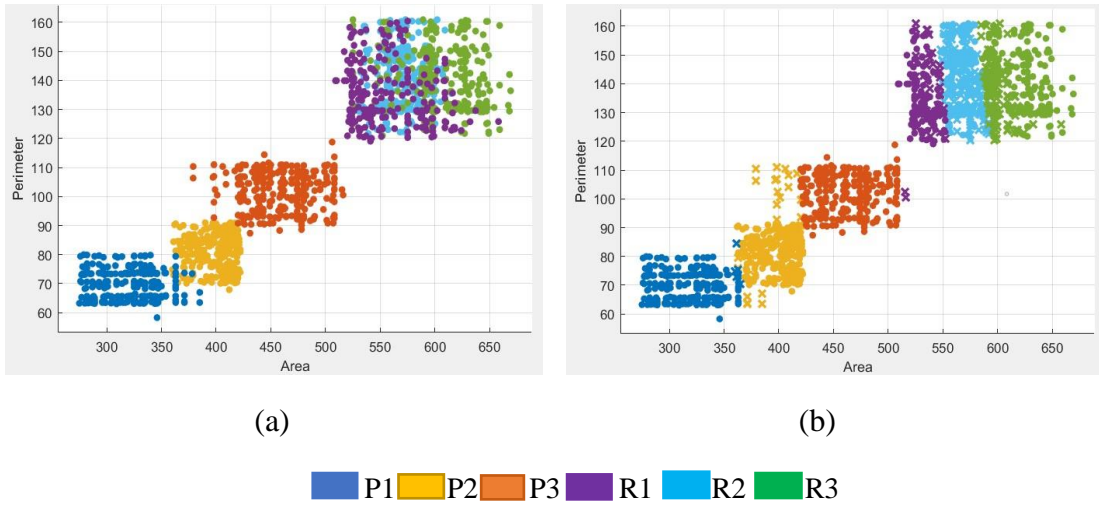


Fig 8.50: Scatter plots for 40% of Cyan for Print sample (P1, P2, P3) and Reprint sample (R1, R2, R3) (a) Original data Perimeter vs. Area before classification (b) Predicted data Perimeter vs. Area after classification.

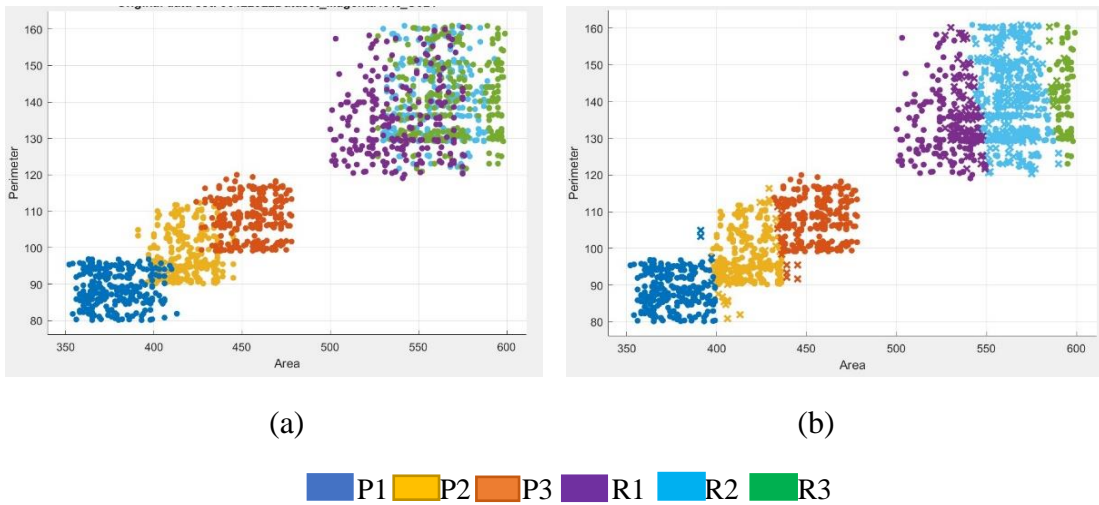


Fig 8.51: Scatter plots for 40% of Magenta for Print sample (P1, P2, P3) and Reprint sample (R1, R2, R3) (a) Original data Perimeter vs. Area before classification (b) Predicted data Perimeter vs. Area after classification.

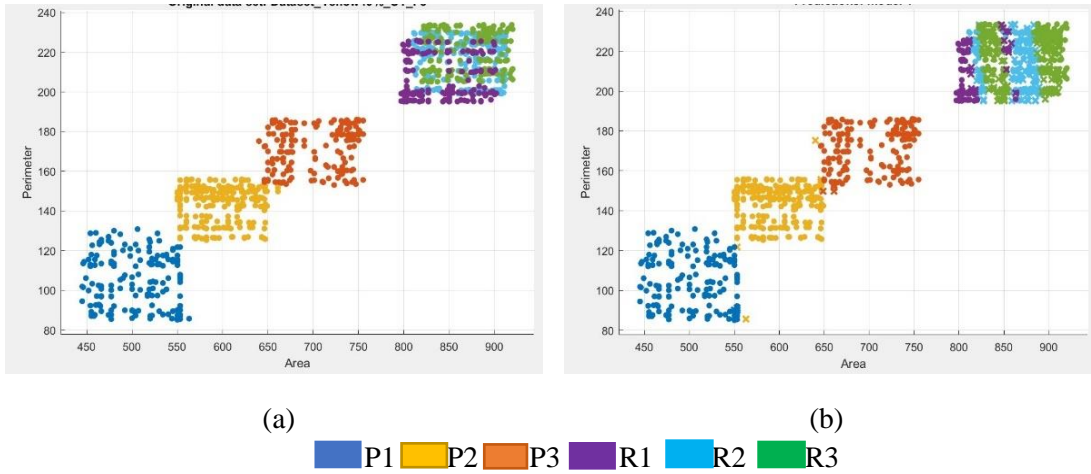


Fig 8.52: Scatter plots for 40% of Yellow for Print sample (P1, P2, P3) and Reprint sample (R1, R2, R3) (a) Original data Perimeter vs. Area before classification (b) Predicted data Perimeter vs. Area after classification.

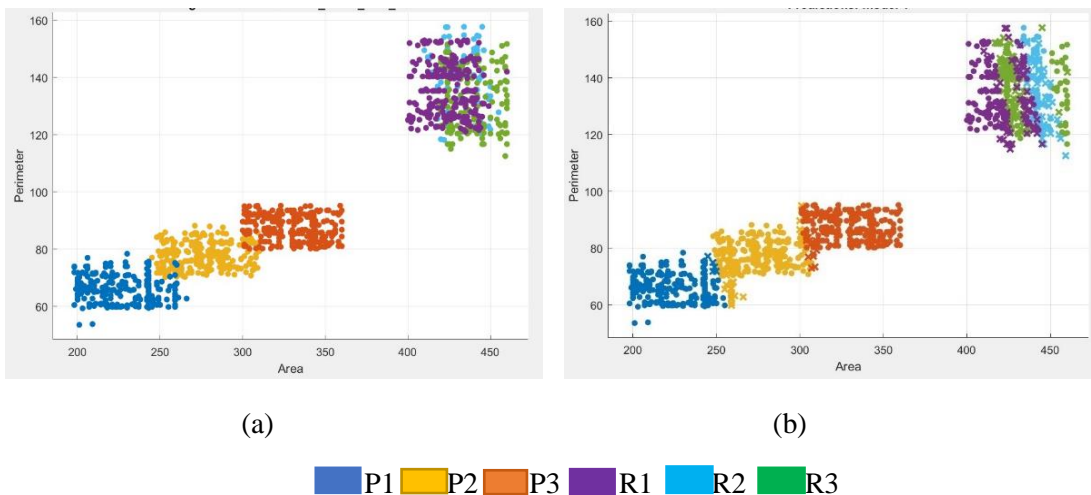


Fig 8.53: Scatter plots for 40% of Black for Print sample (P1, P2, P3) and Reprint sample (R1, R2, R3) (a) Original data Perimeter vs. Area before classification (b) Predicted data Perimeter vs. Area after classification.

Similarly, Fig. 8.54 (a) presents the scatter plot of the perimeter vs. area of the original dots for the printers P1, P2, P3 and for reprints R1, R2, R3 for 50% of cyan color. Additionally, Figs. 8.54 (b) illustrates the scatter plot of the perimeter vs area of the dots for gravure prints and for reprints for 50% of cyan after SVM Classification. Fig. 8.55 (a) and (b) display scatter plots of perimeter vs. dot area for gravure printers P1, P2, and P3 and reprints R1, R2, and R3, specifically for 50% magenta prints and reprints for before and after SVM classification respectively. Similarly, Fig 8.56 (a) and(d) shows the scatter plots of perimeter vs. dot area for original and predicted dot features for 50% yellow prints and reprints, and Fig 8.57 (a)–

(d) depicts similar scatter plots of perimeter vs. dot area for gravure printers P1, P2, and P3 and reprints R1, R2, and R3 for 50% black prints and reprints.

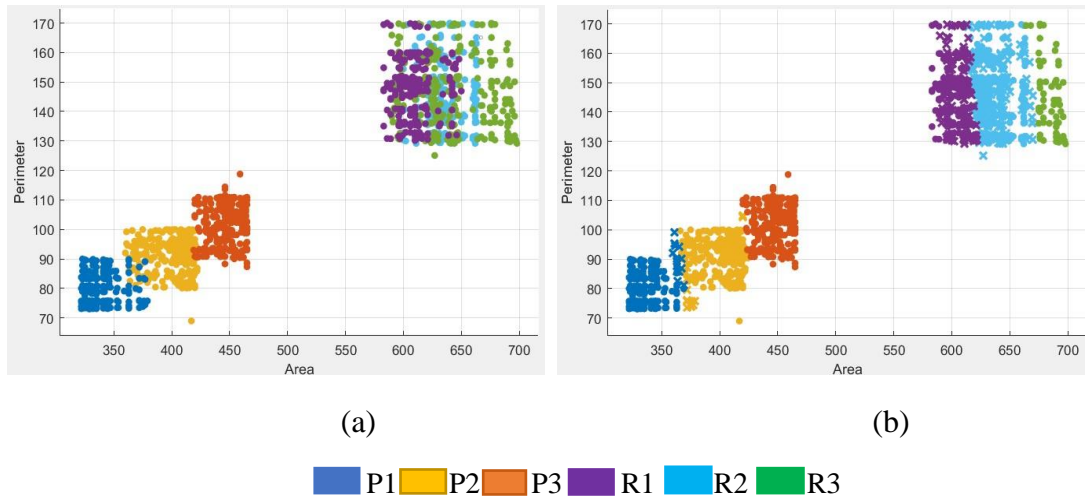


Fig 8.54: Scatter plots for 50% of Cyan for Print sample (P1, P2, P3) and Reprint sample (R1, R2, R3) (a) Original data Perimeter vs. Area before classification (b) Predicted data Perimeter vs. Area after classification.

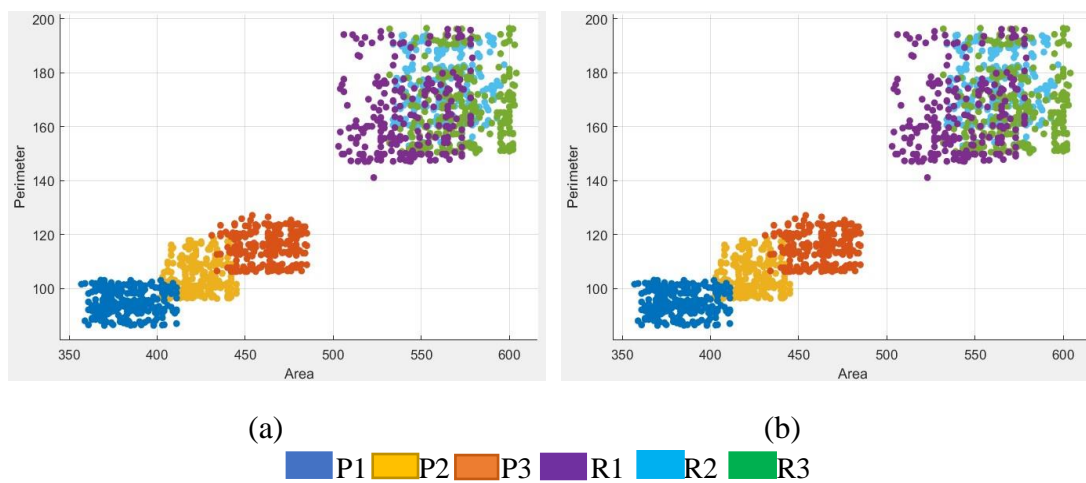


Fig 8.55: Scatter plots for 50% of Magenta for Print sample (P1, P2, P3) and Reprint sample (R1, R2, R3) (a) Original data Perimeter vs. Area before classification (b) Predicted data Perimeter vs. Area after classification.

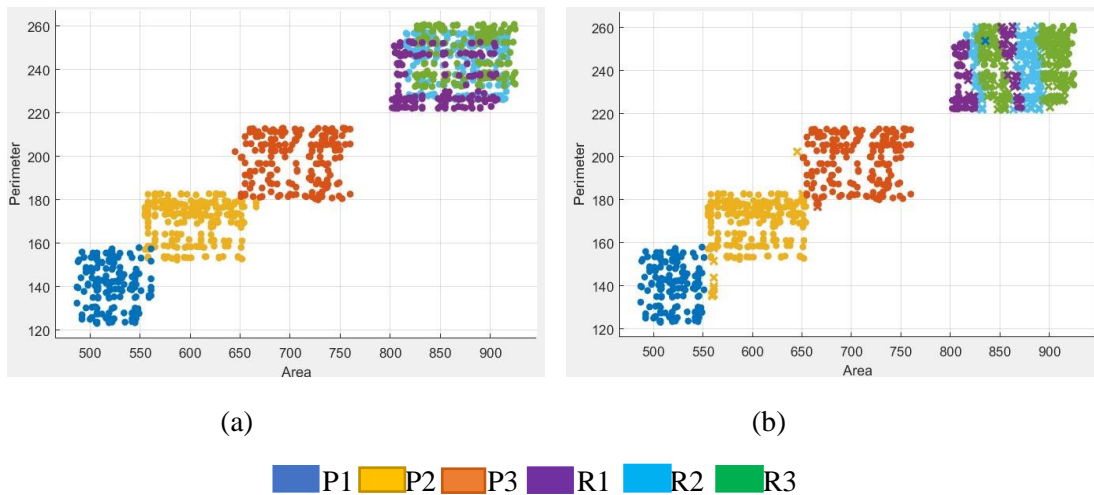


Fig 8.56: Scatter plots for 50% of Yellow for Print sample (P1, P2, P3) and Reprint sample (R1, R2, R3) (a) Original data Perimeter vs. Area before classification (b) Predicted data Perimeter vs. Area after classification.

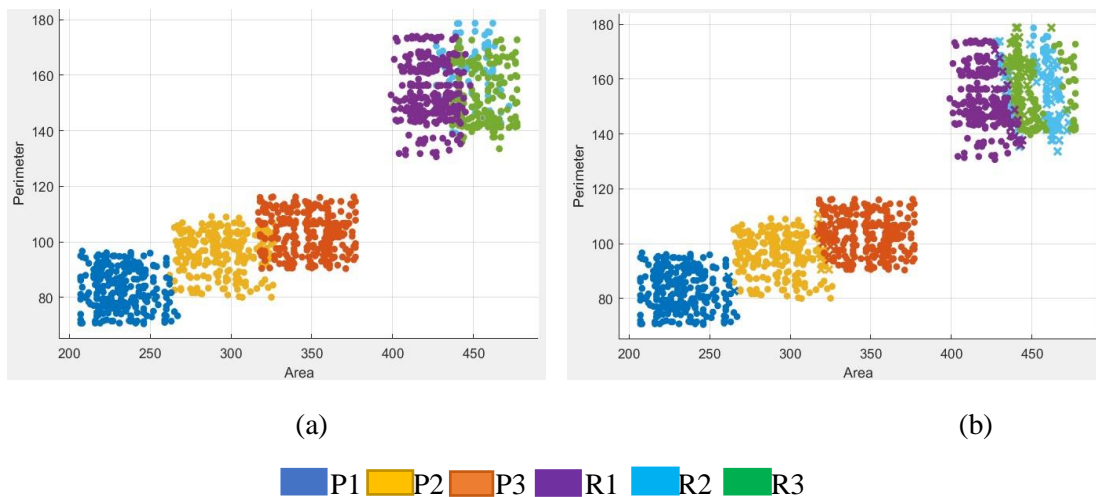


Fig 8.57: Scatter plots for 50% of Black for Print sample (P1, P2, P3) and Reprint sample (R1, R2, R3) (a) Original data Perimeter vs. Area before classification (b) Predicted data Perimeter vs. Area after classification.

In this study, has conducted a comparison of the dot shape index parameter as an input feature, specifically the perimeter versus the dot area of print samples and reprint samples, across various dot percentages. The object was to differentiate between these two types of samples. The study findings indicated that regardless of the color and dot percentage, the dot shape index parameter proved effective in distinguishing between the printed and reprinted samples. Furthermore, in this study, we performed classification using dot shape descriptor indices, specifically examining eccentricity versus area of dots for both print and reprint samples.



Figs 8.58 (a) and 8.58 (b) depict scatter plots that compare the eccentricity and dot area of gravure printers prints (P1, P2, and P3), as well as reprints (R1, R2, and R3), using a 20% cyan concentration. These plots represent the data before and after applying SVM classification to the respective prints and reprints. Similarly, Figs 8.59 (a) and 8.59 (b) display scatter plots of eccentricity versus dot area for the same printers and reprints, but with a 20% magenta concentration. These plots illustrate the data before and after classification of the prints and reprints. Likewise, Figs 8.60 (a) and 8.60 (b) exhibit the original and predicted scatter plots of eccentricity and dot area for 20% yellow prints and reprints, based on the model. Furthermore, Figs 8.61 (a) and (b) present scatter plots of eccentricity versus dot area for the printers and reprints using a 20% black concentration, showing the data before and after prediction.

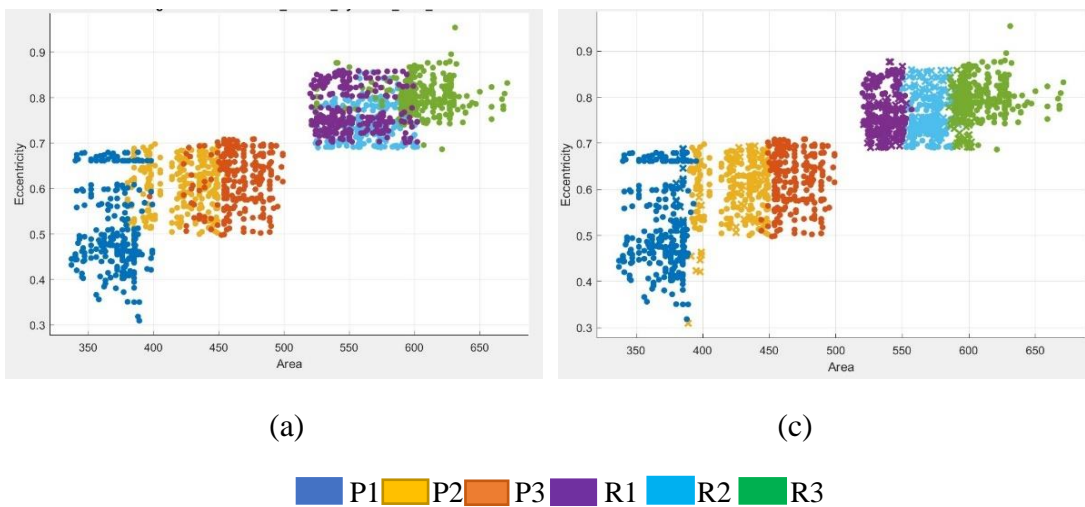


Fig 8.58: Scatter plots for 20% of Cyan for Print sample (P1, P2, P3) and Reprint sample (R1, R2, R3) (a) Original data Eccentricity vs. Area before, (b) Predicted data Eccentricity vs. Area after classification.

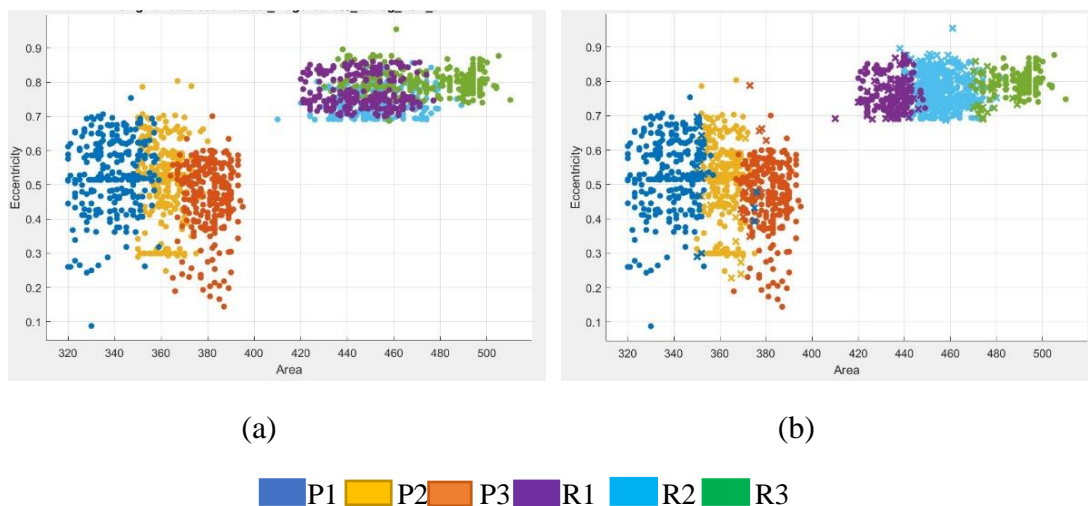


Fig 8.59: Scatter plots for 20% of Magenta for Print sample (P1, P2, P3) and Reprint sample (R1, R2, R3) (a) Original data Eccentricity vs. Area before, (b) Predicted data Eccentricity vs. Area after classification.



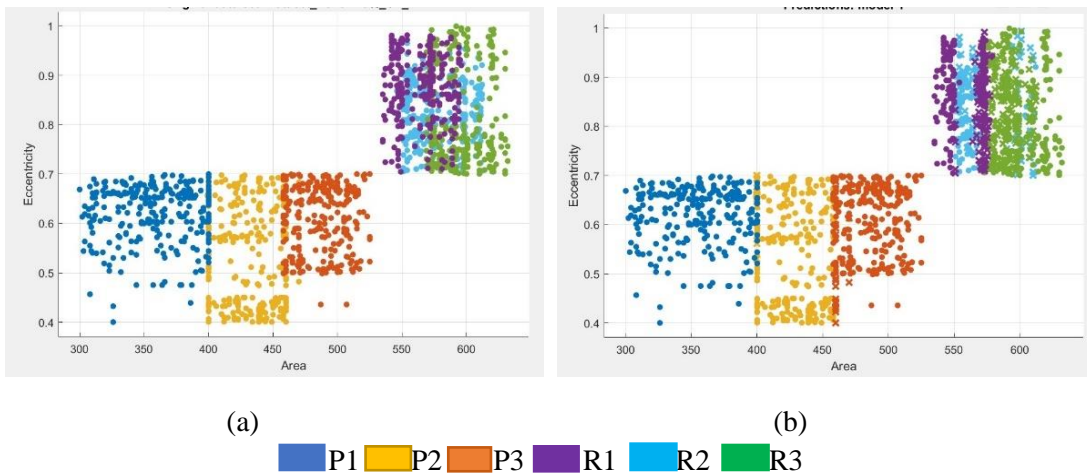


Fig 8.60: Scatter plots for 20% of Yellow for Print sample (P1, P2, P3) and Reprint sample (R1, R2, R3) (a) Original data Eccentricity vs. Area before, (b) Predicted data Eccentricity vs. Area after classification.

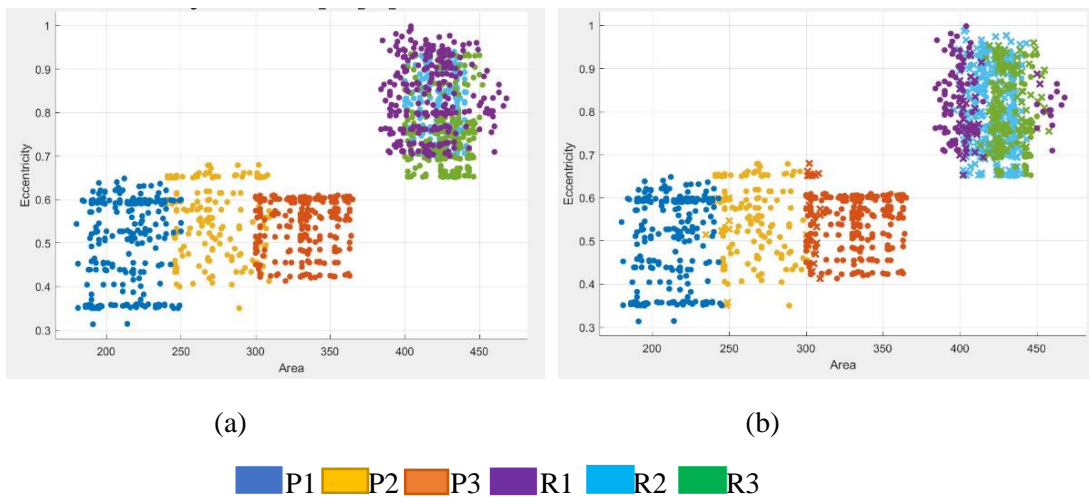
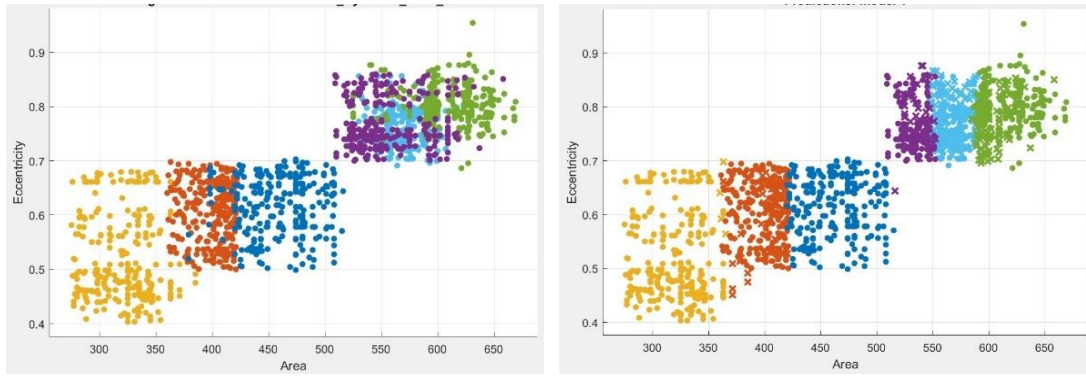


Fig 8.61: Scatter plots for 20% of Black for Print sample (P1, P2, P3) and Reprint sample (R1, R2, R3) (a) Original data Eccentricity vs. Area before classification (b) Predicted data Eccentricity vs. Area after classification.

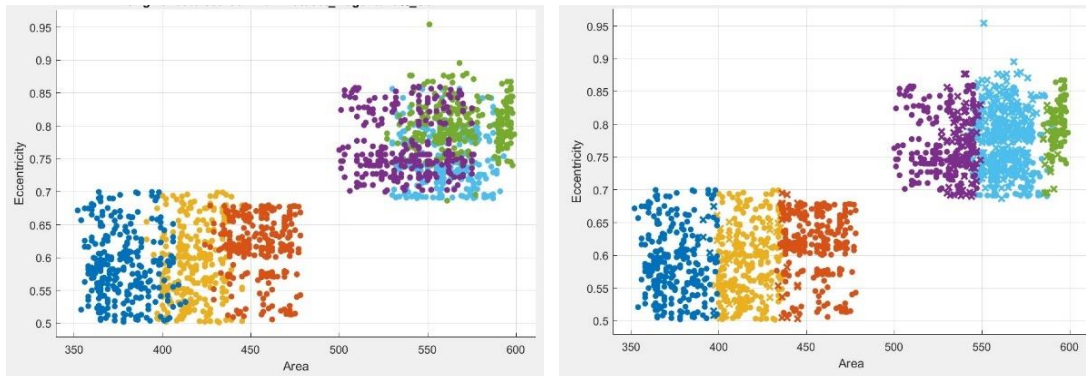
The dot features of prints and reprints were analysed before and after classification, and similar scatter plots were observed for various dot percentages. Figs 8.62 (a) and 8.62 (b) present the scatter plots depicting the relationship between eccentricity and dot area for printers P1, P2, and P3, as well as reprints R1, R2, and R3, using a 40% cyan dot concentration. Similarly, Figs 8.63 (a) and 8.63 (b) show scatter plots for the original and predicted dot features of 40% magenta prints and reprints, respectively. Likewise, Figs 8.64 (a) and 8.64 (b) display scatter plots comparing the original and model-predicted eccentricity versus dot area for 40% yellow dots. Finally, Figs 8.65 (a) and 8.65 (b) illustrate scatter plots of eccentricity versus dot area for gravure printers P1, P2, P3, and reprints R1, R2, R3, considering a 40% black concentration, both before and after SVM classification was applied to the prints and reprints.



(a) (b)

■ P1 ■ P2 ■ P3 ■ R1 ■ R2 ■ R3

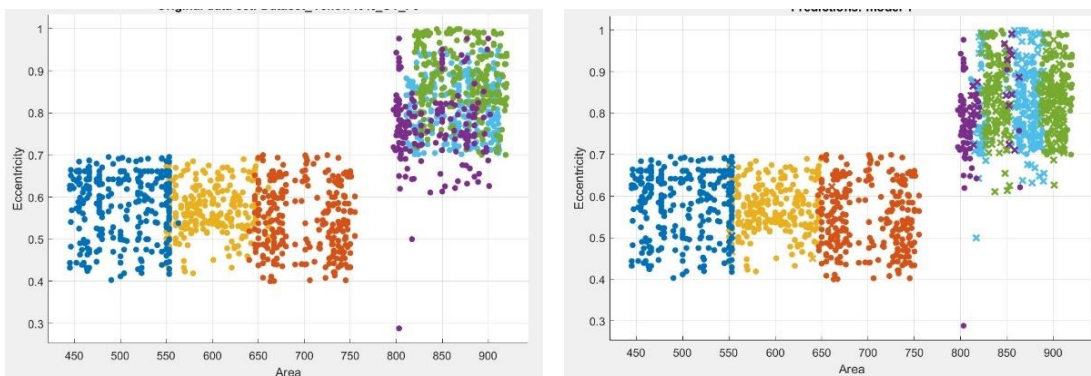
Fig 8.62: Scatter plots for 40% of Cyan for Print sample (P1, P2, P3) and Reprint sample (R1, R2, R3) (a) Original data Eccentricity vs. Area before classification (b) Predicted data Eccentricity vs. Area after classification.



(a) (b)

■ P1 ■ P2 ■ P3 ■ R1 ■ R2 ■ R3

Fig 8.63: Scatter plots for 40% of Magenta for Print sample (P1, P2, P3) and Reprint sample (R1, R2, R3)(a) Original data Eccentricity vs. Area before classification (b) Predicted data Eccentricity vs. Area after classification.



(a) (b)

■ P1 ■ P2 ■ P3 ■ R1 ■ R2 ■ R3

Fig 8.64: Scatter plots for 40% of Yellow for Print sample (P1, P2, P3) and Reprint sample (R1, R2, R3) (a) Original data Eccentricity vs. Area before classification (b) Predicted data Eccentricity vs. Area after classification.

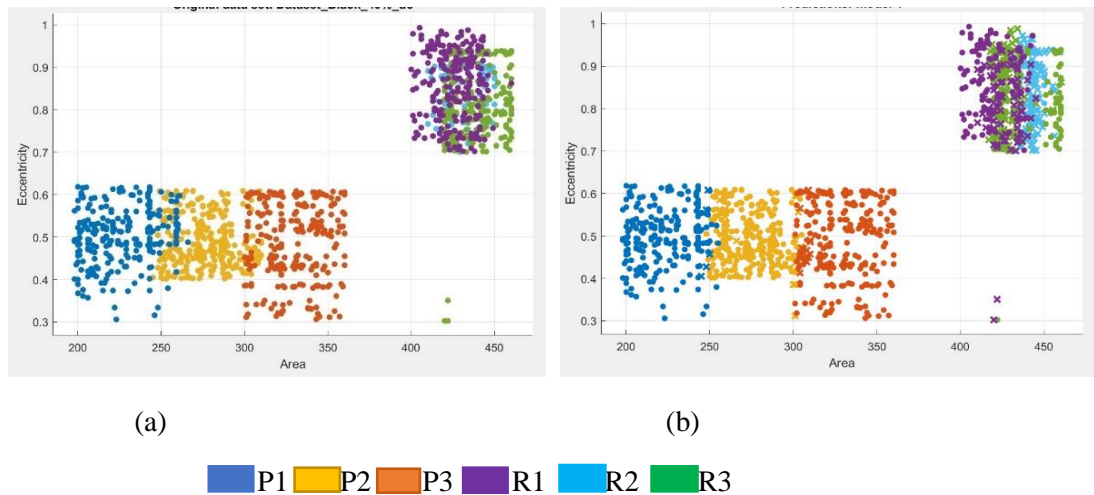
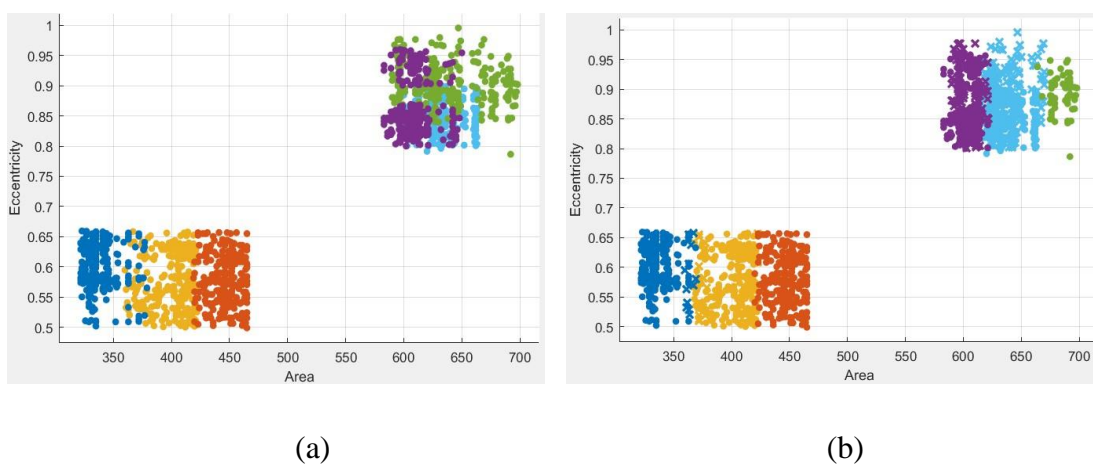


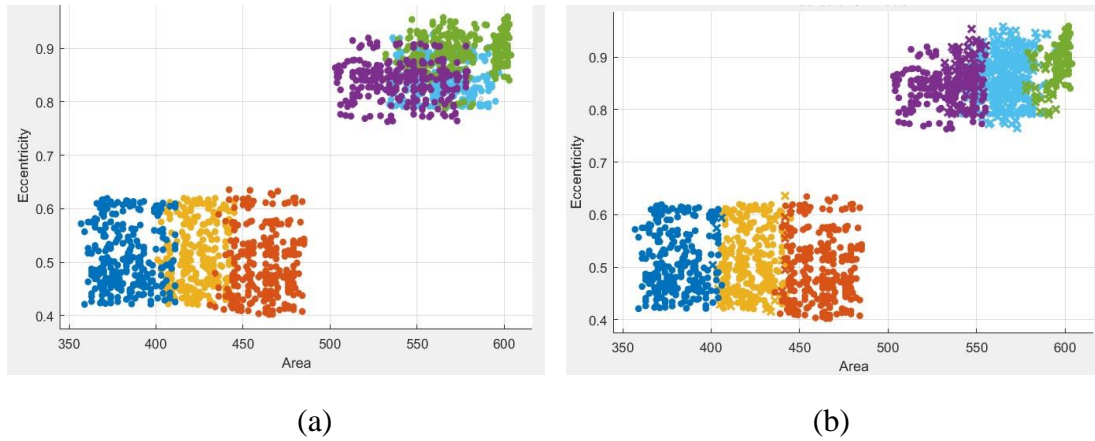
Fig 8.65: Scatter plots for 40% of Black for Print sample (P1, P2, P3) and Reprint sample (R1, R2, R3) (a) Original data Eccentricity vs. Area before classification (b) Predicted data Eccentricity vs. Area after classification.

In a similar vein, Fig 8.66 (a) and (b) display both the original and predicted scatter plots of the eccentricity vs area of the printers P1, P2, and P3 and for reprints R1, R2, and R3 for 50% cyan for before and after SVM classification respectively for the corresponding prints and reprints. These plots represent the data before and after applying SVM classification to the respective prints and reprints. Furthermore, Fig 8.67 (a) and (b) depict scatter plots showcasing the eccentricity versus area of the original and projected dot features for 50% magenta prints and reprints. Correspondingly, Figs. 8.68 (a) and (b) show the scatter plot representing the original and model-predicted relationship between eccentricity and dot area for printers P1, P2, and P3, as well as reprints R1, R2, and R3, using 50% yellow ink. Finally, Figs. 8.69 (a) and 8.69 (b) illustrate scatter plot of eccentricity vs dot area of the dots for 50% black dots, both before and after classification, for the corresponding prints and reprints.



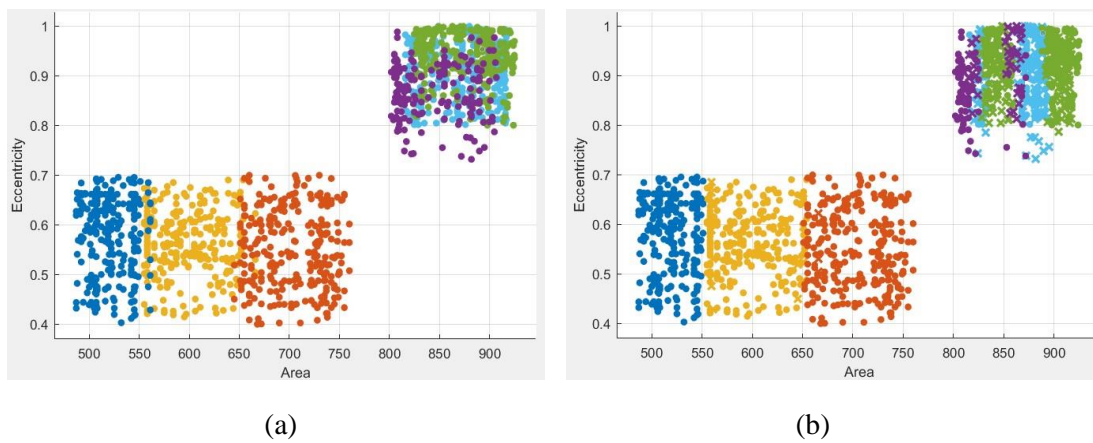
■ P1 ■ P2 ■ P3 ■ R1 ■ R2 ■ R3

Fig 8.66: Scatter plots for 50% of Cyan for Print sample (P1, P2, P3) and Reprint sample (R1, R2, R3) (a) Original data Eccentricity vs. Area before classification (b) Predicted data Eccentricity vs. Area after classification.



■ P1 ■ P2 ■ P3 ■ R1 ■ R2 ■ R3

Fig 8.67: Scatter plots for 50% of Magenta for Print sample (P1, P2, P3) and Reprint sample (R1, R2, R3) (a) Original data Eccentricity vs. Area before classification (b) Predicted data Eccentricity vs. Area after classification.



■ P1 ■ P2 ■ P3 ■ R1 ■ R2 ■ R3

Fig 8.68: Scatter plots for 50% of Yellow for Print sample (P1, P2, P3) and Reprint sample (R1, R2, R3) (a) Original data Eccentricity vs. Area before classification (b) Predicted data Eccentricity vs. Area after classification.



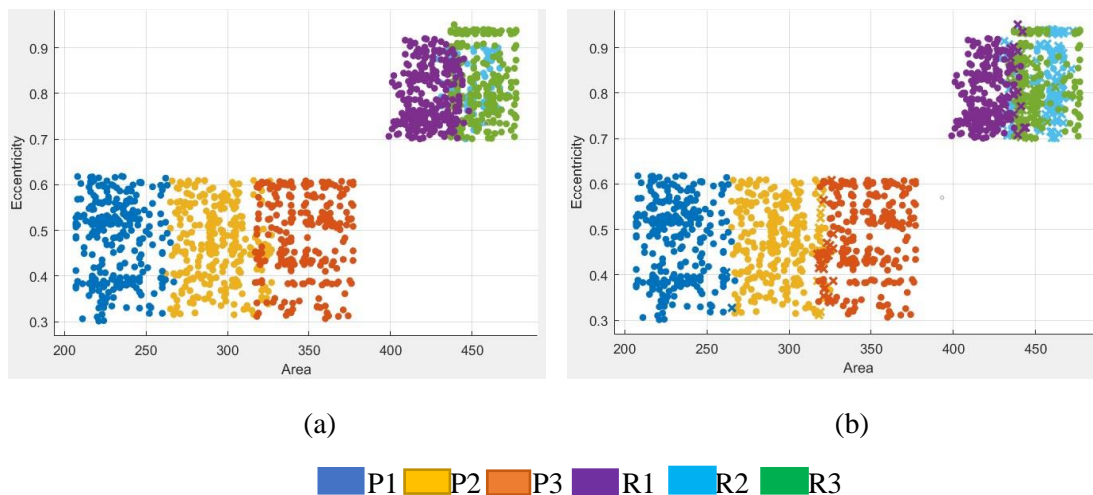


Fig 8.69: Scatter plots for 50% of Black for Print sample (P1, P2, P3) and Reprint sample (R1, R2, R3) (a) Original data Eccentricity vs. Area before classification (b) Predicted data Eccentricity vs. Area after classification.

In this research, we have undertaken a study to compare the dot shape index parameter, focusing on eccentricity versus area of dots as the input feature in the classification model, for print samples and reprint samples at different dot percentages. The main objective was to differentiate between these two sample categories. The results of the scatter plots demonstrated that irrespective of the color and dot percentage, the dot shape index parameter was successful in discerning between the printed and reprinted samples.

The confusion matrices have been created corresponding to the classification performance of dot patterns in print and reprint samples using SVM. Tables 8.11, 8.12, and 8.13 show the confusion matrix of 20% ,40% and 50% dots of cyan, magenta, yellow, and black tints for print and reprint samples. In this table, "O" denotes the predicted output for print and reprint samples, and "A" represents the actual input samples for print and reprint samples. Table 8.11(a) shows the confusion matrix for 20% of cyan, where the precision value is 98% and recall is 90%, which means that the print sample (from the P3 printer) has been classified for 20% cyan dots from the rest of the print and reprint samples. Likewise, Table 8.11(b) depict the confusion matrix for 20% magenta color. In the Table 8.11(c) represent present the confusion matrix for 20% yellow and Tables 8.11(d) represent the confusion matrix for 20% black, respectively, for all print and reprint samples.

In this same way, the confusion matrix for 40% cyan is displayed in Table 8.12(a), while Tables 8.12(b) depict the confusion matrix for 40% magenta, respectively. Furthermore, Tables 8.12(c) present the confusion matrix for 40% yellow, and Tables 8.12(d) represent the confusion matrix for 40% black, respectively, for all print and reprint samples.

Similarly, Table 8.13(a) displayed the confusion matrix for 50% cyan, and Tables 8.13(b) shows the confusion matrix for 50% magenta, respectively. Furthermore, Tables 8.13(c) present the confusion matrix for 50% yellow, and Tables 8.13(d) represent the confusion matrix for 50% black, respectively, for all print and reprint samples.

From the confusion matrix for cyan (20%, 40% and 50%), it is observed that Type 1 and Type 2 errors do not occur in the classification between original print samples (P3, P2, P1), whereas both Type 1 and Type 2 errors occur in the classification between reprint samples (R1, R2, R3). So, these results indicate that the classification model classified the print samples with higher precision and recall percentages compared to reprint samples. Similar results were observed for the 20%, 40%, and 50% magenta, yellow, and black print and reprint samples.

**Table 8.11- (a) Confusion Matrix of SVM Classification results for 20% cyan print and reprint**

O /A	P3C20	P2C20	P1C20	R1C20	R2C20	R3C20	Precision
P3C20	<b>244</b>	9	17				<b>0.98</b>
P2C20	6	<b>261</b>	3				0.94
P1C20		9	<b>261</b>				0.93
R1C20				<b>162</b>	66	42	0.63
R2C20				49	<b>171</b>	50	0.58
R3C20				46	60	<b>164</b>	0.64
Recall	0.90	<b>0.97</b>	<b>0.97</b>	0.60	0.63	0.61	

**Table 8.11- (b) Confusion Matrix of SVM Classification results for 20% magenta print and reprint**

O /A	P3M20	P2M20	P1M20	R1M20	R2M20	R3M20	Precision
P3M20	<b>259</b>	5	6				0.94
P2M20	3	<b>258</b>	9				<b>0.97</b>
P1M20	15	2	<b>253</b>				0.94
R1M20				<b>220</b>	24	26	0.41
R2M20				17	<b>224</b>	29	0.45
R3M20				16	24	<b>230</b>	0.43
Recall	<b>0.96</b>	<b>0.96</b>	0.94	0.40	0.53	0.40	

**Table 8.11- (c) Confusion Matrix of SVM Classification results for 20% yellow print and reprint**

O /A	P3Y20	P2Y20	P1Y20	R1Y20	R2Y20	R3Y20	Precision
P3Y20	<b>268</b>	2					<b>0.98</b>
P2Y20	23	<b>247</b>					0.93
P1Y20		16	<b>254</b>				<b>0.98</b>
R1Y20				<b>164</b>	69	37	0.65
R2Y20				50	<b>120</b>	100	0.54
R3Y20				37	33	<b>200</b>	0.59
Recall	0.90	<b>0.91</b>	<b>0.94</b>	0.61	0.44	0.74	

**Table 8.11- (d) Confusion Matrix of SVM Classification results for 20% black print and reprint**

O /A	P3K20	P2K20	P1K20	R1K20	R2K20	R3K20	Precision
P3K20	<b>260</b>	2	8				0.90
P2K20	30	<b>240</b>					0.95
P1K20		11	<b>259</b>				<b>0.99</b>
R1K20				<b>95</b>	121	54	0.63
R2K20				35	<b>172</b>	63	0.38
R3K20				20	157	<b>93</b>	0.44
Recall	<b>0.96</b>	0.89	<b>0.96</b>	0.35	0.64	0.34	



**Table 8.12- (a) Confusion Matrix of SVM Classification results for 40% cyan print and reprint**

O /A	P3C40	P2C40	P1C40	R1C40	R2C40	R3C40	Precision
P3C40	<b>254</b>	13	3				<b>0.97</b>
P2C40	4	<b>259</b>	7				0.92
P1C40	4	9	<b>257</b>				0.96
R1C40				<b>163</b>	55	52	0.63
R2C40				36	<b>170</b>	64	0.63
R3C40				59	44	<b>167</b>	<i>0.60</i>
Recall	0.94	<b>0.96</b>	0.95	<i>0.60</i>	0.63	0.62	

**Table 8.12- (b) Confusion Matrix of SVM Classification results for 40% magenta print and reprint**

O/A	P3M40	P2M40	P1M40	R1M40	R2M40	R3M40	Precision
P3M40	<b>262</b>	3	5				<b>0.96</b>
P2M40	3	<b>264</b>	3				0.95
P1M40	15	2	<b>253</b>				<b>0.96</b>
R1M40				<b>168</b>	27	75	0.58
R2M40				39	<b>140</b>	91	0.69
R3M40				84	36	<b>150</b>	<i>0.47</i>
Recall	0.97	<b>0.98</b>	0.94	0.62	<b>0.52</b>	0.56	

**Table 8.12- (c) Confusion Matrix of SVM Classification results for 40% yellow print and reprint**

O /A	P3Y40	P2Y40	P1Y40	R1Y40	R2Y40	R3Y40	Precision
P3Y40	<b>264</b>	6					<b>0.98</b>
P2Y40	6	<b>264</b>	3				0.97
P1Y40	3	6	<b>261</b>				<b>0.98</b>
R1Y40				<b>107</b>	72	91	0.64
R2Y40				19	<b>124</b>	127	0.44
R3Y40				5	83	<b>182</b>	<i>0.45</i>
Recall	<b>0.98</b>	<b>0.97</b>	<b>0.98</b>	<i>0.40</i>	0.46	0.60	

**Table 8.12 (d) Confusion Matrix of SVM Classification results for 40% black print and reprint**

O /A	P3K40	P2K40	P1K40	R1K40	R2K40	R3K40	Precision
P3K40	<b>258</b>	12					0.93
P2K40	19	<b>246</b>	5				0.86
P1K40		29	<b>241</b>				<b>0.98</b>
R1K40				<b>128</b>	50	92	<i>0.47</i>
R2K40				90	<b>104</b>	74	0.48
R3K40				52	64	<b>154</b>	0.48
Recall	<b>0.96</b>	0.91	0.89	0.47	<i>0.39</i>	0.57	

**Table 8.13- (a) Confusion Matrix of SVM Classification results for 50% Cyan print and reprint**

O /A	P3C50	P2C50	P1C50	R1C50	R2C50	R3C50	Precision
P3C50	<b>253</b>	16	1				<b>0.99</b>
P2C50	1	<b>263</b>	6				0.90
P1C50		13	<b>257</b>				0.97
R1C50				<b>154</b>	43	73	0.64
R2C50				59	<b>147</b>	64	0.67
R3C50				28	31	<b>211</b>	0.61
Recall	0.94	<b>0.97</b>	0.95	0.57	0.54	0.78	

**Table 8.13 (b) Confusion Matrix of SVM Classification results for 50% Magenta print and reprint**

O /A	P3M50	P2M50	P1M50	R1M50	R2M50	R3M50	Precision
P3M50	<b>261</b>	2	7				<b>0.97</b>
P2M50	5	<b>259</b>	6				0.96
P1M50	4	9	<b>257</b>				0.95
R1M50				<b>161</b>	41	68	0.63
R2M50				58	<b>191</b>	21	0.61
R3M50				36	79	<b>155</b>	0.64
Recall	<b>0.96</b>	<b>0.96</b>	0.95	0.60	0.71	0.57	

**Table 8.13- (c) Confusion Matrix of SVM Classification results for 50% Yellow print and reprint**

O /A	P3Y50	P2Y50	P1Y50	R1Y50	R2Y50	R3Y50	Precision
P3Y50	<b>263</b>	2	5				<b>0.98</b>
P2Y50	3	<b>260</b>	7				0.98
P1Y50	1	2	<b>267</b>				0.97
R1Y50				<b>137</b>	69	64	0.58
R2Y50				49	<b>139</b>	82	0.50
R3Y50				51	71	<b>148</b>	0.50
Recall	0.97	0.96	<b>0.98</b>	0.51	0.52	0.55	

**Table 8.13- (d) Confusion Matrix of SVM Classification results for 50% Black print and reprint**

O /A	P3K50	P2K50	P1K50	R1K50	R2K50	R3K50	Precision
P3K50	<b>259</b>	4	7				0.96
P2K50	7	<b>262</b>	1				0.96
P1K50	3	6	<b>261</b>				<b>0.97</b>
R1K50				<b>134</b>	71	65	0.49
R2K50				72	<b>136</b>	62	0.51
R3K50				68	59	<b>143</b>	0.53
Recall	0.96	<b>0.97</b>	<b>0.97</b>	0.51	0.50	0.53	

The classifier's accuracy  $A_{cc}$  and the harmonic mean  $F_h$  have been shown in Table 8.14(a, b, c, d) for 20% for cyan, magenta, yellow and black. Similarly in Table 8.15(a, b, c, d) for 40% and Table 8.16(a, b, c, d) for 50%. The results indicate that the classification performs well, with good accuracy and F1-scores for print samples P1, P2, and P3, using the SVM model. The print samples provide a very good classification for 20% 40% and 50% dots of cyan, magenta, yellow, and black. It has also been observed in Table 8.14, 8.15 and 8.16 for all the tints that the classifier's accuracy  $A_{cc}$  and the harmonic mean  $F_h$  are relatively lower for R1, R2, and R3 reprint samples.

**Table 8.14(a) – the overall accuracy  $A_{cc}$  and harmonic mean  $F_h$  for each print and reprint using SVM for classification for 20% of Cyan.**

SVM		
Samples	$A_{cc}$	$F_h$
P3	<b>0.98</b>	0.94
P2	<b>0.98</b>	<b>0.95</b>
P1	<b>0.98</b>	<b>0.95</b>
R1	0.87	0.61
R2	0.86	0.60
R3	0.88	0.62

**Table 8.14(b) – the overall accuracy  $A_{cc}$  and harmonic mean  $F_h$  for each print and reprint using SVM for classification for 20% of Magenta.**

SVM		
Samples	$A_{cc}$	$F_h$
P3	0.98	0.95
P2	<b>0.99</b>	<b>0.96</b>
P1	0.98	0.94
R1	0.80	0.39
R2	0.80	0.48
R3	0.81	0.42

**Table 8.14(c) – the overall accuracy  $A_{cc}$  and harmonic mean  $F_h$  for each print and reprint using SVM for classification for 20% of Yellow.**

SVM		
Samples	$A_{cc}$	$F_h$
P3	<b>0.98</b>	<b>0.96</b>
P2	<b>0.97</b>	0.92
P1	<b>0.98</b>	<b>0.95</b>
R1	0.88	0.63
R2	0.84	0.49
R3	0.87	0.66

**Table 8.14(d) – the overall accuracy  $A_{cc}$  and harmonic mean  $F_h$  for each print and reprint using SVM for classification for 20% of Black.**

SVM		
Samples	$A_{cc}$	$F_h$
P3	<b>0.98</b>	0.94
P2	<b>0.97</b>	0.92
P1	<b>0.99</b>	<b>0.97</b>
R1	0.86	0.45
R2	0.77	0.48
R3	0.82	0.39

**Table 8.15(a) – the overall accuracy  $A_{cc}$  and harmonic mean  $F_h$  of each print and reprint using SVM for classification for 40% of Cyan.**

SVM		
Samples	$A_{cc}$	$F_h$
P3	<b>0.99</b>	0.95
P2	0.98	0.94
P1	0.98	<b>0.96</b>
R1	0.88	0.62
R2	0.87	0.63
R3	0.86	0.60

**Table 8.15(b) – the overall accuracy  $A_{cc}$  and harmonic mean  $F_h$  of each print and reprint using SVM for classification for 40% of Magenta.**

SVM		
Samples	$A_{cc}$	$F_h$
P3	0.98	0.95
P2	<b>0.99</b>	<b>0.98</b>
P1	0.98	0.95
R1	0.86	0.60
R2	0.88	0.59
R3	0.82	0.51

**Table 8.15(c) – the overall accuracy  $A_{cc}$  and harmonic mean  $F_h$  for each print and reprint using SVM for classification for 40% of Yellow.**

	SVM	
Samples	$A_{cc}$	$F_h$
P3	<b>0.99</b>	0.98
P2	<b>0.98</b>	<b>0.97</b>
P1	<b>0.99</b>	<b>0.98</b>
R1	0.86	0.49
R2	0.81	0.45
R3	0.81	0.51

**Table 8.15(d) – the overall accuracy  $A_{cc}$  and harmonic mean  $F_h$  for each print and reprint using SVM for classification for 40% of Black.**

	SVM	
Samples	$A_{cc}$	$F_h$
P3	<b>0.98</b>	<b>0.94</b>
P2	<b>0.96</b>	0.91
P1	<b>0.98</b>	<b>0.93</b>
R1	0.82	0.47
R2	0.83	0.43
R3	0.83	0.52

**Table 8.16(a) – the overall accuracy  $A_{cc}$  and harmonic mean  $F_h$  for each print and reprint using SVM for classification for 50% of Cyan.**

	SVM	
Samples	$A_{cc}$	$F_h$
P3	<b>0.98</b>	<b>0.97</b>
P2	0.97	0.94
P1	<b>0.98</b>	0.96
R1	0.87	0.60
R2	0.88	0.59
R3	0.88	0.68

**Table 8.16(b) – the overall accuracy  $A_{cc}$  and harmonic mean  $F_h$  for each print and reprint using SVM for classification for 50% of Magenta.**

	SVM	
Samples	$A_{cc}$	$F_h$
P3	<b>0.98</b>	<b>0.97</b>
P2	<b>0.98</b>	0.96
P1	<b>0.98</b>	0.95
R1	0.87	0.61
R2	0.88	0.66
R3	0.87	0.60



**Table 8.16(c) – the overall accuracy  $A_{cc}$  and harmonic mean  $F_h$  for each print and reprint using SVM for classification for 50% of Yellow.**

Samples	SVM	
	$A_{cc}$	$F_h$
P3	<b>0.99</b>	<b>0.97</b>
P2	<b>0.99</b>	<b>0.97</b>
P1	<b>0.99</b>	<b>0.97</b>
R1	0.85	0.54
R2	0.83	0.51
R3	0.83	0.52

**Table 8.16(d) – the overall accuracy  $A_{cc}$  and harmonic mean  $F_h$  for each print and reprint using SVM for classification for 50% of Black.**

Samples	SVM	
	$A_{cc}$	$F_h$
P3	<b>0.98</b>	<b>0.96</b>
P2	<b>0.98</b>	<b>0.97</b>
P1	<b>0.98</b>	<b>0.97</b>
R1	0.83	0.49
R2	0.84	0.51
R3	0.84	0.53

### 8.4.2 Discussion

In this experimental study, "print" samples (P1, P2, P3) and "reprint" samples (R1, R2, R3) have been categorized based on their dot feature parameters.

Figs. 8.46, 8.47, 8.48, 8.49, 8.50, 8.51, 8.52, 8.53, 8.54, 8.55, 8.56 and 8.57 illustrate that the dot perimeters and areas for cyan, magenta, yellow and black colors in both prints and reprints. These figures demonstrated that, regardless of dot percentage and its color the perimeter and area are larger for reprints compared to prints. Figs. 8.58 to 8.69 exhibit comparable findings regarding the relationship between eccentricity and area for printed and reprinted tints. The eccentricity feature is also greater for reprints. It is possible that this is due to the additional dot gain while copying the print. Specifically, dot gain increases when a scanner or camera captures the original print image. In, Table 8.11-8.13 the confusion matrix evaluating the performance of classification model, classification accuracy of printed dot parameters also indicates that the dot sizes and shapes for reprints have grown irregularly after imaging (simulated counterfeit). The high precision and recall values for classification of P1, P2, and P3 show that the SVM model is quite effective for dot feature classification of prints. Relatively lower accuracy has been obtained with reprints. Tables 8.14, 8.15 and 8.16 demonstrates the accuracy of prints and reprints using SVM classification of printing dot patterns with 20% ,40% and 50% of cyan, magenta, yellow, and black color, respectively. The table indicates that there is a minimal degree of variation in both accuracy and harmonic mean when comparing different original prints across various dot areas. However, for the reprints, the variations in accuracy and harmonic means for different dot areas are wide apart and inevitable. Hence, SVM classification and its associated parameters may be effectively used for identifying counterfeited samples. Thus, printing sources may be established for authentication applications using this model, particularly for forgery detection of printed documents or medicine packages.

This classification model worked well with the dataset of color print and reprint samples

using dot descriptor index parameters as features in the input dataset. The classification model is simple to implement for commercial production due to the simplicity and efficacy of Support Vector Machine. It is possible to identify the original print for authentication, and thus the original prints may be easily differentiated from the counterfeited ones in different packaging applications.

In the next Chapter 9 the conclusion this experimental study to identify the print sample and reprint sample has detailed.

# Chapter 9

## CONCLUSIONS

### 9. Conclusions

In this study, the first method of variable image watermarking can be effectively used for identification of counterfeited printed batch number and expiry dates. The experiments are carried out for inkjet printers on paper and gravure printing on blister foils. However, it can be extended to any printing process with any substrates as it works well with paper and foil.

In the second method, a promising solution based on a pattern recognition process has been proposed to identify a print document (original) from a reprint document (copy or fake). The geometric shape of printed dots can be analyzed at microscopic scale to differentiate an authentic print from its scanned reprint. Six types of dot patterns, including four types of doughnut patterns, have been chosen for the work. A new characterization method which combines several dot pattern features has been suggested. The results demonstrate the relevance of the criteria proposed on the basis of the statistical analysis method.

In the third analysis, it has been observed that dot area as well as the major axis, minor axis and eccentricity for the reprint sample have been increased in comparison to the print samples. The possible reason may be associated dot gain that is unavoidable and irreversible. It may be possible to identify whether a medicine package is printed by the original manufacturer or their authorized printer, or the package is printed by the counterfeiters by this method. As soon as the prints will be copied and reprinted, dot gain will be included in the reprints which are irregular and cannot be manipulated. The increased standard deviation values of dot areas, major or minor axis and eccentricity shows that the homogeneity of the dots produced by original artwork will not be maintained after copying. As soon as the copying is done by any camera or mobile, optical dot gain will be incorporated which increases heterogeneity of the copied reprint samples.

In the fourth analysis of this study a multiclass classification for SVM model has been used to classify the print and reprint samples on the basis of dot structure shape descriptor indexes on blister foil medium, using different color inks and three different gravure machines. The original prints and the reprints sample dot structure, have been statistically analyzed, showing a significant change on dot structure shape descriptor indexes between the prints and the reprints. In the confusion matrix, it has been clearly observed that print samples are classified very well using a SVM multi-class classification model. Relatively lower accuracy is obtained for reprints. It is caused by an optical dot gain linked to the image acquisition of the original print. Since, the counterfeiting of a printed package with color images must involve a stage of imaging through camera or scanner, the associated optical dot gains are unavoidable whatever the quality of the image capture device used.

The analysis of printed dot structure and of reprinted dot structure showed the ability to well perform authentication using microscopic printing. SVM is used to classify the seven-shape descriptor index of the micro-printing dot structure patterns into multiple classes. The accuracy and F1-scores of the experimental results of multi-class classification using SVM shows that the classification is better in all cases of print sample. We have seen that F1- scores for print samples can reach significant as 98%. However, the scores for reprint samples are relatively less as 63%

in this study. Accuracy can reach large as 99% for print samples and can reach large as 88% for reprint samples.

Hence, SVM classification can be effectively utilized to differentiate between an authentic color image print sample from its counterfeited one as imaging is a necessary and unavoidable step for counterfeiters which cannot avoid inherent dot gain. The studied data may be used to identify counterfeit packaging items. According to the manufacturer, this study is useful for determining the authenticity of items that are on the market and is cost-effective.

**Future work:**

In future, there is potential for conducting similar studies using paper laminations or other commonly used polymeric materials for food or cosmetic packaging. Additional experiments could explore other printing processes such as flexography or offset printing, and the process may be extended to include more image capture devices. The focus of the extended process would be to examine the impact of various printing parameters on the authentication of prints produced using different printers and substrates. The efficacy of the methods would be evaluated against counterfeit packaging to ensure secure products for society.

Future research could investigate and explore special dot designs. In addition to analysing dot parameters, dot angles could also be studied to increase the authenticity of prints. Future work could also involve the development of an application that integrates with devices like smartphones or gadgets for the authentication of printed documents or pharmaceutical packages.

# REFERENCE:

1. Q. Su and B. Chen, "Robust color image watermarking technique in the spatial domain" *Soft Comput.*, vol. 22, pp. 91-106, 2018.
2. K.Thongkor and T.Amomraksa, "Improved Watermark Extraction for Printed and Scanned Watermarked Document", *International Symposium on Intelligent Signal Processing and Communication Systems (ISPACS)*,pp.7-9, 2011.
3. TeddyMantoro, M. ImanWahyudi, M. A. Ayu and WendiUsino, "Real-Time Printed Document Authentication Using Watermarked QR Code",*Fourth International Conference on Cyber Security, Cyber Warfare, and Digital Forensic (CyberSec)*, Jakarta, Indonesia, pp. 68-72, 2015.
4. S. Ibrahim, M.Afrakhteh and M. Salleh, "Adaptive watermarking for printed document authentication", *5th International Conference on Computer Sciences and Convergence Information Technology*, Seoul, Korea (South), IEEE, pp. 611-614, 2010.
5. M.Afrakhteh, S. Ibrahim, M. Salleh, "Printed Document Authentication Using Watermarking Technique," *2010 Second International Conference on Computational Intelligence, Modelling and Simulation*, Bali, Indonesia, IEEE, pp. 367-370, 2010.
6. A. Pramila, A.Keskinarkaus, T. Seppänen, "Toward an interactive poster using digital watermarking and a mobile phone camera", *Springer, SIViP 6*, pp. 211–222, 2012.
7. A. Pramila, A.Keskinarkaus, V. Takala and T. Seppänen, "Extracting watermarks from printouts captured with wide angles using computational photography", *Multimedia Tools and Applications*vol. 76, pp.16063–16084, 2017.
8. D. Klein and J. Kruse, "A Comparative Study on Image Hashing for Document Authentication", *2015 International Conference of the Biometrics Special Interest Group (BIOSIG)*, Darmstadt, Germany, pp. 1-5, 2015.
9. K.Gourrame, H.Douzi, R. Harba,R. Riad,F. Ros, M. Amar, M.Elhajji, "A zero-bit Fourier image watermarking for print-cam process", *Multimedia Tools Application*, Springer,vol. 78, pp.2621–2638,2019.
10. S. Hamid Amiri and M.Jamzad, "An Algorithm for Modeling Print and Scan Operations Used for Watermarking", In: Kim, HJ., Katzenbeisser, S., Ho, A.T.S. (eds) *Digital Watermarking, IWDW 2008. Lecture Notes in Computer Science*, Springer, Berlin, Heidelberg, vol. 5450,pp. 254–265, 2009.
11. D.Coltuc, P. Bolon, J. M.Chassery, "Fragile and robust watermarking by histogram specification", *Proc. SPIE, Security and Watermarking of Multimedia Contents IV*,vol. 4675, pp. 701–710, 29 April 2002.
12. D.Coltuc and P. Bolon, "Robust watermarking by histogram specification", *Proceedings 1999 International Conference on Image Processing (Cat. 99CH36348)*, Kobe, Japan, vol.2, pp. 236-239, doi: 10.1109/ICIP.1999.822891, 1999.
13. S. H. Amiri, M.Jamzad, "Robust watermarking against print and scan attack through efficient modeling algorithm", *Signal Processing: Image Communication*,ISSN 0923-5965, vol.29, Issue 10, pp. 1181-1196,2014.

14. P. P. Athichitsakul and S. Phimoltares, A. Mahaweerawat, "Printout verification using a new image hash algorithm based on Radon, Wavelet, and Fast Fourier transforms", 2015 IEEE International Conference on Control System, Computing and Engineering (ICCSCE), Penang, Malaysia, pp. 395-400, 2015.
15. D. Wu, X. Zhou, X. Niu, "A novel image hash algorithm resistant to print-scan", Signal Processing, ScienceDirect, Elsevier, ISSN 0165-1684, Issue 12, vol. 89, pp. 2415-2424, 2009.
16. Y. Zhang, X. Kang, and P. Zhang, "A Practical Print-and-Scan Resilient Watermarking for High Resolution Images", In: Kim, H.J., Katzenbeisser, S., Ho, A.T.S. (eds) Digital Watermarking. IWDW 2008. Lecture Notes in Computer Science, Researchgate, Conference Paper, Springer, Berlin, Heidelberg, vol. 5450, 2009.
17. Y.J. Song, R.Z. Liu, T.N. Tan, "Digital Watermarking for Forgery Detection in Printed Materials", In: Shum, H.Y., Liao, M., Chang, S.F. (eds) Advances in Multimedia Information Processing, Lecture Notes in Computer Science, Springer, Berlin, Heidelberg, vol. 2195, pp. 403-410, 2001.
18. A. Pramila, "Reading watermarks with a camera phone from printed images", 2018.
19. W. L. Linn and W. H. Tsai, "Data Hiding in Image Mosaics by Visible Boundary Regions and Its Copyright Protection Application against Print-And-Scan Attacks", Int. Computer Symposium, Taipei, Taiwan, pp. 15-17, 2004.
20. K. Solanki, U. Madhow, B. S. Manjunath, and S. Chandrasekaran, "Modeling the print-scan process for resilient data hiding", SPIE - The International Society for Optical Engineering, vol. 5681, pp. 418-429, 2005.
21. K. W. Mahmoud, J. M. Blackledge, S. Datta, and A. James, "Print protection using high-frequency fractal noise", Security, Steganography, and Watermarking of Multimedia Contents VI, edited by Edward J. Delp III, Ping W. Wong, Proc. of SPIE-IS&T Electronic Imaging, SPIE vol. 5306, pp. 446-454, 2004.
22. N. Mettripun, R. Lhawchaiyapark and T. Amornraksa, "Method of rearranging watermarked pixels for printed and scanned watermarked documents", 2010 10th International Symposium on Communications and Information Technologies, Tokyo, Japan, IEEE, pp. 492-497, 2010.
23. Q. Su, D. Liu, Z. Yua, G. Wang, X. Zhang, B. Chen, and T. Yao, "New Rapid and Robust Color Image Watermarking Technique in Spatial Domain", in IEEE Access, vol. 7, pp. 30398-30409, 2019.
24. W. Zhang, J. Meng and C. Ma, "Research progress of applying digital watermarking technology for printing", 2018 Chinese Control and Decision Conference (CCDC), Shenyang, China, IEEE, pp. 4479-4482, 2018.
25. Z. Xiao, Y. Zhang, C. Feng, Y. Li and R. Zhang, "A robust and encrypted digital image watermarking method against print-scan", 2015 Chinese Automation Congress (CAC), Wuhan, IEEE, pp. 696-700, 2015.
26. M. K. Kundu and A. Maiti, "An Inexpensive Digital Watermarking Scheme for Printed Document", 2006 IET International Conference on Visual Information Engineering, Bangalore, IEEE, pp. 378-383, 2006.

27. Z. Wang, A. C. Bovik, H. R. Sheikh and E. P. Simoncelli, "Image quality assessment: from error visibility to structural similarity", in *IEEE Transactions on Image Processing*, vol. 13, no. 4, pp. 600-612, 2004.
28. A. M. Bashir, T. E. Eltobely, M. M. Fahmy, M. E. S. Nasr, and M. H. A. El-Aziz. "Fidelity and Robust Digital Watermarking Adaptively Pixel based on Medial Pyramid of Embedding Error Gray Scale Images", *IJCSNS International Journal of Computer Science and Network Security*, vol.10 no.6, June 2010.
29. J. Picard, C. Vielhauer, and N. Thorwirth. "Towards fraud-proof id documents using multiple data hiding technologies and biometrics". *SPIE Proceedings– Electronic Imaging, Security and Watermarking of Multimedia Contents VI*, pages 123–234, 2004.
30. M. Nasedanian, "Characterization of Halftone Prints based on Microscale Image Analysis", (PhD dissertation, Linköping University Electronic Press), 2013.
31. Q. T. Nguyen, Y. Delignon, L. Chagas, and F. Septier, "Printer identification from micrometric scale printing". In *Proc. ICASSP*, pp. 6277–6280, 2014.
32. Q. T. Nguyen, Y. Delignon, L. Chagas, and F. Septier, "Printer technology authentication from micrometric scan of a single printed dot". In *IS&T/SPIE Electronic Imaging*, pp 1–7, 2014.
33. Q. T. Nguyen, Y. Delignon, L. Chagas, and F. Septier, A.T. Phan-Ho, "Probabilistic modelling of printed dots at the microscopic scale. *Signal Process*", *Image Commun*, vol.62, pp.129–138, 2018.
34. Q. T. Nguyen, A. Mai, L. Chagas, N. R. Bruas, "Microscopic printing analysis and application for classification of source printer", *Computers & Security*, vol.108, pp. 102320, ISSN 0167-4048, 2021
35. N. Otsu, "A Threshold Selection Method from Gray-Level Histograms", in *IEEE Transactions on Systems, Man, and Cybernetics*, vol. 9, no. 1, pp. 62-66, 1979. [CrossRef]
36. L.V. Evrard, "Measurement Analysis and Modelling at the Microscale of Printed Dots to Improve the Printed Anti-Counterfeiting Solutions", *Doctoral Dissertation, Chemical and Process Engineering Université Grenoble-Alpes, Grenoble, France, 2019.*
37. E. Olson, "Particle Shape Factors and Their Use in Image Analysis–Part 1: Theory", *J.GXP Compliance*, vol.15, pp.85, 2013.
38. A. Hamblyn, "Effect of Plate Characteristics on Ink Transfer in Flexographic Printing", *Ph.D. Thesis, Swansea University, Swansea, UK, 2021.*
39. I. Tkachenko, A. Trémeau, T. Fournel, "Authentication of Medicine Blister Foils: Characterization of the Rotogravure Printing Process", In *Proceedings of the 14th International Joint Conference on Computer Vision, Imaging and Computer Graphics Theory and Applications (VISIGRAPP 2019)*, Prague, Czech Republic, pp.577–583, 25–27 February 2019. [CrossRef]
40. I. Tkachenko, A. Trémeau and T. Fournel, "Authentication of rotogravure print-outs using a regular test pattern", *Journal of Information Security and Applications*, vol. 66, pp.103133, 2022
41. H. Mathes, "Flexo troubleshooting Most common flexo-printing issues, Part 3", *Flexo Grav. Int.*, vol.4, pp.22–23, 2011.



42. Sosa,R. “Effects of Temperature Control on Gravure Packaging Inks”, Master’s Thesis, Western Michigan University, Kalamazoo, Michigan, pp.4935,2021.
43. M.E.A.Kader,“The Impact of Ink Viscosity on the Enhancement of Rotogravure Optical Print Quality”,*Int.Des.J.*,vol.7,pp.103–107, 2017.
44. S. Joshi, S. Saxena, and N. Khanna,“Source Printer Identification from Document Images Acquired using Smartphone”,vol.2003, pp.12602, 2020.
45. J.Oliver, J.Chen, “Use of Signature Analysis to Discriminate Digital Printing Technologies”, In Proceeding of the IS & T’s NIP 18, International Conference on Digital Printing Technologies, San Diego, CA, USA, pp.218–222, 29 September–4 October 2002.
46. S.Sun, Z.Cao, H.Zhu, J.Zhao, “A Survey of Optimization Methods from a Machine Learning Perspective”, *IEEE Trans. Cybern.*, vol.50,pp.3668–3681, 2020. [CrossRef][PubMed]
47. X.Ying, “An Overview of Overfitting and its Solutions”, *J. Phys. Conf. Ser.*, vol.1168, pp.022022, 2019. [CrossRef]
48. J. Ni, Z. Khan, S. Wang, K. Wang and S. K. Haider, “Automatic detection and counting of circular shaped overlapped objects using circular hough transform and contour detection”, 2016 12th World Congress on Intelligent Control and Automation (WCICA), Guilin, China, pp. 2902-2906, 2016.
49. R. Hussin, M. R.Juhari, N. W. Kang, R.C. Ismail, A. Kamarudin, “Digital Image Processing Techniques for Object Detection from Complex Background Image”, *Procedia Engineering*, vol 41, pp. 340-344, ISSN 1877-7058, 2012.
50. S. Bindu, S. Prudhvi, G. Hemalatha, M. N. R. Sekhar, and M. V. Nanchariah, “Object detection from complex background image using circular hough transform,” *Int. Journal of Engineering Research and Applications*, vol. 4, pp. 23–28, 2014.
51. Abbas, N., Mohamad, D., Abdullah, A. H. “Semi-automatic red blood cells counting in microscopic digital images”, *Jurnal Teknologi*,2015.
52. S. Marcin and I.Dułęba, “Circular object detection using a modified Hough transform”, *International Journal of Applied Mathematics and Computer Science*, vol.18(1) pp.85-91, 2008.
53. OECD and EUIPO, “Trade in counterfeit and pirated goods,” OECD Publishing, pp. 138, 2016.
54. P.J.Chiang, N.Khanna,A. Mikkilineni,K.Segovia, M.V.O.Suh, S. Allebach, J.P., Chiu, G.T.C., E.J. Delp, “Printer and scanner forensics. *Signal Processing Magazine*”, *IEEE*,vol.26, pp.72–83. 2009.
55. S. M.Darwish and H. M. ELgohary. “Building an expert system for printer forensics: A new printer identification model based on niching genetic algorithm”, *Expert Systems*, vol.38(2), pp.e12624, 2021.

56. H.Lee and J.Choi, "Identifying color laser printer using noisy feature and support vector machine", In IEEE International Conference on Ubiquitous Information Technologies and Applications, China, pp. 1–6, 2010.
57. I.Tkachenko, A.Tremeau and T.Fournel, "Fighting against medicine packaging counterfeits: rotogravure press vs. cylinder signatures", Proceedings of IEEE International Workshop on Information Forensics and Security (WIFS),New York, pp. 1-6, 2020.
58. Joshi A. V., Bandyopadhyay S., "Effect of gravure process variables on void area in shrink film, Journal of Coatings Technology and Research", J Coat Technol Res, vol.11, no.5, 2014.
59. Joshi Akshay Vijay, "Investigation of Process Parameters on Gravure Printability for Shrink Sleeves", Thesis, Printing Engineering Department, Jadavpur University, Kolkata, India,2014.
60. P. Kundu, S.Bandyopadhyay, A.Tremeau, "Study on Color Gamut to Authenticate the Gravure Printers Output", International Journal of Computer Applications, vol. 184,no.18, pp. 0975 – 8887, June 2022.
61. P. Kundu, S.Bandyopadhyay, A.Tremeau, "Authentication of a Gravure Printer from Color Values using an Artificial Neural Network", International Journal of Engineering Research & Technology (IJERT), vol. 11, Issue 02, February-2022.
62. P. Kundu, S.Bandyopadhyay, A.Tremeau, "Analysis of Spectral differences between Printers to detect the Counterfeit Medicine Packaging", Journal of Algebraic Statistics, Volume 13, No. 2, p. 798 – 806, 2022.
63. Mandal M., Bandyopadhyay S., "To Predict the Waterfastness Rate of Foil Print", International Journal of Engineering Research & Technology (IJERT), vol. 8,issue 06, June-2019.
64. Mandal M., Bandyopadhyay S., "Study of the lightfastness properties of prints on blister foils by spectral reflectance", Color Research & Application. 45. 10.1002/col.22449, 2019.
65. Manda M., Bandyopadhyay S., "Artificial neural network approach to predict the lightfastness of gravure prints on the plastic film", Color Research & Application, 10.1002/col.22504, vol.45, issue 4, pp.686-698, 2020.
66. Mandal M., Bandyopadhyay S., "To Predict the Waterfastness Rate of Foil Print Applying Artificial Neural Network", International Journal of Computer Applications, vol. 178, No. 35 pp.0975 – 8887, July 2019.
67. Mandal M., Bandyopadhyay S., "To Predict the Lightfastness of Prints on Foil Applying Artificial Neural Network", Society for Imaging Science and Technology,2020.
68. L. Xinguang, L. Chang, W. Yumei, I. Heiner, "Variation of Gravure Printing Characteristic Curves", Proceedings of the 17th IAPRI World Conference on Packaging, 978-1-935068-36-5, 2010.
69. Lee, H., & Choi, J., "Identifying color laser printer using noisy feature and support vector machine", In IEEE International Conference on Ubiquitous Information Technologies and Applications, China, pp. 1–6, 2010.

70. Tsai MJ, Liu J, “Digital forensics for printed source identification”, In IEEE International Symposium on Circuits and Systems (ISCAS), May, pp. 2347–2350. doi: 10.1109/ISCAS.2013.6572349, 2013.
71. M. J. Tsai, and I.Yuadi, “Digital forensics of microscopic images for printed source identification”, *Multimedia Tools and Applications*, vol.77, pp.8729-8758, 2018.
72. M.J.Tsai, J.SYin, I. Yuadi, J. Liu, “Digital forensics of printed source identification for Chinese characters”, *Multimedia Tools and Applications*, vol.73, pp.2129–2155, 2014.
73. M.J.Tsai, H. CL, J.S.Yin, I.Yuadi, “Japanese character based printed source identification”, *IEEE International Symposium on Circuits and Systems (ISCAS)*. May, Lisbon, pp. 2800-2803, 2015.
74. Joshi, S., Khanna, N., “Single classifier-based passive system for source printer classification using local texture features”, *IEEE Transactions on Information Forensics and Security*, vol.13, pp.1603–1614, 2017.
75. R. Schraml, L. Debiasi, C. Kauba, and A. Uhl, “On the feasibility of classification-based product package authentication”, *2017 IEEE Workshop on Information Forensics and Security (WIFS)*, IEEE, pp. 1–6, 2017.
76. S.Voloshynovskiy, M.Diephuis, F.Beekhof, O.Koval, B. Keel, “Towards reproducible results in authentication based on physical non-cloneable functions: The forensic authentication microstructure optical set (famos)”, *Information Forensics and Security (WIFS)*, 2012 IEEE International Workshop on, IEEE. pp. 43–48. 2012.
77. N. Zadbuke, S. Shahi, B. Gulecha, A. Padalkar, M.Thube, “Recent trends and future of pharmaceutical packaging technology”, *Journal of pharmacy & bioallied sciences*, vol. 5(2), pp.98, 2013.
78. A.Singh, P.K. Sharma and R. Malviya, “Eco Friendly Pharmaceutical Packaging Material *World Applied Sciences Journal*”, vol.14(11), pp.1703-1716, 2011.
79. S. Kumar, and S.K. Gupta. “Applications of biodegradable pharmaceutical packaging materials: a review”, *Middle-East Journal of Scientific Research*, vol.12(5), pp. 699-706, 2012.
80. WHO Expert Committee on Specifications for Guidelines on packaging for pharmaceutical products. WHO Technical report, World Health Organization, 2002. (WHO Technical Report Series, No. 902)
81. L. Lachman, H.A. Lieberman and J.L. Kanig, “The theory and practice of industrial pharmacy”, Varghese Publishing House, pp. 412-428, 2008.
82. R.Pilchik, “Pharmaceutical Blister Packaging, Part I Rationale and Materials”, *The Techmark Group*, 1040 North Kings Highway, Suite 707, Cherry Hill, vol.24(11), pp.68-68, 2000.
83. E. Pongrácz, "The Environmental Impacts of Packaging", 2007
84. A. Singh et. al “Eco Friendly Pharmaceutical Packaging Material”, 2013.
85. J. Nieminen, I.Anugwom, M.Kallioinen, M.Mänttari, “Green solvents in recovery of aluminium and plastic from waste pharmaceutical blister packaging”, *Waste Management*, vol.107, pp.20-27, ISSN 0956-053X, 2020.
86. M. Lamberti & F. Escher, “Aluminium Foil as a Food Packaging Material in Comparison with Other Materials”, *Food Reviews International*, vol.2(4), pp.407-433, 2007.

87. P. Y. Dave, "Short Review on Printing Ink Technology to Prevent Counterfeit of the Products", *Journal of Advanced Chemical Sciences*, vol.6, Issue 4, pp.693– 697, 2020.
88. R.Y. Shah, P.N. Prajapati, Agrawal YK., "Anticounterfeit packaging technologies", *J Adv Pharm Technol Res.*, vol.1(4), pp.368-73, 2010.
89. J. M. Soon, and L. Manning, "Developing anti-counterfeiting measures: The role of smart packaging", *Food Research International*, vol.123, pp.135-143, 2019.
90. Counterfeit medicines, QA counterfeit, World Health Organization (WHO) 2009. Available from: <http://www.who.int/medicines/services/counterfeit/faqs/QACounterfeit>.
91. V. Pareek, and A. Khunteta, "Pharmaceutical packaging: Current trends and future", vol. 6, pp.480-485, 2014.
92. An ICC initiative Business Action to Stop Counterfeiting and Piracy (BASCAP) Brand protection directory. The World Business Organization. Available from: <http://www.iccwbo.org/bascap>
93. Helmut Kipphan, "Handbook of Print Media", Technologies and Production Methods, Publisher: Springer-Verlag, Berlin Heidelberg, 2001.
94. R. H. Leach, "The Printing Ink Manual", 5 th Edition, London: Springer; 173p. 1988
95. N.R. Eldred, "Package Printing", 1998.
96. Hennig, G., Selbmann, K. H., Mattheus, S., Kecke, R., Bruning S. , Laser Precision Micro Fabrication in the Printing Industry. *Journal of Laser Micro/Nanoengineering*, vol.1 (2), pp.89-9, 2006.
97. B. Sharma, S. Singh, A. Pandey, D. Dutt, & A. Kulshreshtha, "Sustainable and green manufacturing of gravure printing cylinder for flexible packaging printing application", *Scientific Reports*, 2022.
98. Philip Pimlott, "Gravure Association of America, A comprehensive guide to essential gravure technology", Gravure Association of America, 2003.
99. Donald E. Troxel, William F. Schreiber, Samuel M. Goldwasser, Malik M. A. Khan, Len Picard, Michael A. Ide, and Carolyn J. Turcio, "Automated Engraving of Gravure Cylinders", *IEEE Transactions on Systems, Man, and Cybernetics*, vol. SMC- 11, no. 9, September 1981.
100. X. Rong, J. Pekarovic, A. Pekarovicova, "Gravure Printability from Laser and Electromechanically Engraved Cylinder", *Proceedings of International printing Graphics Arts Conference*, Vancouver, British Columbia, Canada, pp. 151-154, October 2004.
101. Chiawei Wu, "Engraving Manager Packaging corporation of America", Waco, Texas, Cylinder Specifications, RIT, 2010.
102. S. Lee, Y. Na, "Effect of roll patterns on the Ink transfer in R2R printing process", *Int. J. Precis. Eng. Manuf*, vol. 10, pp.123–130, 2009.



103. Pujun, Deng, Wang Yu, and Fang Wei. "Influences of Cell Angles on Ink Transferring in Gravure", Proceedings of the 17th IAPRI World Conference on Packaging.
104. Li A., "The gravure atom: An evaluation of cell structure", vol.21, pp.32-38, 2007.
105. Janoschka (n. d), Cell Wall, Retrieved October 02, 2012.
106. S. Wu, J. Xing, L. Dong, H. Zhu, Multi-Objective Optimization of Microstructure of Gravure Cell Based on Response Surface Method, Processes, vol.9(2), pp.403, 2021.
107. G. G. Laurent, "Measurement and prediction procedures for printability in flexography", (MP3 Flexo) (Doctoral dissertation, Doctoral dissertation, Royal Institute of Technology, Stockholm, Sweden), 2002.
108. C. Cortes, and V. Vapnik, "Support-vector networks", Machine Learning, vol.20, pp.273-297,1995.
109. Y. Ahuja, and S. K. Yadav, "Multiclass Classification and Support Vector Machine", 2012.
110. A. Patle and D. S. Chouhan, "SVM kernel functions for classification", 2013 International Conference on Advances in Technology and Engineering (ICATE), Mumbai, India, pp.1-9, 2013.
111. G. Lychock, "Dot Area, Dot Gain, and n-Factors", Brochure, X-Rite, Incorporated Brochure, Grandville, MI ,1995.

*J. Indira Das*  
04.07.2023